A novel route to ionogels using polymerisation-induced self-assembly in ionic liquid

GEORGIA LUCY MAITLAND

Doctor of Philosophy

ASTON UNIVERSITY

March 2024

Abstract: A novel route to ionogels using polymerisation-induced self-assembly in ionic liquid

Georgia Lucy Maitland

Thesis presented for the degree of Doctor of Philosophy

2024

This Thesis describes the ionic liquid-directed self-assembly of block copolymers via reversible addition-fragmentation chain transfer (RAFT)-mediated polymerisation-induced self-assembly (PISA) to conveniently generate so-called ionogels.

Firstly, polymer solubility screenings were conducted in two hydrophilic ionic liquids (ILs), 1-ethyl-3-methylimidazolium dicyanamide ([EMIM][DCA]) and 1-ethyl-3-methylimidazolium ethyl sulphate ([EMIM][$EtOSO_3$]). Subsequently, suitable polymers were identified for proceeding PISA syntheses. Poly(2-hydroxyethyl methacrylate) (PHEMA) and poly(benzyl methacrylate) (PBzMA) were identified as a suitable stabiliser block and core-forming block, respectively. Additionally, benzyl methacrylate (BzMA) monomer was shown to be miscible with both ILs, enabling the development of dispersion PISA formulations which provide the most accessible route to worm gels.

A PHEMA macromolecular chain transfer agent was synthesised via RAFT solution polymerisation and subsequently chain extended via RAFT dispersion polymerisation of BzMA in [EMIM][DCA] to afford block copolymer nanoparticles, specifically spheres, worms and vesicles, as confirmed by dynamic light scattering (DLS), small-angle X-ray scattering (SAXS) and transmission electron microscopy (TEM). The presence of worms enabled the formation of free-standing gels at copolymer concentrations >4% w/w. These gels that exhibited comparable electrochemical properties and thermal stability to [EMIM][DCA] alone. Moreover, rheological studies indicated that stiffer gels were formed when an increasing proportion of worms was present. This PISA formulation in [EMIM][DCA] facilitates the *in situ* formation of worm ionogels without the need for crosslinkers, co-solvents or post-polymerisation processing/purification.

PHEMA-*b*-PBzMA nanoparticle syntheses were also conducted in [EMIM][$EtOSO_3$]. The presence of spheres and vesicles was confirmed by DLS and SAXS, however no gelation occurred for the PBzMA DP range at 15% w/w and 20% w/w copolymer, indicating the absence or an insufficient proportion of worm-like nanoparticles. This could be due to the length of the PHEMA stabiliser block being sufficiently large to prevent fusion of 2D spheres in this specific IL, thus hindering the ability to form anisotropic worms.

Key words: Ionic liquids; ionogels; polymerisation-induced self-assembly; block copolymers; reversible addition-fragmentation chain transfer; polymerisation; nanoparticles; gel electrolytes.

Acknowledgements

I would firstly like to thank my main supervisor, Dr. Matthew Derry, for his incredible support and guidance throughout the whole of my PhD, which I am extremely grateful. I don't think I could have asked for a better supervisor. I would also like to thank my associate supervisor, Prof. Paul Topham for his invaluable input in my research, and for making me laugh when I needed it the most. I would like to thank them both for the several traveling opportunities I have been given, both national and international. Most importantly, I am thankful for the Diamond Light Source trips, which have had some of the funniest, side-splitting memorable moments from the whole of my PhD.

A huge thank you is given to Dr. Stephen Worrall, firstly for aiding with my electrochemical analyses, but more importantly, for essentially helping kickstart the beginning of my PhD career, and for his mentoring during my BSc that has proven to be invaluable. I would not be here if it was not for your encouragement and support. I am indebted to Dr. Helena Hutchins, whom without her, I would not have settled into PhD life so quickly. Thank you for always being so patient and answering all my silly questions when I was first starting out.

A massive part of my amazing PhD experience is owed to the MB111 PhD members, both past and present. Thanks to those who were there in my last few months of my PhD: Nawal, Alice and Ben for entertaining office conversations. Thank you Bawan, Hana and Lauren, for your company when travelling, and giving me some of my most favourite memories. Thank you, Joe, for all the insane conversations in the office that have always left me crying with laughter. Anisha, thank you for being an amazing travel buddy, as well as being one of the best, most supportive friends I could ask for. Thank you, Bridget, for journeying with me through this PhD since the very beginning and being one of the best friends I've ever had. From the bottom of my heart, I love you all so much.

I am also indebted to the Derry-Topham research group, both past and present members. In particular, I would like to thank Dr. Amit Kumar Sarkar for always checking in on me and helping me whenever I needed it. I am very excited to be working with you again in the near future. Thank you to Jem, our incredible lab technician who was always on hand to aid with all analytical equipment. Thank you to MEDIPOL, for allowing me to make some amazing friends from across the world. In particular, all the researchers that have visited from Thailand, who have enhanced my PhD experience and have been my biggest supporters. Each and every one of you have made a huge impact in my life, and I'm so grateful to have so many new friends.

I would like to thank my family for supporting me from the start. Mom and Steve, thank you for your unwavering love and support. Without you both, I would not be writing this. I am also unbelievably grateful for the encouragement and love I have constantly been given by the Alexander-Luck crew, particularly Mark and Lynsay. Thank you for always asking me about my work and celebrating every little milestone along the way. I would also like to thank the rest of my family, including Dad, Lynne, and all of my brothers, for all the nights out and pub trips that have kept me going. I love you all so much.

Lastly, I would like to thank my best friend and partner, Cole. For always being there and supporting me unconditionally. Thank you for pushing me to be the best version of myself, and for being endlessly patient with me. I am so excited to journey through life with you.

List of publications

1. S. Varlas; **G. L. Maitland**; M. J. Derry, Protein-, (Poly)peptide-, and Amino Acid-Based Nanostructures Prepared via Polymerization-Induced Self-Assembly, *Polymers*, **2021**, 13(16), 2603
2. **G. L. Maitland**; M. Liu; T. J. Neal; J. Hammerton; Y. Han; S. D. Worrall; P. D. Topham; M. J. Derry, Block copolymer synthesis in ionic liquid via polymerisation-induced self-assembly: A convenient route to gel electrolytes, *Chemical Science,* **2024**, 15, 4416-4426

Table of contents

Abbreviations

AA	Acrylic acid
ACVA	4,4'-Azobis(4-cyanovaleric acid)
AIBN	2,2'-Azobisisobutyronitrile
ATRP	Atom transfer radical polymerisation
BCP	Block copolymer
BzMA	Benzyl methacrylate
CGC	Critical gel concentration
CPTP	4-Cyano-4-(phenylcarbonothioylthio) pentanoic acid
CTA	Chain transfer agent
D_h	Hydrodynamic diameter
D_{sphere}	Spherical nanoparticle diameter
$D_{vesicle}$	Overall vesicle diameter
DAAM	Diacetone acrylamide
DLS	Dynamic light scattering
$Đ_M$	Dispersity
DMA	*N,N*-Dimethylacrylamide
DMF	*N,N*-Dimethyl formamide
DP	Degree of polymerisation
EIS	Electrochemical impendence spectroscopy
[EMIM][DCA]	1-ethyl-3-methylimidazolium dicyanamide
[EMIM][EtOSO$_3$]	1-ethyl-3-methylimidazolium ethyl sulphate
EtOH	Ethanol
FRP	Free radical polymerisation
G'	Storage modulus
G''	Loss modulus
GPC	Gel permeation chromatography

HEMA	2-Hydroxyethyl methacrylate
IL	Ionic liquid
L_{worm}	Worm length
MA	Methyl acrylate
Macro-CTA	Macromolecular chain transfer agent
MeOH	Methanol
M_n	Number-average molecular weight
M_w	Weight-average molecular weight
MWD	Molecular weight distribution
***n*-BuMA**	*n*-Butyl methacrylate
NMP	Nitroxide-mediated polymerisation
NMR	Nuclear magnetic resonance
***n*-PMA**	*n*-Propyl methacrylate
PDI	Polydispersity index
PBzMA	Poly(benzyl methacrylate)
PDAAM	Poly(diacetone acrylamide)
PDMA	Poly*(N,N*-dimethylacrylamide)
PHEMA	Poly(2-hydroxyethyl methacrylate)
PMMA	Poly(methyl methacrylate)
PISA	Polymerisation-induced self-assembly
PS	Polystyrene
q	Scattering vector
R_g	Radius of gyration
$R_{g,\,cop}$	Radius of gyration of dissolved copolymer chains
R_m	Centre of vesicle to centre of membrane
R_s	Sphere core radius

R_w	Worm core cross-sectional radius
RAFT	Reversible addition-fragmentation chain transfer
RDRP	Reversible deactivation radical polymerisation
RI	Refractive index
SAXS	Small-angle X-ray scattering
St	Styrene
T_g	Glass transition temperature
T_{worm}	Worm thickness
TEM	Transmission electron microscopy
TGA	Thermal gravimetric analysis
THF	Tetrahydrofuran
V_h	Hydrodynamic volume

List of figures

List of schemes

List of tables

1. Introduction

1.1 Polymers

A polymer is a long chain molecule consisting of repeating structural units, or monomers, covalently bonded together via a polymerisation reaction. When the same monomer is used as the repeating unit, this yields a homopolymer. Simply put, the terminology of the formed homopolymer is poly(monomer). An example of this would be polyethylene, which is formed when ethylene is polymerised. In order for a unit or monomer to form a polymer, functionality of the unit is required. Simply put, the unit requires two or more sites to bond so it can link on to another unit to form a molecular chain. For example, a diol with the functionality of two hydroxyl groups can link to another unit that also has functionality, such as a dicarboxylic acid (with two carboxyl groups) to form a polyester.

Polymers cannot be designated an exact molar mass and so instead, polymer molar masses in one given sample are expressed as an average of a molecular weight distribution (MWD) whose breadth can be characterised by a polydispersity index (PDI) or preferably, dispersity ($Đ_M$). $Đ_M$ can be calculated by dividing the number-average molecular weight (M_n) by the weight-average molecular weight (M_w) as shown in Equation 1.1

$$Đ_M = \frac{M_w}{M_n} \quad 1.1$$

M_n (defined in Equation 1.2[1]) can be calculated by analytical techniques such as ^{1}H NMR spectroscopy using end group analysis or using size exclusion chromatography (SEC) such as gel permeation chromatography (GPC) in which polymer chains are separated and measured by their hydrodynamic volume (V_h) (see Section 1.2.2). M_w can also be determined by GPC, as well as other techniques such as light scattering.

$$M_n = \frac{\Sigma N_i M_i}{\Sigma N_i} = \frac{\Sigma w_i}{\Sigma(\frac{w_i}{M_i})} \quad 1.2$$

Where M_i is the molar mass and N_i is the number of molecules of given M_i. M_w is defined as seen in Equation 1.3[1]:

$$M_w = \frac{\Sigma N_i M_i^2}{\Sigma N_i M_i} = \frac{\Sigma w_i M_i}{\Sigma w_i} \quad 1.3$$

The average number of repeat units in a polymer chain is known as the mean degree of polymerisation (DP). If every polymer chain in a given sample has the same M_w and M_n (so $Đ_M$ = 1), the sample is said to be perfectly monodisperse. If $Đ_M$ < 1.5, the MWD of the sample is arguably considered to be narrow, whereas a $Đ_M$ > 2.0 suggests the MWD is broad. However, these definitions of 'narrow' and 'broad' MWDs are not objectively assigned.[2]

1.2 Polymer characterisation

1.2.1 Gel permeation chromatography (GPC)

Another method of characterising polymers is size exclusion chromatography (SEC), or more specifically known as gel permeation chromatography (GPC). GPC works by separating polymer chains based on their hydrodynamic volume thus polymer chains with different molecular weights can be distinguished by their retention time in the GPC columns and subsequently analysed. The process typically involves introducing a given polymer sample into the mobile phase solvent by passing the sample through columns packed with porous beads[3] such as covalently crosslinked polystyrene beads. Depending on the hydrodynamic volume of the chains, the time at which they elute through the columns differs. Polymer chains that are smaller in size can travel through the porous beads, take a longer path through the columns and thus elute slower, whereas larger polymer chains cannot enter as many of the pores and thus take a shorter path through the column and elute faster. Once the chains have eluted, they are detected, typically by using a refractive index (RI) detector.

It is important to note that GPC is a relative technique, meaning that molecular weights that are determined relative to a calibration standard such as poly(methyl methacrylate) (PMMA) or polystyrene (PS) that have known molecular weights and narrow MWDs. Therefore, it is not entirely accurate to rely on GPC to determine the exact molecular weight of polymer samples that are not the same polymer as the calibrant. Ultimately, it is more appropriate to use this technique in conjunction with ^{1}H NMR spectroscopy, where M_n values can be determined via end-group analysis, albeit with its own corresponding disadvantages (e.g. the assumption that all polymer chains contain the required end group functionality)

1.2.2 Dynamic Light Scattering (DLS)

The hydrodynamic volume (D_h) of particles in a dispersion can be measured by dynamic light scattering (DLS). DLS takes in to account the Brownian motion of particles in order to determine

the size of the particles[1]. The fundamental theory behind Brownian motion is that when particles are dispersed in a liquid, the solvent molecules and particles are constantly colliding. Particle movement occurs as a result of energy transmitted by other collisions. Smaller particles move faster and are more likely to collide within a dispersion as energy transfer from collisions is approximately constant. By contrast, larger particles will move slower. D_h can then be calculated based on the speed at which the particles are moving, assuming that all other parameters required such as the translational diffusion coefficient, temperature and solution viscosity are known too. This is shown in the Stokes-Einstein equation below:

$$D_h = \frac{k_B T}{3\pi\eta D} \quad 1.4$$

Where k_B is the Boltzmann constant, T is the absolute temperature, η is the solution viscosity and D is the translational diffusion coefficient[4] (also commonly known as the velocity of the Brownian motion). In relation to particle size and D, smaller particles exhibit a larger D as a result of faster movement. Despite some advantages of DLS such as being a non-invasive and fast technique, requiring very simple sample preparation, there are also limitations. Most notably, the Stokes-Einstein equation assumes that the particles are all spherical, thus any D_h values given is only comparable to the diameter of a sphere.

1.2.3 Rheology of viscoelastic materials

Rheology is defined as the study of how the application of force influences deformation of states of matter.[5] Deformation arises as a result of stress being applied to a material. The simplest example of materials deformation can be shown as the process of the deformation of a cuboid upon the application of an external force (Figure 1.1). When force is applied in one direction, this is known as shear stress. Stress (σ), in essence, is defined as force per unit area and is expressed in Pascals (Pa). Strain (γ) is defined as the deformation per unit length and arises as a result of the application of shear stress. In other words, strain denotes the relative deformation.

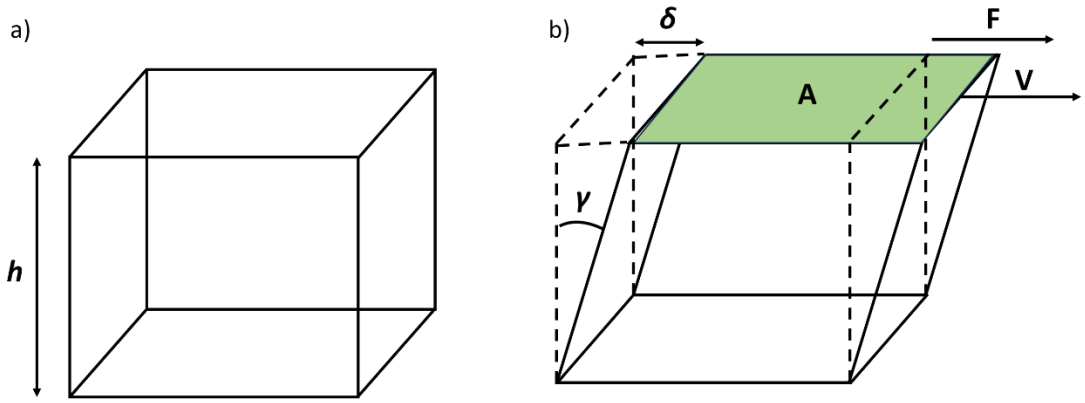

Figure 1.1. a) Cuboid which has not deformed as a result of shear deformation. The height of the cuboid is denoted as *h*. b) Cuboid that has undergone shear deformation as a result of the application of stress to one face with an area (*A*). Strain is denoted as *γ,* the displacement is denoted by δ, and F and V denote force applied and velocity, respectively. Adapted from Cowie.[1]

The rheological behaviour of polymers can be characterised macroscopically by i) the flow of viscous liquids, ii) mechanical properties of elastic solids, and iii) viscoelasticity.[1] The flow of viscous liquids can be described by Newton's law, which states that applied stress is independent of resultant strain, but is proportional to the rate of strain, therefore when stress is applied, deformation will continue until the strain rate reaches zero. In contrast, mechanical properties of elastic solids can be expressed by Hooke's law, which states that applied stress is proportional to resultant strain, but independent of rate of strain, therefore a Hookean solid will reversibly return to its original state once applied stress is removed. Both of these laws assume that only small strains or rates of strain occur, in which typically linear behaviour is observed. However, at larger stress or strains, non-linear behaviour is observed.

Viscoelastic materials are those that exhibit characteristics of both a liquid and a solid. Neither Hooke's law nor Newton's law alone can describe this phenomenon sufficiently. Upon application of a given frequency, viscoelastic materials can exist in either of five distinct states: viscous/terminal, transition to flow, rubbery plateau, leathery/transition, or glassy. Typical rheological behaviour of a polymer as a function of angular frequency is shown in Figure 1.2, where the storage modulus (*G*') represents the contribution of solid-like behaviour to the overall properties and the loss modulus (*G*'') represents the liquid-like contribution. Such viscoelastic behaviour is explored in more detail in Chapter 4, with a specific focus on gel-like materials.

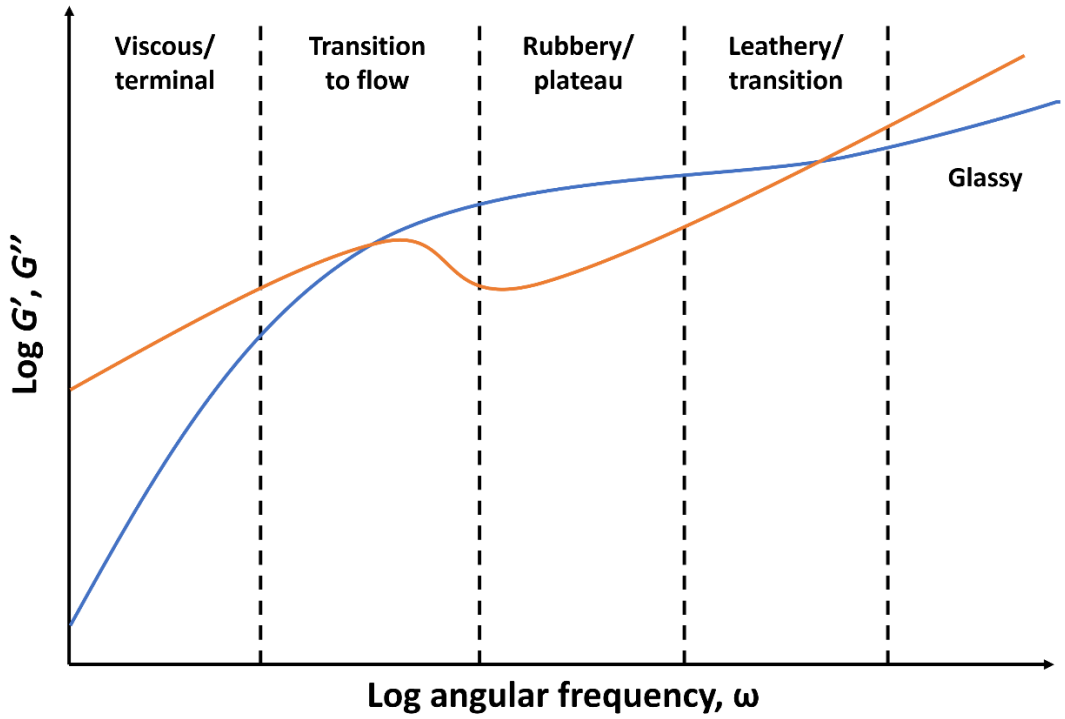

Figure 1.2. Dependence of storage (blue) and loss modulus (orange) (*G*' and *G*'', respectively) with angular frequency (ω) of a viscoelastic material during oscillatory measurements.[6]

The viscoelastic properties of a material can be analysed by various different methods, for example, stress-relaxation and creep measurements. However, most relevant to this Thesis is measuring the viscoelastic behaviour by oscillatory measurements, where viscoelasticity can be measured as a function of frequency, temperature and strain using a rheometer.[1] This viscoelastic properties of the worm ionogels synthesised in Chapter 3 are measured using oscillatory measurements. A range of geometries are able to be used to conduct oscillatory measurements, such as parallel plates and cone-and-plate. The cone-and-plate geometry is used for all oscillatory measurements in this Chapter (Figure 1.3) as it offers a constant shear rate across the sample. Conversely, when using a parallel plate, the shear rate is zero at the centre of the plate and its maximum value at the edge of the plate.

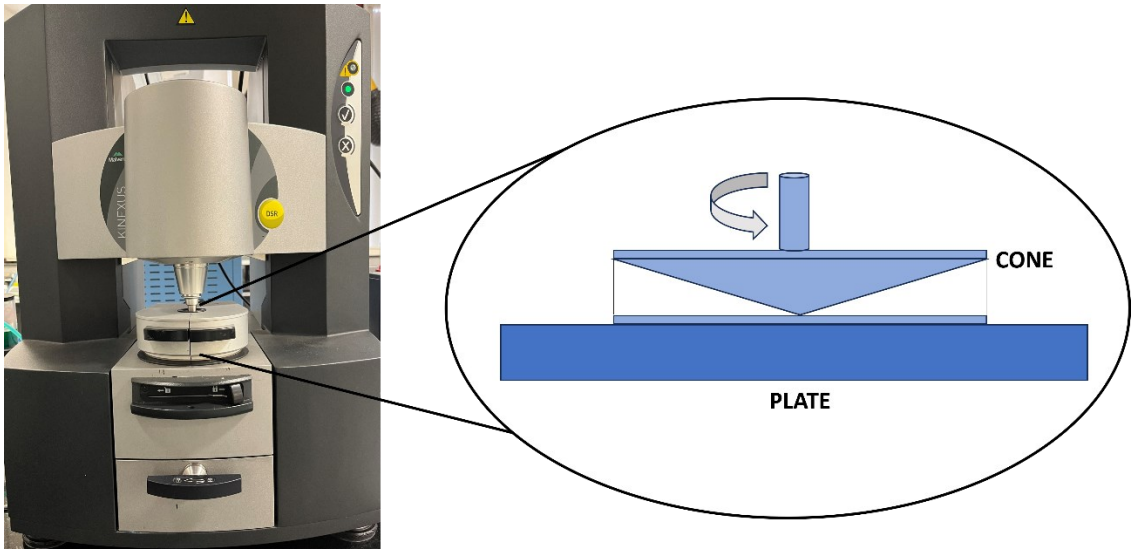

Figure 1.3. Kinexus Dynamic Shear Rheometer-III from Netzsch Analyzing and Testing, used for oscillatory measurements in this Thesis. The cone-and-plate geometry used for these measurements is illustrated. This geometry can be found under the hood in the rheometer.

1.2.4 Electrochemical impedance spectroscopy (EIS)

Electrochemical impedance spectroscopy (EIS)[7] enables the study of electrochemical properties of conductive materials such as diffusion and ion exchange between materials and their interfaces.[8] Upon the application of a small-amplitude stimulus (i.e. a current or voltage) to a given electrochemical material over a broad range of frequencies, the resulting response (i.e. a voltage or current, respectively) can be measured.

In this Thesis, EIS is used to determine electrochemical properties of ionogels (Section 1.6) synthesised. The bulk resistance of the ionogels is extracted from the x-intercept at high frequencies of plotted Nyquist plots (example shown in Figure 1.4).

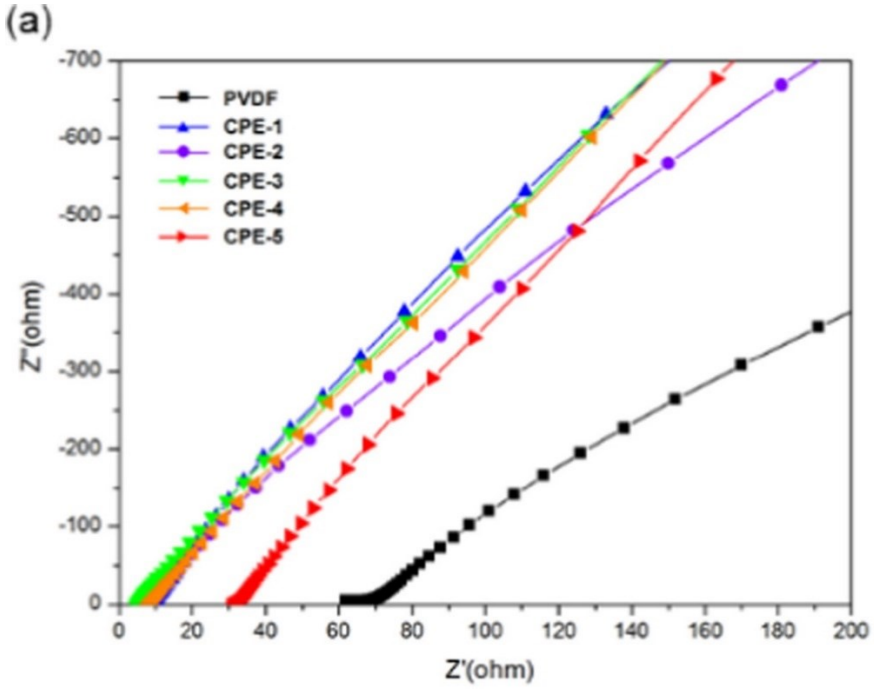

Figure 1.4. Example of Nyquist plot obtained from electrochemical impedance spectroscopy of an ionogel.[9]

1.3 Polymerisation methods

Two key categories for polymerisation reactions are step growth (e.g. condensation polymerisation) and chain (i.e. addition polymerisation). Step growth or condensation polymerisation involves the use of monomers with polyfunctionality to yield a polymer.[1] An example of this would be a simple polyester chain, which is synthesised by a condensation reaction between a bifunctional carboxylic acid (i.e. a dicarboxylic acid) and a bifunctional alcohol (i.e. a diol). Chain polymerisation typically utilises the reactivity of the π-bonds in a C=C bond in a vinyl monomer to yield a polymer by forming single σ bonds. In order for this to proceed, a reactive initiating species such as a free radical or ionic initiator is required to activate the polymerisation process.[1] Only chain polymerisation methods will be discussed in more detail in this Thesis.

1.3.1 Free radical (uncontrolled) polymerisation

Free radical polymerisation (FRP) is a widely known example of chain polymerisation and can be described in three principal steps: initiation, propagation and termination. These are illustrated in the equations below:

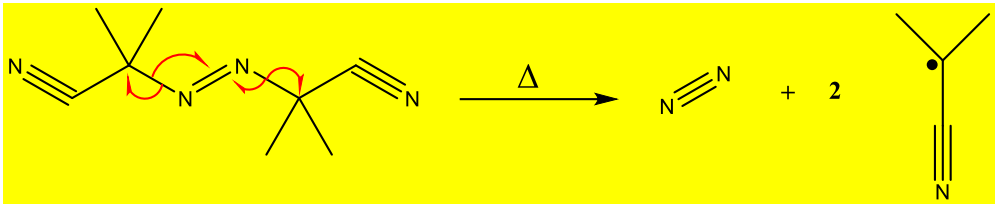

During initiation, the reactive initiating species typically undergoes either UV or thermally induced decomposition via homolytic cleavage to form radical species.

Initiation $I_2 \xrightarrow{\text{UV or heat}} 2I^{\bullet} \xrightarrow{+ M} I\text{-}M^{\bullet}$

The radical species immediately react with a monomer unit to form a new radical, which begins the propagation step.

Propagation $I\text{-}M^{\bullet} \xrightarrow{+ M} I\text{-}M\text{-}M^{\bullet} \left(= P_m^{\bullet}\right)$

During propagation, monomer units are then sequentially added to the active species, growing the polymer chain. This yields a polymer with a degree of polymerisation m.

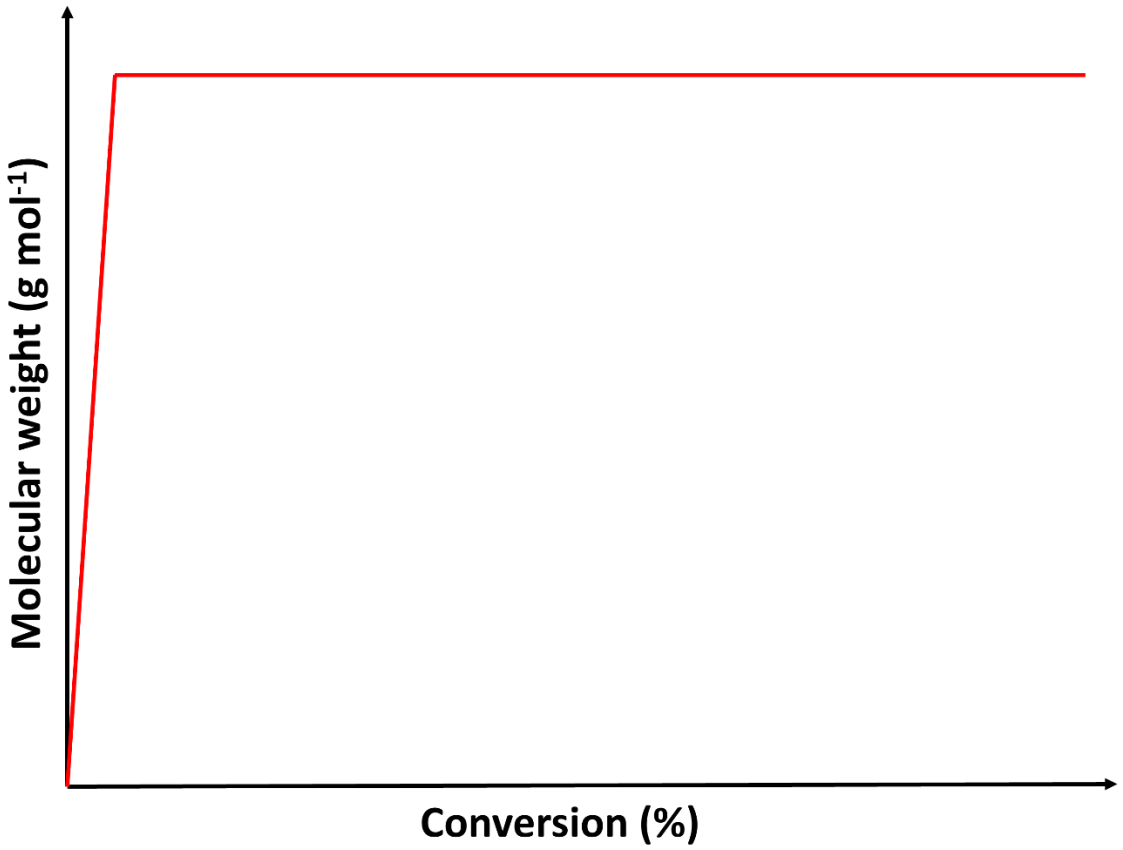

Figure 1.5. Progression of molecular weight with respect to monomer conversion during free radical (uncontrolled) polymerisation.

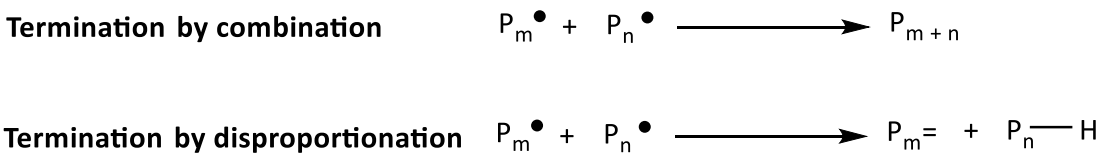

Termination can then occur in one of two ways: combination or disproportionation. Termination by combination involves the direct coupling of two radical species that results in a 'dead' polymer[2] with a DP of m+n, the sum of the DPs of both radical species involved in this termination event. Termination by disproportionation occurs from the transfer of an atom from one radical to another, e.g. hydrogen, resulting in the formation of two dead polymer chains where one possesses an unsaturated chain end, and one containing the transferred hydrogen.

As well as the three key steps that occur during free-radical polymerisation, a number of side reactions can also occur which can terminate the growth of the original polymer chain.[2] Transfer to initiator occurs when an initiator that has not yet decomposed (i.e. has not yet undergone

homolytic cleavage) reacts with an active polymer chain to yield an active initiator species and a dead polymer chain that is initiator-capped which can then continue on to form new polymer chains.

Transfer to initiator $P_m^{\bullet} + I_2 \longrightarrow P_m\text{-}I^{\bullet} + I^{\bullet}$

Transfer to polymer occurs when a hydrogen abstracts from a polymer chain onto a polymer radical, leading to branching, both short and chain by either intra- or intermolecular transfer, respectively.

Transfer to polymer $P_m^{\bullet} + P_x \longrightarrow P_m + P_x^{\bullet}$

Transfer to monomer or solvent is also possible, where a solvent or monomer hydrogen atom is transferred to a polymer radical to form monomer or solvent active radical species.

Transfer to monomer $P_m^{\bullet} + M \longrightarrow P_m + M^{\bullet}$

Transfer to solvent $P_m^{\bullet} + S \longrightarrow P_m + S^{\bullet}$

All active species formed during these side reactions can be seen as initiator fragments which are then able to form new polymer chains, therefore are assumed to not hinder polymerisation kinetics.

1.3.2 Reversible deactivation radical polymerisation (RDRP)

Reversible deactivation radical polymerisation (RDRP), also known as pseudo-living polymerisation [10] has been and is continuing to become a substantially popular polymerisation method. RDRP has become particularly prevalent over the past 30 years due to the exquisite control and versatility that it provides for the polymerisation of vinyl monomers.[11] In comparison to free radical (uncontrolled) polymerisation, RDRP is facilitated by reversible deactivation of propagating radicals which in turn provides an equilibrium between dormant and active polymer chains.[12] Examples of RDRP techniques include atom transfer radical polymerisation (ATRP), nitroxide-mediated polymerisation (NMP) and reversible addition-fragmentation chain transfer (RAFT) polymerisation. This allows for the synthesis of well-defined polymers (notably block copolymers) with narrow MWDs and control over pre-determined molecular weight.[13]

Block copolymers generally consist of two or more discrete blocks that are covalently bonded together and are chemically distinct.[14, 15] The simplest example of a block copolymer is an AB diblock copolymer, which is synthesised by a two-step process.[16] The synthesis of block copolymers can be carried out via sequential monomer addition or post-polymerisation coupling reactions, both of which give access to a range of polymer architectures (Figure 1.6). In particular, sequential addition polymerisation via controlled polymerisations techniques enables the use of a versatile range of monomers and conditions with a conveniently facile experimental setup.[15]

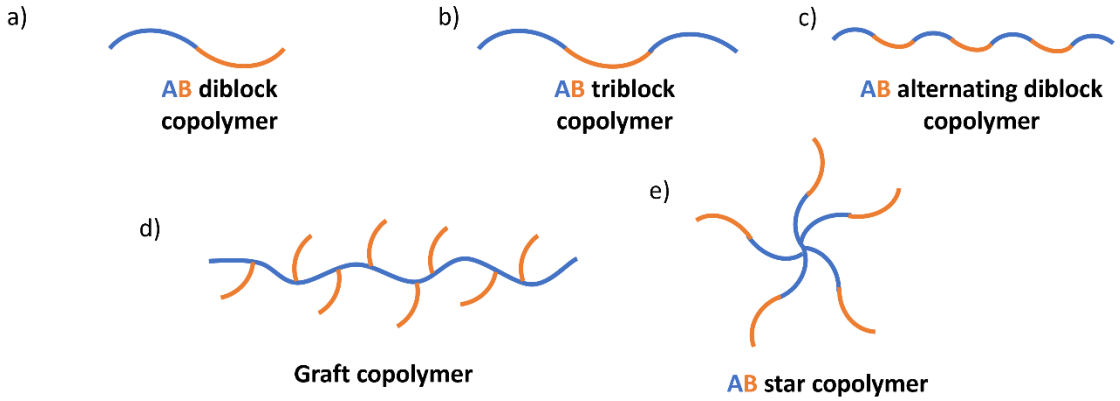

Figure 1.6. Examples of copolymer architectures that can be generated by the syntheses of block copolymers, where a), b) and c) are examples of linear architectures. Non-linear architecture examples are shown in d), and e).[11]

1.3.2.1 Reversible addition-fragmentation chain transfer (RAFT) polymerisation

Reversible addition-fragmentation chain transfer (RAFT) has been established as a widely popular and convenient polymerisation technique, ever since it was first reported in 1998 by Chiefari *et al.*[17] Unlike other previously mentioned RDRP techniques, RAFT is alternatively termed a degenerative chain transfer process which enables the reversible deactivation of propagating radicals thus reducing the concentration of active species and subsequently limiting termination events [18] (Scheme 1.1). RAFT polymerisation has received considerably increased attention in recent years due to being more amenable to some functional groups that techniques such as ATRP is not able to accommodate such as polymers that contain carboxyl groups (-COOH) and sulphonic acid groups ($-SO_3H$).[19]

A 2017 review by Perrier[10] highlighted the continuous increase in the utilisation of RAFT polymerisation, particularly over the past two decades. At the time of publication of this review, there were over 8000 publications utilising RAFT including 300 reviews and over 1000 patents covering a vast range of applications such as biomedical and materials science etc. RAFT requires

the use of a chain transfer agent (CTA)[20] which have a general structure S=C(Z)-S-R. Examples of CTAs include trithiocarbonates and dithioesters, both of which display the highest rates of radical addition and contain a sulphur or carbon atom adjacent to the thiocarbonyl group, respectively. Termination events that occur during free radical polymerisation are significantly suppressed during RAFT polymerisation. This is the primary role of the CTA, which enables the rapid establishment of an equilibrium between active and dormant polymer chains[19]. A RAFT agent can also be a xanthate or a dithiocarbamate, both of which exhibit slower rates of radical addition than the former CTAs mentioned.[10, 18] These possess an oxygen and nitrogen atom adjacent to the thiocarbonyl group, respectively. The former more reactive and latter less reactive examples are illustrated in Figure 1.7.

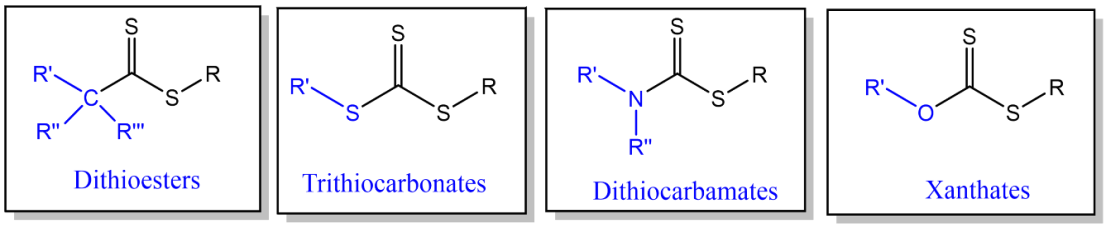

Figure 1.7. General structures of RAFT CTAs. CTA selection is dependent on the choice of monomer. The groups in blue represent the Z-group of the CTA.

Similar to free radical polymerisation, RAFT polymerisation comprises an initiation, propagation, and termination step. The mechanism for RAFT polymerisation technique is illustrated in Scheme 1.1, as this is the technique that is utilised throughout this Thesis.

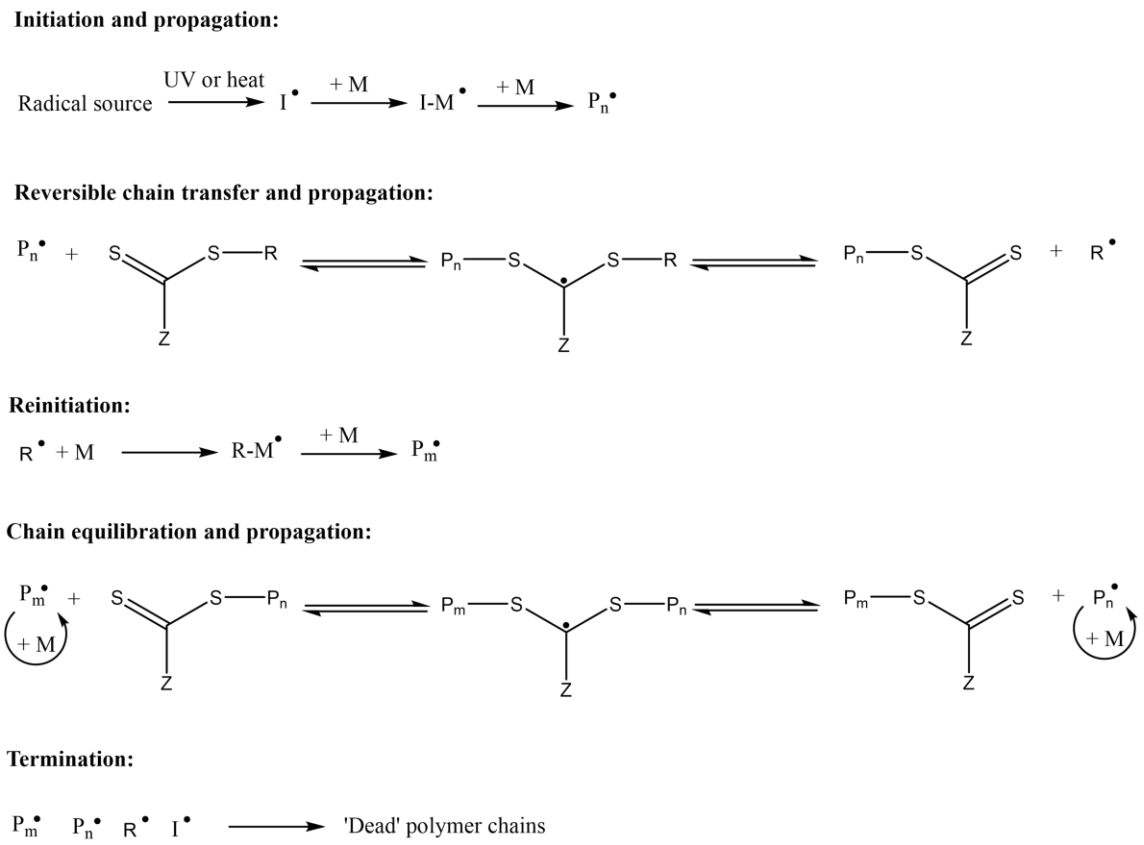

Scheme 1.1. The mechanism of RAFT polymerisation[10]

To initiate a RAFT polymerisation, radicals are introduced into the system by thermal- or photo-decomposition of a radical source, as with free-radical polymerisation. After the radical species are initiated, propagation results in the insertion of monomer units between the R- and S=C(Z)-S groups. The reactivity and therefore the choice of CTA for a reaction is dependent on its compatibility with the selected monomer. More specifically, for a RAFT polymerisation to be successful, the Z- and R- groups of the CTA need to be mindfully chosen such that the C=S bond is more reactive to radical addition relative to the C=C bond of the monomer as this will give optimum control of the RAFT polymerisation. This is primarily the responsibility of the Z-group in addition to maintaining stability of the intermediate radical. For the most effective R-group, a fine balance between steric effects and radical stability needs to be achieved. In order to attain this balance, the R-group must have the ability to form radicals with sufficient stability to promote R$^{\bullet}$ as a leaving group with this new radical species exhibiting appropriate reactivity so that it can add to monomer and initiate the growth of new polymer chains.[10] For this reason, the R$^{\bullet}$ radical species formed during reversible chain transfer (Scheme 1.1) should ideally be of similar reactivity to the monomer radical, M$^{\bullet}$.

Vinyl monomers are assigned in two different groups on the basis of their reactivity: more activated monomers (MAMs) and less activated monomers (LAMs). The vinyl group in MAMs is conjugated to one of the following four groups: a nitrile (e.g. acrylonitrile), an aromatic ring (e.g. styrene), a carbonyl group (acrylates and methacrylates). To achieve controlled polymerisation of MAMs, dithioester and trithiocarbonate RAFT agents are most suitable. LAMs possess a double bond beside an electron-rich atom or group such as oxygen, nitrogen, halogens, sulphur or a saturated carbon. In order to attain controlled polymerisation of LAMs, dithiocarbamates or xanthates are a most appropriate choice of CTA. Examples of LAMs include vinyl chlorides and 1-alkenes[10]. Keddie *et al.*[21] reported a comprehensive guide to selecting appropriate CTAs for the polymerisation of a given monomer class (Figure 1.8).

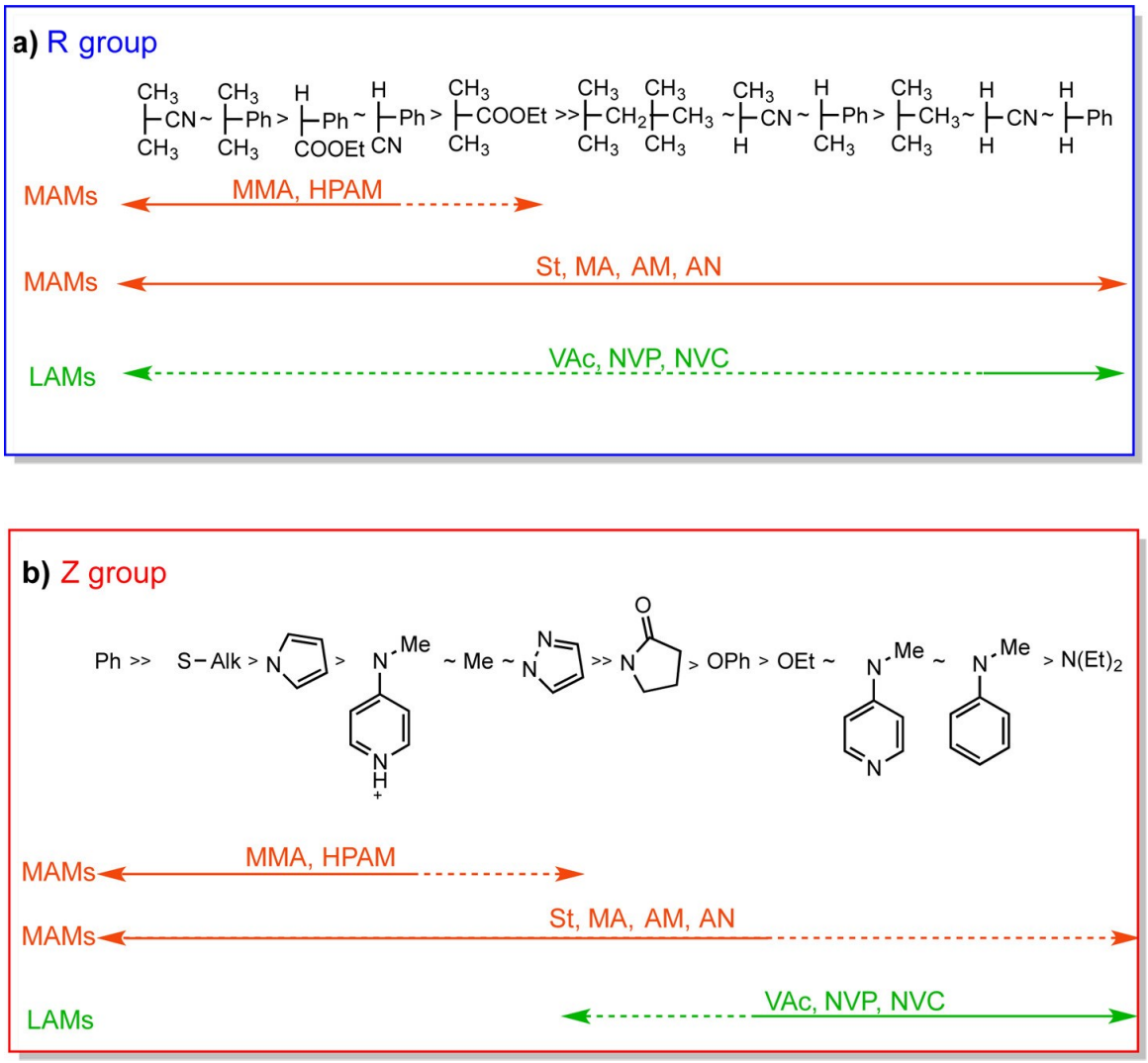

Figure 1.8. Guidelines for the selection of a) R groups and b) Z groups within chain transfer agents to provide control over RAFT polymerisations.[10, 18, 21]

1.3.3 Block copolymer synthesis via RAFT polymerisation

RAFT polymerisation is conceivably the most adaptable RDRP technique for developing block copolymers, as a result of the extensive choice for functional monomers, solvents and reaction conditions that RAFT is compatible with.[21] Typically, block copolymers prepared via RAFT polymerisation involves the incorporation of two or more monomers through sequential polymerisation (Scheme 1.2). Prior to each additional polymerisation, a purification step is often required to remove residual unreacted monomer.

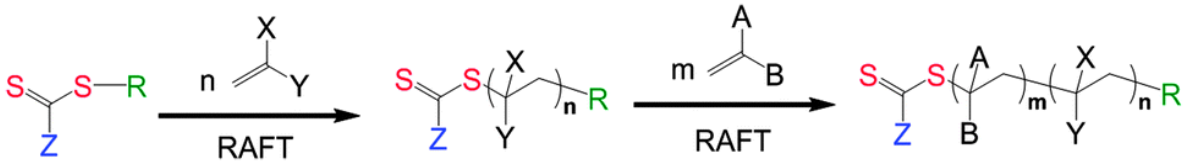

Scheme 1.2. Sequential RAFT polymerisations to form block copolymers.[21]

The order of which the monomers can be sequentially added into a block copolymer is crucial. The macro-CTA formed (i.e. the first block) must have, as previously discussed, an R group that is sufficient as a homolytic leaving group with respect to the propagating radical of the second monomer and should also have the ability to reinitiate the growth of further polymer chains of the second monomer. Moreover, monomers that produce stable tertiary propagating radicals such as methacrylates and methacrylamides should be utilised to prepare macro-CTAs for the chain extension of monomers that produce stabilised secondary propagating radicals such as styrenes, acrylamides and acrylates. Vinyl esters and vinyl amides should be sequentially added onto macro-CTAs of either of the former groups (methacrylates, methacrylamides, styrenes, acrylamides, acrylates) as they exhibit the most reactive secondary propagating radicals out of the potential R groups mentioned.[21]

1.4 Self-assembly

1.4.1 Block copolymer self-assembly

Analogous to surfactants, block copolymers can undergo self-assembly in the bulk and in solution. Microphase separation can be observed in the bulk as a result of enthalpic incompatibility between the two blocks. Essentially, microphase separation occurs in order to minimise the Gibbs-free energy of mixing. Because the blocks are bonded covalently, macroscopic phase separation is prevented.[16] In a typical AB diblock copolymer, microphase separation is dependent on three

parameters: i) the relative volume fractions of the two blocks, denoted as f_A and f_B where the sum of these is always equal to 1; ii) the total degree of polymerisation, denoted as N, which is the sum of each block's degree of polymerisation, further denoted as N_A and N_B; and iii) the Flory-Huggins parameter, χ_{AB}. This χ_{AB} parameter dictates the degree of incompatibility between the A and B blocks, which essentially drives the microphase separation.[14] The incompatibility between the A and B blocks is dependent on temperature, which the relationship is given by:

$$\chi_{AB} = \left(\frac{z}{k_B T}\right)[\varepsilon_{AB} - \frac{1}{2}(\varepsilon_{AA} + \varepsilon_{BB})] \quad 1.5$$

Where z is the number of nearest neighbours per repeat unit in the polymer, k_B is the Boltzmann constant, $k_B T$ is the thermal energy, $\varepsilon_{AB,}$ $\varepsilon_{AA,\text{ and }}$ ε_{BB} are the interaction energies per repeat unit for A-B, A-A and B-B, respectively. With increasing temperature, the incompatibility between the A and B block decreases and the copolymers can become homogenous. In other words, an increase in temperature enables an order-to-disorder transition (ODT), and so the copolymer becomes disordered. The temperature at which this transition occurs is denoted as T_{ODT}.[14] Likewise, ODT can be observed upon decreasing χN. Generally, with increasing f_A at a fixed χN above the (ODT) where $\chi N > 10.5$, order-to-order transitions are seen, progressing from closely packed spheres (CPS), to spherical (S), cylindrical (C), gyroidal (G) and lamellae (L).[16] When the compositions are inverted i.e. when $f_A > f_B$, morphological inversion is observed. These morphological changes were theorised by Liebler[22] as well as Bates *et al.*[23, 24] and Matsen *et al*.[25-27] The changes were also experimentally observed by Khandpur *et al.*[28] as shown in Figure 1.6c. The self-consistent mean-field (SCMF) theory has been used for phase behaviour predictions for bulk self-assembly of block copolymers (Figure 1.9).

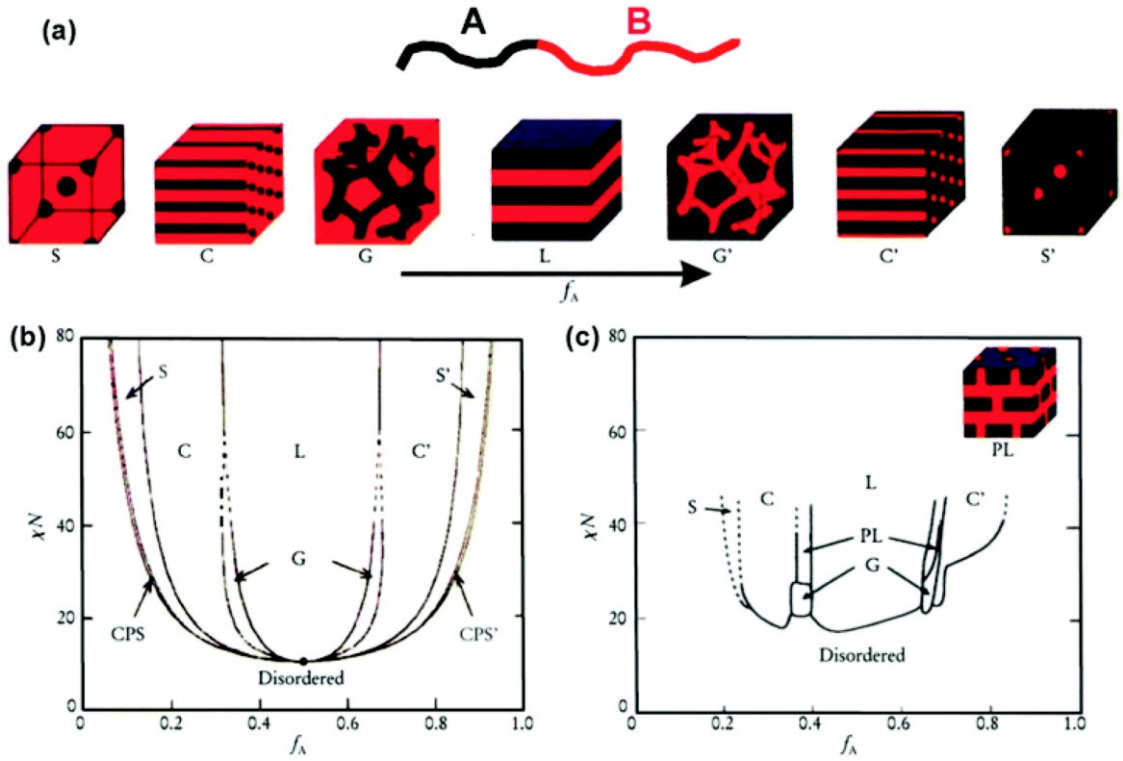

Figure 1.9. a) Illustrations of microphase-separated structures which can be observed upon bulk self-assembly of block copolymers where S and S' are body centred cubic spheres, C and C' are hexagonally packed cylinders, G and G' are bicontinuous gyroids, and L is lamellae. b) Phase diagram predicted by the self-consistent mean-field theory, where morphology is dictated by the block volume fraction (f) and the segregation parameter (χN). Closely packed spheres is denoted as CPS and CPS'. c) phase diagram for experimentally-determined polyisoprene-*block*-polystyrene block copolymers where f_A is the volume fraction of the polyisoprene block. Perforated lamellae is abbreviated to PL.[14, 16, 28]

When a solvent is introduced into the block copolymer system, self-assembly in solution becomes increasingly complex. For example, when an AB diblock copolymer is in a single solvent that is selective towards one of the blocks, there are three notable χ parameters to consider: A block-solvent interaction (χ_{AS}), B block-solvent interaction (χ_{BS}) and A block-B block interaction (χ_{AB}).

1.4.2 Polymerisation-induced self-assembly (PISA)

Self-assembly of block copolymers can be undertaken in solution. Polymerisation-induced self-assembly (PISA) has been well established as an efficient and versatile method for generating well-defined block copolymer nanoparticles. Unlike traditional solution self-assembly, which is typically conducted in dilute solutions (<1% w/w),[29] nanoparticles can be generated at high solids content (≤50% w/w)[30] when utilising PISA. Additionally, PISA eliminates the requirement for post-polymerisation processing such as thin film rehydration, and pH or solvent switching.[29] In a typical PISA synthesis, a functionalised polymer that is selective towards the chosen reaction solvent

(therefore termed the solvophilic block) is synthesised via a chosen RDRP technique. The polymer is then chain extended with a monomer that yields a solvophobic block, which induces self-assembly and gives rise to a range of different nano-objects varying in size and shape.[30] PISA can be conducted via either emulsion or dispersion polymerisation, depending on whether the monomer is immiscible or miscible with the chosen solvent, respectively.

A range of RDRP-mediated PISA formulations have been reported. Nitroxide mediated polymerisation-induced self-assembly (NMPISA) has been thoroughly investigated by Charleux and co-workers[31-36] amongst others,[34, 37-40] which typically involves the chain extension of a solvophilic (macro)alkoxyamine via the polymerisation of vinyl monomers to yield block copolymers with a solvophobic second block.[41] Additionally, atom transfer radical polymerisation (ATRP)-mediated PISA has been utilised.[42-45] However, this method is limited to its application output as a result of the requirement of a transition metal catalyst, which can introduce toxicity into the polymeric nanoparticles upon self-assembly, which is particularly unsuitable for biomedical applications.[46] On the other hand, post polymerisation processes such as dialysis can be implemented in order to combat this issue.[42]

Although it was previously not the preferred term, PISA was first developed over 20 years ago by Ferguson *et al*.[47] where a water-soluble poly(acrylic acid) macromolecular chain transfer agent (macro-CTA) was chain extended via the slow-feed emulsion polymerisation of *n*-butyl acrylate to yield micelles. Today, RAFT-PISA has arguably had the most academic interest amongst all of the RDRP-mediated PISA techniques.[48] This is due to the versatility of RAFT, where a vast range of monomer and solvent choices including water,[20, 49-51] other polar solvents,[51-55] and non-polar solvents.[29, 56-61] can be employed, as well as being highly compatible with reaction conditions.[62] This means robust and convenient protocols for developing block copolymer nanoparticles such as spheres, worms and vesicles can be readily achieved. Of particular interest, PISA has been, though not extensively, conducted in ionic liquids.[63, 64] Importantly, synthesising worm-like micelles via PISA can provide a route to fabricating soft gel materials at considerably low polymer concentrations (≥3% w/w)[65]

The typical synthesis of a block copolymer via RAFT-PISA dispersion polymerisation is shown in Figure 1.10.

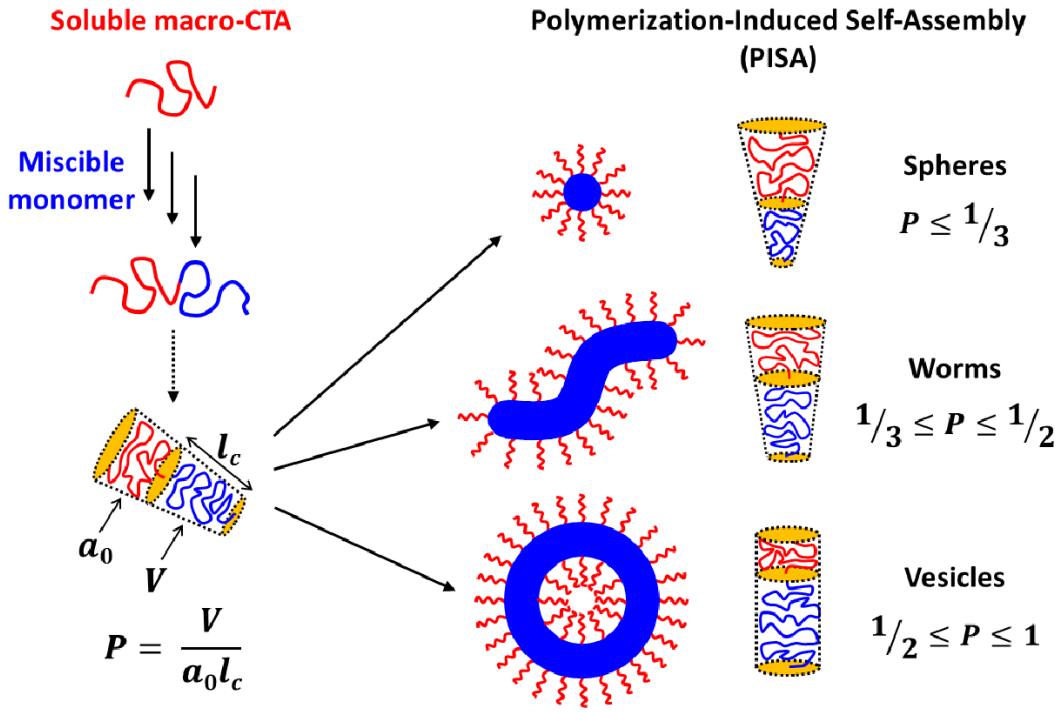

Figure 1.10. Schematic representation of RAFT-PISA under dispersion conditions, in which a solvophilic macromolecular chain transfer agent (red) is chain extended with a miscible monomer to yield an insoluble polymer block, also known as the core-forming block (blue). This can give rise to a range of morphologies such as spheres, worms and vesicles, primarily dictated by the value of the packing parameter, *P*. *P* is defined in terms of: *V*, which denotes the volume of the core-forming block; a_0, which denotes the optimal head-group area inhabited by the stabiliser block; and l_c, which denotes the length of the core-forming block.[66]

1.4.3 Synthesis of worm gels via RAFT-PISA

As previously stated, synthesising worm-like micelles can provide a convenient route to generating soft gels with low polymer concentrations. Soft gels can be formed when there are sufficient inter-worm contacts to result in physical entanglement thus inducing gelation. This interesting method can be used to develop so-called ionogels (discussed in more detail in Section 1.6) in which traditionally, copolymer concentrations are required to be relatively higher (up to 10% w/w)[67] in order to form the ionogels. The fabrication of worm gels via the synthesis of diblock copolymers has been explored for over two decades[65] for a wide range of applications such as sterilisable gels (Figure 1.11),[68] cell culture[69] drug delivery,[70, 71] and viscosity modification.[72]

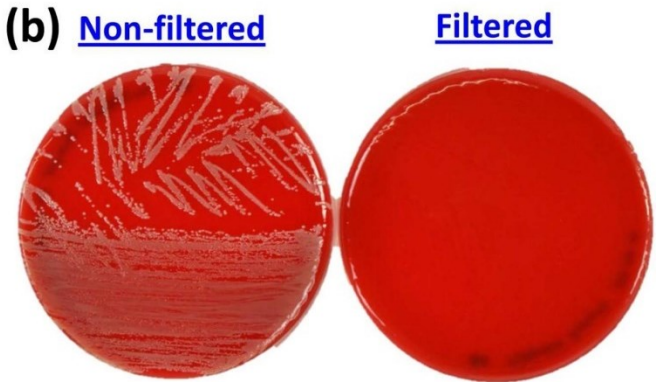

Figure 1.11. Non-filtered and ultrafiltered copolymer worm gels. The non-filtered worm gel shows substantial bacterial growth, whereas the ultrafiltered worm gel indicates complete removal of *S. aureus* bacteria.[68]

In particular, RAFT-PISA has enabled the synthesis of diblock copolymer worm gels in a wide range of media, including water,[44, 49, 68, 73, 74] polar solvents (such as lower alcohols)[75-77] and non-polar solvents (such as *n*-alkanes).[57, 59, 78] Worms typically occupy a relatively narrow phase space between spheres and vesicles, and therefore can be more challenging to obtain.[79] However, with sufficient synthetic endeavour and exploring a range of experimental parameters, the preparation of worms as well as spheres and vesicles can be achieved.

Interestingly, worm gels prepared via dispersion PISA can often display thermoresponsive behaviour, in which reversible worm-to-sphere morphological transitions can be observed upon cooling in aqueous formulations[68] (Figure 1.12), or heating in *n*-alkanes and ethanol. Armes and co-workers have comprehensively investigated these phenomena.[59, 68, 73, 80-83] For example, Blanazs *et al*.[68] reported the formation of well-defined biocompatible block copolymers that could be used as promising sterilisable gels for biomedical applications. A poly(glycerol monomethacrylate) (PGMA) macro-CTA was synthesised via RAFT solution polymerisation of glycerol monomethacrylate. The PGMA macro-CTA was then chain extended using 2-hydroxypropyl methacrylate via RAFT aqueous dispersion polymerisation, affording a poly(glycerol monomethacrylate)-*block*-poly(2-hydroxypropyl methacrylate) (PGMA-*b*-PHPMA) diblock copolymer. Free-standing soft gels were formed as a result of the presence of worm-like nanoparticles, which upon cooling to 4 °C, transitioned into spheres causing immediate degelation (Figure 1.11). Utilising this unique property, the worm gels were deliberately contaminated with dye-tagged bacteria, *S. aureus,* and subsequently ultrafiltered at 4 °C to assess the sterilisable capabilities of the worm gels.

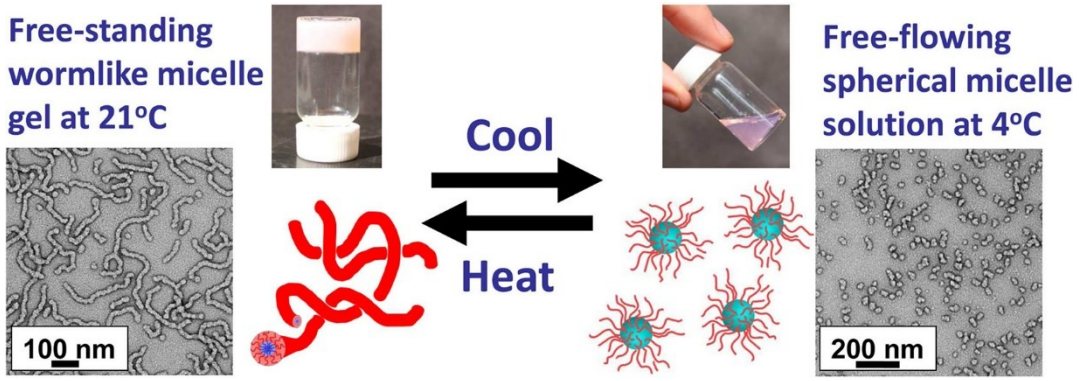

Figure 1.12. Thermoresponsive diblock copolymer nanoparticles prepared in water reported by Blanazs *et al*. where upon heating, worm-like micelles are observed, and upon cooling a free-flowing solution containing spherical nanoparticles are present, as confirmed by TEM.[68]

More recently, phosphorylcholine-based thermoresponsive worm gels were investigated for their suitability for biomedical applications. Based on prior research,[44] Beattie *et al*.[83] reported the synthesis of thermoresponsive poly(2-(methacryloyloxy)ethyl phosphorylcholine)-*block*-poly(2-hydroxypropyl methacrylate) (PMPC-*b*-PHPMA) diblock copolymer worm gels. Two PMPC precursors (actual DP = 15 and 26) were synthesised and utilised as the stabiliser block for the synthesis of the PMPC-*b*-PHPMA block copolymers via RAFT dispersion polymerisation of HPMA in water to afford worms with differing thicknesses. Block copolymers synthesised using $PMPC_{15}$ macro-CTA enabled thin worm formation that in turn enabled thermoresponsive behaviour. In contrast, using $PMPC_{26}$ macro-CTA afforded thicker worms which did not exhibit any thermoresponsive behaviour.

The length of the stabiliser block has been shown to affect the range of morphologies obtained in some formulations. In some cases, if the stabiliser block is too long, this can lead to kinetically trapped spherical morphologies. It has been reported that shortening the stabiliser block has successfully enabled the formation of worm-like morphologies. Fielding *et al*.[57] reported accessing higher order morphologies as a result of using a relatively shorter stabiliser block in the synthesis of poly(lauryl methacrylate)-*block*-poly(benzyl methacrylate) ($PLMA_x$-*b*-$PBzMA_y$) block copolymers in *n*-heptane. When chain extending $PLMA_{37}$ macro-CTA via RAFT dispersion polymerisation of benzyl methacrylate (BzMA), only spheres were generated. In contrast, chain extension using a shorter stabiliser block, a $PLMA_{17}$ macro-CTA to yield (for example) $PLMA_{17}$-*b*-$PBzMA_{63}$, anisotropic worms were observed.

On the contrary, reducing the length of the stabiliser block has also been reported to have been unsuccessful in some cases. Docherty *et al.*[84] reported the synthesis of epoxy functional block copolymers via RAFT dispersion polymerisation of glycidyl methacrylate in mineral oil to yield functionalised spheres. Two different poly(stearyl methacrylate) (PSMA) macro CTAs, $PSMA_{18}$ and $PSMA_{13}$ were chain extended with BzMA, targeting PBzMA DPs between 50-300 and 50-400 for each macro-CTA, respectively, in an effort to access higher order morphologies such as worms. Despite shortening the stabiliser block, worms could not be accessed as a result of ample steric stabilisation provided by the stabiliser block therefore preventing 1D fusion of the spheres to yield worms.[29] To combat this, the stabiliser block was shortened more, to $PSMA_9$ macro-CTA to afford access to spheres, worms and vesicles (Figure 1.13).[85]

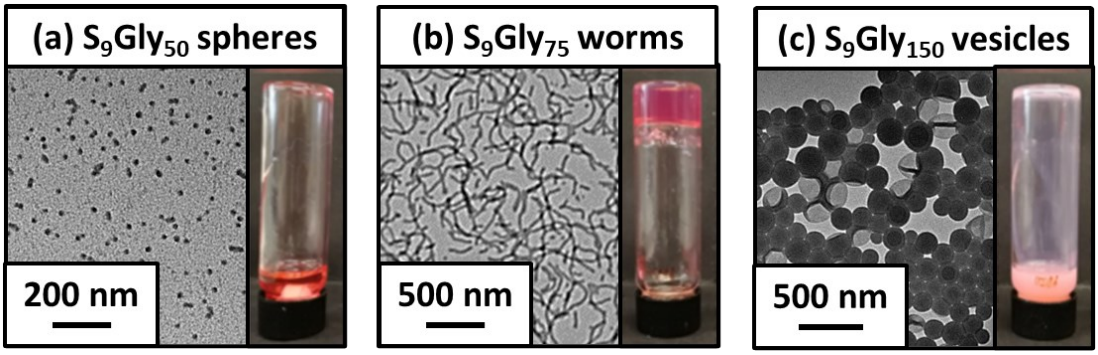

Figure 1.13. Representative TEM images of 0.10% w/w dispersions of poly(stearyl methacrylate)-block-poly(glycidyl methacrylate) ($PSMA_9$-b-$PGlyMA_y$ or S_9-Gly_y) for a) S_9-Gly_{50} (spheres), b) S_9-Gly_{75} (worms) and c)S_9-Gly_{150} (vesicles). Digital images of each dispersion is also shown to the right of each TEM image.[85]

Higher order morphologies can also be accessed by tuning the glass transition temperature (T_g) of the core-forming block. György *et al.*[86] reported the RAFT statistical copolymerisation of lauryl methacrylate (LMA) with methyl methacrylate (MMA) in mineral oil, which subsequently afforded access to spheres, worms and vesicles (Figure 1.14). Incorporating LMA into the core-forming block enabled the T_g to be lowered, therefore the growing polymer chains were more mobile than in a previous study[87] where only poly(methyl methacrylate (PMMA) was present in the core-forming block. Furthermore, the higher T_g of the PMMA block led to the formation of only kinetically trapped spheres, as a result of the PMMA block's stiffness and immobility.

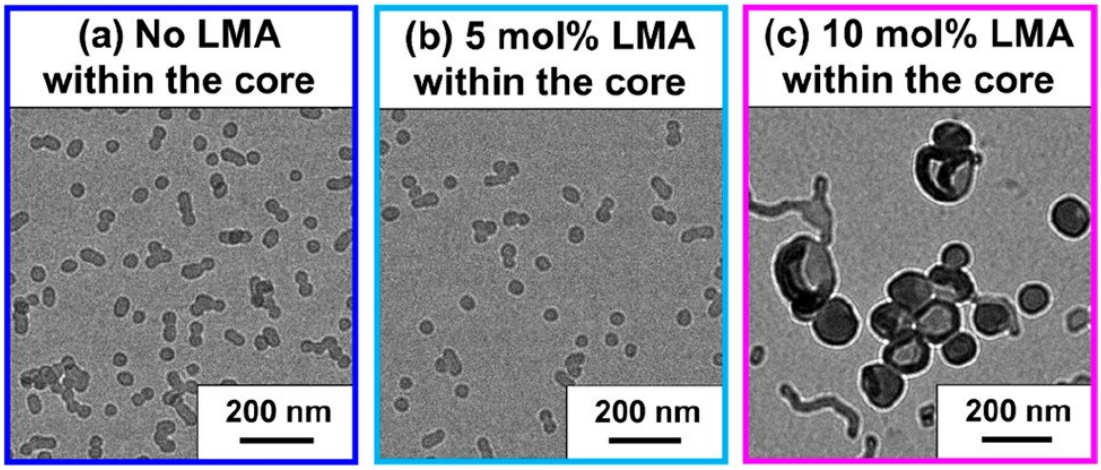

Figure 1.14. Transmission electron microscopy images obtained when targeting (a) $PLMA_{22}$–$PMMA_{200}$ (T_g of core forming block 111°C), (b) $PLMA_{22}$-b-$P(0.95MMA\text{-}stat\text{-}0.05LMA)_{200}$ (T_g = 99 °C), or (c) $PLMA_{22}$-b-$P(0.9MMA\text{-}stat\text{-}0.1LMA)_{200}$ (T_g = 82 °C).[86]

Interestingly, PISA has been conducted in an extensive range of solvents such as alcohols[52, 54, 55, 75, 88-93], non-polar[29, 56, 57, 61, 94-97] and aqueous.[49, 98-102] In addition to the previously discussed variables, the choice of solvent has also been shown to affect which morphologies can be accessed in some formulations. For example, Jones *et al.*[103] reported the synthesis of poly(*N,N*-dimethylacrylamide)-*block*-(poly(benzyl methacrylate) ($PDMA_x$-*b*-$PBzMA_y$) block copolymers via dispersion polymerisation of BzMA in ethanol and ethanol/water mixtures. By systematically increasing the proportion of water in a particular system, faster kinetics was observed. When anhydrous ethanol was used, 35% BzMA monomer conversion was reached after 300 minutes. In contrast, when water was introduced into the system at 20% w/w, 90% conversion was reached after 300 minutes. Despite leading to faster kinetics, introduction of water into the system, so that the solvent system was 80:20 w/w ethanol/water, hindered access to higher order morphologies and only kinetically trapped spheres were formed, whereas using anhydrous ethanol allowed for formation of spheres, worms and vesicles (Figure 1.15).

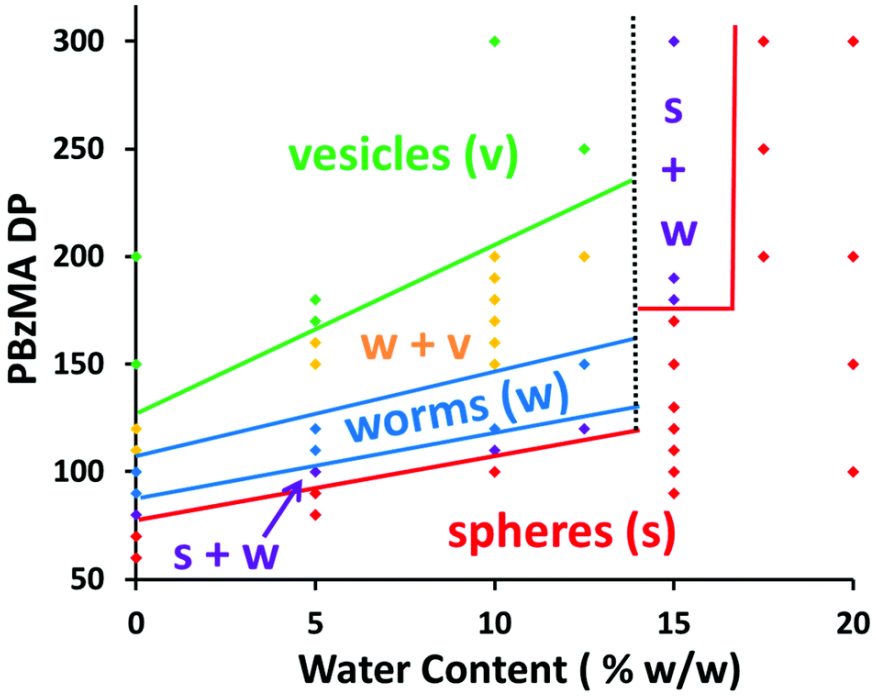

Figure 1.15. Phase diagram showing morphologies obtained for $PDMA_{43}$-b-$PBzMA_y$ diblock copolymers with respect to water content in the ethanol/water mixtures for the RAFT dispersion polymerisation of BzMA.[103]

Kang *et al*.[104] described the preparation of nucleobase-containing block copolymers via reversible addition-fragmentation chain transfer (RAFT) dispersion polymerisation of adenine-containing methacrylate or an adenine containing- and thymine-containing methacrylate mixture in both chloroform and 1,4-dioxane. When PISA was conducted in chloroform, only spherical micelles could be accessed. On the other hand, when using 1,4-dioxane, higher order morphologies such as cylinders and lamellae could be accessed as a result of improved chain mobility of the core-forming blocks. This was attributed the increased solubility of the core-forming blocks in 1,4-dioxane compared to chloroform.

Derry *et al*.[29] investigated and reported the preparation of poly(lauryl methacrylate)-*block*-poly(benzyl methacrylate) ($PLMA_x$-*b*-$PBzMA_y$) block copolymer nanoparticles in mineral oil and poly(α-olefin) (PAO) oil as the continuous phases at a range of copolymer concentrations. It was found that worm phases could be accessed in both solvents (Figure 1.16).

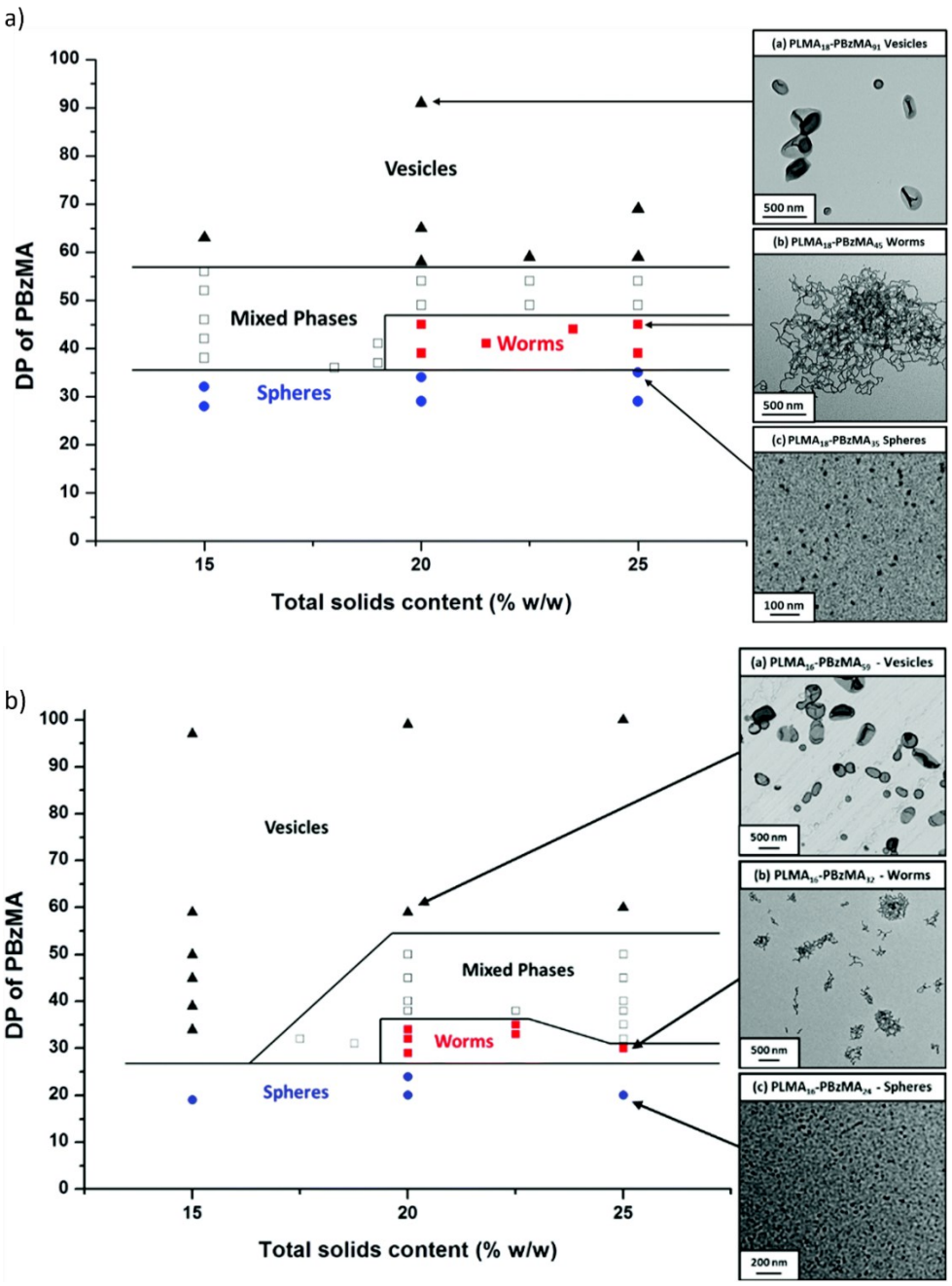

Figure 1.16. Phase diagrams constructed for a) $PLMA_{18}$-b-$PBzMA_y$ diblock nanoparticles prepared by RAFT dispersion polymerisation of BzMA in mineral oil, and b) $PLMA_{16}$-b-$PBzMA_y$ diblock copolymer nanoparticles prepared by RAFT dispersion polymerisation of benzyl methacrylate in poly(α-olefin) oil.[29]

Furthermore, pure worm phases could be observed at 20% w/w solids for $PLMA_{18}$-*b*-$PBzMA_{45}$ in mineral oil. On the other hand, the same block copolymer at this concentration in PAO yielded a mixed phase of spheres, worms and vesicles (Figure 1.17), thus emphasising the effect of solvent on the obtained block copolymer nanoparticles formed via PISA.

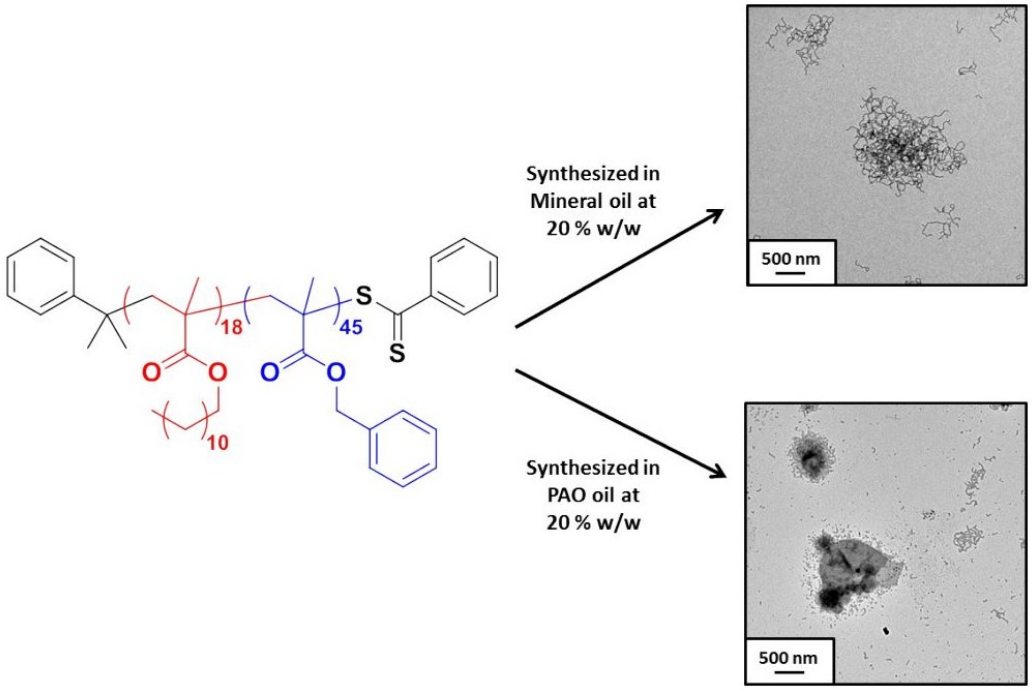

Figure 1.17.TEM images of morphologies obtained of $PLMA_{18}$-b-$PBzMA_{35}$ in mineral oil and PAO at 20% w/w solids. $PLMA_{18}$-b-$PBzMA_{35}$ block copolymers formed in mineral oil results in the formation of pure worm phases. In contrast, a mixed phase of spheres, worms and vesicles is obtained in PAO.[29]

1.5 Ionic liquids

Since their first introduction into the literature in 1914,[105] there has been extensive academic interest of ionic liquids (ILs). More specifically, there has been an emerging trend in the scientific community for utilising ILs over the past two decades.[106] This is due to their beneficial physicochemical properties, such as their high ionic conductivity and thermal stability and being practically non-volatile and non-flammable. Thus, ILs have been investigated as a more desirable alternative to conventional organic solvents in a range of applications. ILs generally constitute an anion and a cation component, of which there is an almost inexhaustible combination. As a result, ILs can be tailored towards specific applications depending on the selected combination, a characteristic that conventional organic solvents cannot offer.[107] For example, they can be tuned to offer the ability to hydrogen bond or be designed such that they are more hydrophobic or hydrophilic. However, this is not a comprehensive list. Some examples of anions and cations that are commonly used are illustrated in Figure 1.18.

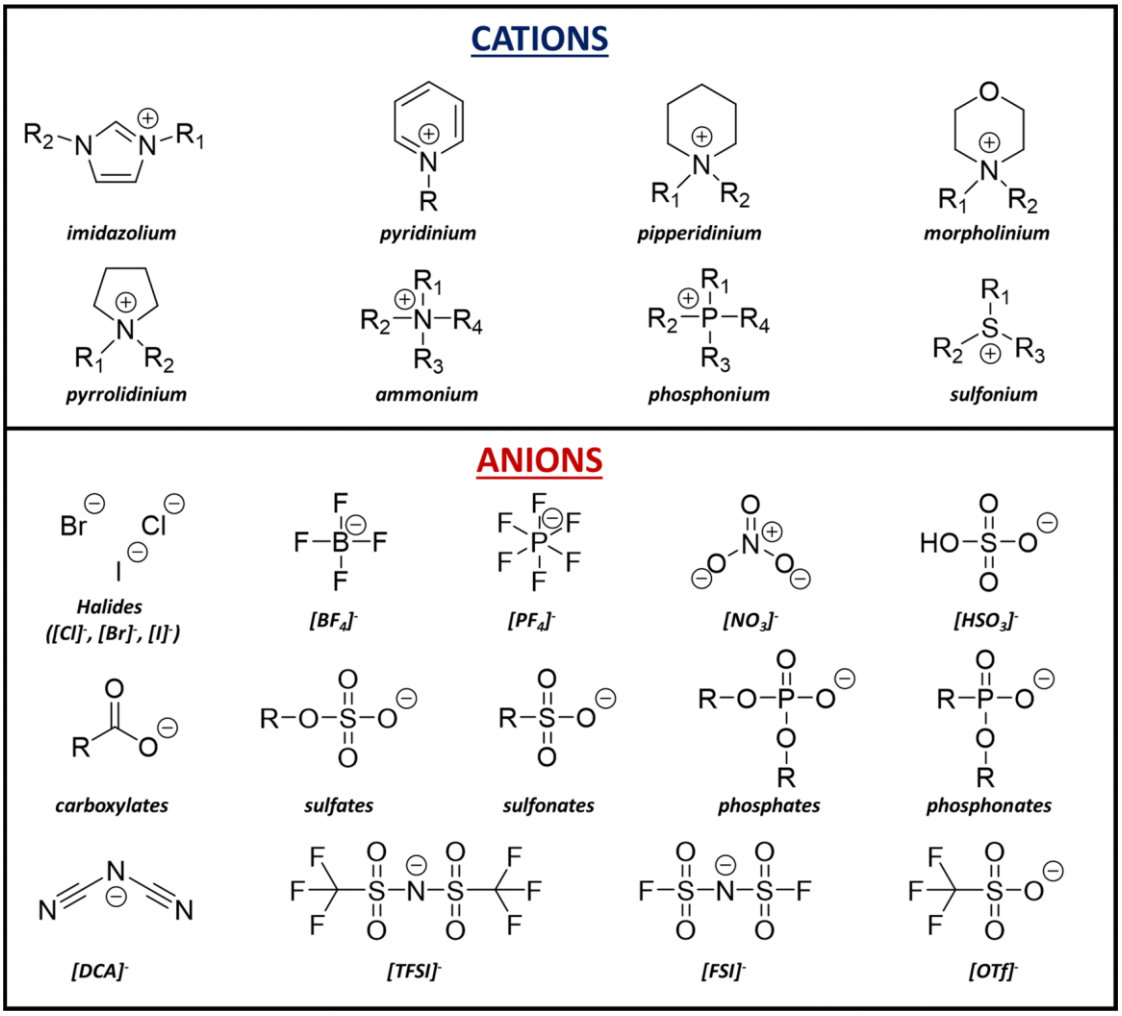

Figure 1.18. Common anions and cations that can be combined to yield ionic liquids. R = H or alkyl group[30]

Ionic liquids have substantial industrial relevance.[107] Despite being relatively more expensive to obtain than organic solvents, their ability to be readily recovered by distillation or extraction and therefore recycled means that the cost can be conveniently reduced in order to utilise them.[108-110] Interestingly, ILs have received interest in the biomedical field for applications such as drug/gene delivery,[111-114] tissue engineering,[115-117] and antimicrobial agents.[118, 119]

1.5.1 Block copolymer self-assembly in ionic liquids

Block copolymer self-assembly in ionic liquids over the past few years has been extensively reported.[120] The earliest example of this method is demonstrated by He *et al.*[121] where block copolymer micelles were prepared by the self-assembly of a range of amphiphilic poly((1,2-butadiene)-*block*-ethylene oxide) (PB-*b*-PEO) block copolymers in the hydrophobic 1-butyl-3-methylimidazolium hexafluorophosphate ([BMIM][PF_6]) at 1% w/w solids. By varying the length of the core-forming PEO block, a range of morphologies could be systematically generated,

progressing from spheres, to cylindrical micelles, to vesicles, all of which were confirmed by cryo-transmission electron microscopy (cryo-TEM) analysis. Simone *et al.*[122] also demonstrated block copolymer self-assembly in [BMIM][PF_6]. Varying in their block composition, three polystyrene-*block*-poly(methyl methacrylate) (PS-*b*-PMMA) diblock copolymers were synthesised via anionic polymerisation in tetrahydrofuran (THF) before dissolution in [BMIM][PF_6] with the aid of dichloromethane co-solvent, which was subsequently removed alongside any residual absorbed water. As a result, block copolymer micelles were yielded as confirmed by cryo-TEM and DLS, following progression from spheres to cylinders upon relatively shortening the [BMIM][PF_6]-selective PMMA block. Frozen micellar morphologies were observed, attributed to the high glass transition temperature of the PS core-forming block.

Stimuli-responsive polymers can be utilised for block copolymer self-assembly in ionic liquids to yield specifically desired morphologies.[123-129] For example, Lan *et al.*[127] reported the self-assembly of photo- and thermoresponsive diblock copolymers in ionic liquids that showed promise to be utilised as actuators. The solvent-selective block, poly(*N,N*-dimethylacrylamide) was synthesised via RAFT solution polymerisation, and subsequently chain extended via RAFT copolymerisation of 4-phenylazophenylmethacrylate (AzoMA) and *n*-butyl acrylate (*n*-BA) in 1,4-dioxane to ultimately yield a poly(*N,N*-dimethylacrylamide)-*block*-poly(4-phenylazophenylmethacrylate-*random*-butyl acrylate) (PDMA-*b*-(P(AzoMA-*r*-BA)) block copolymer, in which the P(AzoMA-*r*-BA) exhibited a lower critical solution temperature (LCST), enabling complete dissolution in the ILs at low temperatures. In two different imidazolium-based ionic liquids, the block copolymer exhibited a varied lower critical micellisation temperature (LCMT) depending on the ratio mixture of ionic liquids, and the content as well as the conformation of the azo group present in the core-forming block. This tunability enabled reversible micellisation/dissolution to occur upon exposure to either visible or ultraviolet light near room temperature (Figure 1.19).

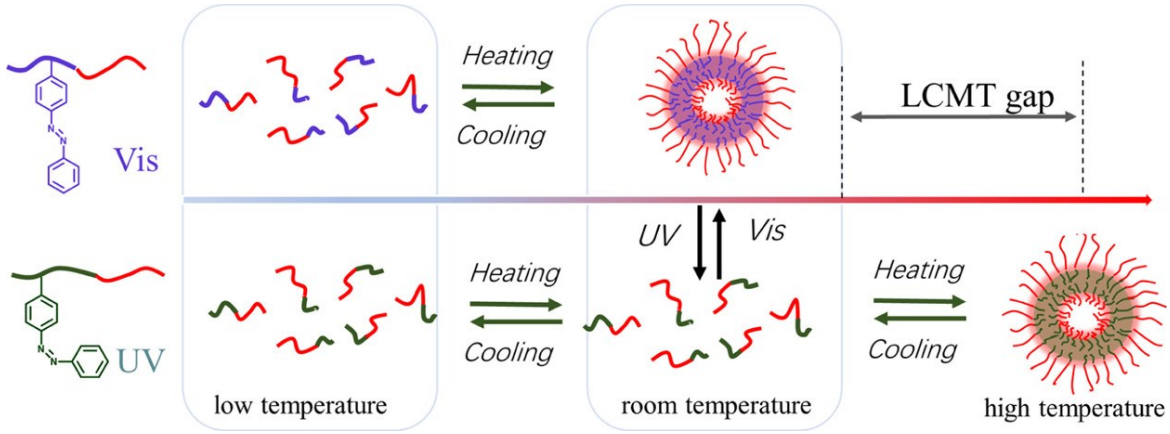

Figure 1.19. Schematic representation of reversible micellisation/dissolution at room temperature upon exposure to visible or ultraviolet light.[127]

1.5.2 RAFT-PISA in ionic liquids

Thus far, there have been very few reports of PISA being conducted in ILs. Zhang and Zhu[63] reported the synthesis of a series of diblock copolymers in a relatively hydrophobic ionic liquid, 1-butyl-3-methylimidazolium hexafluorophosphate ([BMIM][PF_6]), whereby a functionalised poly(ethylene glycol) (PEG) was chain extended using three different monomers (2-hydroxyethyl methacrylate, styrene and *n*-butyl methacrylate) via RAFT dispersion polymerisation (Figure 1.20). This seminal work demonstrates the potential for preparing dispersions of functional block copolymer nanoparticles in ILs via convenient PISA protocols, however only isotropic nanoparticles (spheres and vesicles) were successfully obtained as confirmed by transmission electron microscopy (TEM) studies.

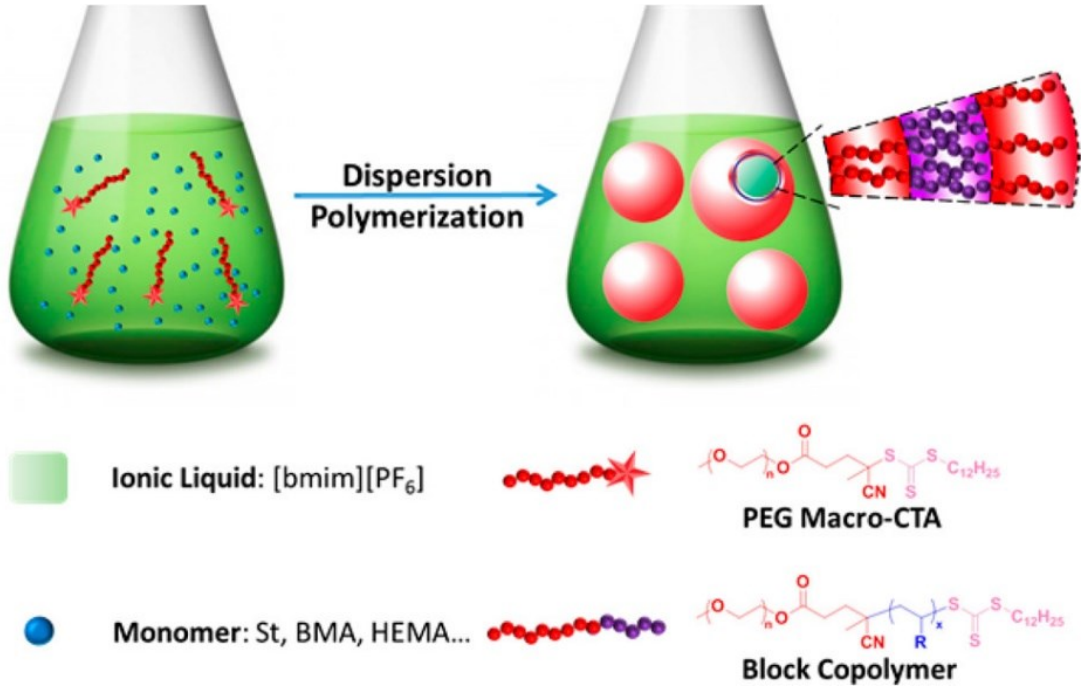

Figure 1.20. Schematic image of RAFT dispersion polymerisation of a range of monomer via polymerisation-induced self-assembly in 1-butyl-3-methylimidazolium hexafluorophosphate ([BMIM][PF_6]) to yield vesicular morphologies. Reproduced from Zhang *et al.*[63]

Similarly, Zhou *et al.*[64] also reported the preparation of spherical nanoparticles, specifically nanospheres and vesicles, by RAFT dispersion polymerisation of styrene in [BMIM][PF_6] using a PEG macro-CTA. In this study, the same block copolymer was also synthesised using an alcoholic PISA formulation in order to assess the effect of solvent choice on reaction time, determined by kinetic studies. It was concluded that block copolymer synthesis carried out in the IL was faster (monomer conversion reached 94.5% within 12 hours) than the syntheses conducted in both methanol and a methanol/water mixture where monomer conversions reached only approximately 19% and 65.7%, respectively, within 12 hours.

More recently, Yamanaka *et al.*[130] carried out *in-situ* monitoring of PISA and gelation of triblock copolymers in [BMIM][PF_6]. For the first time, the gelation process of a PHEMA-*b*-PEG-*b*-PHEMA triblock copolymer was monitored by time-resolved X-ray scattering and rheology (Figure 1.21). Gelation in this case occurred as a result of the interconnection of the spherical PHEMA domains by the PEG blocks, leading to kinetically trapped spherical morphologies. Additionally, gelation was only possible at ≥10% w/w solids concentration. Gelation was not observed at a concentration of 5% w/w as evidenced by the lack of increase in storage and loss moduli throughout the polymerisation.

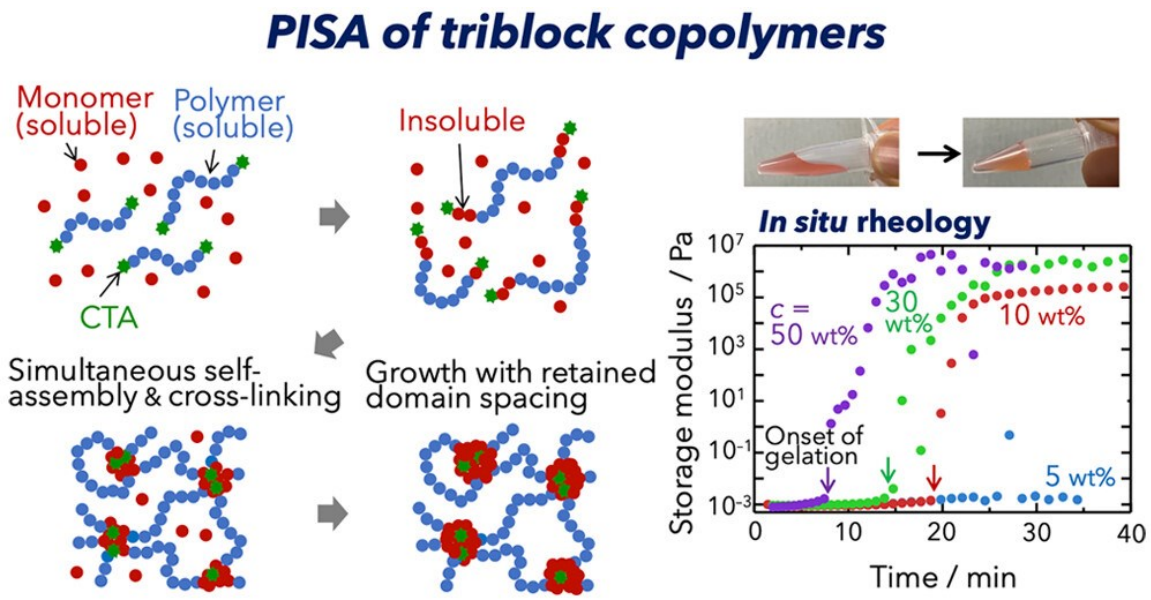

Figure 1.21. Schematic illustration of the PISA process of triblock copolymers to induce gelation monitored by time-resolved rheology.[130]

Demarteau *et al.* [131] reported the synthesis of poly(ionic liquid)-containing block copolymers via emulsion PISA yielding spherical particles with diameters ranging from 200 to 300 nm. The hydrophilic IL diallyldimethylammonium chloride (DADMAC) was functionalised using a two different macromolecular design via the interchange of xanthates (MADIX) agents via a RAFT polymerisation to form mono- and di- functional poly (diallyldimethylammonium chloride) macro-CTAs (PDADMAC). Di- and tri-block copolymers were then synthesised via RAFT emulsion polymerisation of styrene to yield polyelectrolyte latexes of spherical morphologies (Figure 1.22).

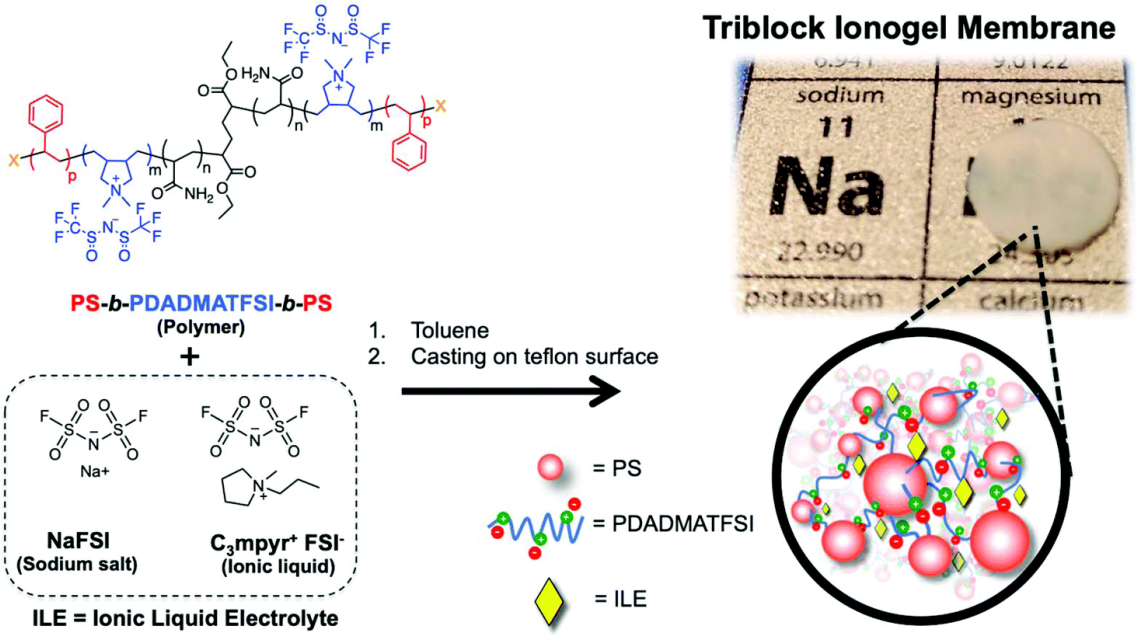

Figure 1.22. Schematic representation of the formation of ionogels by chain extending difunctional poly(dimethyldiallylammonium-bis(trifluoromethanesulfonyl)imide) (PDADMATFSI) macro-CTAs via RAFT emulsion polymerisation of styrene in water, followed by a solvent-casting process.[131]

Yang *et al.*[132] described the synthesis of poly(ionic liquid)-containing nano-objects via RAFT dispersion polymerisation of 1-butyl-3-(4-vinylbenzyl)imidazolium tetrafluoroborate ([BVBIm][BF4]) in ethanol using a PDMA macro-CTA as the stabiliser block. Interestingly, this formulation yielded spheres, worms, and vesicles as confirmed by TEM, all observed by systematically changing parameters such as the weight concentration and target DP of the poly(ionic liquid) block.

As shown from the literature reported, PISA in ILs has been somewhat overlooked. Furthermore, only spherical nanoparticles have been yielded in such formulations whereas worms have not yet been demonstrated.[63] Therefore, there is much promise to extend the scope of ionic liquid PISA formulations.

1.6 Ionogels and their electrochemical applications

Ionogels are defined as gel materials that are composed of ionic liquids immobilised in a matrix made up of organic[133] or inorganic networks[30]. Inorganic networks can be composed of, for example, SiO_2[134-136] or TiO_2[137], and can be obtained by sol-gel processing[134, 138, 139], physical crosslinking, or dispersing silica nanoparticles in to the IL.[140] Organic networks can be synthesised

by incorporating the IL in to matrices consisting of polymers or small molecules such as peptides.[30] Ionogels can also be hybridised materials, incorporating an inorganic-organic network.[140] Depending on the method of ionogel fabrication, ionogels can be characterised as physically or chemically crosslinked networks.[140] Physically crosslinked ionogels are generated as a result of non-covalent interactions such as hydrogen bonding or host-guest interactions. On the other hand, chemically crosslinked ionogel networks can be formed as a result of covalent interactions such as polymerisation or the incorporation of chemical crosslinkers.[30, 141]

Polymers are abundantly used as gelators to yield ionogels as a result of high IL encapsulation ability and their versatility.[30] The most straightforward methods reported include the swelling of a polymer in an IL[142], or mixing together the pre-synthesised polymer and IL with the aid of a cosolvent[143], which is thereafter removed to yield the ionogel.[30, 140] Other methods include *in situ* gelation using monomers or polymers where the IL is used as a solvent. This was first reported by Noda *et al.*[144] who fabricated ionogels by *in situ* radical polymerisation of 2-hydroxyethyl methacrylate in both 1-ethyl-3-methylimidazolium tetrafluoroborate ([EMIM][BF_4]) and 1-butylpyridinium tetrafluoroborate ([BPM][BF_4]) in the presence of a covalent crosslinker. The ionogels yielded had a considerably lower ionic conductivity than the ionic liquids alone. For example, the ionic conductivities of [BPM][BF_4] alone and the PHEMA/[BPM][BF_4] ionogel were measured at 30 °C to be 3 x 10^{-3} S cm^{-1} and 1 x 10^{-3} S cm^{-1}, respectively. Other ionic liquids have also been investigated for their suitability in ionogel formulations. Susan *et al.*[145] reported an ionogel formulation by the *in situ* free radical polymerisation of methyl methacrylate in 1-ethyl-3-methylimidazolium bis(trifluoromethane sulfonyl) imide ([EMIM][TFSI]) with the aid of covalent crosslinker to afford self-standing polymer films (Figure 1.23).

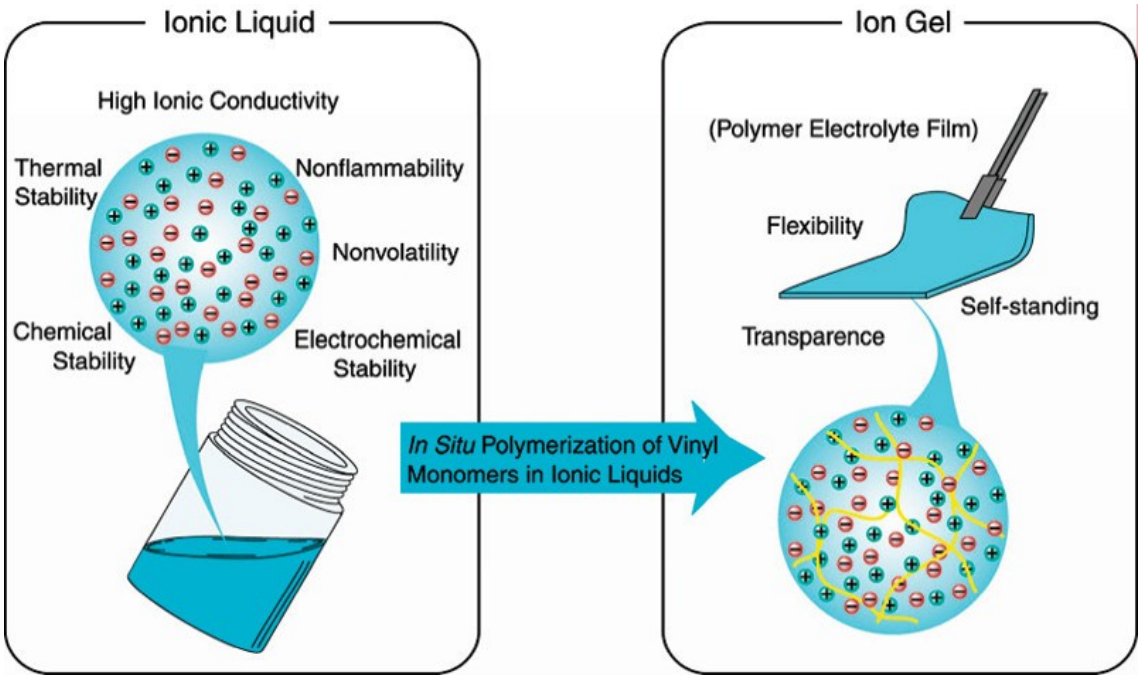

Figure 1.23. Synthesis of free-standing ionogels via *in situ* free radical polymerisation of vinyl monomers in ionic liquids. Reproduced from Susan *et al.*[145]

Self-assembly of di- and tri-block copolymers in ionic liquids is an extensively reported method for developing physically crosslinked ionogels. The earliest example of this method is demonstrated by Lodge *et al.*[67] whereby a poly(styrene-*block*-ethylene oxide-*block*-styrene) (SOS) triblock copolymer and 1-butyl-3-methylimidazolium hexafluorophosphate ([BMIM][PF_6]) was dissolved in dichloromethane at SOS concentrations of 1, 3, 4, 5, 7 and 10 wt%. The dichloromethane co-solvent was then subsequently removed from the solution by evaporation to yield the SOS/[BMIM][PF_6] polymer electrolytes. Transparent gels were generated at concentrations ≥ 5 wt% and ionic conductivity measurements indicated a moderate decline of ionic conductivity when the triblock copolymer network was present, compared to the bulk ionic liquid. Interestingly, ionogels can be generated by utilising thermoresponsive block copolymers that are capable of undergoing gel-liquid phase transitions in responsive to thermal stimulus.[146-148] For example, He *et al.*[147] reported the preparation of a thermoresponsive triblock copolymer, poly(*N*-isopropyl acrylamide-*block*-ethylene oxide-*block*-*N*-isopropyl acrylamide) (PNIPAm-*b*-PEO-*b*-PNIPAm). This block copolymer was dissolved in 1-ethyl-3-methylimidazolium bis(trifluoromethylsulfonyl)imide ([EMIM][TFSI]) at room temperature affording a viscous liquid. Upon further cooling, a transparent ionogel was formed, thermoreversible behaviour was observed during heating-cooling cycles. Temperature-dependant rheological studies of ionogels demonstrated good mechanical strength at 5 °C, which decreased with respect to increased temperature. Furthermore, transition from gel

to solution was determined as 20 °C, which agreed with previously reported temperatures of phase separation of PNIPAM-based ionogels in [EMIM][TFSI].[149]

Ionogels can also be generated by use of poly(ionic liquids) (PILs). Using PILs incorporates the desirable properties offered by the polymer network as well as the ionic liquid, so that the ionogel exhibits preferable ionic conductivity as well as mechanical strength. As a result of their durability and the structural versatility of the ILs, PILs have received considerable interest in a range of interesting applications such as biomedicine,[150, 151] catalysis and a range of energy storage applications.[152-156] With regards to electronic applications, creating ionogels using PILs can reduce the risk of leakage of ILs, as a result of strong electrostatic attractions between the PIL networks and the IL.[157] Two strategies for the preparation of PILS have been reported: i) the direct polymerisation of IL monomers via free-radical or RDRP for example; and ii) functionalisation of non-ionic polymers via post polymerisation processes.[30]

Another typical method for the preparation of ionogels is by use of small molecule gelators.[30, 158-160] The process of fabricating ionogels using this method entails adding the small molecule gelator (for example, small amides, ionic molecules etc.) into an IL at higher temperatures. Upon cooling, supramolecular bonding of the gelators via weak interactions such as hydrogen bonding and π-π interactions enable physical gelation, affording the ionogel. Only a small concentration of gelators are required (≤1% w/w) in order to fabricate an ionogel, thus the ionic conductivity provided by the IL is minimally compromised. However, the gelators offer poor mechanical integrity, therefore the gels formed are limited in their application. For example, they can be used for application in flexible electronics.[161] As previously stated, inorganic matrices can also be used as host networks for the preparation of ionogels. SiO_2- and TiO_2-based ionogels made via this method have attracted interest in applications such as lithium ion batteries[162]

In recent years, so-called ionogels have attracted considerable interest due to their advantageous properties in a range of applications as well as the various fabrication methods. Interestingly, new ionogels have been formulated for use in biomedical applications such as drug delivery[163-165] and wound healing[166-168], owing to their self-healing and anti-bacterial properties.[30, 169]

Dye-sensitised solar cells (DSSCs) (Figure 1.24) are an excellent example of ionogel utilisation.[107, 155, 170-173] DSSCs comprise a semiconducting IL-based electrolyte, dye-sensitised titanium dioxide (TiO_2) for harvesting light, dye to boost the cell's sensitivity to visible light, and a platinum cathode.[108]

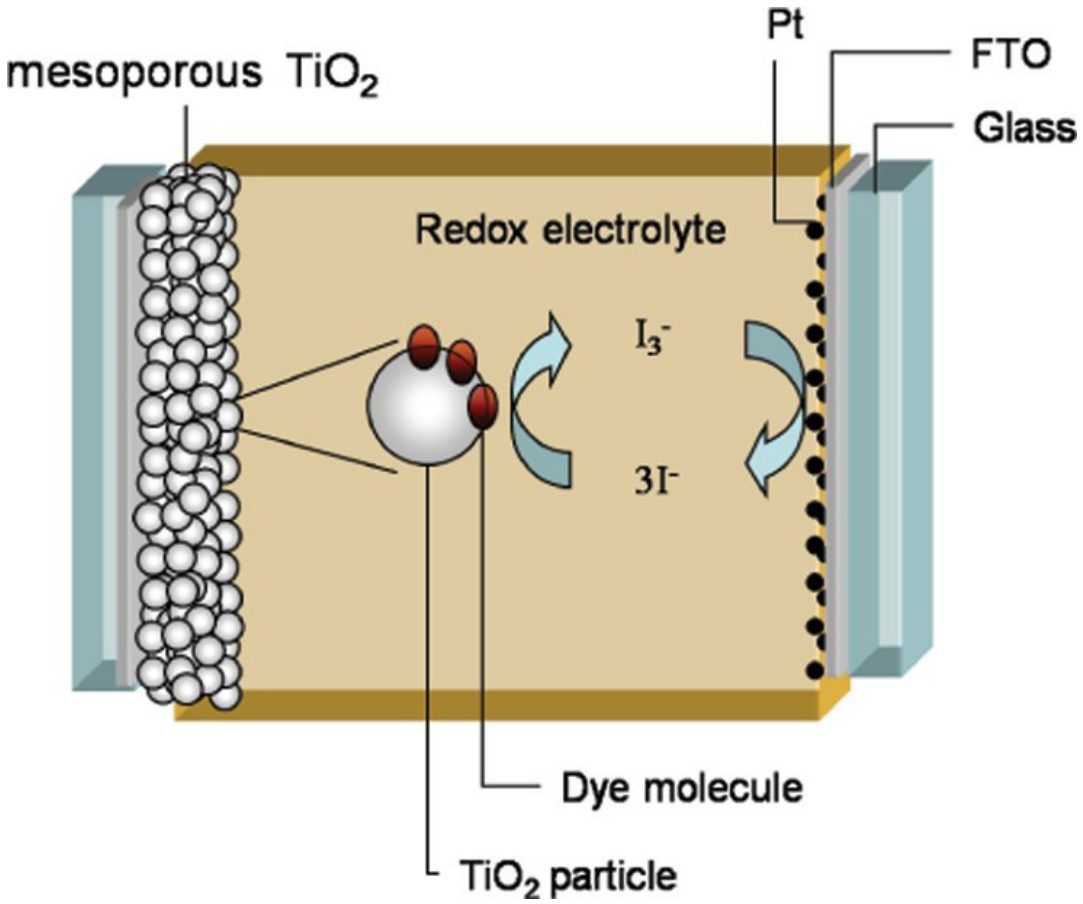

Figure 1.24. Schematic representation of a dye-sensitised solar cell (DSSC).[173] FTO denotes fluorine-doped tin oxide, which coats glass. This acts as a substrate for the deposition of mesoporous TiO_2.

Yoon *et al.*[174] reported a new ionogel formulation for DSSC applications, by incorporating a triblock copolymer, poly(styrene-block-ethylene oxide-block-styrene) (SEOS) into 1-propyl-3-methylimidazolium iodide (PMII), an IL that has been previously used in such applications owing to its high ionic conductivity. Polymer concentration was only required up to 5% w/w to induce gelation, therefore maximising the ionic conductivity of the materials whilst being provided with mechanical integrity. The incorporation of the quasi-solid ionogel enabled the DSSC to maintain an efficiency of 92% under 1440 hours of operation as opposed to a DSSC with solely an ionic liquid electrolyte that had an efficiency of 78%.

Similarly, Zhang *et al.*[175] also utilised PMII as a solvent to generate ionogels for DSSC application. The ionogel was fabricated by encapsulating bis-imidazolium ionic liquid (Bis-C_{12}(mim)Br) into β-Cyclodextrin (β-CD) prior to mixing with PMII to yield the supramolecular ionogel. The ionogel demonstrated long term stability as confirmed by an accelerating aging test of sealed devices. In

comparison to an IL electrolyte, the ionogel showed better long term stability as a result of the gel network preventing leakage in the DSSC device.

More recently, Syairah *et al.*[176] described the fabrication of ionogels containing iodine, sodium iodide, poly(ethylene oxide), and ethylene and propylene carbonate for DSSC applications. Each ionogel also contained one of the following ionic liquids: 1-butyl-3-methylimidazole (BMII), 1-hexyl-3-methylimidazole (HMII), and 1-methyl-3-propylimidazolium iodide (MPII). The gel containing MPII showed superior ionic conductivity (9.41 mS cm^{-1}) relative to the other gels containing BMII and HMII with ionic conductivities of 8.48 and 7.73 mS cm^{-1}, respectively. This is as a result of the structure of the ionic liquids. As the alkyl group chain length decreases, the viscosity decreases thus enhancing the mobility of the ions within the electrolyte.

Interestingly, ionogels for DSSCs have also been formulated from poly(ionic liquids). For example, Zhao *et al.*[153] reported the preparation of organic solvent-free gel electrolytes from the synthesis of poly(1-butyl-3-vinylimidazolium bromide) ([PBVIm][Br]) and poly(1-butyl-3-vinylimidazolium bis(trifluoromethanesulfonyl)imide) ([PBVIm][TFSI]) followed by dissolution in a liquid electrolyte. In particular, it was found that the [PBVIm][TFSI]-containing gel electrolyte showcased superior long-term stability when compared to the native liquid electrolyte as confirmed by photon-to-current conversion efficiency plots. Additionally, leakage was not an observed issue for the gel electrolytes.

1.7 Thesis outline and aims

The overarching objective of this research is to generate so-called ionogels by an *in situ* method to eliminate the requirement for co-solvent or crosslinking agents, as well as removing the necessity for any post-polymerisation processing. This is achieved by using a previously well-established self-assembly technique called polymerisation-induced self-assembly to generate worm-like morphologies that, providing there is sufficient physical worm entanglement, enables the formation of free-standing gels. In order to achieve this, the block copolymer that is synthesised during this process needs to be appropriately designed such that one block is IL-philic (i.e. the stabiliser block), and the other block is IL-phobic (i.e. the core-forming block). Importantly, this can enable the formation of soft gels at polymer concentrations of <4% w/w despite the use of no additional agents to induce gelation. This preparation method can allow the electrochemical properties that the ionic liquid provides to be maximised, yet maintaining mechanical integrity attributed to the polymer content.

The synthesis and solubility screenings of a range of polymers in commercially available [EMIM][DCA] and [EMIM]$EtOSO_3$] acquired from BASF in order to aid in designing subsequent block copolymers is described in Chapter 2. Chapter 3 describes the synthesis of poly(2-hydroxyethyl methacrylate)-*block*-poly(benzyl methacrylate) (PHEMA-*b*-PBzMA) diblock copolymer spheres, worms or vesicles in [EMIM][DCA] at 15% w/w solids. Confirmation of morphologies in select samples Is determined using DLS, SAXS and TEM. Importantly, critical gel concentration (CGC) screenings are conducted for $PHEMA_{30}$-*b*-$PBzMA_{291}$ which contained the highest proportion of worm like morphologies as confirmed by SAXS. CGC screenings are carried out to determine the lowest concentration at which freestanding gels can still be generated. The characterisation of worm gels is discussed in Chapter 4, in particular the rheological, electrochemical and thermal characteristics are studied. This study shows that comparable desirable properties are observed in the worm gels, and furthermore how negligible the effects of the polymer network present in the gel have on the benefits that the ionic liquid provide. These studies alongside the syntheses described in Chapter 3 showcase the promise of the convenient and facile synthesis route to generating ionogels with desirable properties for electrochemical applications. Chapter 5 describes a new formulation for generating spherical nanoparticles including spheres and vesicles via polymerisation-induced self-assembly in an additional ionic liquid to that of [EMIM][DCA], which is used in Chapter 3. More specifically, [EMIM][$EtOSO_3$] is used as the solvent for RAFT dispersion polymerisation of benzyl methacrylate. The syntheses of the block copolymers in [EMIM][DCA] in Chapter 3, compared to syntheses in [EMIM][$EtOSO_3$] is also explored in terms of kinetic insights as well as differences in morphologies. The concluding remarks and future work suggestions are provided in Chapter 6.

1.8 References

1. J. M. G. Cowie and V. Arrighi, *Polymers: chemistry and physics of modern materials*, CRC Press, Boca Raton, 3rd edn., 2007.
2. T. Lodge and P. C. Hiemenz, *Polymer chemistry*, CRC Press, Boca Raton, Florida, 3rd edn., 2020.
3. A. Lambert, *Br. Polym. J.*, 1971, **3**, 13-23.
4. S. E. Harding, D. B. Sattelle and V. A. Bloomfield, *Laser light scattering in biochemistry*, The Royal Society of Chemistry, Cambridge, 1992.
5. J. W. Goodwin and R. W. Hughes, *Rheology for Chemists : An Introduction*, Royal Society of Chemistry, Cambridge, 2008.
6. H. A. Barnes, *A Handbook of Elementary Rheology*, University of Wales Institute of Non-Newtonian Fluid Mechanics, Aberystwyth, 2000.
7. A. C. Lazanas and M. I. Prodromidis, *ACS Meas. Sci. Au*, 2023, **3**, 162-193.
8. N. Gil-González, T. Akyazi, E. Castaño, F. Benito-Lopez and M. C. Morant-Miñana, *Sens. Actuators B: Chem*, 2018, **260**, 380-387.

9. Q. Xiao, C. Deng, Q. Wang, Q. Zhang, Y. Yue and S. Ren, *ACS Omega*, 2019, **4**, 95-103.
10. S. Perrier, *Macromolecules*, 2017, **50**, 7433-7447.
11. N. Corrigan, K. Jung, G. Moad, C. J. Hawker, K. Matyjaszewski and C. Boyer, *Prog. Polym. Sci*, 2020, **111**, 101311.
12. V. A. Bobrin, J. Zhang, N. Corrigan and C. Boyer, *Adv. Mater. Technol*, 2023, **8**, 2201054.
13. G. Moad, E. Rizzardo and S. H. Thang, *Acc. Chem. Res*, 2008, **41**, 1133-1142.
14. Y. Mai and A. Eisenberg, *Chem. Soc. Rev*, 2012, **41**, 5969-5985.
15. H. Feng, X. Lu, W. Wang, N.-G. Kang and J. W. Mays, *Polymers*, 2017, **9**, 494.
16. R. Tamate, K. Hashimoto, T. Ueki and M. Watanabe, *Phys. Chem. Chem. Phys*, 2018, **20**, 25123-25139.
17. J. Chiefari, Y. K. Chong, F. Ercole, J. Krstina, J. Jeffery, T. P. T. Le, R. T. A. Mayadunne, G. F. Meijs, C. L. Moad, G. Moad, E. Rizzardo and S. H. Thang, *Macromolecules*, 1998, **31**, 5559-5562.
18. D. J. Keddie, G. Moad, E. Rizzardo and S. H. Thang, *Macromolecules*, 2012, **45**, 5321-5342.
19. C. L. McCormick, B. S. Sumerlin, B. S. Lokitz and J. E. Stempka, *Soft Matter*, 2008, **4**, 1760-1773.
20. N. J. Warren and S. P. Armes, *J. Am. Chem. Soc*, 2014, **136**, 10174-10185.
21. D. J. Keddie, *Chem. Soc. Rev*, 2014, **43**, 496-505.
22. L. Leibler, *Macromolecules*, 1980, **13**, 1602-1617.
23. F. S. Bates and G. H. Fredrickson, *Phys. Today*, 1999, **52**, 32-38.
24. F. S. Bates and G. H. Fredrickson, *Annu. Rev. Phys. Chem*, 1990, **41**, 525-557.
25. M. W. Matsen and M. Schick, *Phys. Rev. Lett*, 1994, **72**, 2660-2663.
26. M. W. Matsen and M. Schick, *Macromolecules*, 1994, **27**, 6761-6767.
27. M. W. Matsen and F. S. Bates, *Macromolecules*, 1996, **29**, 1091-1098.
28. A. K. Khandpur, S. Foerster, F. S. Bates, I. W. Hamley, A. J. Ryan, W. Bras, K. Almdal and K. Mortensen, *Macromolecules*, 1995, **28**, 8796-8806.
29. M. J. Derry, L. A. Fielding and S. P. Armes, *Polym. Chem*, 2015, **6**, 3054-3062.
30. X. Fan, S. Liu, Z. Jia, J. J. Koh, J. C. C. Yeo, C.-G. Wang, N. E. Surat'man, X. J. Loh, J. Le Bideau, C. He, Z. Li and T.-P. Loh, *Chem. Soc. Rev*, 2023, **52**, 2497-2527.
31. G. Delaittre, J. Nicolas, C. Lefay, M. Save and B. Charleux, *Chem. Commun*, 2005, 614-616.
32. G. Delaittre, C. Dire, J. Rieger, J.-L. Putaux and B. Charleux, *Chem. Commun*, 2009, 2887-2889.
33. X. G. Qiao, M. Lansalot, E. Bourgeat-Lami and B. Charleux, *Macromolecules*, 2013, **46**, 4285-4295.
34. X. G. Qiao, O. Lambert, J. C. Taveau, P. Y. Dugas, B. Charleux, M. Lansalot and E. Bourgeat-Lami, *Macromolecules*, 2017, **50**, 3796-3806.
35. S. Brusseau, J. Belleney, S. Magnet, L. Couvreur and B. Charleux, *Polym. Chem*, 2010, **1**, 720-729.
36. G. Delaittre, M. Save and B. Charleux, *Macromol. Rapid Commun*, 2007, **28**, 1528-1533.
37. E. Yoshida, *J. Dispers. Sci. Technol*, 2020, **41**, 763-770.
38. E. Yoshida, *J. Polym. Res*, 2018, **25**, 109.
39. A. Darabi, A. R. Shirin-Abadi, J. Pinaud, P. G. Jessop and M. F. Cunningham, *Polym. Chem*, 2014, **5**, 6163-6170.
40. D. Keller, A. Beloqui, M. Martínez-Martínez, M. Ferrer and G. Delaittre, *Biomacromolecules*, 2017, **18**, 2777-2788.
41. J. Nicolas, Y. Guillaneuf, C. Lefay, D. Bertin, D. Gigmes and B. Charleux, *Prog. Polym. Sci*, 2013, **38**, 63-235.

42. S. Sugihara, K. Sugihara, S. P. Armes, H. Ahmad and A. L. Lewis, *Macromolecules*, 2010, **43**, 6321-6329.
43. W.-M. Wan and C.-Y. Pan, *Macromolecules*, 2007, **40**, 8897-8905.
44. S. Sugihara, A. Blanazs, S. P. Armes, A. J. Ryan and A. L. Lewis, *J. Am. Chem. Soc*, 2011, **133**, 15707-15713.
45. G. Wang, M. Schmitt, Z. Wang, B. Lee, X. Pan, L. Fu, J. Yan, S. Li, G. Xie, M. R. Bockstaller and K. Matyjaszewski, *Macromolecules*, 2016, **49**, 8605-8615.
46. X. Zhao, C. Sun, F. Xiong, T. Wang, S. Li, F. Huo and X. Yao, *Research*, **6**, 0113.
47. C. J. Ferguson, R. J. Hughes, B. T. T. Pham, B. S. Hawkett, R. G. Gilbert, A. K. Serelis and C. H. Such, *Macromolecules*, 2002, **35**, 9243-9245.
48. N. J. W. Penfold, J. Yeow, C. Boyer and S. P. Armes, *ACS Macro Lett*, 2019, **8**, 1029-1054.
49. S. Boissé, J. Rieger, K. Belal, A. Di-Cicco, P. Beaunier, M.-H. Li and B. Charleux, *Chem. Commun*, 2010, **46**, 1950-1952.
50. S. J. Hunter, N. J. W. Penfold, E. R. Jones, T. Zinn, O. O. Mykhaylyk and S. P. Armes, *Macromolecules*, 2022, **55**, 3051-3062.
51. Y. Li and S. P. Armes, *Angew. Chem. Int. Ed*, 2010, **49**, 4042-4046.
52. M. Semsarilar, N. J. W. Penfold, E. R. Jones and S. P. Armes, *Polym. Chem*, 2015, **6**, 1751-1757.
53. J. Zhou, W. Zhang, C. Hong and C. Pan, *Polym. Chem*, 2016, **7**, 3259-3267.
54. W. Zhao, G. Gody, S. Dong, P. B. Zetterlund and S. Perrier, *Polym. Chem*, 2014, **5**, 6990-7003.
55. G. Desnos, A. Rubio, C. Gomri, M. Gravelle, V. Ladmiral and M. Semsarilar, *Polymers*, 2021, **13**, 2502.
56. L. P. D. Ratcliffe, B. E. McKenzie, G. M. D. Le Bouëdec, C. N. Williams, S. L. Brown and S. P. Armes, *Macromolecules*, 2015, **48**, 8594-8607.
57. L. A. Fielding, M. J. Derry, V. Ladmiral, J. Rosselgong, A. M. Rodrigues, L. P. D. Ratcliffe, S. Sugihara and S. P. Armes, *Chem. Sci*, 2013, **4**, 2081-2087.
58. M. J. Derry, L. A. Fielding, N. J. Warren, C. J. Mable, A. J. Smith, O. O. Mykhaylyk and S. P. Armes, *Chem. Sci*, 2016, **7**, 5078-5090.
59. L. A. Fielding, J. A. Lane, M. J. Derry, O. O. Mykhaylyk and S. P. Armes, *J. Am. Chem. Soc*, 2014, **136**, 5790-5798.
60. A. P. Lopez-Oliva, N. J. Warren, A. Rajkumar, O. O. Mykhaylyk, M. J. Derry, K. E. B. Doncom, M. J. Rymaruk and S. P. Armes, *Macromolecules*, 2015, **48**, 3547-3555.
61. L. Houillot, C. Bui, M. Save, B. Charleux, C. Farcet, C. Moire, J.-A. Raust and I. Rodriguez, *Macromolecules*, 2007, **40**, 6500-6509.
62. J. Wan, B. Fan and S. H. Thang, *Chem. Sci*, 2022, **13**, 4192-4224.
63. Q. Zhang and S. Zhu, *ACS Macro Lett.*, 2015, **4**, 755-758.
64. H. Zhou, C. Liu, C. Gao, Y. Qu, K. Shi and W. Zhang, *J. Polym. Sci. Part A: Polym Chem*, 2016, **54**, 1517-1525.
65. J. R. Lovett, M. J. Derry, P. Yang, F. L. Hatton, N. J. Warren, Patrick W. Fowler and S. P. Armes, *Chem. Sci*, 2018, **9**, 7138-7144.
66. M. J. Derry, L. A. Fielding and S. P. Armes, *Prog. Polym. Sci*, 2016, **52**, 1-18.
67. Y. He, P. G. Boswell, P. Bühlmann and T. P. Lodge, *J. Phys. Chem. B*, 2007, **111**, 4645-4652.
68. A. Blanazs, R. Verber, O. O. Mykhaylyk, A. J. Ryan, J. Z. Heath, C. W. I. Douglas and S. P. Armes, *J. Am. Chem. Soc*, 2012, **134**, 9741-9748.
69. M. Sponchioni, C. T. O'Brien, C. Borchers, E. Wang, M. N. Rivolta, N. J. W. Penfold, I. Canton and S. P. Armes, *Chem. Sci*, 2020, **11**, 232-240.

70. Y. Kim, D. A. Dalhaimer P Fau - Christian, D. E. Christian Da Fau - Discher and D. E. Discher, *Nanotechnology*, 2005, **16**, 484-489.
71. B. Karagoz, L. Esser, H. T. Duong, J. S. Basuki, C. Boyer and T. P. Davis, *Polym. Chem*, 2014, **5**, 350-355.
72. M. J. Derry, O. O. Mykhaylyk and S. P. Armes, *Angew. Chem. Int. Ed*, 2017, **56**, 1746-1750.
73. R. Verber, A. Blanazs and S. P. Armes, *Soft Matter*, 2012, **8**, 9915-9922.
74. A. Blanazs, A. J. Ryan and S. P. Armes, *Macromolecules*, 2012, **45**, 5099-5107.
75. Y. Pei and A. B. Lowe, *Polym. Chem*, 2014, **5**, 2342-2351.
76. Y. Pei, N. C. Dharsana, J. A. van Hensbergen, R. P. Burford, P. J. Roth and A. B. Lowe, *Soft Matter*, 2014, **10**, 5787-5796.
77. M. Semsarilar, E. R. Jones, A. Blanazs and S. P. Armes, *Adv. Mater*, 2012, **24**, 3378-3382.
78. E. Raphael, M. J. Derry, M. Hippler and S. P. Armes, *Chem. Sci*, 2021, **12**, 12082-12091.
79. F. L. Hatton, M. J. Derry and S. P. Armes, *Polym. Chem*, 2020, **11**, 6343-6355.
80. S. J. Byard, C. T. O'Brien, M. J. Derry, M. Williams, O. O. Mykhaylyk, A. Blanazs and S. P. Armes, *Chem. Sci*, 2020, **11**, 396-402.
81. S. J. Hunter and S. P. Armes, *J. Colloid. Interface. Sci*, 2023, **634**, 906-920.
82. J. M. Cumming, O. J. Deane and S. P. Armes, *Macromolecules*, 2022, **55**, 788-798.
83. D. L. Beattie, O. O. Mykhaylyk, A. J. Ryan and S. P. Armes, *Soft Matter*, 2021, **17**, 5602-5612.
84. P. J. Docherty, M. J. Derry and S. P. Armes, *Polym. Chem*, 2019, **10**, 603-611.
85. P. J. Docherty, C. Girou, M. J. Derry and S. P. Armes, *Polym. Chem*, 2020, **11**, 3332-3339.
86. C. György, T. J. Neal, T. Smith, D. J. Growney and S. P. Armes, *Macromolecules*, 2022, **55**, 4091-4101.
87. C. György, C. Verity, T. J. Neal, M. J. Rymaruk, E. J. Cornel, T. Smith, D. J. Growney and S. P. Armes, *Macromolecules*, 2021, **54**, 9496-9509.
88. C.-Q. Huang and C.-Y. Pan, *Polymer*, 2010, **51**, 5115-5121.
89. W. Cai, W. Wan, C. Hong, C. Huang and C. Pan, *Soft Matter*, 2010, **6**, 5554-5561.
90. S. Dong, W. Zhao, F. P. Lucien, S. Perrier and P. B. Zetterlund, *Polym. Chem*, 2015, **6**, 2249-2254.
91. W.-M. Wan and C.-Y. Pan, *Polym. Chem*, 2010, **1**, 1475-1484.
92. B. Karagoz, C. Boyer and T. P. Davis, *Macromol. Rapid Commun*, 2014, **35**, 417-421.
93. C. Gonzato, M. Semsarilar, E. R. Jones, F. Li, G. J. P. Krooshof, P. Wyman, O. O. Mykhaylyk, R. Tuinier and S. P. Armes, *J. Am. Chem. Soc*, 2014, **136**, 11100-11106.
94. S. Sahoo, Y. D. Gordievskaya, K. Bauri, A. A. Gavrilov, E. Y. Kramarenko and P. De, *Macromolecules*, 2022, **55**, 1139-1152.
95. L. Houillot, C. Bui, C. Farcet, C. Moire, J.-A. Raust, H. Pasch, M. Save and B. Charleux, *ACS Appl. Mater. Interfaces*, 2010, **2**, 434-442.
96. R. R. Gibson, A. Fernyhough, O. M. Musa and S. P. Armes, *Polym. Chem*, 2021, **12**, 2165-2174.
97. C. György, S. J. Hunter, C. Girou, M. J. Derry and S. P. Armes, *Polym. Chem*, 2020, **11**, 4579-4590.
98. J. Rieger, C. Grazon, B. Charleux, D. Alaimo and C. Jérôme, *J. Polym. Sci. A. Polym. Chem*, 2009, **47**, 2373-2390.
99. A. Blanazs, J. Madsen, G. Battaglia, A. J. Ryan and S. P. Armes, *J. Am. Chem. Soc*, 2011, **133**, 16581-16587.
100. G. Liu, Q. Qiu, W. Shen and Z. An, *Macromolecules*, 2011, **44**, 5237-5245.

101. C. A. Figg, A. Simula, K. A. Gebre, B. S. Tucker, D. M. Haddleton and B. S. Sumerlin, *Chem. Sci*, 2015, **6**, 1230-1236.
102. I. Chaduc, W. Zhang, J. Rieger, M. Lansalot, F. D'Agosto and B. Charleux, *Macromol. Rapid Commun*, 2011, **32**, 1270-1276.
103. E. R. Jones, M. Semsarilar, P. Wyman, M. Boerakker and S. P. Armes, *Polym. Chem*, 2016, **7**, 851-859.
104. Y. Kang, A. Pitto-Barry, H. Willcock, W.-D. Quan, N. Kirby, A. M. Sanchez and R. K. O'Reilly, *Polym. Chem*, 2015, **6**, 106-117.
105. P. Walden, *Russ. Acad. Sci*, 1914, **8**, 405-422.
106. Z. Lei, B. Chen, Y.-M. Koo and D. R. MacFarlane, *Chem. Rev*, 2017, **117**, 6633-6635.
107. A. J. Greer, J. Jacquemin and C. Hardacre, *Molecules*, 2020, **25**, 5207.
108. G. Kaur, H. Kumar and M. Singla, *J. Mol. Liq*, 2022, **351**, 118556.
109. J. Zhou, H. Sui, Z. Jia, Z. Yang, L. He and X. Li, *RSC Adv*, 2018, **8**, 32832-32864.
110. N. L. Mai, K. Ahn and Y.-M. Koo, *Process. Biochem*, 2014, **49**, 872-881.
111. J. Chen, F. Xie, X. Li and L. Chen, *Green. Chem*, 2018, **20**, 4169-4200.
112. S. N. Pedro, C. S. R. Freire, A. J. D. Silvestre and M. G. Freire, *Encyclopedia*, 2021, **1**, 324-339.
113. M. Halayqa, M. Zawadzki, U. Domańska and A. Plichta, *J. Mol. Struct*, 2019, **1180**, 573-584.
114. A. Júlio, S. A. Costa Lima, S. Reis, T. Santos de Almeida and P. Fonte, *J. Drug. Deliv. Sci. Technol*, 2020, **56**, 100915.
115. R. M. Meira, D. M. Correia, S. Ribeiro, P. Costa, A. C. Gomes, F. M. Gama, S. Lanceros-Méndez and C. Ribeiro, *ACS Appl. Polym. Mater*, 2019, **1**, 2649-2658.
116. J. C. Dias, D. C. Correia, A. C. Lopes, S. Ribeiro, C. Ribeiro, V. Sencadas, G. Botelho, J. M. S. S. Esperança, J. M. Laza, J. L. Vilas, L. M. León and S. Lanceros-Méndez, *J. Mater. Sci*, 2016, **51**, 4442-4450.
117. R. M. Meira, D. M. Correia, A. García Díez, S. Lanceros-Mendez and C. Ribeiro, *J. Mater. Chem. B*, 2022, **10**, 6472-6482.
118. J. N. Pendleton and B. F. Gilmore, *Int. J. Antimicrob. Agents*, 2015, **46**, 131-139.
119. Z. Fang, X. Zheng, L. Li, J. Qi, W. Wu and Y. Lu, *Pharm. Res*, 2022, **39**, 2391-2404.
120. F. Ghorbanizamani, H. Moulahoum, F. Zihnioglu and S. Timur, *J. Mol. Liq*, 2021, **323**, 115076.
121. Y. He, Z. Li, P. Simone and T. P. Lodge, *J. Am. Chem. Soc*, 2006, **128**, 2745-2750.
122. P. M. Simone and T. P. Lodge, *Macromol. Chem. Phys*, 2007, **208**, 339-348.
123. T. Ueki, M. Watanabe and T. P. Lodge, *Macromolecules*, 2009, **42**, 1315-1320.
124. Y. Kobayashi, Y. Kitazawa, T. Komori, K. Ueno, H. Kokubo and M. Watanabe, *Macromol. Rapid Commun*, 2016, **37**, 1207-1211.
125. H.-N. Lee and T. P. Lodge, *J. Phys. Chem. B*, 2011, **115**, 1971-1977.
126. H.-N. Lee, Z. Bai, N. Newell and T. P. Lodge, *Macromolecules*, 2010, **43**, 9522-9528.
127. X. Lan, X. Ma, L. Wang, Y. Shi, Q. Gu, L. Wu, X. Gu and Z. Luo, *ACS Omega*, 2019, **4**, 11229-11236.
128. C. L. Seitzinger, C. C. Hall and T. P. Lodge, *Macromolecules*, 2022, **55**, 3811-3820.
129. C. L. Seitzinger and T. P. Lodge, *Macromolecules*, 2023, **56**, 850-857.
130. R. Yamanaka, A. Sugawara-Narutaki and R. Takahashi, *Macromolecules*, 2023, **56**, 4354-4361.
131. J. Demarteau, A. Fernandez de Añastro, A. S. Shaplov and D. Mecerreyes, *Polym. Chem*, 2020, **11**, 1481-1488.
132. Y. Yang, J. Zheng, S. Man, X. Sun and Z. An, *Polym. Chem*, 2018, **9**, 824-827.

133. Y. Gao, J. Guo, J. Chen, G. Yang, L. Shi, S. Lu, H. Wu, H. Mao, X. Da, G. Gao and S. Ding, *Chem. Eng. J*, 2022, **427**, 131057.
134. S. Dai, Y. H. Ju, H. J. Gao, J. S. Lin, S. J. Pennycook and C. E. Barnes, *Chem. Commun*, 2000, 243-244.
135. S. Wang, B. Hsia, J. P. Alper, C. Carraro, Z. Wang and R. Maboudian, *J. Power Sources*, 2016, **301**, 299-305.
136. P. Chen, Z. Zhao, G. Zhang, X. Jin, L.-M. Wang and Y. D. Liu, *Mater. Today Commun*, 2021, **28**, 102532.
137. Y. L. Verma, A. K. Tripathi, Shalu, V. K. Singh, L. Balo, H. Gupta, S. K. Singh and R. K. Singh, *Mater. Sci. Eng. B*, 2017, **220**, 37-43.
138. D. Li, F. Shi, S. Guo and Y. Deng, *Tetrahedron. Lett*, 2004, **45**, 265-268.
139. M.-A. Néouze, J. L. Bideau, F. Leroux and A. Vioux, *Chem. Commun*, 2005, 1082-1084.
140. J. Le Bideau, L. Viau and A. Vioux, *Chem. Soc. Rev*, 2011, **40**, 907-925.
141. X. Wan, Y. He, Z. Xu, C. Li and C. Yang, *Macromol. Rapid Commun*, 2023, **44**, 2200957.
142. P. Izák, Š. Hovorka, T. Bartovský, L. Bartovská and J. G. Crespo, *J.Membr. Sci*, 2007, **296**, 131-138.
143. A. Lewandowski and A. Świderska, *Solid. State. Ion*, 2004, **169**, 21-24.
144. A. Noda and M. Watanabe, *Electrochim. Acta*, 2000, **45**, 1265-1270.
145. M. A. B. H. Susan, T. Kaneko, A. Noda and M. Watanabe, *J. Am. Chem. Soc*, 2005, **127**, 4976-4983.
146. J. C. Ribot, C. Guerrero-Sanchez, R. Hoogenboom and U. S. Schubert, *J. Mater. Chem*, 2010, **20**, 8279-8284.
147. Y. He and T. P. Lodge, *Chem. Commun*, 2007, 2732-2734.
148. Y. He and T. P. Lodge, *Macromolecules*, 2008, **41**, 167-174.
149. T. Ueki and M. Watanabe, *Chem. Lett*, 2006, **35**, 964-965.
150. A. Muñoz-Bonilla and M. Fernández-García, *Eur. Polym. J*, 2018, **105**, 135-149.
151. X. Zhang, S. Zeng, Z. Hu, X. Liang, Q. Sun, J. Huang and G. Zu, *ACS Materials. Lett*, 2022, **4**, 2459-2468.
152. H. Srour, M. Leocmach, V. Maffeis, A. C. Ghogia, S. Denis-Quanquin, N. Taberlet, S. Manneville, C. Andraud, C. Bucher and C. Monnereau, *Polym. Chem*, 2016, **7**, 6608-6616.
153. J. Zhao, X. Shen, F. Yan, L. Qiu, S. Lee and B. Sun, *J. Mater. Chem*, 2011, **21**, 7326-7330.
154. J. Rao, X. Wang, R. Yunis, V. Ranganathan, P. C. Howlett, D. R. MacFarlane, M. Forsyth and H. Zhu, *Electrochim. Acta*, 2020, **346**, 136224.
155. C.-P. Lee and K.-C. Ho, *Eur. Polym. J*, 2018, **108**, 420-428.
156. D. Zhou, R. Liu, J. Zhang, X. Qi, Y.-B. He, B. Li, Q.-H. Yang, Y.-S. Hu and F. Kang, *Nano Energy*, 2017, **33**, 45-54.
157. C.-C. Yan, W. Li, Z. Liu, S. Zheng, Y. Hu, Y. Zhou, J. Guo, X. Ou, Q. Li, J. Yu, L. Li, M. Yang, Q. Liu and F. Yan, *Adv. Funct. Mater*, 2023, **34**, 2314408.
158. W. P. Singh, U. Koch and R. S. Singh, *Soft. Mater*, 2020, **18**, 386-410.
159. N. Kimizuka and T. Nakashima, *Langmuir*, 2001, **17**, 6759-6761.
160. A. Wu, F. Lu, P. Sun, X. Qiao, X. Gao and L. Zheng, *Langmuir*, 2017, **33**, 13982-13989.
161. L. Zhang, D. Jiang, T. Dong, R. Das, D. Pan, C. Sun, Z. Wu, Q. Zhang, C. Liu and Z. Guo, *Chem. Rec*, 2020, **20**, 948-967.
162. N. Chen, H. Zhang, L. Li, R. Chen and S. Guo, *Adv. Energy. Mater*, 2018, **8**, 1702675.
163. K. Peng, Y. Shi, A. LaBarbiera and S. Mitragotri, *ACS Biomater Sci & Eng*, 2023, **9**, 2838-2845.

164. M. Mokhtarpour, H. Shekaari and A. Shayanfar, *J. Drug. Deliv. Sci. Technol*, 2020, **56**, 101512.
165. L. Viau, C. Tourné-Péteilh, J.-M. Devoisselle and A. Vioux, *Chem. Commun*, 2010, **46**, 228-230.
166. E. R. D. Seiler, K. Koyama, T. Iijima, T. Saito, Y. Takeoka, M. Rikukawa and M. Yoshizawa-Fujita, *Polymers*, 2021, **13**.
167. Q. Xu, Z. Zheng, B. Wang, H. Mao and F. Yan, *ACS Appl. Mater. Interfaces*, 2017, **9**, 14656-14664.
168. G. C. Luque, M. A.-O. Moya, M. A.-O. Picchio, V. Bagnarello, I. Valerio, J. Bolaños, M. Vethencourt, S. H. Gamboa, L. A.-O. X. Tomé, R. A.-O. Minari and D. A.-O. Mecerreyes, *Polymers*, 2023, **15**, 1076.
169. L. C. Tomé, L. Porcarelli, J. E. Bara, M. Forsyth and D. Mecerreyes, *Mater. Horiz*, 2021, **8**, 3239-3265.
170. S. Rahman, A. Haleem, M. Siddiq, M. K. Hussain, S. Qamar, S. Hameed and M. Waris, *RSC. Adv*, 2023, **13**, 19508-19529.
171. P. A.-O. Raut, V. Kishnani, K. A.-O. Mondal, A. A.-O. Gupta and S. A.-O. X. Jana, *Micromachines*, 2022, **13**, 680.
172. M. Gorlov and L. Kloo, *Dalton. Trans*, 2008, 2655-2666.
173. A. Hagfeldt, G. Boschloo, L. Sun, L. Kloo and H. Pettersson, *Chem. Rev*, 2010, **110**, 6595-6663.
174. J. Yoon, D. k. Kang, J. Won, J.-Y. Park and Y. S. Kang, *J. Power Sources*, 2012, **201**, 395-401.
175. J. Zhang, W. Zhang, J. Guo, C. Yuan and F. Yan, *Electrochim. Acta*, 2015, **165**, 98-104.
176. A. Syairah, M. H. Khanmirzaei, N. M. Saidi, N. K. Farhana, S. Ramesh, K. Ramesh and S. Ramesh, *Ionics*, 2019, **25**, 2427-2435.

2. Synthesis of homopolymers via free radical and RAFT polymerisation and solubility screenings in ionic liquids

2.1 Introduction

Ionic liquids (ILs) are defined as molten salts with a melting point <100 °C comprising anions and cations[1], of which there is an almost inexhaustible combination. Moreover, properties of ionic liquids can be tuned for a multitude of applications. For example, ionic liquids can be tailored to enhance their hydrogen bonding ability, or hydrophilic/hydrophobic properties etc.[2] Owing to their versatility, ionic liquids have been used for a multitude of applications.[3, 4] Importantly, they have been utilised for the solvation of polymers, particularly as a solvent for the synthesis of polymers,[5, 6] as well as for polymer processing.[7-10] As a result of their good thermal stability and low flammability, they have also been considered as alternatives to traditional organic solvents in a variety of electrochemical applications such as lithium-ion batteries,[11-13] dye-sensitised solar cells[14-16] and sensors[17-21] to name but a few.[22]

Polymerisation-induced self-assembly (PISA) has been shown to be a versatile method for generating well-defined block copolymers with a range of morphologies. As discussed in Chapter 1, PISA is generally a two-step process. The first step is synthesising a functionalised solvophilic polymer (for example a macromolecular chain transfer agent via RAFT solution polymerisation). The second step is the chain extension of the solvophilic polymer via dispersion or emulsion polymerisation of a monomer that yields a solvophobic polymer. In order for the polymerisation to proceed via either dispersion or emulsion polymerisation, the monomer chosen should be miscible or immiscible with the solvent, respectively.[23]

In order to design an appropriate PISA synthesis in a given solvent, it is important to understand monomer miscibilities and polymer solubilities in that solvent. Of particular relevance to this research, dispersion polymerisation is the favourable method for generating block copolymers via RAFT-PISA. This is because it has been established that worm morphologies (which occupy a very narrow phase space between spheres and vesicles[24]) can be more readily accessed via dispersion polymerisation compared to emulsion polymerisation.[25] Block copolymer worms are particularly attractive as they can form free-standing gels when dispersed at copolymer concentrations exceeding the critical gelation concentration (CGC).[26] Such worm gels have potential applications as viscosity modifiers,[27, 28] sterilisable gels[29] and stem cell storage media.[30] Given their promise in such applications, we believe that worm gels offer much promise in the way of generating so-called ionogels which are comprised of ionic liquid trapped in a polymer matrix. Several methods have been reported on the fabrication of ionogels, most typically requiring the aid of co-solvent,

crosslinkers or post-polymerisation processing. In the absence of additives such as crosslinking agents, worm gel formation essentially relies on the formation of a sufficient proportion and length of wormlike micelles in the ionic liquid to enable physical entanglement and therefore yield gels. As a result of this, the requirement for co-solvents and crosslinkers is removed, thus enhancing desirable properties of ionogels such as ionic conductivity. Worm gel formation via PISA has been extensively reported previously in a range of solvents.[31-37] Despite some advances on worm formation via emulsion polymerisation,[38-41] this route have more typically lead to kinetically trapped spheres,[25, 42-45] therefore worm formation is comparably less probable.

Herein, a series of monomers are tested for their miscibility with two different commercially available ionic liquids, 1-ethyl-3-methylimidazolium dicyanamide, [EMIM][DCA], and 1-ethyl-3-methylimidazolium ethyl sulphate, [EMIM][$EtOSO_3$], to assess their suitability to be polymerised to form a core-forming block during PISA. Both of these ILs have been utilised previously for ionogel formation using different crosslinking strategies.[21, 46-48] Furthermore, series of homopolymers are synthesised via either free radical polymerisation or RAFT solution polymerisation and subsequently investigated for their solubility in these ILs to screen them as potential core-forming blocks in [EMIM][DCA] and [EMIM][$EtOSO_3$] (Figure 2.1).

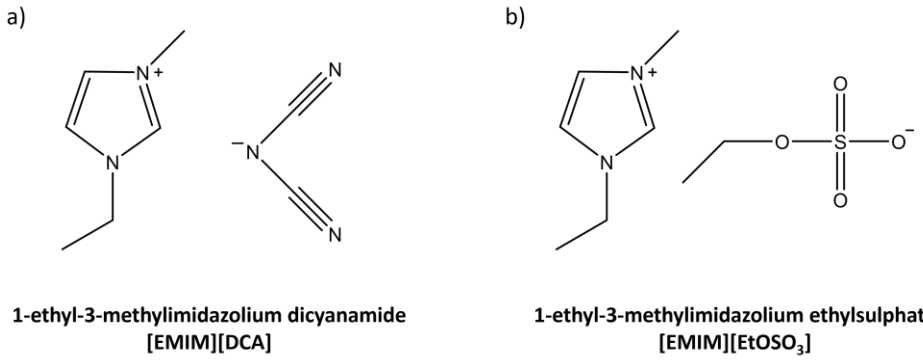

Figure 2.1. Hydrophilic ionic liquids used for miscibility and solubility screenings of monomers and polymers.

2.2 Experimental

2.2.1 Materials

Methyl acrylate (MA) and acrylic acid (AA) were purchased from Fisher Scientific. 2-Hydroxyethyl methacrylate (HEMA), *N,N*-dimethylacrylamide (DMA), diacetone acrylamide (DAAM), benzyl methacrylate (BzMA), *n*-propyl methacrylate (*n*-PMA), *n*-butyl methacrylate (*n*-BuMA) and styrene (St) were purchased from Sigma Aldrich. All monomers were passed through a basic alumina column prior to use to remove inhibitor, with the exception of DAAM which was used as received. 2,2'-Azobisisobutyronitrile (AIBN) was purchased from Molekula and was recrystallised from methanol prior to use. 4,4'-Azobis(4-cyanovaleric acid) (ACVA) and 4-cyano-4-(phenylcarbonothioylthio) pentanoic acid (CPTP) RAFT agents were purchased from Sigma Aldrich and used as received. All reagent grade organic solvents used were purchased from Fisher Scientific and used as received. 1-Ethyl-3-methylimidazolium dicyanamide ([EMIM][DCA]) and 1-ethyl-3-methylimidazolium ethyl sulphate ([EMIM][$EtOSO_3$]) were acquired from BASF and used as received. Dimethyl sulfoxide-d6, chloroform-d and methanol-d4 for ^{1}H NMR analysis were purchased from Goss Scientific and used as received.

2.2.2 ^{1}H Nuclear Magnetic Resonance (NMR) Spectroscopy

^{1}H NMR spectra were obtained in either MeOD-d4, DMSO-d6 or $CDCl_3$-d using a Bruker Avance Neo 300 MHz spectrometer. Typically 16 scans were averaged per spectrum and all chemical shifts are expressed in ppm. Both crude and pure samples were prepared by dissolving approximately 40 mg of sample in 0.7 mL of appropriate deuterated solvent. ^{1}H NMR spectra were referenced using peaks present as a result of residual solvent.

2.2.3 Gel Permeation Chromatography (GPC)

Molecular weight distributions were obtained by GPC using either DMF eluent or water eluent. The DMF system was composed of an Agilent Infinity II multi-detector gel permeation chromatography (GPC) instrument comprising a guard column and two PL gel mixed-C columns. The mobile phase contained 0.10% w/v LiBr in HPLC grade DMF and the flow rate was fixed at 1 mL min^{-1} at 80 °C. The DMF GPC was calibrated using near-monodispersed poly(methyl methacrylate) standards (M_p range = 535-1,591,000 g mol^{-1}). The aqueous system was composed of an Agilent Infinity II multi-detector GPC instrument comprising a guard column and two aquagel OH mixed-H columns. The mobile phase contained 0.05% w/v NaN_3 in HPLC grade water and the

flow rate was fixed at 1 mL min^{-1} at 35 °C. The aqueous GPC was calibrated using near-monodispersed poly(ethylene glycol) standards (M_p range = 106-1,511,000 g mol^{-1})

2.2.4 Ionic liquid miscibility screenings of monomers

All miscibility screenings of the selected monomers in [EMIM][DCA] and [EMIM][$EtOSO_3$] were conducted at 10% w/w monomer concentration. This concentration was selected as it approximates as the monomer concentration that will be employed during block copolymer syntheses in subsequent work.

Confirmation of miscibility or immiscibility was determined by eye. In order to conduct dispersion polymerisations for subsequent block copolymer syntheses in IL, the insoluble core-forming block (i.e. the IL-phobic block) requires its precursor monomer to be fully miscible with the IL. Therefore, those that were immiscible with the IL were eliminated from the monomer selection. The monomers that underwent miscibility screenings are shown in Figure 2.2.

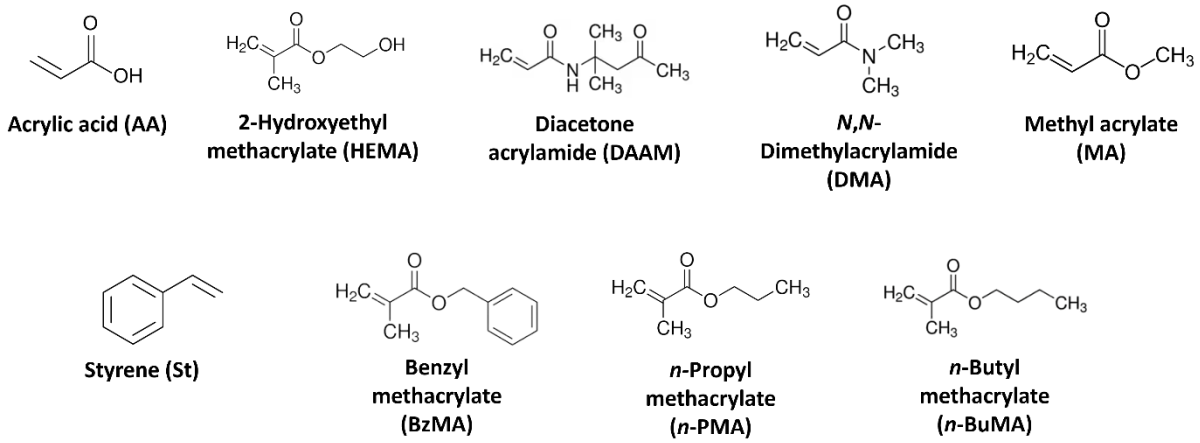

Figure 2.2. Monomer selection for miscibility screenings in 1-ethyl-3-methylimidazolium dicyanamide, [EMIM][DCA], and 1-ethyl-3-methylimidazolium ethyl sulphate, [EMIM][$EtOSO_3$].

2.2.5 Synthesis of homopolymers via free radical polymerisation

All free radical polymerisations were conducted at 25% w/w solids at 60 °C for 2 hours. The AIBN quantity used for all reactions was 0.5 mol% with respect to monomer.[49]

2.2.5.1 Synthesis of poly(methyl acrylate) (PMA) via free radical polymerisation

The polymerisation of methyl acrylate via free radical polymerisation at 25% w/w was conducted as follows. A 50 mL round bottomed flask was charged with methyl acrylate (5 g; 58.1 mmol), AIBN (45.7 mg; 278 µmol) and THF (15.1 g). The sealed flask was purged with nitrogen for 30 minutes and placed in a preheated oil bath at 60 °C for 2 hours. The resulting poly(methyl acrylate) (PMA, DMF GPC: M_n = 10,500 g mol^{-1}, $Đ_M = M_w/M_n$ = 1.85) was purified by twice precipitating into excess methanol before drying using a rotary evaporator. The resulting PMA was obtained as a viscous free-flowing transparent liquid.

2.2.5.2 Synthesis of poly(2-hydroxyethyl methacrylate) (PHEMA) via free radical polymerisation

The polymerisation of 2-hydroxyethyl methacrylate (HEMA) via free radical polymerisation at 25% w/w was conducted as follows. A 50 mL round bottomed flask was charged with 2-hydroxyethylmethacrylate (5g; 38.4 mmol), AIBN (33.7 mg; 205 µmol), and methanol (15.1 g). The sealed flask was purged with nitrogen for 30 minutes and placed in a preheated oil bath at 60 °C for 2 hours. The resulting poly(2-hydroxyethyl methacrylate) (PHEMA, DMF GPC: M_n = 305,500 g mol^{-1}, $Đ_M$ = 2.22) was purified by twice precipitating into excess diethyl ether before drying using a rotary evaporator. The resulting PHEMA was obtained as a transparent gel.

2.2.5.3 Synthesis of poly(acrylic acid) (PAA) via free radical polymerisation

The polymerisation of acrylic acid via free radical polymerisation at 25% w/w was conducted as follows. A 50 mL round bottomed flask was charged with acrylic acid (5g; 69.4 mmol), AIBN (59.9 mg; 365 µmol), and THF (15.2 g). The sealed flask was purged with nitrogen for 30 minutes and placed in a preheated oil bath at 60 °C for 2 hours. The resulting poly(acrylic acid) (PAA, Aqueous GPC: M_n = 23,700 g mol^{-1}, $Đ_M$ = 1.74) was purified by twice precipitating into excess hexane before drying using a rotary evaporator. The resulting PAA was obtained as a viscous, free-flowing liquid.

2.2.5.4 Synthesis of poly(N, N-dimethyl acrylamide) (PDMA) via free radical polymerisation

The polymerisation of *N,N*-dimethyl acrylamide (DMA) via free radical polymerisation at 25% w/w was conducted as follows. A 50 mL round bottomed flask was charged with DMA (5g; 50.4 mmol), AIBN (39.8 mg; 242 µmol), and methanol (15.1 g). The sealed flask was purged with nitrogen for 30 minutes and placed in a preheated oil bath at 60 °C for 2 hours. The resulting poly(*N,N*-dimethylacrylamide) (PDMA, DMF GPC: M_n = 80,100 g mol^{-1}, $Đ_M$ = 2.72) was purified by twice

precipitating into excess diethyl ether before drying using a rotary evaporator. The resulting PDMA was obtained as a transparent gel.

2.2.5.5 Synthesis of poly(diacetone acrylamide) (PDAAM) via free radical polymerisation

The polymerisation of diacetone acrylamide (DAAM) via free radical polymerisation at 25% w/w was conducted as follows. A 50 mL round bottomed flask was charged with DAAM (5g; 29.5 mmol), AIBN (23.9 mg; 145.5 µmol), and ethanol (20 g). The sealed flask was purged with nitrogen for 30 minutes and placed in a preheated oil bath at 60 °C for 2 hours. The resulting poly(diacetone acrylamide) (PDAAM, DMF GPC: M_n = 22,200 g mol^{-1}, $Đ_M$ = 2.47) was purified by twice precipitating into excess diethyl ether before drying using a rotary evaporator. The resulting PDAAM was obtained as a white solid.

2.2.5.6 Synthesis of poly(benzyl methacrylate) (PBzMA) via free radical polymerisation

The polymerisation of benzyl methacrylate (BzMA) via free radical polymerisation at 25% w/w was conducted as follows. A 50 mL round bottomed flask was charged with BzMA (5.2 g; 28.4 mmol), ACVA (41.4 mg; 147.7 µmol), and THF (15.7 g). The sealed flask was purged with nitrogen for 30 minutes and placed in a preheated oil bath at 60 °C for 2 hours. The resulting poly(benzyl methacrylate) (PBzMA, DMF GPC: M_n = 66,300 g mol^{-1}, $Đ_M$ = 2.13) was purified by twice precipitating into excess methanol before drying using a rotary evaporator. The resulting PBzMA was obtained as a white solid.

2.2.6 Synthesis of macro-CTAs via RAFT solution polymerisation

2.2.6.1 Synthesis of PHEMA macromolecular chain transfer agent (macro-CTA) via RAFT solution polymerisation

A typical synthesis of $PHEMA_{31}$ macro-CTA was conducted as follows. A 10 mL round bottom flask was charged with 2-hydroxyethyl methacrylate (HEMA; 3.21 g; 24.7 mmol), 4-cyano-4-(phenylcarbonothioylthio) pentanoic acid (CPTP; 0.138 g; 494 µmol; target degree of polymerisation, DP = 50), 2,2'-azobisisobutyronitrile (AIBN; 40 mg; 247 µmol; [CPTP]/[AIBN] molar ratio = 5) and methanol (MeOH; 5.1 g; total solids content = 40% w/w). The sealed reaction flask was purged with nitrogen for 30 minutes and placed in a preheated oil bath at 60 °C for 6 hours. The resulting PHEMA (HEMA conversion = 54%, M_n = 5,000 g mol^{-1}, $Đ_M$ = 1.36) was purified by twice precipitating into excess diethyl ether and dried using a rotary evaporator. The degree of

polymerisation (DP) of the PHEMA macro-CTA was calculated to be 30 using ^{1}H NMR spectroscopy by comparing the integrated signals that correspond to the CPTP aromatic protons at 7.4-7.9 ppm with the integrated signals corresponding to the two oxymethylene protons at 3.8-4.0 ppm (Figure 2.3 and Equations 2.1 and 2.2) The resulting PHEMA was obtained as a pink solid.

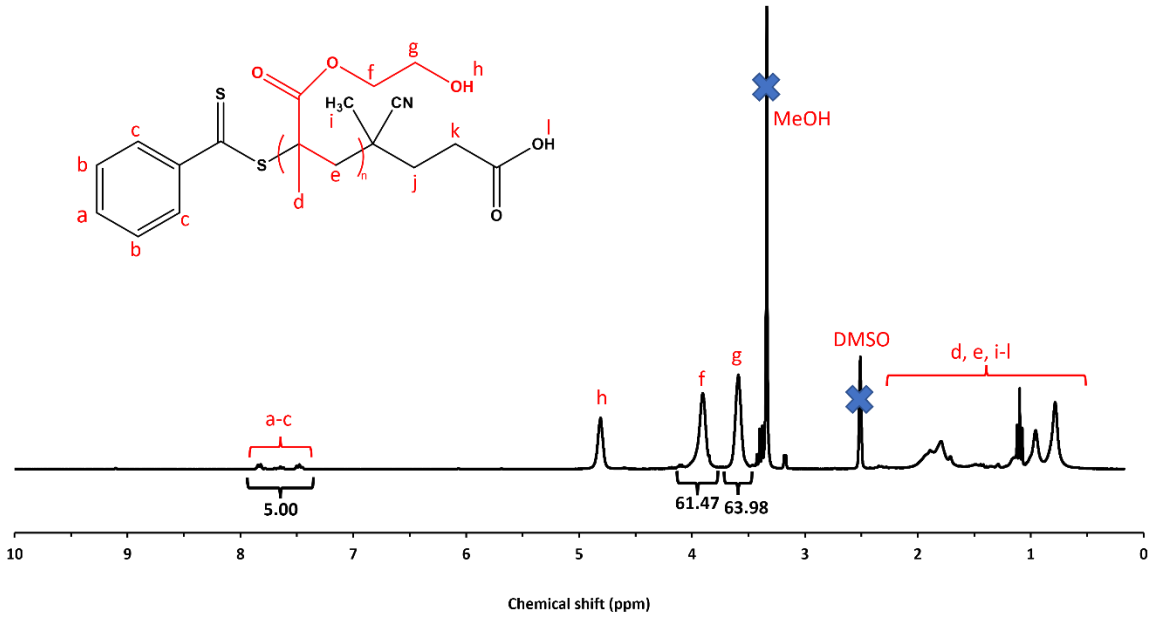

Figure 2.3. Assigned ^{1}H NMR spectrum of purified $PHEMA_{31}$ macro-CTA in DMSO-d6.

$$[Integral\ (a\text{-}c)] = 5H \quad (2.1)$$

$$PHEMA\ DP = \frac{[Integral\ (f)]}{2} = 31 \quad (2.2)$$

2.2.6.2 Synthesis of PDMA macro-CTA via RAFT solution polymerisation

A typical synthesis of $PDMA_{50}$ macro-CTA was conducted as follows. A 10 mL round bottomed flask was charged with *N*,*N*-dimethylacrylamide (DMA; 2.886 g; 29.1 mmol), 4-cyano-4-(phenylcarbonothioylthio) pentanoic acid (CPTP; 0.163 g; 582 µmol; target degree of polymerisation, DP = 50), ACVA initiator (81.6 mg; 291 µmol; [CPTP]/[ACVA] molar ratio = 2) and ethanol (1.3 g; total solids content = 70% w/w). The sealed flask was purged with nitrogen for 30 minutes and then placed in a preheated oil bath at 70 °C for 6 hours. The resulting PDMA (DMA conversion = 53%, M_n = 5,200 g mol^{-1}, $Đ_M$ = 1.41) was purified by twice precipitating into diethyl ether and dried using a rotary evaporator. The degree of polymerisation (DP) of the PDMA macro-

CTA was calculated to be 50 using ^{1}H NMR spectroscopy by comparing the integrated signals that correspond to the CPTP aromatic protons at 7.4-7.9 ppm with the integrated signals corresponding to the six alkyl protons at 2.8-3.3 ppm (Figure 2.4 and Equations 2.3 and 2.4). The resulting PDMA was obtained as an orange solid.

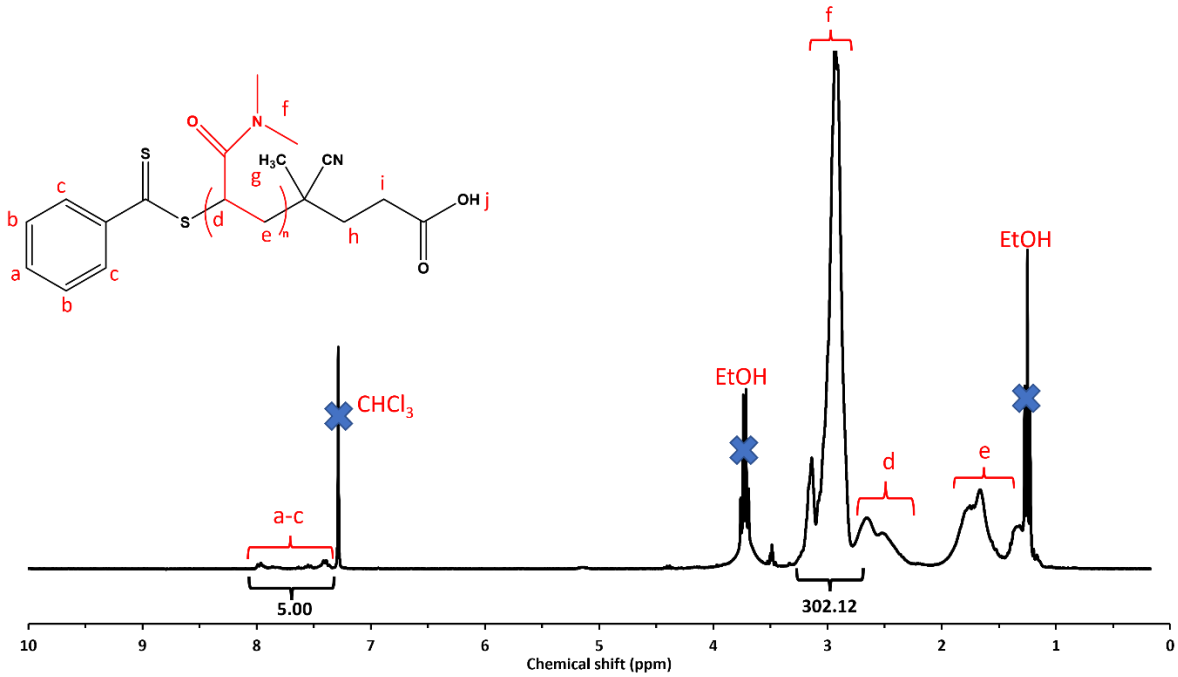

Figure 2.4. Assigned ^{1}H NMR spectrum of purified $PDMA_{50}$ macro-CTA in $CDCl_3$-d.

$$[Integral\ (a\text{-}c)] = 5H \quad (2.3)$$

$$PHEMA\ DP = \frac{[Integral\ (f)]}{6} = 50 \quad (2.4)$$

2.2.6.3 Synthesis of PDAAM macro-CTA via RAFT solution polymerisation

A typical synthesis of $PDAAM_n$ macro-CTA was conducted as follows. A 10 mL round bottomed flask was charged with diacetone acrylamide (DAAM; 3g; 17.7 mmol), 4-cyano-4-(phenylcarbonothioylthio) pentanoic acid (CPTP; 0.099 g; 355 µmol; target degree of polymerisation, DP = 50), ACVA initiator (19.9 mg; 70.9 µmol; [CPTP]/[ACVA] molar ratio = 5) and methanol (4.68 g; total solids content = 40% w/w). The sealed flask was purged with nitrogen for 30 minutes and then placed in a preheated oil bath at 70 °C for 6 hours. The resulting PDAAM (M_n = 600 g mol^{-1} , $Đ_M$ = 1.42) was purified by twice precipitating into diethyl ether and dried using a

rotary evaporator. The DP of the PDAAM macro-CTA was unable to be determined experimentally by ^{1}H NMR spectroscopy as end-group analysis was not feasible due to polymeric peaks crowding in the same region as the peaks corresponding to the CPTP aromatic protons between 7.4-8.1 ppm (Figure 2.5). The resulting PDAAM was obtained as a red solid.

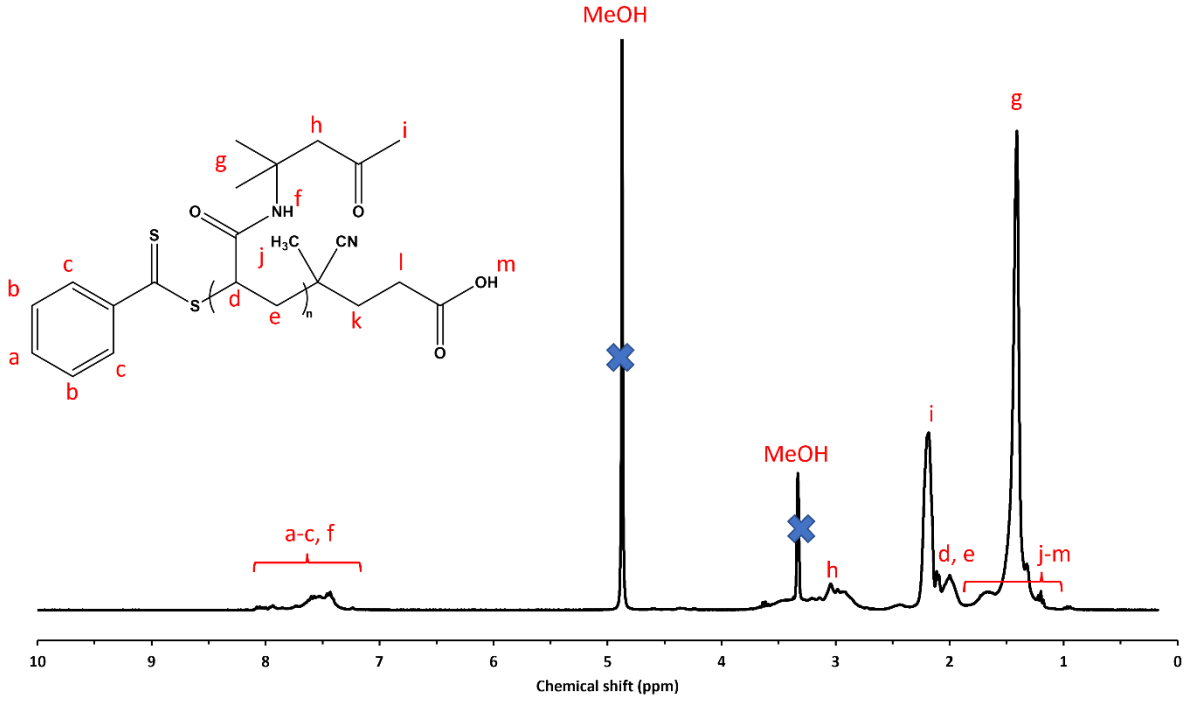

Figure 2.5. Assigned ^{1}H NMR spectrum of purified PDAAM macro-CTA in MeOD-d4.

2.2.6.4 Synthesis of PBzMA macro-CTA via RAFT solution polymerisation

A typical synthesis of $PBzMA_n$ macro-CTA was conducted as follows. A 10 mL round bottomed flask was charged with benzyl methacrylate (BzMA; 3g; 17.0 mmol), 4-cyano-4-(phenylcarbonothioylthio) pentanoic acid (CPTP; 0.0951 g; 341 µmol; target degree of polymerisation, DP = 50), ACVA initiator (19.1 mg; 68.1 µmol; [CPTP]/[ACVA] molar ratio = 5) and THF (4.67 g; total solids content = 40% w/w). The sealed flask was purged with nitrogen for 30 minutes and then placed in a preheated oil bath at 70 °C for 6 hours. The resulting PBzMA (BzMA conversion = 51%, M_n = 1,900 g mol^{-1} , $Đ_M$ = 1.60) was purified by twice precipitating into methanol and dried using a rotary evaporator. The DP of the PBzMA macro-CTA was unable to be determined experimentally by ^{1}H NMR spectroscopy as end-group analysis was not feasible due to peaks corresponding to aromatic protons present in PBzMA crowding in the same region as the peaks corresponding to the CPTP aromatic protons between 7.4-8.1 ppm (Figure 2.6). The resulting

PBzMA was obtained as a red solid. The degree of polymerisation (DP) of the PBzMA macro CTA was calculated to be 26 by estimation based on the BzMA monomer conversion obtained (Equation 2.5)

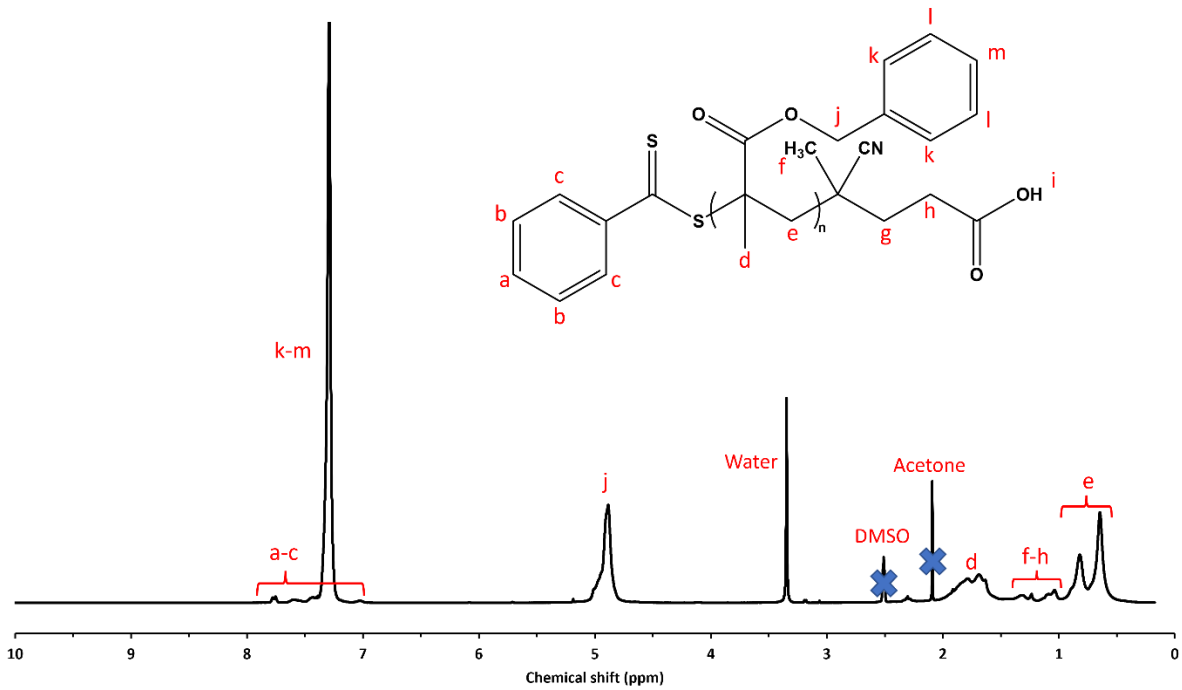

Figure 2.6. Assigned ^{1}H NMR spectrum of purified $PBzMA_{25}$ macro-CTA in DMSO-d6

$$PBzMA\ DP = PBzMA\ target\ DP \times BzMA\ monomer\ conversion \quad (2.5)$$

2.2.7 Solubility screenings of polymers in ionic liquids

Solubility screenings of all polymers synthesised, both via free radical polymerisation and RAFT solution polymerisation, were conducted in two hydrophilic ionic liquids, 1-ethyl-3-methylimidazolium ethyl sulphate, [EMIM][$EtOSO_3$], and 1-ethyl-3-methylimidazolium dicyanamide, [EMIM][DCA], in order to guide subsequent block copolymer syntheses. The polymers selected for these screenings are shown in Figure 2.7.

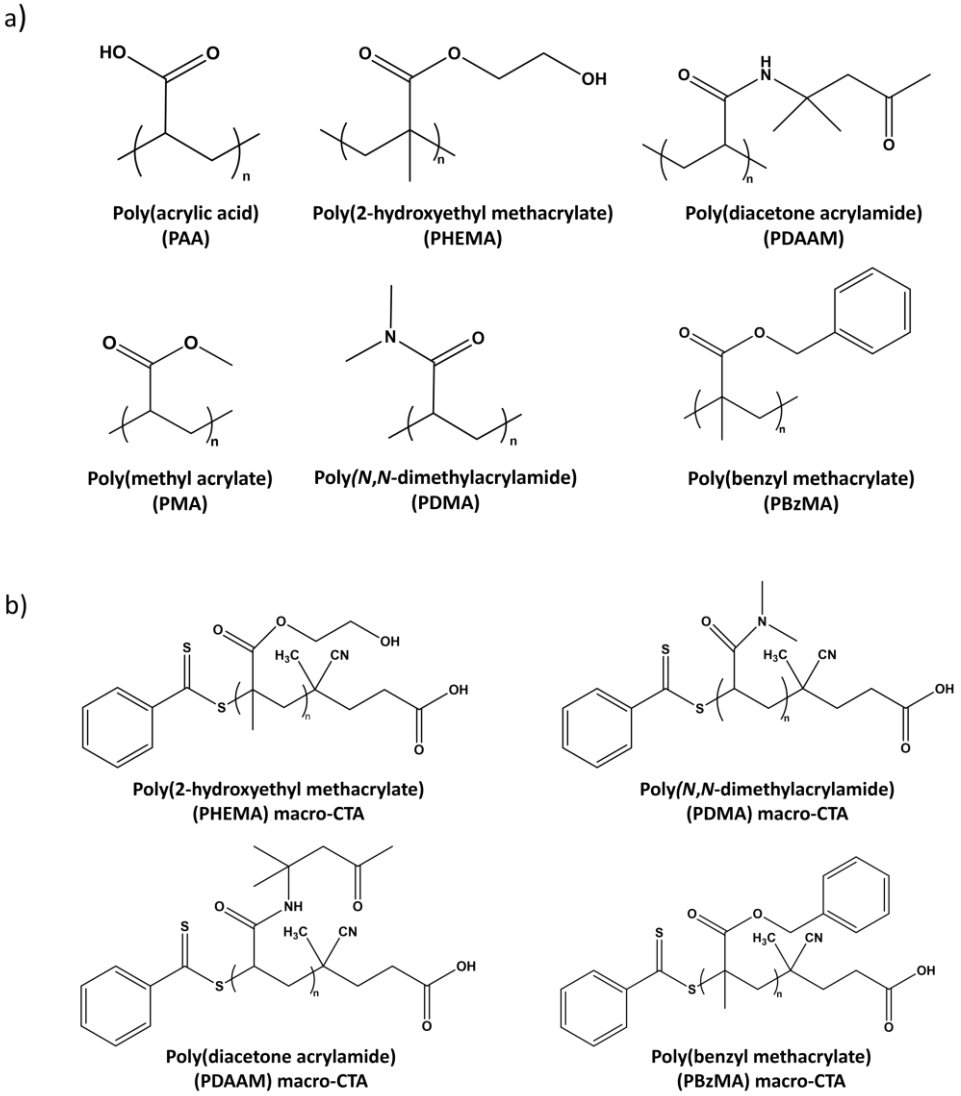

Figure 2.7. Polymers selected for solubility screenings in 1-ethyl-3-methylimidazolium dicyanamide, [EMIM][DCA], and 1-ethyl-3-methylimidazolium ethyl sulphate, [EMIM][$EtOSO_3$]. a) Homopolymers synthesised via free radical polymerisation and b) macromolecular chain transfer agents synthesised via RAFT solution polymerisation.

In a typical screening, a 5 mL round bottomed flask was charged with a stirrer bar, polymer (75 mg) and ionic liquid (1.5g) to form a 4.76% w/w solution. The solution was heated in an oil bath at 70 °C for up to 4 hours. This temperature was selected as this was the predicted temperature at which subsequent PISA syntheses were conducted. As the block copolymer polymer solutions would then be left at room temperature post-polymerisation, the polymer solubilities in the ILs were also assessed at room temperature.

2.3 Results and discussion

2.3.1 Miscibility screenings of monomer

A selection of monomers were screened for their miscibility in hydrophilic ILs at room temperature and 10 % w/w. The results from this study are as shown in Table 2.1:

Table 2.1. Monomers and their respective miscibilities with both ILs investigated at room temperature. A tick indicates miscibility with the IL up to 10 % w/w and a cross indicates immiscibility with the ILs.

Monomer	[EMIM][$EtOSO_3$] miscibility at room temperature	[EMIM][DCA] miscibility at room temperature
AA	✓	✓
MA	✓	✓
MMA	✓	✓
n-PMA	×	×
n-BuMA	×	×
BzMA	✓	✓
2-HPMA	✓	✓
4-HBA	✓	✓
2-HEMA	✓	✓
HEA	✓	✓
DMA	✓	✓
DAAM	✓	✓
St	×	×

As seen in Table 2.1, a range of monomer were investigated for their miscibility with two different ILs. In order to yield worm gels, RAFT dispersion polymerisation has been shown to be the most suitable technique for block copolymer syntheses to proceed.[24] Therefore, it was important that any monomer that could be used to generate the core-forming block of the block copolymer, was miscible with the ILs. For this reason, monomers with a range of hydrophilicity/hydrophobicity were tested to assess their suitability. *n*-Propyl methacrylate (*n*-PMA), *n*-butyl methacrylate (*n*-BuMA) and styrene (St) were shown to be immiscible with both ILs, thus were not selected as suitable monomers to generate the core-forming block for polymerisation-induced self-assembly (PISA) syntheses, nor were solubility screenings for their respective polymers conducted. The remaining monomers were all miscible with both of the ILs, therefore were investigated further for their potential in dispersion PISA syntheses.

2.3.2 Synthesis of homopolymers via free radical polymerisation

Based on miscibility screenings of a range of monomers (Section 2.3.1), a series of homopolymers were synthesised using IL-miscible monomers via free radical polymerisation to assess their solubilities in the ILs once polymerised. All homopolymers were synthesised via solution polymerisation and extracted and purified via precipitation methods. The solvents used for each purification is tabulated below in Table 2.2:

Table 2.2. Homopolymers synthesised via free radical solution polymerisation and solvents used for each for polymer purification

Homopolymer	Precipitation solvent
Poly(methyl acrylate)	Methanol
Poly(2-hydroxyethyl methacrylate)	Diethyl ether
Poly(acrylic acid)	Hexane
Poly(*N, N*-dimethyl acrylamide)	Diethyl ether
Poly(diacetone acrylamide)	Diethyl ether
Poly(benzyl methacrylate)	Methanol

Free radical polymerisation was conducted owing to preparation and synthesis being facile and relatively quick compared to other polymerisation techniques. As a result, a range of polymers could be generated rapidly. Success of polymerisation was determined by ^{1}H NMR spectroscopy (Figures 2.8, 2.10, 2.12 and 2.14).

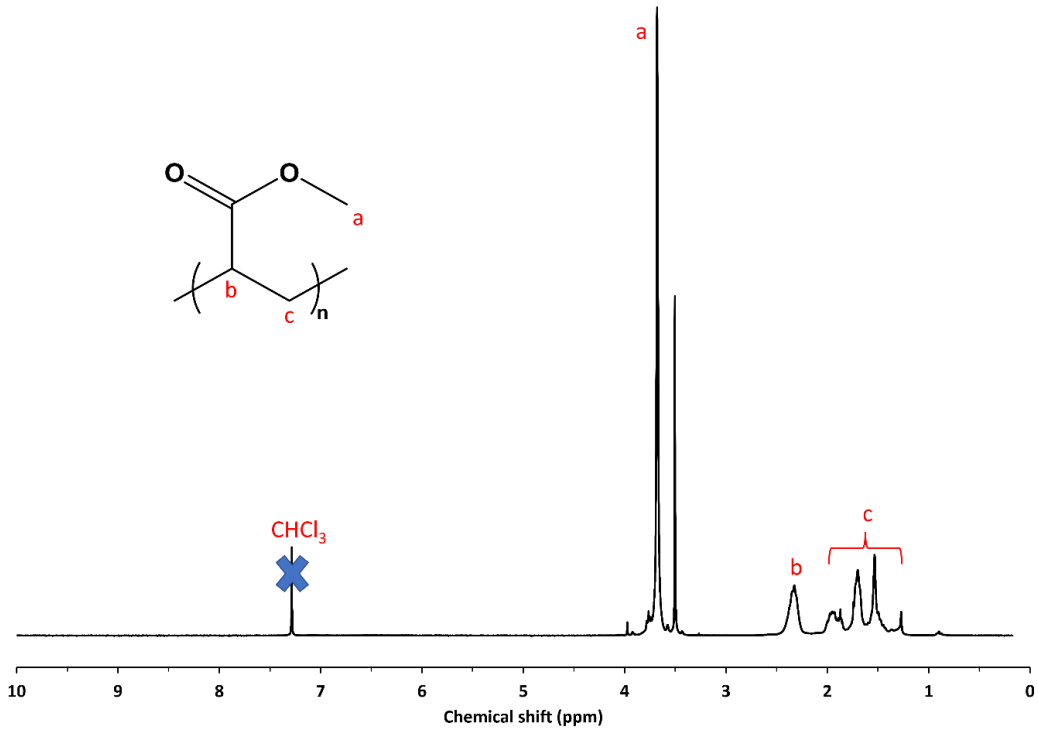

Figure 2.8. Assigned ^{1}H NMR spectrum of purified poly(methyl acrylate) in $CDCl_3$-d.

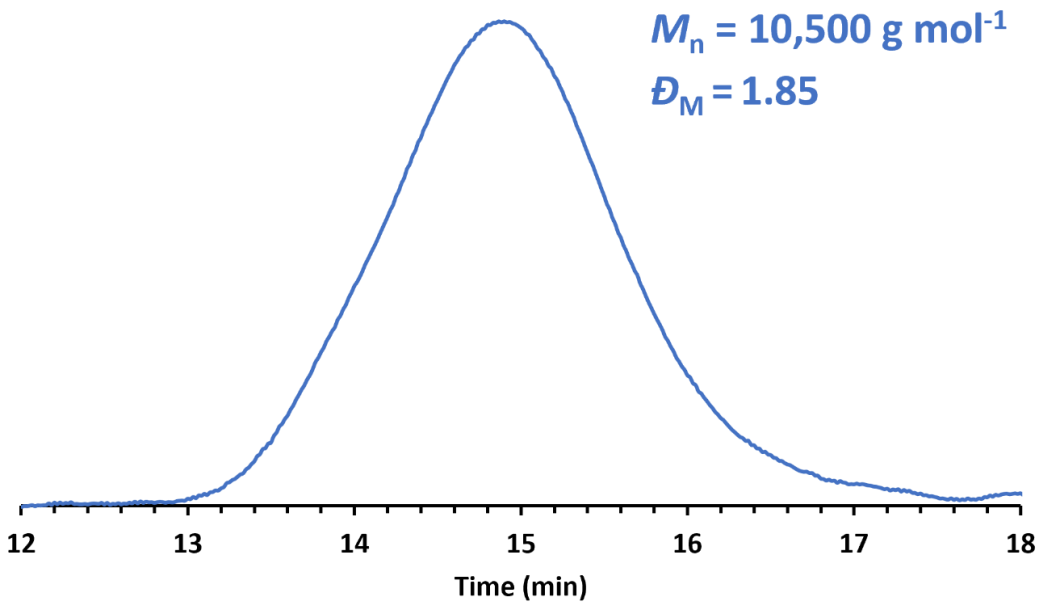

Figure 2.9. DMF GPC chromatogram obtained of poly(methyl acrylate) synthesised via free radical polymerisation of methyl acrylate for 2 hours at 60 °C in THF at 25% w/w solids.

^{1}H NMR spectroscopic analysis confirmed the successful synthesis of PMA. Furthermore, the absence of residual monomer peaks was evidenced by ^{1}H NMR spectroscopy (Figure 2.8). GPC analysis also showed a polymer had successfully been synthesised as shown by the trace obtained for PMA (Figure 2.9).

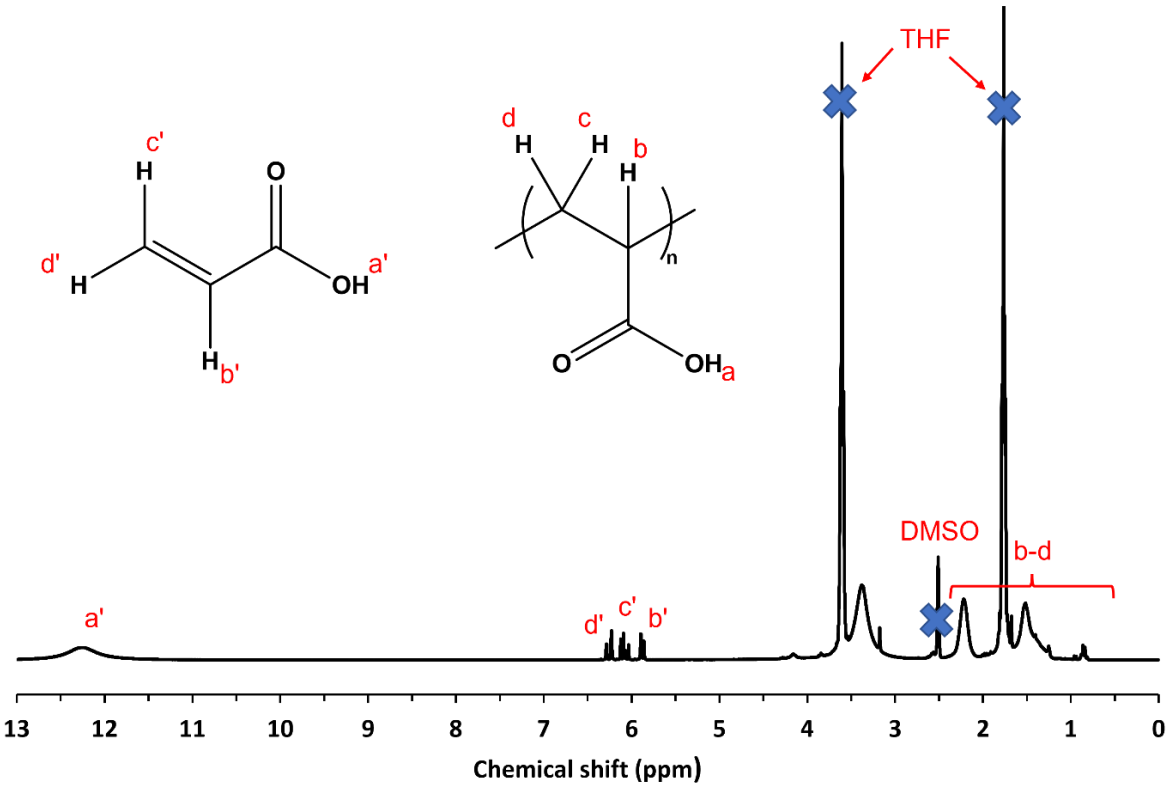

Figure 2.10. Assigned ^{1}H NMR spectrum of precipitated poly(acrylic acid) in DMSO-d6.

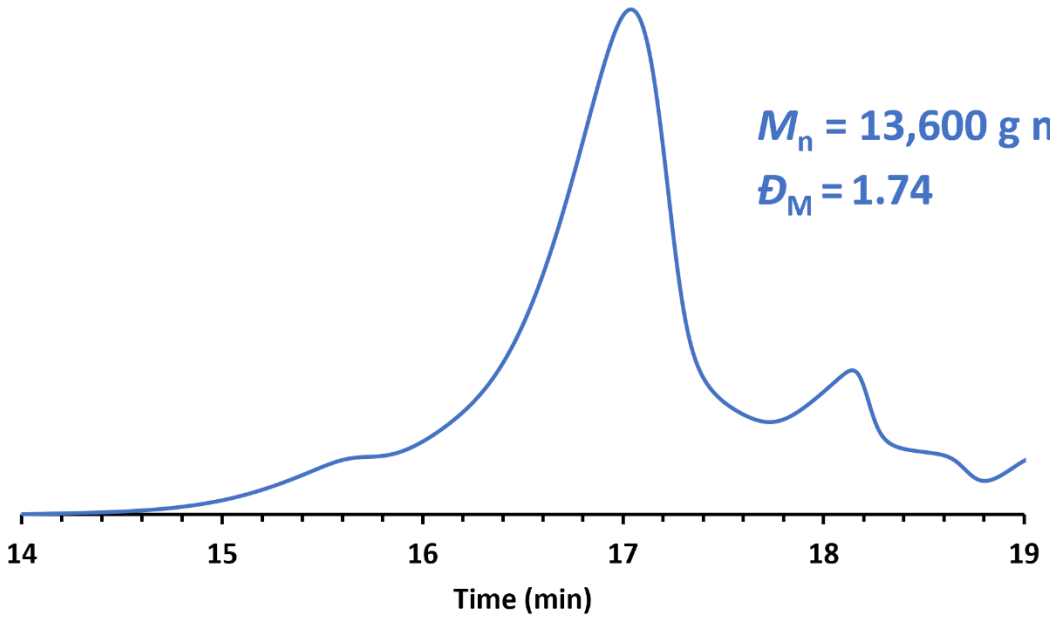

Figure 2.11. Aqueous GPC chromatogram obtained of poly(acrylic acid) synthesised via free radical polymerisation of acrylic acid for 2 hours at 60 °C in THF at 25% w/w solids.

^{1}H NMR spectroscopic analysis confirmed the success of the synthesis of PAA. However, the resulting polymer was not 100% pure as judged by the presence residual vinyl monomer peaks in the ^{1}H NMR spectrum between 5.5 and 6.5 ppm (see Figure 2.10), indicating. Despite two rounds of precipitation and purification, isolation of pure polymer was difficult as a result of its highly viscous consistency. It is clear that more efficient purification and drying methods were required for this synthesis. GPC analysis also indicated successful polymer synthesis (Figure 2.11). As a result of the charged nature of the poly(acrylic acid), the quality of the chromatograms obtained were comparatively poor as a result of the interactions between the polymer and columns in the GPC.

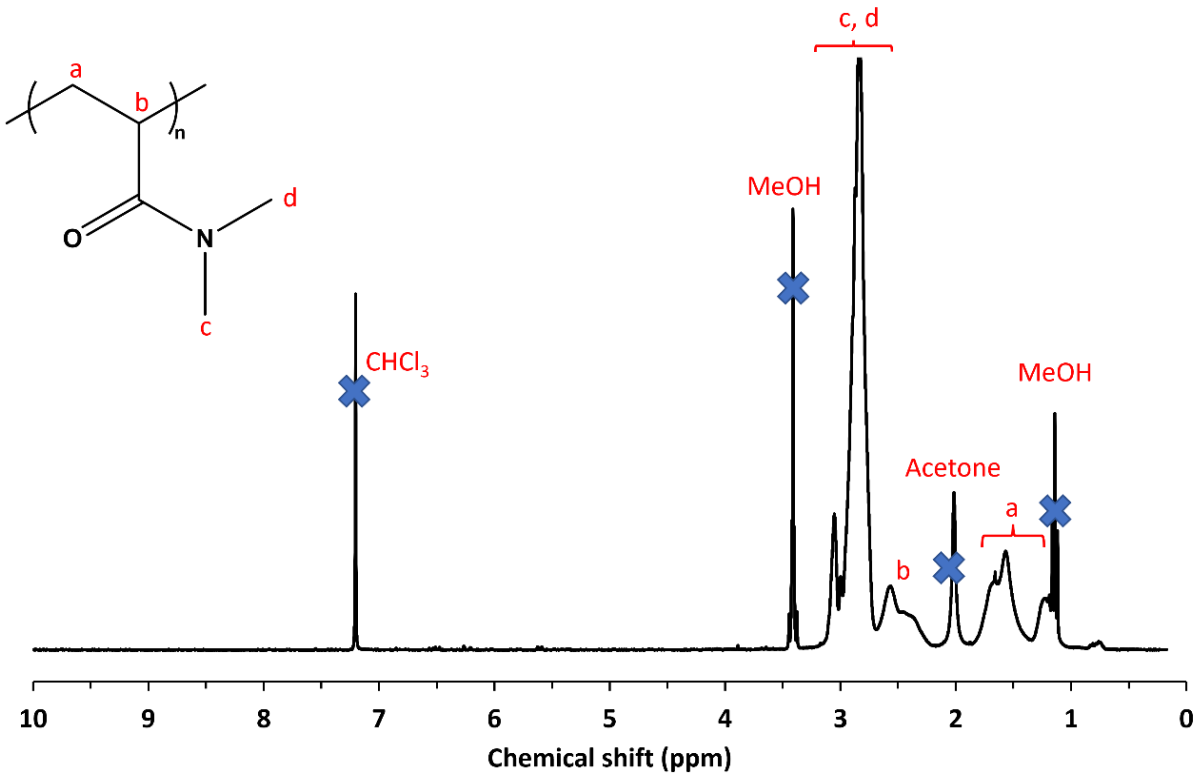

Figure 2.12. Assigned ^{1}H NMR spectrum of precipitated poly(*N,N*-dimethylacrylamide) in $CDCl_3$-d.

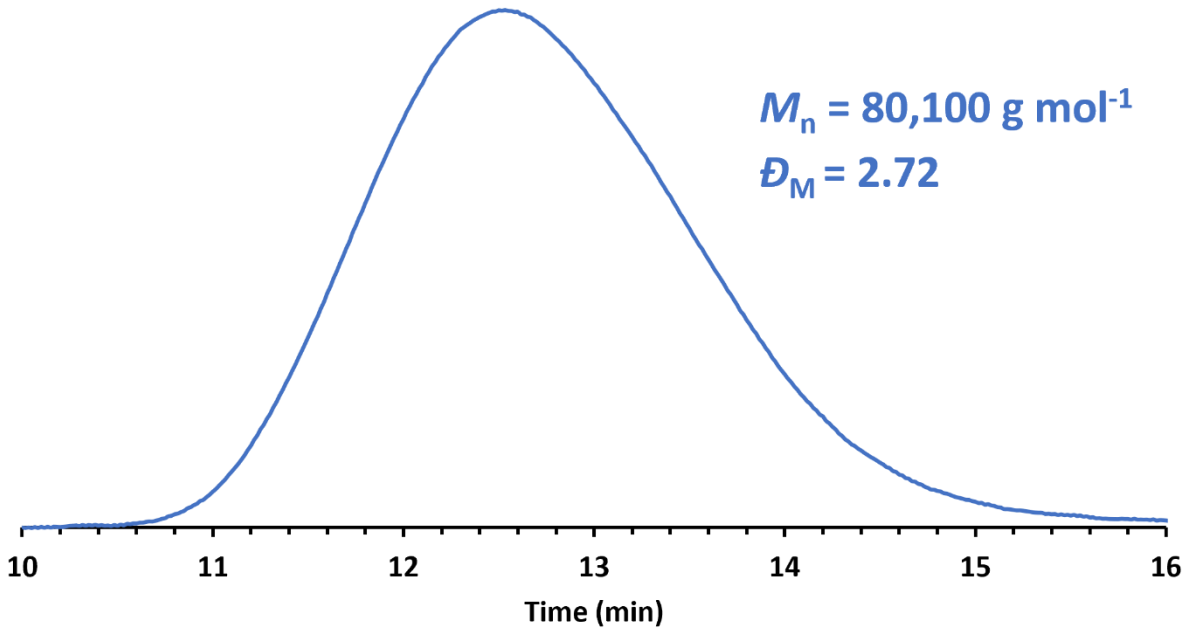

Figure 2.13. DMF GPC chromatogram obtained of poly(*N,N*-dimethylacrylamide) synthesised via free radical polymerisation of *N,N*-dimethylacrylamide for 2 hours at 60 °C in methanol at 25% w/w solids.

PDMA was shown to have a more substantially improved purification compared to PAA, as evidenced by the comparatively weaker vinyl proton peaks in the ^{1}H NMR spectrum (Figure 2.12). It is clear there is still monomer present in the sample. GPC analysis also indicated successful polymerisation (Figure 2.13), as well evidencing that some branching or crosslinking may have occurred based on the dispersity obtained ($Đ_M$ = 2.72).

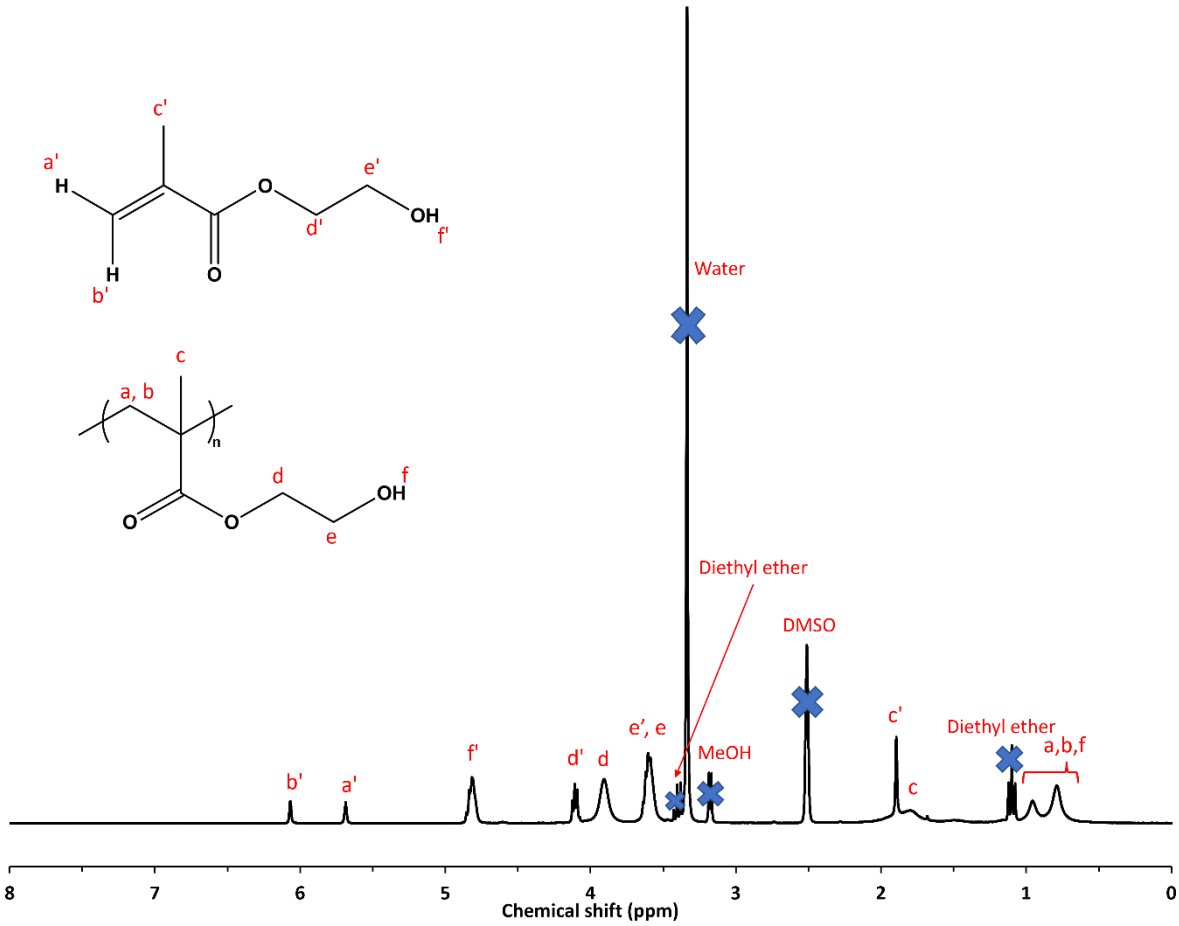

Figure 2.14. Assigned ^{1}H NMR spectrum of twice precipitated poly(2-hydroxyethyl methacrylate) in DMSO-d6.

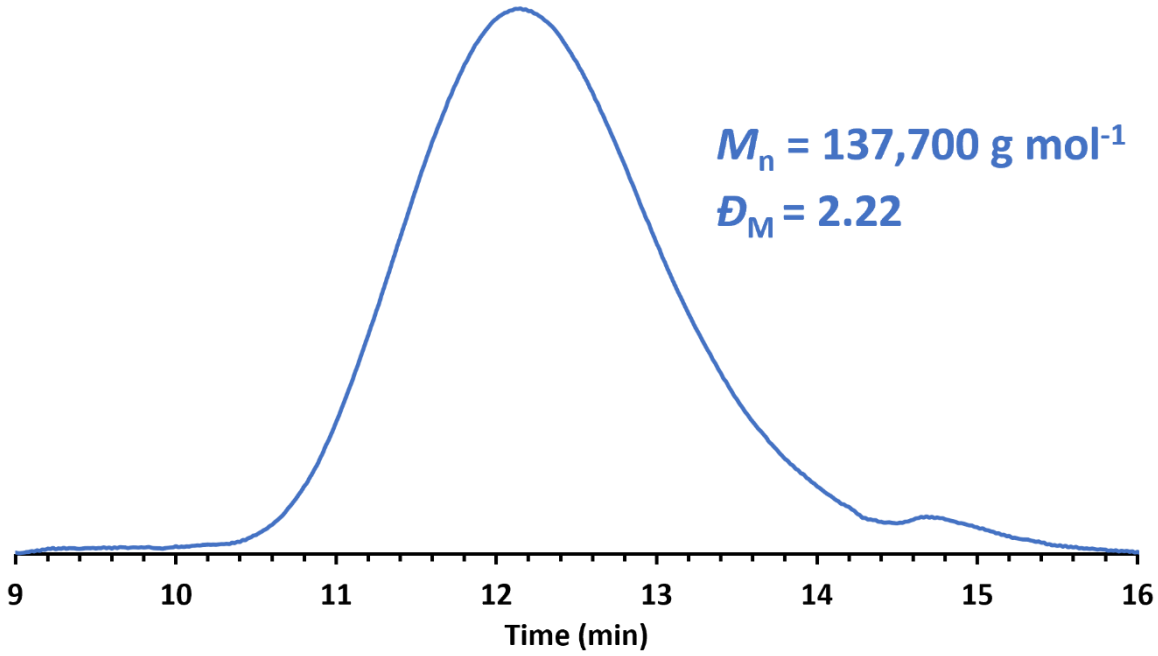

Figure 2.15. DMF GPC chromatogram obtained of poly(2-hydroxyethyl methacrylate) synthesised via free radical polymerisation of 2-hydroxyethyl methacrylate for 2 hours at 60 °C in methanol at 25% w/w solids.

As with the purification of PAA, ^{1}H NMR spectroscopic analysis indicated a successful synthesis of PHEMA but with residual HEMA monomer (Figure 2.14). Additionally, as seen with the GPC analysis of PDMA (Figure 2.13), the GPC data obtained for PHEMA (Figure 2.15) also showed a broader molecular weight distribution, indicated by the obtained dispersity ($Đ_M$ = 2.22). In all cases where polymer purification was challenging, there was also a higher degree of residual solvent content. Importantly, this may have adversely affected subsequent solubility screenings of the polymers.

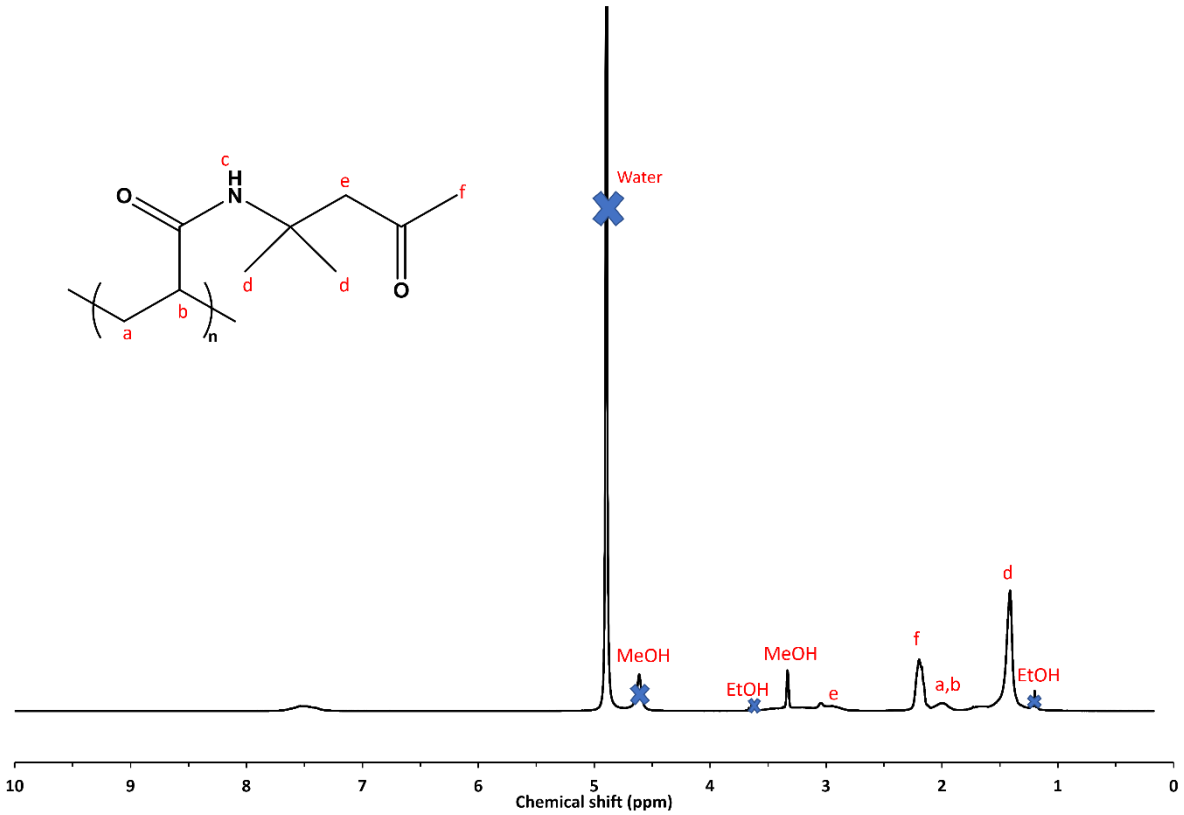

Figure 2.16. Assigned ^{1}H NMR spectrum of purified poly(diacetone acrylamide) in MeOD-d4.

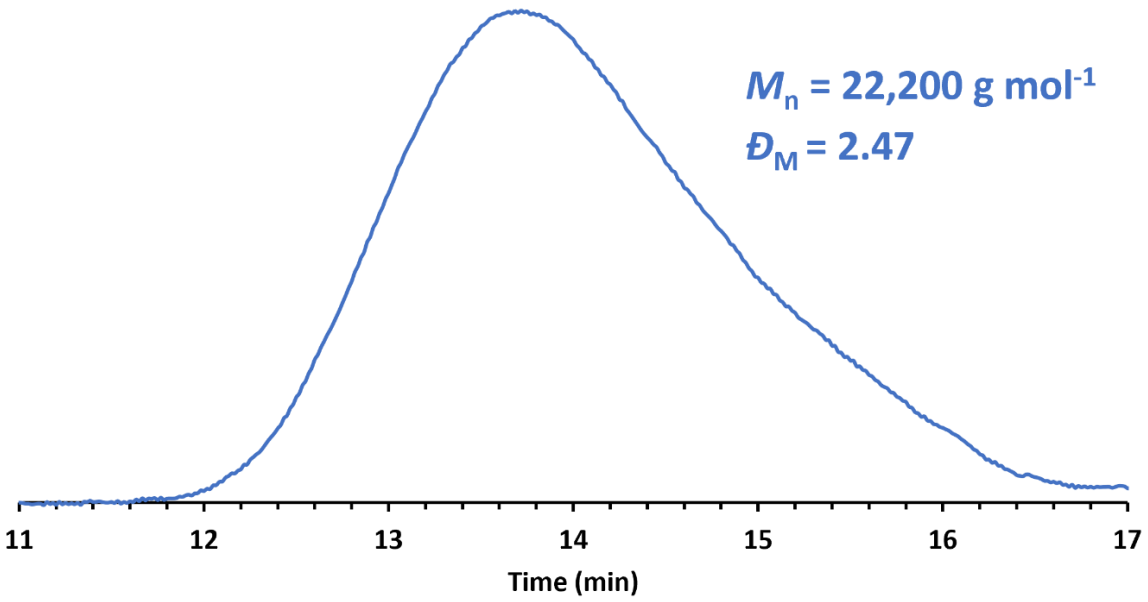

Figure 2.17. DMF GPC chromatogram obtained of poly(diacetone acrylamide) synthesised via free radical polymerisation of diacetone acrylamide for 2 hours at 60 °C in ethanol at 25% w/w solids.

^{1}H NMR analysis showed the success of the polymerisation of DAAM (Figure 2.16) as shown by the absence of vinyl monomer peaks, usually present between 5.5 and 6.0 ppm. Despite having some residual solvent peaks, they appear to comparably lower than those with more difficult purification processes. GPC analysis indicated success of polymer synthesis (Figure 2.17).

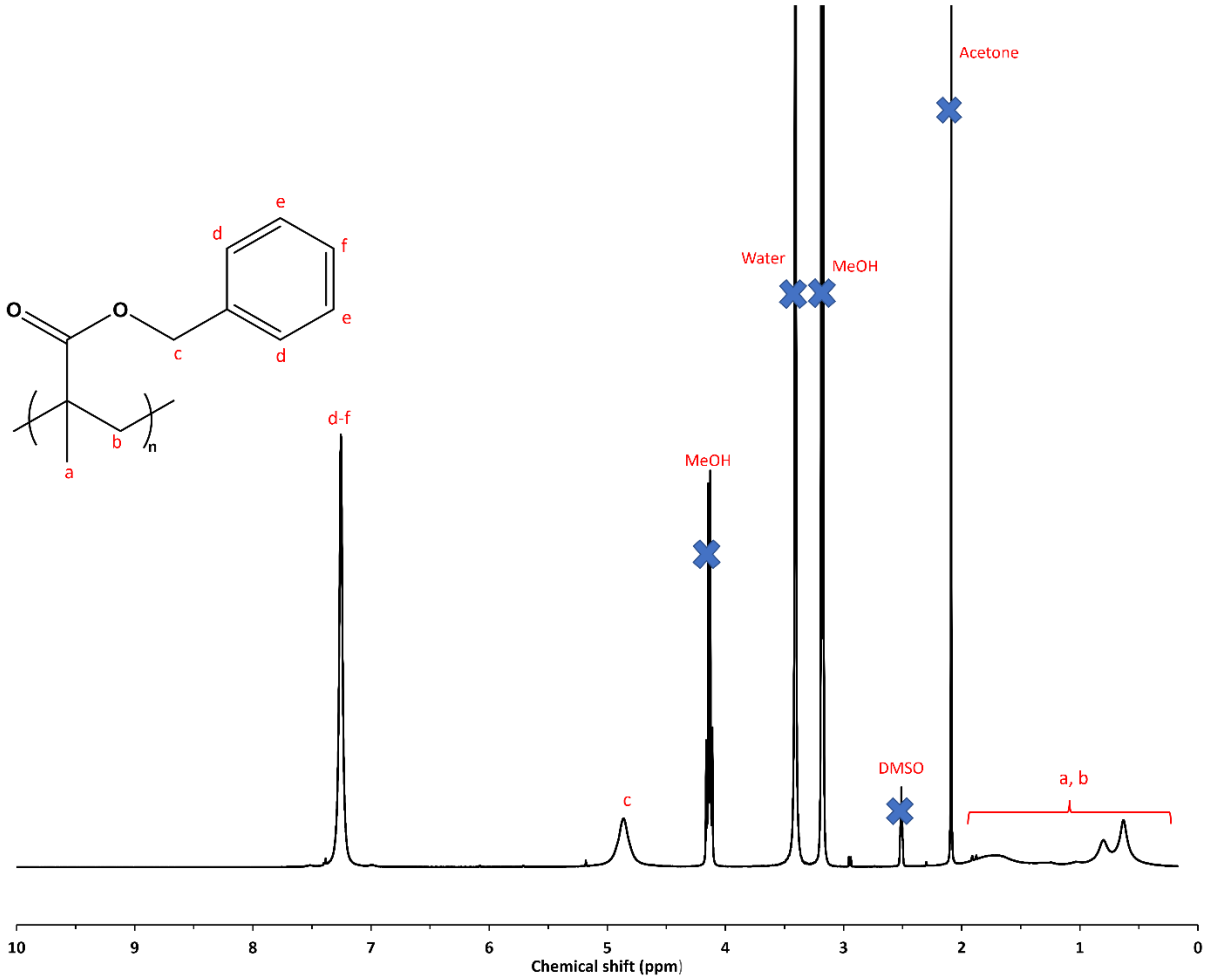

Figure 2.18. Assigned ^{1}H NMR spectrum of purified poly (benzyl methacrylate) in DMSO-d6.

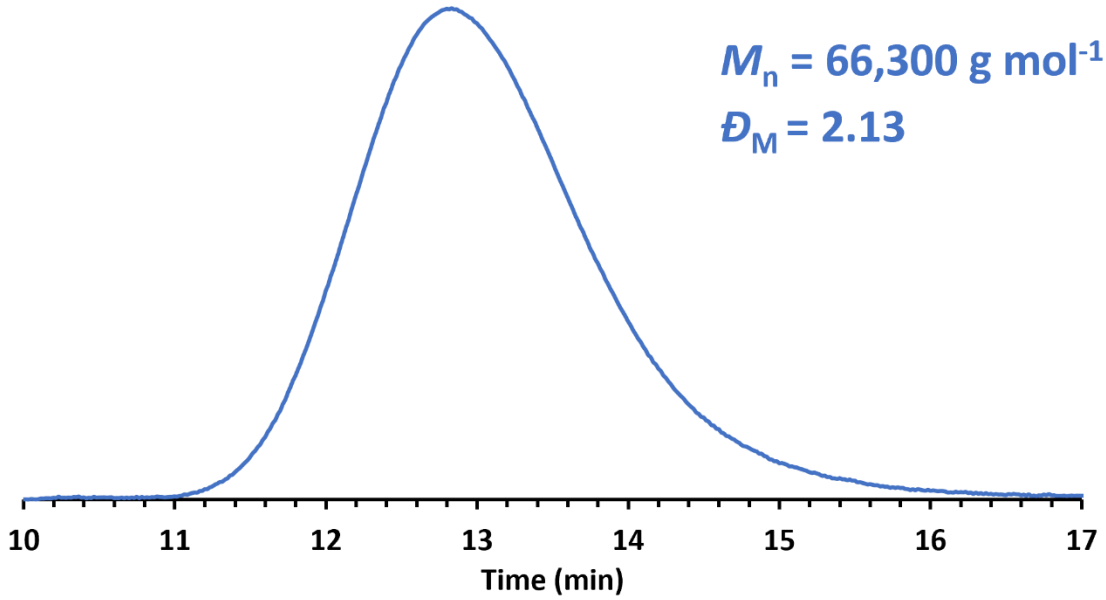

Figure 2.19. DMF GPC chromatogram obtained of poly(benzyl methacrylate) synthesised via free radical polymerisation of benzyl methacrylate for 2 hours at 60 °C in THF at 25% w/w solids.

Confirmation of successful synthesis and purification of PBzMA is shown in Figure 2.18, where no monomer peaks are observed. As with other polymers such as PDMA, PHEMA and PDAAM, broad molecular weight distribution for this polymer was demonstrated by the relatively high dispersity obtained by GPC analysis ($Đ_M$ = 2.13 in Figure 2.19).

2.3.3 Synthesis of macro-CTAs via RAFT solution polymerisation

A series of macro-CTAs were synthesised via RAFT solution polymerisation for the purpose of investigating their solubilities in [EMIM][DCA] and [EMIM][$EtOSO_3$]. This was conducted in addition to free radical polymerisations in order to assess the effect the RAFT end-group functionality on the ability of the given polymer to solubilise in the ILs. All macro-CTAs were synthesised with a target DP of 50 as future block copolymer syntheses would require a relatively short stabiliser block to yield worms. Furthermore, in order to be considered as a stabiliser block, it was necessary that the macro-CTAs synthesised were soluble in the ILs. All macro-CTAs were characterised by ^{1}H NMR spectroscopy (Figures 2.3-2.6) and GPC (Figures 2.20-2.23).

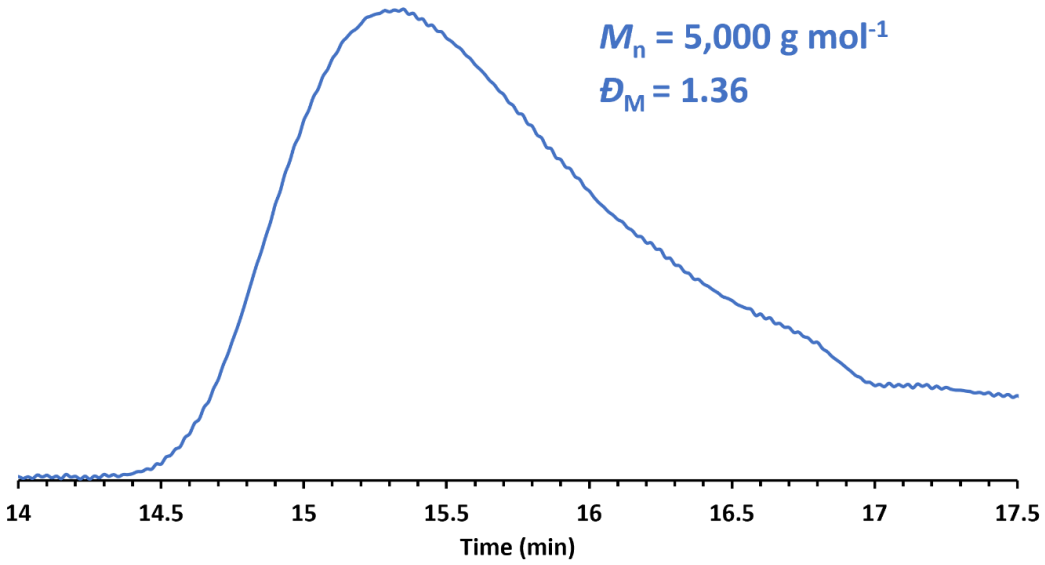

Figure 2.20. DMF GPC chromatogram obtained of poly(2-hydroxyethyl methacrylate) synthesised via RAFT solution polymerisation of 2-hydroxyethyl methacrylate for 6 hours at 70 °C in methanol at 40% w/w solids.

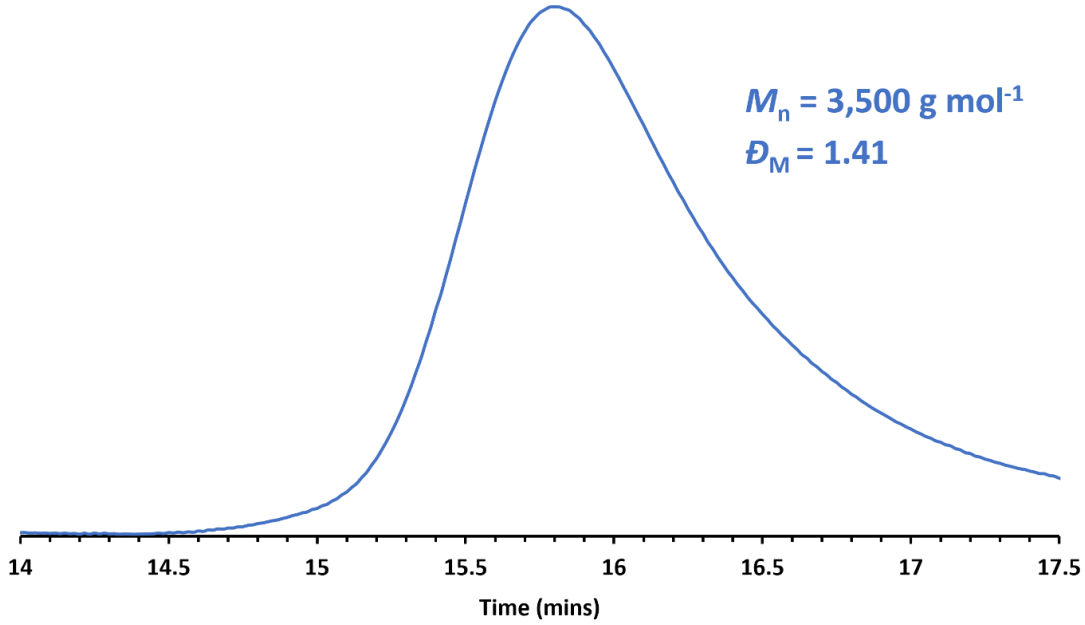

Figure 2.21. DMF GPC chromatogram obtained of poly(N,N-dimethylacrylamide) synthesised via RAFT solution polymerisation of N,N-dimethylacrylamide for 6 hours at 70 °C in ethanol at 70% w/w solids.

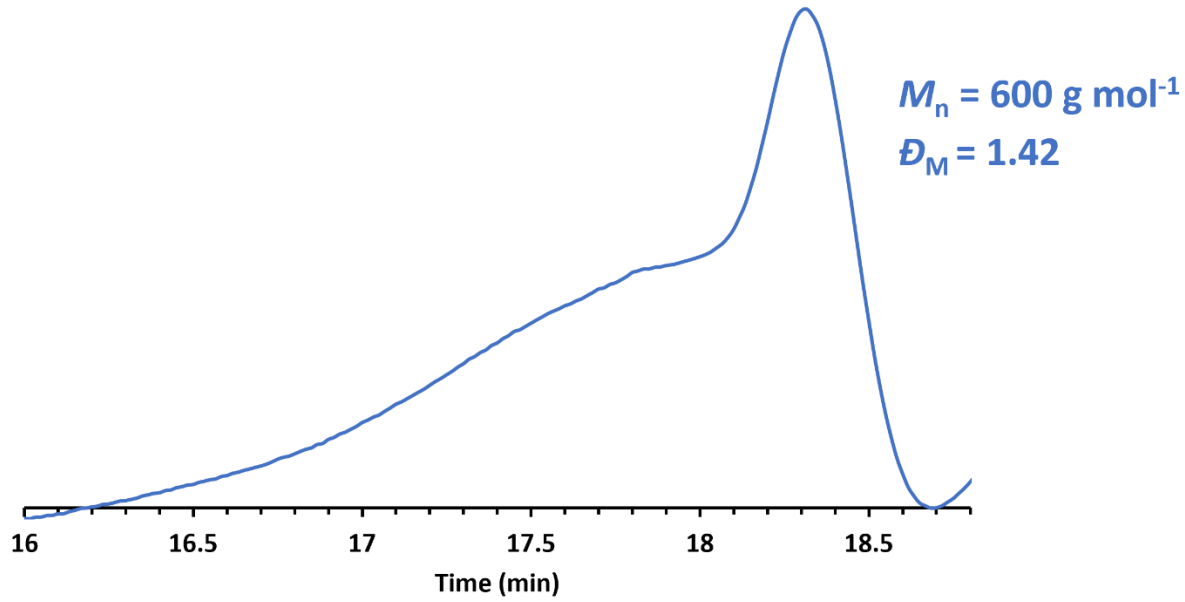

Figure 2.22. DMF GPC chromatogram obtained of poly(diacetone acrylamide) synthesised via RAFT solution polymerisation of diacetone acrylamide for 6 hours at 70 °C in methanol at 40% w/w solids.

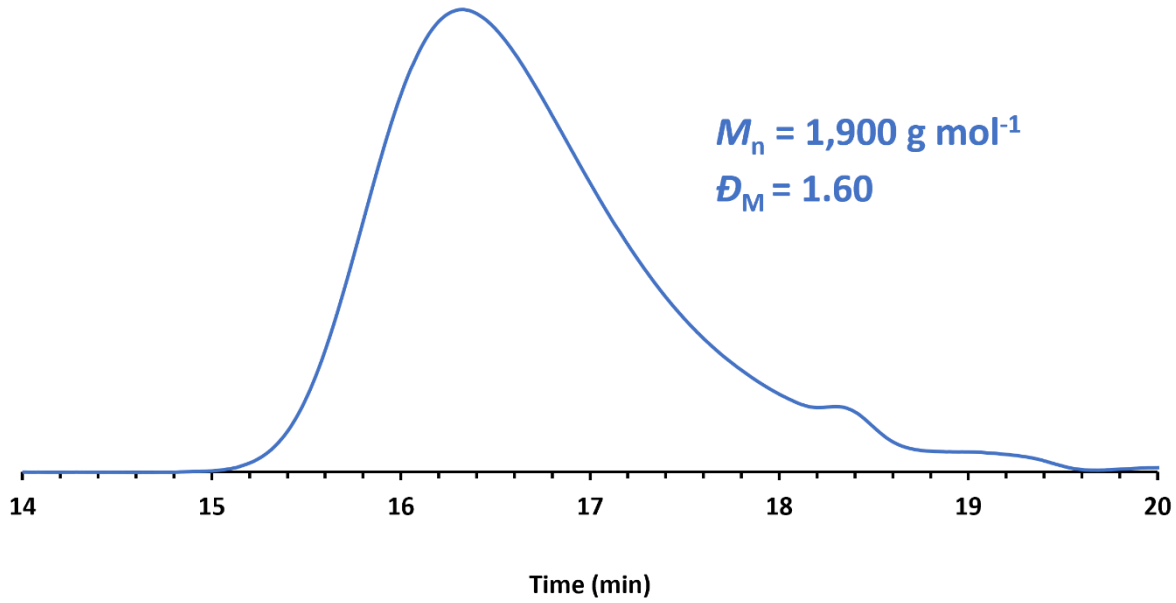

Figure 2.23. DMF GPC chromatogram obtained of poly(benzyl methacrylate) synthesised via RAFT solution polymerisation of benzyl methacrylate for 6 hours at 70 °C in THF at 40% w/w solids.

Table 2.3. Comparison of molecular weight and dispersity values of free radical homopolymers and their RAFT macro-CTA counterpart. All data presented is obtained via GPC analysis.

	Free radical homopolymer		Macro-CTA	
	M_n (g mol^{-1})	$Đ_M$	M_n (g mol^{-1})	$Đ_M$
PHEMA	137,700	2.22	5,000	1.36
PDMA	80,100	2.72	3,500	1.41
PDAAM	22,200	2.47	600	1.42
PBzMA	66,300	2.13	1,900	1.60

When synthesising the polymers via RAFT polymerisation, it is clear that the polymerisations were more controlled as confirmed by the relatively lower molecular weight (M_n) and dispersity of these polymers despite longer reaction time (6 hours for RAFT polymerisation, 2 hours for free radical polymerisation), as obtained by GPC analysis. For example, PHEMA synthesised via free radical polymerisation exhibited an M_n of 305,500 g mol^{-1}, which is substantially larger when compared to the PHEMA macro-CTA synthesised by RAFT polymerisation, which had an M_n of 5,000 g mol^{-1}. Furthermore, the dispersity of PHEMA formed via free radical polymerisation ($Đ_M$ = 2.22) was also noticeably higher than the RAFT-synthesised PHEMA macro-CTA ($Đ_M$ = 1.36). The difference between molecular weight and dispersity is observed in all the cases where a free radical homopolymer and macro-CTA were synthesised. (See Table 2.3)

2.3.4 Polymer solubility screenings in ionic liquids

A series of homopolymers synthesised by both free radical polymerisation and RAFT solution polymerisation was synthesised in order to assess their solubilities in two hydrophilic ILs, [EMIM][DCA] and [EMIM][$EtOSO_3$]. The homopolymers were added to the selected IL at 4.76% w/w solids and gently heated to 70 °C for up to 4 hours. This temperature was selected as this was the estimated temperature at which subsequent PISA syntheses would take place. The results from the solubility screenings of the homopolymers synthesised via free radical polymerisation is summarised in Table 2.4:

Table 2.4. Summary of solubility screenings conducted for homopolymers synthesised via free radical polymerisation. A tick indicates successful solubilisation into the corresponding IL, and a cross indicates insolubility.

	Solubility at room temperature		**Solubility at 70 °C**	
Polymer	**[EMIM][DCA]**	**[EMIM][$EtOSO_3$]**	**[EMIM][DCA]**	**[EMIM][$EtOSO_3$]**
PAA	×	×	✓	×
PMA	✓	✓	✓	✓
PHEMA	✓	×	✓	×
PDMA	✓	×	✓	×
PDAAM	×	×	×	×
PBzMA	×	×	×	×

Based on the findings of the free radical polymer solubility screenings, PAA was initially found to be insoluble in both ILs. Interestingly, when PAA was heated to 70 °C in [EMIM][DCA], the IL appeared to solubilise the polymer forming a free-flowing solution, however upon removing the solution from the oil bath, the solution became much more viscous and turbid, suggesting PAA was insoluble in [EMIM][DCA] at room temperature and therefore potentially displaying some thermoresponsive behaviour. Moreover, PAA was found to be insoluble in [EMIM][$EtOSO_3$]. However, the use of this polymer and [EMIM][$EtOSO_3$] for the generation of ionogels has been previously reported by Chen *et al.*[50] where AA was synthesised via free radical polymerisation with the aid of a crosslinker in the IL to yield stretchable ionogels. Based on this, it may be reasonable to assume that the inefficiency of the purification process of PAA could have had an adverse effect on the solubility in the [EMIM][$EtOSO_3$] in this research, and therefore was seen to be insoluble.

PDAAM and PBzMA appeared to be insoluble in both ILs up to 70 °C. Based on this, in addition to the miscibility of their respective monomers with these ILs, these polymers show promise as the core-forming block in block copolymer syntheses via RAFT dispersion polymerisation. In contrast, PMA was found to be soluble in both ILs up to 70 °C and therefore could be considered as an appropriate stabiliser block. Interestingly, PHEMA and PDMA were both found to be soluble in [EMIM][DCA] but insoluble in [EMIM][$EtOSO_3$]. This could potentially be due to these polymers having a higher affinity to [EMIM][DCA] relative to [EMIM][$EtOSO_3$] as a result of the former's relatively higher hydrophilicity and lower viscosity (14.6 cP for [EMIM][DCA], and 94.2 cP for [EMIM][$EtOSO_3$] at room temperature). Moreover, the comparatively lower viscosity of the [EMIM][DCA] may have resulted in the increased polymer affinity as a result of more efficient

solution mixing. Based on these observations, PHEMA and PDMA showed promise to be used as stabiliser blocks for PISA syntheses in [EMIM][DCA].

Further screenings were conducted for selected homopolymers, or macromolecular chain transfer agents (macro-CTAs) that were synthesised via RAFT solution polymerisation. The results for these screenings are summarised in Table 2.5 below:

Table 2.5. Summary of solubility screenings conducted for macro-CTAs synthesised via RAFT solution polymerisation. A tick indicates successful solubilisation into the corresponding IL, and a cross indicates insolubility.

	Solubility at room temperature		**Solubility at 70 °C**	
Polymer	**[EMIM][DCA]**	**[EMIM][$EtOSO_3$]**	**[EMIM][DCA]**	**[EMIM][$EtOSO_3$]**
PHEMA macro-CTA	✓	✓	✓	✓
PDMA macro-CTA	✓	✓	✓	✓
PDAAM macro-CTA	✓	×	✓	×
PBzMA macro-CTA	×	×	×	×

When synthesised via RAFT solution polymerisation, PHEMA was shown to be soluble in both ILs. This was also observed for PDMA, where both of these polymers were insoluble in [EMIM][$EtOSO_3$] as free radical homopolymers. This showed that the macro-CTAs formed had a higher affinity for the less hydrophilic IL than the free radical counterparts. The ability of [EMIM][DCA] to solubilise these macro-CTAs but not the homopolymers synthesised via free radical polymerisation is attributed to the more controlled RAFT polymerisation that yields a lower molecular weight polymer. For example, free-radical PHEMA homopolymer had a substantially larger molecular weight (M_n) of 137,000 g mol^{-1}, whereas the PHEMA macro-CTA had a molecular weight (M_n) of 5,000 g mol^{-1}. Also, it is much more likely that the macro-CTAs exhibit a more linear structure compared to the potentially crosslinked/branched structure formed during the uncontrolled free radical polymerisation. This is also reflected in the dispersities obtained for each polymer, where the macro-CTA dispersities were all shown to be comparably lower then the free radical polymers. These observations and results may be due to one, or both of the following: (i) the RAFT CTA functionality aids IL solubility; (ii) the much lower molecular weight of the macro-CTAs provides better IL solubility.

Overall, both of these polymers can in fact be considered as potential stabiliser blocks for subsequent RAFT dispersion polymerisations. Additionally, PDAAM was found to be soluble in [EMIM][DCA] when synthesised via RAFT solution polymerisation yet remained insoluble in [EMIM][$EtOSO_3$]. Thus, PDAAM could be considered as a potential stabiliser block or core-forming block in [EMIM][DCA] or [EMIM][$EtOSO_3$], respectively. This observation further shows the stronger affinity that [EMIM][DCA] has towards the solubilisation of this selection of polymers.

2.4 Conclusions

In summary, extensive preliminary work was conducted in order to design appropriate subsequent block copolymers. Firstly, miscibility screenings of monomers in two different ionic liquids, [EMIM][DCA] and [EMIM][$EtOSO_3$], were conducted in order to assess suitability of monomers should they be selected as forthcoming stabiliser or core-forming blocks. Ideally, they were required to be fully miscible with the ILs, most importantly for dispersion polymerisations when synthesising the block copolymers. This is because worm-like micelles have been reported to be more readily accessible via dispersion polymerisation as opposed to other polymerisation routes such as emulsion polymerisation. For this reason, monomers that were found to be immiscible with the ILs such as *n*-butyl methacrylate, *n*-propyl methacrylate and styrene were eliminated and no longer investigated for future use. Following on from miscibility screenings, polymers were then synthesised via free radical polymerisation, with varying degrees of success regarding polymer purification as judged by ^{1}H NMR spectroscopy, which may have adversely affected the solubility screening studies. Alongside this, a series of polymers were synthesised via RAFT solution polymerisation, which demonstrated that RAFT polymerisation provided enhanced control of the synthesis as expected, with narrower molecular weight distributions and lower molecular weight for each polymer being confirmed by GPC analysis. This was also reflected in the solubility screenings where some RAFT-synthesised polymers were soluble in the ILs, whereas their free radical counterparts were not, potentially due to branching or crosslinking. Those that were soluble in the ILs could be considered as future stabiliser blocks. On the other hand, those that were shown to be insoluble in the ILs could be considered as core-forming blocks for subsequent RAFT dispersion polymerisations, providing that the respective monomers were miscible with the ILs. Specifically, it was deduced that PBzMA was the most suitable as the core-forming block, given that it was insoluble in both ILs up to 70 °C, and BzMA monomer was miscible with the ILs. In contrast, PHEMA and PDMA could potentially be used as suitable stabiliser blocks, as their monomer were miscible with both ILs, and solubility studies showed that they were both soluble

in the ILs up to 70 °C. However, PHEMA was selected as the stabiliser block for forthcoming block copolymer syntheses as this particular polymer is able to chain extend with BzMA due to PHEMA's better leaving group ability as a macro-CTA as a result of greater steric stabilisation. PDMA in the form of a macro-CTA would comparatively be a poorer leaving group for chain extension using BzMA, there would be poorer control of the RAFT polymerisation during chain extension.[51] These studies enable the design of appropriate block copolymer syntheses via RAFT dispersion PISA that would increase the likelihood of generating worm gels.

2.5 References

1. S. K. Singh and A. W. Savoy, *J. Mol. Liq*, 2020, **297**, 112038.
2. R. Tamate, K. Hashimoto, T. Ueki and M. Watanabe, *Phys. Chem. Chem. Phys*, 2018, **20**, 25123-25139.
3. K. Ueno, H. Tokuda and M. Watanabe, *Phys. Chem. Chem. Phys*, 2010, **12**, 1649-1658.
4. G. Kaur, H. Kumar and M. Singla, *J. Mol. Liq*, 2022, **351**, 118556.
5. M. A. B. H. Susan, T. Kaneko, A. Noda and M. Watanabe, *J. Am. Chem. Soc*, 2005, **127**, 4976-4983.
6. A. Noda and M. Watanabe, *Electrochim. Acta*, 2000, **45**, 1265-1270.
7. S. Zhang, K. H. Lee, C. D. Frisbie and T. P. Lodge, *Macromolecules*, 2011, **44**, 940-949.
8. P. M. Simone and T. P. Lodge, *Macromol. Chem. Phys*, 2007, **208**, 339-348.
9. Y. He, Z. Li, P. Simone and T. P. Lodge, *J. Am. Chem. Soc*, 2006, **128**, 2745-2750.
10. Y. He, P. G. Boswell, P. Bühlmann and T. P. Lodge, *J. Phys. Chem. B*, 2007, **111**, 4645-4652.
11. A. Balducci, *Top. Curr. Chem*, 2017, **375**, 20.
12. X. Ma, J. Yu, Y. Hu, J. Texter and F. Yan, *Ind. Chem. Mater*, 2023, **1**, 39-59.
13. S. Rana, R. C. Thakur and H. S. Dosanjh, *Solid. State. Ion*, 2023, **400**, 116340.
14. R. A. Abu Talip, W. Z. Yahya and M. A. Bustam, *Sustainability*, 2020, **12**, 7598.
15. M. Gorlov and L. Kloo, *Dalton. Trans*, 2008, 2655-2666.
16. N. I. Mohd Faridz Hilmy, W. Z. N. Yahya and K. A. Kurnia, *J. Mol. Liq*, 2020, **320**, 114381.
17. K. Mishra, N. Devi, S. S. Siwal, Q. Zhang, W. F. Alsanie, F. Scarpa and V. K. Thakur, *Adv. Sci*, 2022, **9**, 2202187.
18. S. Al-Sodies, A. M. Asiri, A. Khan, K. A. Alamry and M. A. Hussein, *Eur. Polym. J*, 2024, **205**, 112719.
19. K. Mi, L. Tong, M. Yu, Y. Zhao, H. Dong and S. Hou, *Anal. Methods*, 2023, **15**, 3522-3531.
20. D. Wei and A. Ivaska, *Anal. Chim. Acta*, 2008, **607**, 126-135.
21. D. Weng, F. Xu, X. Li, S. Li, Y. Li and J. Sun, *ACS. Appl. Mater. Interfaces*, 2020, **12**, 57477-57485.
22. A. J. Greer, J. Jacquemin and C. Hardacre, *Molecules*, 2020, **25**, 5207.
23. M. J. Derry, L. A. Fielding and S. P. Armes, *Prog. Polym. Sci*, 2016, **52**, 1-18.
24. S. J. Byard, M. Williams, B. E. McKenzie, A. Blanazs and S. P. Armes, *Macromolecules*, 2017, **50**, 1482-1493.
25. A. A. Cockram, T. J. Neal, M. J. Derry, O. O. Mykhaylyk, N. S. J. Williams, M. W. Murray, S. N. Emmett and S. P. Armes, *Macromolecules*, 2017, **50**, 796-802.

26. J. R. Lovett, M. J. Derry, P. Yang, F. L. Hatton, N. J. Warren, Patrick W. Fowler and S. P. Armes, *Chem. Sci*, 2018, **9**, 7138-7144.
27. M. J. Derry, O. O. Mykhaylyk and S. P. Armes, *Soft Matter*, 2021, **17**, 8867-8876.
28. M. J. Derry, O. O. Mykhaylyk and S. P. Armes, *Angew. Chem. Int. Ed*, 2017, **56**, 1746-1750.
29. A. Blanazs, R. Verber, O. O. Mykhaylyk, A. J. Ryan, J. Z. Heath, C. W. I. Douglas and S. P. Armes, *J. Am. Chem. Soc*, 2012, **134**, 9741-9748.
30. I. Canton, N. J. Warren, A. Chahal, K. Amps, A. Wood, R. Weightman, E. Wang, H. Moore and S. P. Armes, *ACS Cent. Sci*, 2016, **2**, 65-74.
31. M. J. Derry, L. A. Fielding and S. P. Armes, *Polym. Chem*, 2015, **6**, 3054-3062.
32. S. Sugihara, A. Blanazs, S. P. Armes, A. J. Ryan and A. L. Lewis, *J. Am. Chem. Soc*, 2011, **133**, 15707-15713.
33. E. Raphael, M. J. Derry, M. Hippler and S. P. Armes, *Chem. Sci*, 2021, **12**, 12082-12091.
34. L. A. Fielding, J. A. Lane, M. J. Derry, O. O. Mykhaylyk and S. P. Armes, *J. Am. Chem. Soc*, 2014, **136**, 5790-5798.
35. C. György, T. J. Neal, T. Smith, D. J. Growney and S. P. Armes, *Macromolecules*, 2022, **55**, 4091-4101.
36. J. Zhou, W. Zhang, C. Hong and C. Pan, *Polym. Chem*, 2016, **7**, 3259-3267.
37. P. J. Docherty, C. Girou, M. J. Derry and S. P. Armes, *Polym. Chem*, 2020, **11**, 3332-3339.
38. S. J. Hunter, J. R. Lovett, O. O. Mykhaylyk, E. R. Jones and S. P. Armes, *Polym. Chem*, 2021, **12**, 3629-3639.
39. S. J. Hunter, N. J. W. Penfold, E. R. Jones, T. Zinn, O. O. Mykhaylyk and S. P. Armes, *Macromolecules*, 2022, **55**, 3051-3062.
40. W. Zhang, F. D'Agosto, P.-Y. Dugas, J. Rieger and B. Charleux, *Polymer*, 2013, **54**, 2011-2019.
41. S. Boissé, J. Rieger, K. Belal, A. Di-Cicco, P. Beaunier, M.-H. Li and B. Charleux, *Chem. Commun*, 2010, **46**, 1950-1952.
42. D. H. H. Chan, A. A. Cockram, R. R. Gibson, E. L. Kynaston, C. Lindsay, P. Taylor and S. P. Armes, *Polym. Chem*, 2021, **12**, 5760-5769.
43. I. Chaduc, M. Girod, R. Antoine, B. Charleux, F. D'Agosto and M. Lansalot, *Macromolecules*, 2012, **45**, 5881-5893.
44. V. J. Cunningham, A. M. Alswieleh, K. L. Thompson, M. Williams, G. J. Leggett, S. P. Armes and O. M. Musa, *Macromolecules*, 2014, **47**, 5613-5623.
45. F. L. Hatton, M. J. Derry and S. P. Armes, *Polym. Chem*, 2020, **11**, 6343-6355.
46. Y. Fang, H. Cheng, H. He, S. Wang, J. Li, S. Yue, L. Zhang, Z. Du and J. Ouyang, *Adv. Funct. Mater*, 2020, **30**, 2004699.
47. M. Yang, Y. Hu, X. Wang, H. Chen, J. Yu, W. Li, R. Li and F. Yan, *Adv. Mater*, 2024, **36**, 2312249.
48. Y. Yao, Y. Hui, Z. Wang, H. Chen, H. Zhu and N. Zhou, *Research*, 2023, **6**, 0104.
49. H. J. Hutchins-Crawford, P. Ninjiaranai, M. J. Derry, R. Molloy, B. J. Tighe and P. D. Topham, *Polym. Chem*, 2021, **12**, 4317-4325.
50. B. Chen, J. J. Lu, C. H. Yang, J. H. Yang, J. Zhou, Y. M. Chen and Z. Suo, *ACS Appl. Mater. Interfaces*, 2014, **6**, 7840-7845.
51. D. J. Keddie, *Chem. Soc. Rev*, 2014, **43**, 496-505.

3. Polymerisation-induced self-assembly in 1-ethyl-3-methylimidazolium dicyanamide: RAFT dispersion polymerisation of benzyl methacrylate

Reproduced in part with permission from [G. L. Maitland; M. Liu; T. J. Neal; J. Hammerton; Y. Han; S. D. Worrall; P. D. Topham; M. J. Derry, *Chemical Science*, **2024**, 15, 4416-4426

3.1 Introduction

Ionic liquids (ILs) are typically defined as liquid electrolytes, with melting points below 100 °C, solely comprising ions.[1, 2] Compared to many traditional organic solvents, ILs exhibit advantageous properties such as high ionic conductivity, good thermal stability and low vapour pressure.[3] Owing to the vast number of unique combinations of cations and anions, key physicochemical properties of ILs can be tailored for specific applications.[2, 4] Hence, ILs have been utilised for a diverse number of applications in electrochemistry, catalysis and analysis as well as being used as performance additives such as anti-static agents[5, 6] and dispersing agents.[4, 7, 8] Due to their low vapour pressure and high thermal stability, utilising ILs as electrolyte components in batteries can potentially address flammability issues associated with traditional organic solvent-based electrolytes.[2, 9] Of particular relevance to this work, ILs have been used to develop so-called polymeric ionogels,[10, 11] which are a class of gel electrolyte formed from the immobilisation of IL in a polymer matrix. Ionogels have been used in a range of electrochemical applications such as electrolytes in lithium-ion batteries, [12-18] dye-sensitized solar cells[19-22] and actuators[1, 23-25], and offer an alternative to liquid electrolytes thus significantly reducing the risk of potentially hazardous leakage.

There have been several different approaches reported that use polymers to prepare ionogels. Generally, physically crosslinked or chemically crosslinked ionogels can be generated depending on the preparation method.[26, 27] For example, chemically crosslinked ionogels can be prepared by (i) the polymerisation of vinyl monomers in an IL with the addition of a crosslinker to immobilise the IL[16, 28-32] or (ii) utilising poly(ionic liquids).[33-36] In contrast, physically crosslinked ionogels have been prepared utilising (i) hydrogen bonding,[37-40] (ii) ion-dipole interactions,[39] (iii) the self-assembly of block copolymers[9-11, 41-43] or random copolymers[44] in an IL with the aid of a co-solvent. Over the past few decades, reversible addition-fragmentation chain transfer (RAFT) polymerisation has emerged as a popular method of reversible deactivation radical polymerisation (RDRP) to generate an extensive range of functional, well-defined diblock copolymers.[45] Exploiting its versatility, RAFT-mediated polymerisation-induced self-assembly (PISA)[46-49] has been demonstrated as a convenient tool to synthesise block copolymer nanoparticles in a range of media such as alcohols[50-52], non-polar solvents[53-55] and water[56-61]. PISA has many advantages over traditional block copolymer self-assembly methods, for example it can be conducted at high copolymer concentrations (up to 50% w/w)[62, 63] and does not require post-polymerisation processing steps such as solvent/pH switching and film rehydration.[56, 64] In a typical PISA reaction, a soluble macromolecular chain transfer agent (macro-CTA, i.e. the stabilizer block) is chain

extended using a monomer that polymerises to form an insoluble block, resulting in the formation of nanoparticles comprising amphiphilic AB diblock copolymer chains.[65] PISA can be conducted under dispersion or emulsion conditions, depending on whether the monomer that is polymerised to form the insoluble structure-directing block is miscible (dispersion)[46, 54, 65-67] or immiscible (emulsion).[68, 69]

To date, there have been very few reports of PISA being conducted in IL. Zhang and Zhu[3] reported the synthesis of a series of diblock copolymers via RAFT dispersion polymerisation in a relatively hydrophobic IL, 1-butyl-3-methylimidazolium hexafluorophosphate ([BMIM][PF_6]), whereby a functionalised poly(ethylene glycol) macro-CTA was chain extended using three different monomers (2-hydroxyethyl methacrylate, styrene or *n*-butyl methacrylate). This seminal work demonstrated the potential for preparing dispersions of functional block copolymer nanoparticles in IL via convenient PISA protocols, however only isotropic nanoparticles (spheres or vesicles) were successfully obtained as confirmed by transmission electron microscopy (TEM) studies. We do note one instance in this study where the formation of so-called 'rod-like aggregates' or 'stretched vesicles' species was demonstrated, however these anisotropic objects were only present as a minor population. Similarly, Zhou *et al.*[70] reported the preparation of poly(ethylene glycol)-*b*-polystyrene (PEG-*b*-PS) nanospheres and vesicles via RAFT dispersion polymerisation in [BMIM][PF_6]. In this further study, the same PEG-*b*-PS block copolymer was also synthesised via alcoholic PISA in order to assess the effect of solvent choice on polymerisation kinetics. It was demonstrated that block copolymer synthesis conducted in this IL was faster: 95% monomer conversion was achieved within 12 hours in [BMIM][PF_6] compared to only 20% and 65% within the same time frame for reactions conducted in methanol and a methanol/water mixture, respectively. Demarteau *et al.*[71] reported the synthesis of poly(ionic liquid)-containing block copolymers via aqueous emulsion PISA, yielding spherical particles with diameters >300 nm as confirmed by TEM analysis. Specifically, the hydrophilic IL diallyl dimethylammonium chloride (DADMAC) was functionalised to form mono- and di- functional poly(diallyl dimethylammonium chloride) (PDADMAC) macro-CTAs that were subsequently used to prepare di- and triblock copolymers via RAFT aqueous emulsion polymerisation of styrene to yield spherical polyelectrolyte latex particles. Ionogel membranes were prepared in this previous study via post-polymerisation formulation, where the particles dispersed in aqueous medium were mixed with ionic liquid electrolyte with the aid of toluene co-solvent for 10 hours before being casted onto Teflon.

Despite PISA formulations being developed in ILs, there have been no reports of a system that yields worm-like micelles, which typically occupy phase space where the degree of polymerisation of the structure-directing block lies between those for spherical micelles and vesicles.[62] Worm-like micelles provide a route to soft gel materials at lower copolymer concentrations (≥3% w/w)[72] than the polymer concentrations typically required for ionogel preparation (up to 10% w/w).[11] Whilst there have been recent advances in this area, developing PISA formulations that provide access to worm gels in ILs would represent a much more facile route to functional ionogel materials using straightforward synthesis and preparation routes without the need for post-polymerisation processing or purification.

Herein, for the first time, a RAFT-PISA formulation that yields diblock copolymer spheres, worms and vesicles in IL is described. Specifically, poly(2-hydroxyethyl methacrylate)-*b*-poly(benzyl methacrylate) (PHEMA-*b*-PBzMA) block copolymer nanoparticles were synthesised via RAFT dispersion polymerisation in 1-ethyl-3-methylimidazolium dicyanamide ([EMIM][DCA]) (Scheme 3.1). PHEMA was selected as the stabiliser block for this system as a result of successful solubility screenings carried out in Chapter 2, that indicated PHEMA was soluble in [EMIM][DCA] up to 70 °C and 10% w/w solids concentration. Additionally, solubility screenings conducted on PBzMA homopolymer in Chapter 2 indicated suitability of its use as a core-forming block in a potential PISA system in [EMIM][DCA]. Detailed characterisation of the block copolymer nanoparticles was conducted, including ^{1}H nuclear magnetic resonance (NMR) spectroscopy, gel permeation chromatography (GPC), dynamic light scattering (DLS), transmission electron microscopy (TEM), small-angle X-ray scattering (SAXS), oscillatory rheology, thermogravimetric analysis (TGA) and electrochemical impedance spectroscopy (EIS). For the first time, this new PISA formulation facilitates the *in situ* formation of self-standing worm ionogel electrolyte materials at copolymer concentrations >4% w/w via efficient and convenient synthesis routes without the need for organic co-solvents, crosslinkers, post-polymerisation processing or purification. Importantly, we demonstrate that the worm ionogels developed in this work exhibit comparable electrochemical properties to that of the ionic liquid alone, showcasing their potential as gel electrolytes.

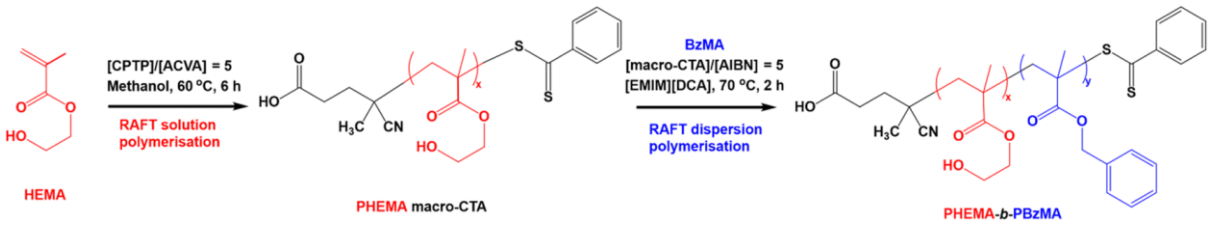

Scheme 3.1. Synthesis of poly(2-hydroxymethacrylate) (PHEMA) macro-CTA via RAFT solution polymerisation in methanol at 60 °C, followed by RAFT dispersion polymerisation of benzyl methacrylate (BzMA) in 1-ethyl-3-methylimidazolium dicyanamide ([EMIM][DCA]) at 70 °C to yield PHEMA-*b*-PBzMA diblock copolymers.

3.2 Experimental

3.2.1 Materials

2-Hydroxyethyl methacrylate (HEMA) and benzyl methacrylate (BzMA) were purchased from Sigma Aldrich and passed through a basic alumina column prior to use in order to remove the inhibitor. 2,2'-Azobisisobutyronitrile (AIBN) was purchased from Molekula and was recrystallised from methanol prior to use. 4-Cyano-4-(phenylcarbonothioylthio) pentanoic acid (CPTP) RAFT agent was purchased from Sigma Aldrich and used as received. Reagent grade methanol and diethyl ether were purchased from Fisher Scientific. Dimethyl sulfoxide-d6 and methanol-d4 for ^{1}H NMR analysis were purchased from Goss Scientific. 1-Ethyl-3-methylimidazolium dicyanamide [EMIM][DCA] was acquired from BASF.

3.2.2 ^{1}H Nuclear magnetic resonance (NMR) spectroscopy

^{1}H NMR spectra were obtained in either MeOD-d4 or DMSO-d6 using a Bruker Avance Neo 300 MHz spectrometer. Both crude and pure samples were prepared by dissolving approximately 40 mg of sample in 0.7 mL of appropriate deuterated solvent. Typically, 16 scans were averaged per spectrum and all chemical shifts are expressed in ppm. ^{1}H NMR spectra were referenced using peaks present as a result of residual solvent.

3.2.3 Gel permeation chromatography (GPC)

Molecular weight distributions were obtained by using an Agilent Infinity II multi-detector gel permeation chromatography (GPC) instrument comprising a guard column and two PL gel mixed-C columns. The mobile phase contained 0.10% w/v LiBr in HPLC grade DMF and the flow rate was fixed at 1 mL min^{-1} at 80 °C. The GPC was calibrated using near-monodispersed poly(methyl methacrylate) standards (M_p range = 535-1,591,000 g mol^{-1}).

3.2.4 Dynamic light scattering (DLS)

Dynamic light scattering (DLS) studies were conducted using a Zetasizer Nano ZS instrument (Malvern Panalytical, UK) at a fixed scattering angle of 173°. The block copolymer dispersions were diluted in [EMIM][DCA] (Refractive index = 1.51 as determined by Soriano *et al*.[73], viscosity = 14.6 cP) to 0.10% w/w prior to light scattering studies at 25 °C. The polydispersity index (PDI) and average diameter (*D*) were calculated, and data were averaged over three sets of approximately thirteen runs each of 30 seconds duration.

3.2.5 Transmission electron microscopy (TEM)

Bright field transmission electron microscopy (TEM) studies were conducted using a JEOL2100 instrument operating at 200 kV. Prior to analysis, block copolymer dispersions were diluted with [EMIM][DCA] to 0.15% w/w, placed on carbon-coated copper grids, blotted using filter paper and allowed to dry overnight, following a previously reported protocol.[74] No staining agent was required.

3.2.6 Small-angle X-ray scattering (SAXS)

Small-angle X-ray scattering (SAXS) patterns were recorded for 1.0% w/w copolymer dispersions in [EMIM][DCA] in 1.5 mm diameter polycarbonate capillaries at a synchrotron source (beamline B21[75], Diamond Light Source, UK) using monochromatic X-ray radiation (X-ray wavelength λ = 0.9408 Å, sample-to-detector distance of 3.712 m corresponding to scattering vector *q* ranging from 0.0045 to 0.34 $Å^{-1}$) and an EigerX 4M detector (Dectris, Switzerland). Scattering data were reduced using standard protocols from the beamline and were further analyzed using Irena SAS macros for Igor Pro[76]. Background-subtracted SAXS data were fitted to an appropriate model (or a combination models when a mixed phase is observed): (i) Gaussian chains[77], (ii) spherical micelles[78], (iii) worm-like micelles[78], (iv) vesicles.[79]

3.2.7 Helium pycnometry

The solid-state density of $PHEMA_{30}$ macro-CTA was determined using a Micromeritics AccuPyc II 1345 pycnometer at 20 °C using a 1 cm^3 cup. The instrument was calibrated using a 0.718537 cm^3 ball bearing calibrant. The reported value was an average of 10 measurements. The solid-state density of PBzMA was previously determined using helium pycnometry to be 1.15 g cm^{-3}. [80]

3.2.8 Synthesis of poly(2-hydroxyethyl methacrylate) (PHEMA) macromolecular chain transfer agent (macro-CTA) via RAFT solution polymerisation

The synthesis of the $PHEMA_{30}$ macro-CTA at 50% w/w solids was conducted as follows. A 100 mL round-bottomed flask was charged with 2-hydroxyethyl methacrylate (HEMA; 20 g; 154 mmol), 4-cyano-4-(phenylcarbonothioylthio)pentanoic acid (CPTP; 0.859 g; 3.0 mmol), 2,2'-azobisisobutyronitrile (AIBN; 100.9 mg; 615 µmol; CPTP/AIBN molar ratio = 5) and methanol (21 g). The sealed reaction flask was purged with nitrogen for 30 minutes prior to being placed in a preheated oil bath at 60 °C and stirred for 6 hours. The resulting PHEMA (Figure 3.1) (HEMA conversion = 40%; M_n = 8,000 g mol^{-1}, $Đ_M = M_w/M_n$ = 1.25) was purified by twice precipitating into a ten-fold excess of diethyl ether and dried on a rotary evaporator until all solvent was removed as judged by ^{1}H NMR spectroscopy (see Figure 3.2). The resulting PHEMA macro-CTA was obtained as a pink solid.

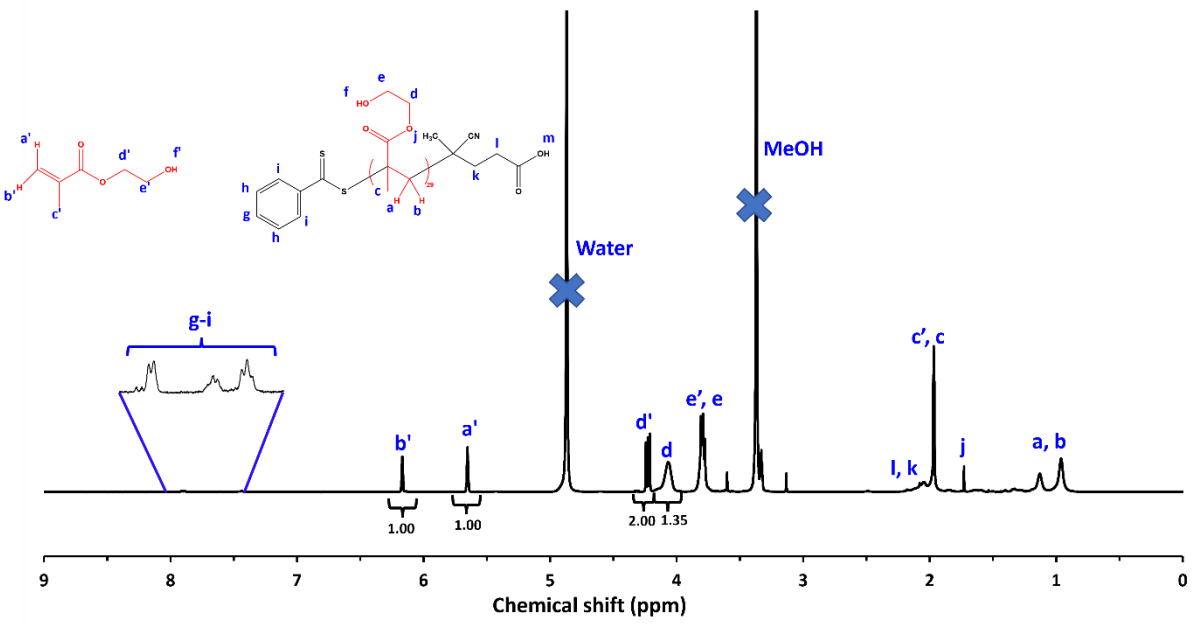

Figure 3.1. Assigned ^{1}H NMR spectrum of crude PHEMA macro-CTA in MeOH-d_4.

$$I_m = [Integral\ (d')] = 2H \qquad 3.1$$

$$I_p = [Integral\ (d)] \qquad 3.2$$

$$\% \text{ Conversion} = \frac{I_p}{I_m + I_p} \times 100\% = \frac{1.35}{2.00 + 1.35} \times 100\% = \mathbf{40\%} \qquad 3.3$$

The mean degree of polymerisation (DP) of this macro-CTA was calculated to be 30 using ^{1}H NMR spectroscopy by comparing the integrated signals corresponding to the five CPTP aromatic protons at 7.2-8.0 ppm relative to the peak at 4.0-4.1 ppm corresponding to the two oxymethylene protons of PHEMA (see Figure 3.2). Thus the CTA efficiency of the CPTP RAFT agent was estimated to be 67% (see Equation 3.6).

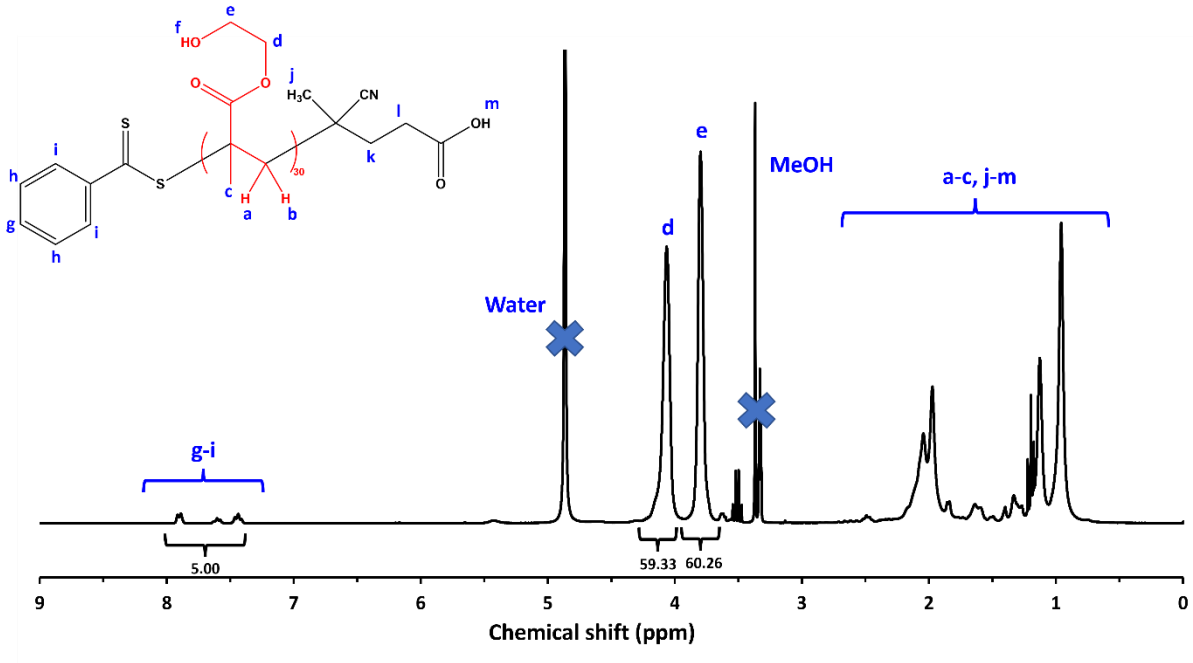

Figure 3.2. Assigned ^{1}H NMR spectrum of purified $PHEMA_{30}$ macro-CTA in MeOH-d_4.

The degree of polymerisation (DP) of the PHEMA macro-CTA and the CTA efficiency was calculated using the following equations:

$$[\text{Integral (g-i)}] = 5H \qquad 3.4$$

$$\text{PHEMA DP} = \frac{[Integral\ (d)]}{2} = \frac{59.33}{2} = \mathbf{30} \qquad 3.5$$

$$\%\ CTA\ efficiency = \frac{Target\ DP\ x\ NMR\ conversion}{Actual\ PHEMA\ DP}\ x\ 100 \qquad 3.6$$

3.2.9 Synthesis of poly(2-hydroxyethyl methacrylate)-*block*-poly(benzyl methacrylate) (PHEMA-*b*-PBzMA) diblock copolymer via RAFT dispersion polymerisation in 1-ethyl-3-methylimidazolium dicyanamide ([EMIM][DCA])

A typical RAFT dispersion polymerisation for the synthesis of $PHEMA_{30}$-$PBzMA_{291}$ at 15% w/w solids was conducted as follows. Benzyl methacrylate (BzMA; 0.52 g; 2.96 mmol), 2,2'-azobisisobutyronitrile (AIBN; 0.3 mg; 1.97 µmol), $PHEMA_{30}$ macro-CTA (0.04 g; 9.87 µmol; macro-CTA/initiator molar ratio = 5; PBzMA target degree of polymerisation = 300) and 1-ethyl-3-methylimidazolium dicyanamide ([EMIM][DCA]; 3.18 g) were added to a 14 mL sample vial. The sealed reaction mixture was purged with nitrogen for 30 minutes prior to being placed in a preheated oil bath at 70 °C whilst stirring for 2 hours (BzMA conversion = 98%; M_n = 52,900 g mol^{-1}, $Đ_M$ = 1.35).

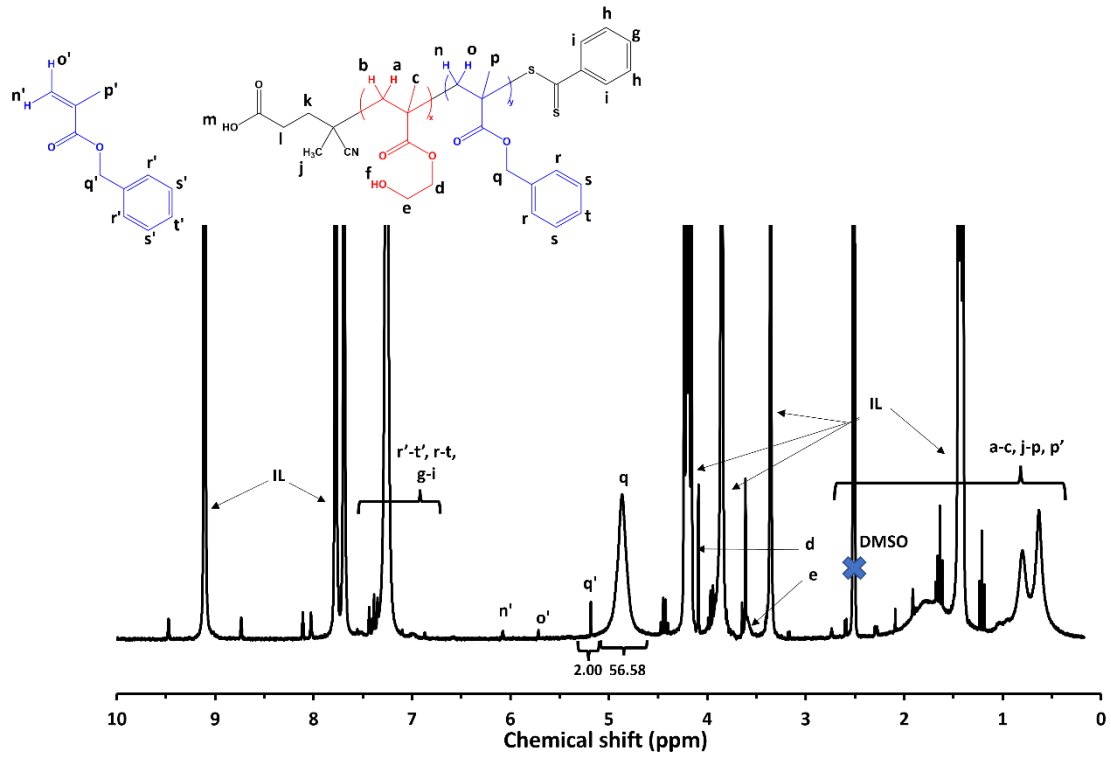

Figure 3.3. Assigned representative ^{1}H NMR spectrum of crude $PHEMA_{30}$-*b*-$PBzMA_y$ in DMSO-d_6.

Example calculation:

I_m = [Integral (q')] = 2H *3.6*

I_p = [Integral (q)] *3.7*

$$\% \text{ Conversion} = \frac{I_p}{I_m + I_p} \times 100\% = \frac{56.58}{2.00 + 56.58} \times 100\% = \mathbf{97\%} \quad 3.8$$

3.3 Results and discussion

3.3.1 Synthesis of PHEMA macro-CTA

A PHEMA macromolecular chain transfer agent (macro-CTA) with a mean degree of polymerisation (DP) of 30 was synthesised via RAFT solution polymerisation in methanol at 60 °C using 4-cyano-4-(phenylcarbonothioylthio)pentanoic acid (CPTP) as a chain transfer agent (Scheme 3.1). Commonly in macro-CTA syntheses, polymerisations are quenched before reaching high (≥ 80%) monomer conversion in order to retain RAFT end groups by avoiding monomer-starved conditions,[81] thus enabling high blocking efficiencies in subsequent block copolymer syntheses. In this study, the RAFT solution polymerisation of HEMA was quenched after 6 hours, affording a monomer conversion of 40% as judged by ^{1}H NMR spectroscopy (Figure 3.1). This yielded a relatively short PHEMA$_{30}$ macro-CTA stabiliser block, which is often favourable for the proceeding PISA syntheses when targeting higher order nanoparticle morphologies (i.e. worms and vesicles).[82] The retention of RAFT end groups was confirmed by the ^{1}H NMR spectrum of the purified macro-CTA by presence of the aromatic protons within the Z-group of the RAFT agent (see Figure 3.2). The synthesised PHEMA$_{30}$ macro-CTA exhibited a relatively narrow molecular weight distribution ($Đ_M$ = 1.25), indicating that this RAFT solution polymerisation of HEMA was well-controlled. Additionally, helium pycnometry measurements indicated a solid-state PHEMA$_{30}$ density of 1.26 g cm^{-3}, which is in good agreement with previously reported values.[83]

3.3.2 Synthesis and characterisation of PHEMA-*b*-PBzMA block copolymers in [EMIM][DCA]

A representative kinetic study of the chain extension of PHEMA$_{30}$ with benzyl methacrylate (BzMA) in [EMIM][DCA] at 70 °C and 15% w/w solids was conducted when targeting a PBzMA DP of 300

(Figure 3.4). Aliquots from the reaction solution were taken at 5 minute intervals during the first hour, then every 10 minutes thereafter to monitor the polymerisation kinetics. An induction period up to 25 minutes is observed, followed by a relatively slow rate of polymerisation up to 60 minutes, as is common for RAFT solution polymerisation (i.e. where block copolymer chains are fully soluble). After 60 minutes, a significant rate enhancement was observed, which typically indicates the onset of micellar nucleation where a critical length of the solvophobic block is reached, above which the propagating block becomes insoluble. This rate enhancement arises due to the preferential migration of unreacted monomer into the nanoparticle cores within which the polymerisation proceeds, thus providing a higher effective local monomer concentration at the site of polymerisation.[62, 84] At 120 minutes, monomer conversion reached 90%. In the present PISA formulation, the critical PBzMA DP for the assembly of $PHEMA_{30}$-*b*-$PBzMA_y$ nanoparticles during PISA in [EMIM][DCA] was determined to be 72. At this critical point in the PISA synthesis (when BzMA monomer conversion reaches 24%), the observed rate of polymerisation increased by a factor of approximately 6 (Figure 3.4a). GPC data obtained showed good control over the as judged by the low mass dispersities throughout and linear evolution of molecular weight with monomer conversion (Figure 3.4b). Additionally, GPC traces confirm efficient chain extension of the $PHEMA_{30}$ macro-CTA during the RAFT dispersion polymerisation of benzyl methacrylate in [EMIM][DCA] (Figure 3.4c).

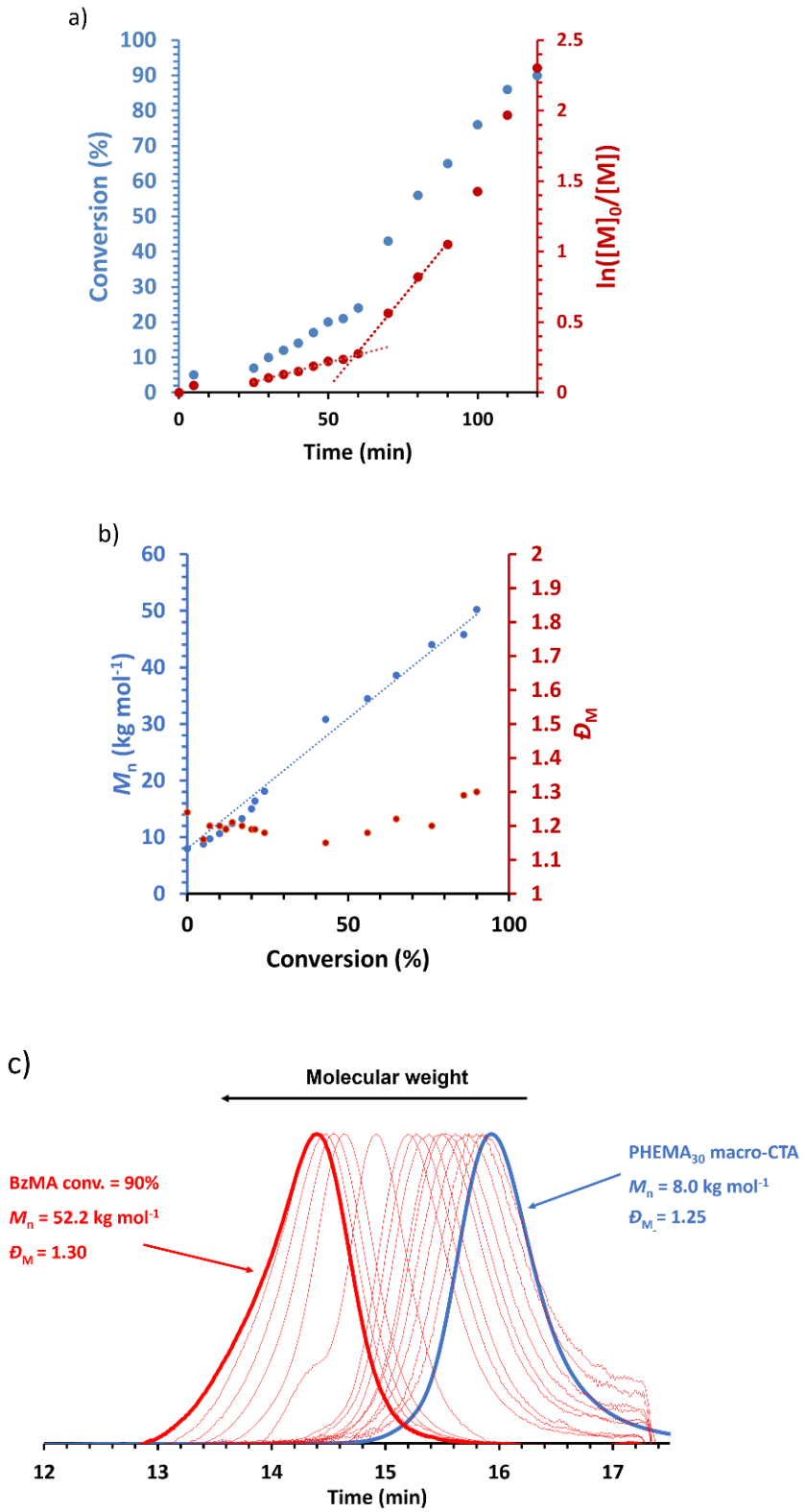

Figure 3.4. Kinetic study for the RAFT dispersion polymerisation of BzMA (target PBzMA DP = 300) in [EMIM][DCA] at 15% w/w solids using a $PHEMA_{30}$ macro-CTA: a) BzMA conversion vs. time (blue data) and semi-log kinetic (red data) plots; b) M_n and $Đ_M$ vs. BzMA conversion. Dashed blue line indicates linear progression of molar mass growth; c) DMF GPC chromatograms of aliquots taken during the reaction where the growth of molecular weight is indicated by a shift to the left over time. GPC data was obtained against poly(methyl methacrylate) standards.

Following this kinetic study, the optimum polymerisation time for complete monomer conversion was identified as 2 hours. Thus, a series of $PHEMA_{30}$-*b*-$PBzMA_y$ block copolymers at 15% w/w with varying target DPs of the core-forming PBzMA block (i.e. 'y' values) was synthesised (Table 3.1 and Figure 3.5). Importantly, high monomer conversions (≥96%) were obtained for all syntheses as determined by ^{1}H NMR spectroscopy. The determination of the PBzMA DP was not possible by end-group analysis via ^{1}H NMR spectroscopy analysis as a result of the region in which the aromatic protons appearing in the spectra (7.2-8.0 ppm) being crowded with additional peaks attributed to protons present in the IL (Figure 3.3). Therefore, the actual PBzMA DP was calculated by multiplying the BzMA monomer conversion by the targeted PBzMA DP. A range of dispersions were formed (Figure 3.5), with initial observations indicating that varying morphologies were synthesised based on comparisons to previous PISA formulations.[80] Transparent fluids formed at lower PBzMA DPs typically indicate the presence of either dissolved polymer chains (i.e. no PISA occurred) or spheres. Dispersions of $PHEMA_{30}$-*b*-$PBzMA_y$ where y = 233-317 yielded free-standing gels, suggesting the formation of worm-like nanoparticles that can form an extended percolating gel network.[72] Beyond this gel phase, turbid free-flowing solutions at higher PBzMA DPs (>330) are characteristic of the presence of vesicles.

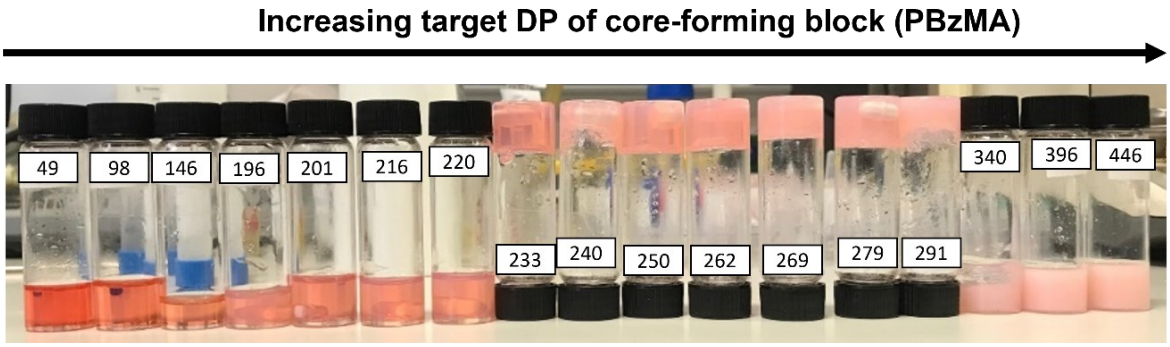

Figure 3.5. Digital image showing the physical appearance of the series of $PHEMA_{30}$-b-$PBzMA_y$ block copolymer dispersions in [EMIM][DCA] at 15% w/w solids. Number labels on sample vials denote the actual PBzMA core-forming block DP, as determined using ^{1}H NMR spectroscopy. Inverted sample vials indicate free-standing gels.

Table 3.1. Summary of targeted copolymer composition, BzMA conversion, actual copolymer composition, GPC M_n and $Đ_M$ (= M_w/M_n), and DLS diameter and PDI for the series of $PHEMA_{30}$-*b*-$PBzMA_y$ diblock copolymers prepared by RAFT dispersion polymerisation of BzMA in [EMIM][DCA] at 70 °C and 15% w/w, using AIBN initiator ([$PHEMA_{30}$ macro-CTA]/[AIBN] molar ratio = 5.0). $PHEMA_{30}$-*b*-$PBzMA_y$ is denoted as H_{30}-B_y for brevity.

		^{1}H NMR spectroscopy		DMF GPC		DLS	
Target composition	**BzMA conversion (%)**	**Actual composition**	$M_{n,th}$ (g mol^{-1})	M_n (g mol^{-1})	$Đ_M$	**Diameter (nm)**	**PDI**
H_{30}	-	H_{30}	4,184	8,000	1.24	-	-
H_{30}-B_{50}	97	H_{30}-B_{49}	12,688	18,100	1.24	34	0.99
H_{30}-B_{100}	98	H_{30}-B_{98}	21,322	24,900	1.21	39	0.98
H_{30}-B_{150}	97	H_{30}-B_{146}	29,780	24,000	1.20	47	0.85
H_{30}-B_{200}	98	H_{30}-B_{198}	38,591	42,500	1.24	90	0.32
H_{30}-B_{210}	98	H_{30}-B_{201}	40,353	40,600	1.21	137	1.00
H_{30}-B_{220}	98	H_{30}-B_{216}	42,115	40,000	1.34	100	0.67
H_{30}-B_{230}	99	H_{30}-B_{228}	44,230	41,400	1.39	134	0.57
H_{30}-B_{240}	97	H_{30}-B_{233}	45,111	45,500	1.30	88	0.84
H_{30}-B_{250}	97	H_{30}-B_{240}	46,873	47,800	1.23	153	0.14
H_{30}-B_{260}	96	H_{30}-B_{250}	48,107	46,700	1.30	129	0.04
H_{30}-B_{270}	98	H_{30}-B_{262}	50,750	50,700	1.34	210	0.24
H_{30}-B_{280}	96	H_{30}-B_{269}	51,455	53,100	1.26	221	0.11
H_{30}-B_{290}	96	H_{30}-B_{279}	53,217	48,700	1.43	134	0.13
H_{30}-B_{300}	97	H_{30}-B_{291}	55,331	52,900	1.31	238	0.06
H_{30}-B_{310}	98	H_{30}-B_{301}	57,093	56,800	1.33	31	0.60
H_{30}-B_{320}	98	H_{30}-B_{314}	59,384	57,000	1.29	146	0.28
H_{30}-B_{330}	96	H_{30}-B_{317}	59,913	60,200	1.34	145	0.47
H_{30}-B_{340}	97	H_{30}-B_{330}	62,203	57,500	1.36	245	0.07
H_{30}-B_{350}	97	H_{30}-B_{340}	63,966	57,300	1.49	356	0.07
H_{30}-B_{400}	99	H_{30}-B_{396}	73,833	66,700	1.43	272	0.08
H_{30}-B_{450}	99	H_{30}-B_{446}	82,644	67,200	1.53	273	0.08
H_{30}-B_{500}	98	H_{30}-B_{490}	90,397	79,900	1.56	692	0.58

As expected, the molecular weight of the block copolymer increases as the DP of the PBzMA core-forming block increases. GPC confirms a clear shift to shorter retention times for the block copolymers compared to the $PHEMA_{30}$ macro-CTA with negligible precursor macro-CTA chains remaining in all block copolymer samples, characteristic of both an increase in molecular weight and efficient macro-CTA chain-extension during the PISA synthesis (Figure 3.6). The slight discrepancies between the molecular weight obtained by GPC and that obtained by end-group analysis via ^{1}H NMR spectroscopy (Figure 3.6b) can be attributed to the poly(methyl methacrylate) calibration standards used for GPC analysis.[66] In contrast to the molar mass dispersity of the $PHEMA_{30}$ macro-CTA ($Đ_M$ = 1.25), the dispersities obtained for the block copolymers shown in

Figure 3.6 were similar up to a target PBzMA DP of 200 ($Đ_M$ ≤ 1.24), indicating good control of the molecular weight distribution during the PISA syntheses. Some loss of control was observed when targeting higher PBzMA DPs, for example a target DP of 400 where $Đ_M$ = 1.43, which is often a characteristic of block copolymers synthesised via RAFT-PISA when targeting relatively high core-forming block DPs.[65, 68, 72] The high molecular weight tailing observed in GPC traces when targeting higher PBzMA DPs is most likely due to some low level of termination by combination as has been previously observed for PISA formulations involving BzMA.[85]

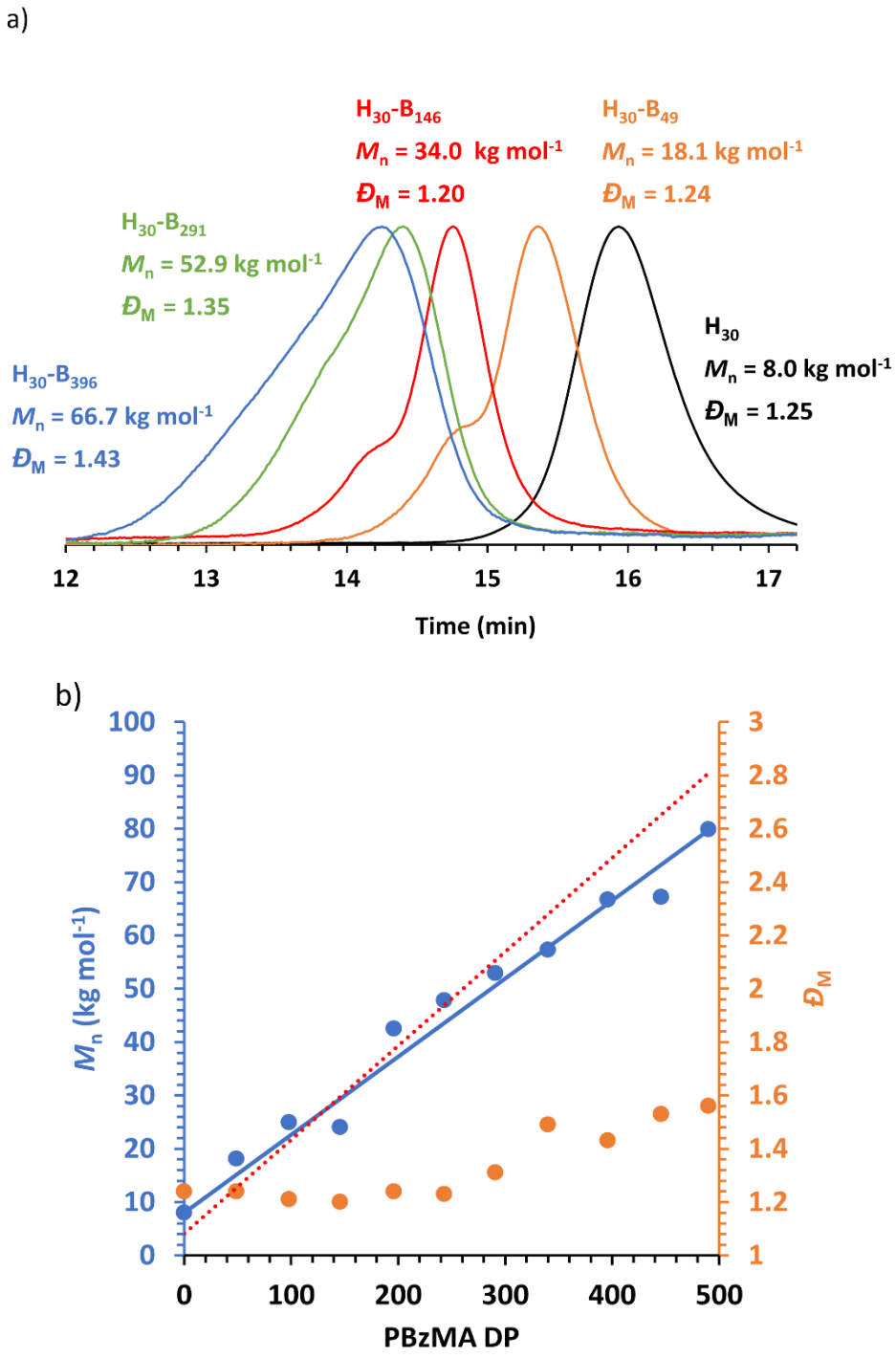

Figure 3.6. DMF GPC data obtained for $PHEMA_{30}$-*b*-$PBzMA_y$ block copolymers synthesised via RAFT dispersion polymerisation of benzyl methacrylate in [EMIM][DCA] at 15% w/w solids. GPC data was obtained against poly(methyl methacrylate) standards. A) Chromatograms obtained for a selection of $PHEMA_{30}$-*b*-$PBzMA_y$ block copolymers, where PHEMA is denoted as H and PBzMA is denoted as B. b) M_n vs. PBzMA DP (blue), where the blue line indicates the line of best fit, and $Đ_M$ vs. PBzMA DP (orange), where the red dashed line indicates the theoretical M_n vs. PBzMA DP. Theoretical M_n and DP were obtained by ^{1}H NMR spectroscopy, and actual M_n and $Đ_M$ were obtained by GPC analysis.

3.3.3 Characterisation of $PHEMA_{30}$-*b*-$PBzMA_y$ nanoparticles

DLS studies were conducted to characterise the $PHEMA_{30}$-*b*-$PBzMA_y$ nanoparticles in [EMIM][DCA], indicating the formation of nano-objects ranging in DLS diameter from ~40 nm to ~700 nm (see Table 3.1 and Figure 3.7a). Whilst DLS analysis is not ideally suited to the analysis of anisotropic nanoparticles, the apparent diameter returned can provide a 'sphere equivalent' size. It is noteworthy that nanoparticles formed when targeting PBzMA DPs of 340-450 were ~250-350 nm in diameter with narrow size distributions (DLS polydispersity index, PDI ≤ 0.08) which, given that this PBzMA DP range is above the range where gels are obtained, suggests the formation of vesicles. DLS size distributions of selected $PHEMA_{30}$-*b*-$PBzMA_y$ dispersions are shown in Figure 3.7a.

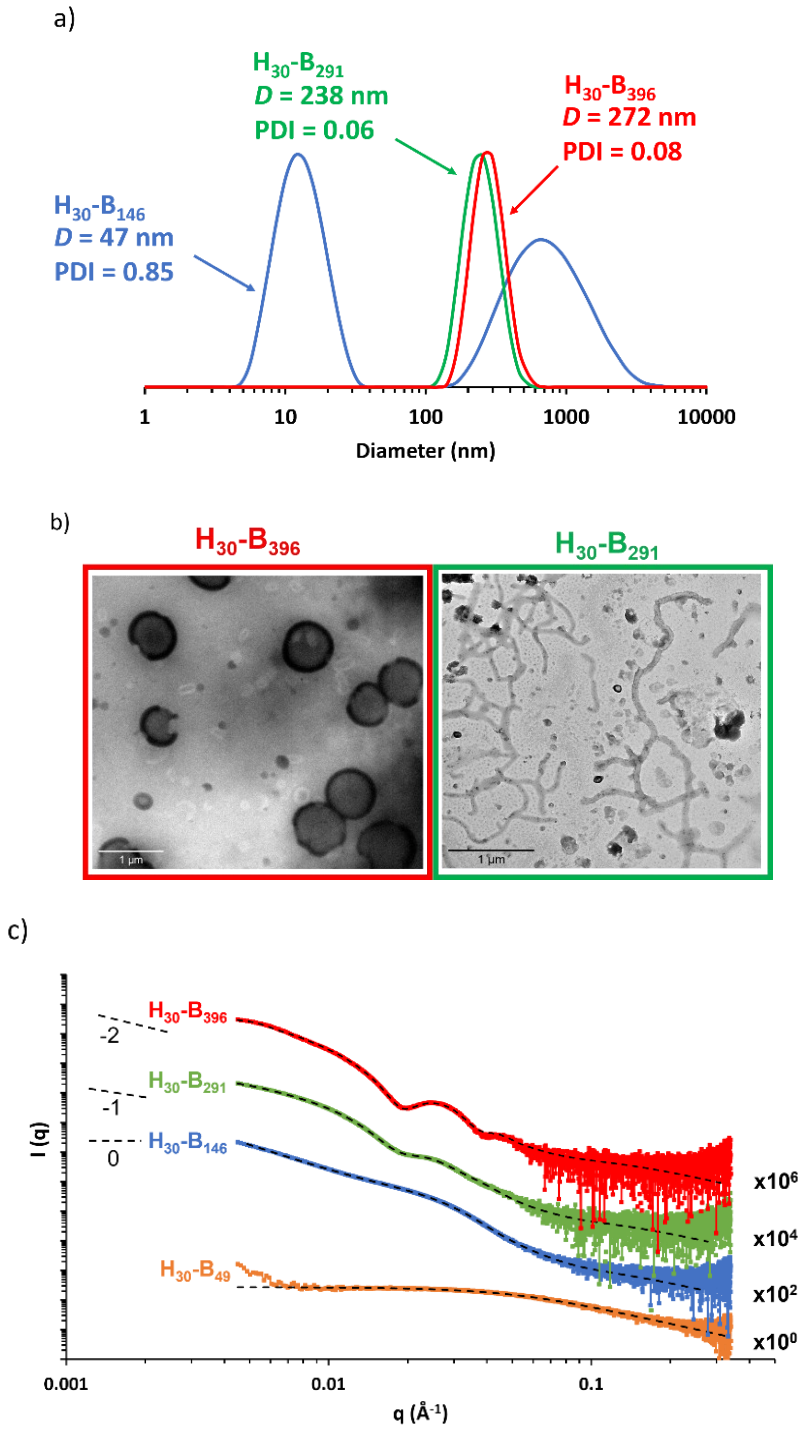

Figure 3.7. a) DLS data obtained for 0.15% w/w dispersions of $PHEMA_{30}$-*b*-$PBzMA_{396}$ (red), $PHEMA_{30}$-*b*-$PBzMA_{291}$ (green) and $PHEMA_{30}$-*b*-$PBzMA_{146}$ (blue) in [EMIM][DCA], b) TEM images obtained for 0.15 % w/w dispersions of $PHEMA_{30}$-*b*-$PBzMA_{396}$ (red) and $PHEMA_{30}$-*b*-$PBzMA_{291}$ (green) in [EMIM][DCA], and c) Background-subtracted SAXS patterns recorded at 1.0% w/w for $PHEMA_{30}$-*b*-$PBzMA_{y}$ chains (orange), spheres and chains mixture (blue), spheres and worms mixture (green) and vesicles (red) in [EMIM][DCA]. Dashed lines represent model fits obtained, where the Gaussian chain model (Appendix 7.1.4) was used for H_{30}-B_{49}, the spherical micelle model (Appendix 7.1.1) was employed for H_{30}-B_{146}, a combination of spherical micelle and worm like micelle model (Appendix 7.1.2) was used for H_{30}-B_{291}, and the vesicle model (Appendix 7.1.3) was employed for fitting H_{30}-B_{396}.. Gradients of 0, -1 and -2 are shown as a guide to the eye indicate the presence of spheres, worms and vesicles, respectively.

The presence of nanoparticles was also confirmed by TEM and SAXS (Figures 3.7b, 3.7c, 3.8 and 3.9-3.30). In particular, TEM analysis of $PHEMA_{30}$-b-$PBzMA_{396}$ in [EMIM][DCA] indicated the presence of vesicles, which was further evidenced by SAXS analysis by fitting background-subtracted data to a well-established vesicle model.[79] For this sample, SAXS data were successfully fitted using a vesicle model alone indicating a pure phase of vesicles with a mean overall vesicle diameter of 315 nm, which is comparable to the overall DLS diameter observed by DLS, and the mean membrane thickness was determined to be 29 nm. Most importantly, TEM analysis indicated the presence of $PHEMA_{30}$-b-$PBzMA_{291}$ worms (Figure 3.7b), suggesting that the corresponding 15% w/w free-standing ionogel was formed as a result of the presence of worm-like micelles.[86] The presence of worms was further evidenced by fitting the background-subtracted SAXS data for $PHEMA_{30}$-*b*-$PBzMA_{291}$ to a worm-like micelle model,[78] which indicated a mean worm thickness of 43 nm and a worm length of ~150 nm. In addition to the worm-like micelle model, fitting the SAXS data for this 1% w/w $PHEMA_{30}$-*b*-$PBzMA_{291}$ dispersion required a population (17.4% v/v) of spherical nanoparticles with 21 nm in diameter. SAXS data obtained for $PHEMA_{30}$-*b*-$PBzMA_{146}$ nano-objects suggested the presence of aggregated particles as indicated by the significant upturn in scattering intensity at low q values. Nevertheless, this background-subtracted scattering pattern was well fitted to a spherical micelle model[78] that indicated the presence of spheres with a mean diameter of 20 nm, with the upturn at low q being represented by an additional power-law relationship. DLS analysis of these nanoparticles also supports the presence of aggregates, with a clear bimodal distribution of smaller particles with similar diameters to those observed by SAXS and larger aggregates between approximately 100 nm and 5 μm in diameter. As a result of this bimodal and broad distribution, the mean DLS diameter was 47 nm with a high PDI value (0.85). TEM analysis also appears to support these observations, however high quality TEM images were difficult to obtain (see Figure 3.8).

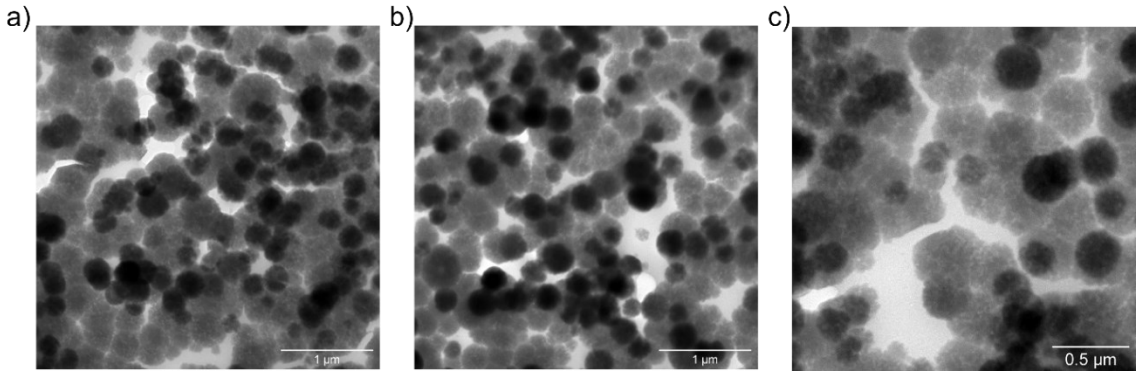

Figure 3.8. TEM images obtained for a 0.15% w/w dispersion of $PHEMA_{30}$-*b*-$PBzMA_{146}$.

Finally, SAXS data for a 1% w/w $PHEMA_{30}$-*b*-$PBzMA_{49}$ in [EMIM][DCA] were obtained, which confirmed the presence of molecularly dissolved block copolymer chains. This supports the detailed kinetic study of this PISA formulation (see Figure 3.4) that identified the critical PBzMA DP for self-assembly in [EMIM][DCA] as approximately 72. Indeed these data were well fitted to a Gaussian chain model[77], indicating polymer chains with a radius of gyration of 2.9 nm. In addition to the four datasets presented in Figure 3.7c, SAXS analysis was conducted on all $PHEMA_{30}$-*b*-$PBzMA_y$ samples and fitted to appropriate models (see Figures 3.9-3.30 and Table 3.2), further confirming that this new PISA formulation yields nanoparticle dispersions containing spheres, worms and vesicles in [EMIM][DCA] ionic liquid.

Table 3.2. Summary of parameters obtained when fitting SAXS data to appropriate models (Appendix 7.1). φ_{sphere}, φ_{worm} and $\varphi_{vesicle}$ are the volume fraction of spheres, worms and vesicles, respectively. D_{sphere} is the spherical nanoparticle diameter ($D_{sphere} = 2R_s + 4R_g$, where R_g is the radius of gyration of the stabiliser block and R_s is the core radius). T_{worm} is the worm thickness ($T_{worm} = 2R_w + 4R_g$, where R_w is the worm core cross-sectional radius). L_{worm} is the worm length. $D_{vesicle}$ is the overall vesicle diameter ($D_{vesicle} = R_m + T_m + 4R_g$, where R_m is the centre of the vesicle to the centre of the membrane and T_m is the membrane thickness). $R_{g_{cop}}$ is the radius of gyration of dissolved copolymer chains. υ is the extended volume parameter. PHEMA$_{30}$-*b*-PBzMA$_y$ is denoted as H_{30}-B_y for brevity.

	Spherical micelle model		Worm-like micelle model			Vesicle model			Gaussian chain model	
Sample	$\boldsymbol{\varphi_{\mathrm{sphere}}}$	$\boldsymbol{D_{\mathrm{sphere}}}$ **(nm)**	$\boldsymbol{\varphi_{\mathrm{worm}}}$	$\boldsymbol{T_{\mathrm{worm}}}$ **(nm)**	$\boldsymbol{L_{\mathrm{worm}}}$ **(nm)**	$\boldsymbol{\varphi_{\mathrm{vesicle}}}$	$\boldsymbol{D_{\mathrm{vesicle}}}$ **(nm)**	$\boldsymbol{T_{\mathrm{m}}}$ **(nm)**	$\boldsymbol{R_{\mathrm{g_{cop}}}}$ **(nm)**	$\boldsymbol{\upsilon}$
H_{30}-B_{49}									2.90	0.5
H_{30}-B_{98}	0.0141	20.0								
H_{30}-B_{146}	0.0227	20.4								
H_{30}-B_{198}	0.0066	20.7	0.0124	35.6	140					
H_{30}-B_{201}	0.0118	22.7	0.0085	34.5	256					
H_{30}-B_{216}	0.0160	21.1	0.0068	32.2	600					
H_{30}-B_{228}	0.0084	21.3	0.0123	35.4	212					
H_{30}-B_{233}	0.0127	21.9	0.0080	35.1	156					
H_{30}-B_{240}	0.0036	22.3	0.0121	38.7	159					
H_{30}-B_{250}			0.0050	17.4	600					
H_{30}-B_{265}	0.0052	21.3	0.0223	39.0	212					
H_{30}-B_{269}	0.0020	21.5	0.0127	42.8	216					
H_{30}-B_{279}	0.0054	21.4	0.0111	40.3	197					
H_{30}-B_{291}	0.0017	20.7	0.0079	42.7	149					
H_{30}-B_{301}	0.0172	21.6	0.0056	39.2	240					
H_{30}-B_{314}			0.0012	19.6	100	0.0175	409	24.6		
H_{30}-B_{317}			0.0007	17.8	100	0.0174	440	25.1		
H_{30}-B_{330}			0.0040	59.2	100	0.0155	348	25.4		
H_{30}-B_{340}			0.0008	38.1	104	0.0166	311	26.3		
H_{30}-B_{396}						0.0147	315	29.0		
H_{30}-B_{446}						0.0162	302	31.3		
H_{30}-B_{490}						0.0530	307	33.3		

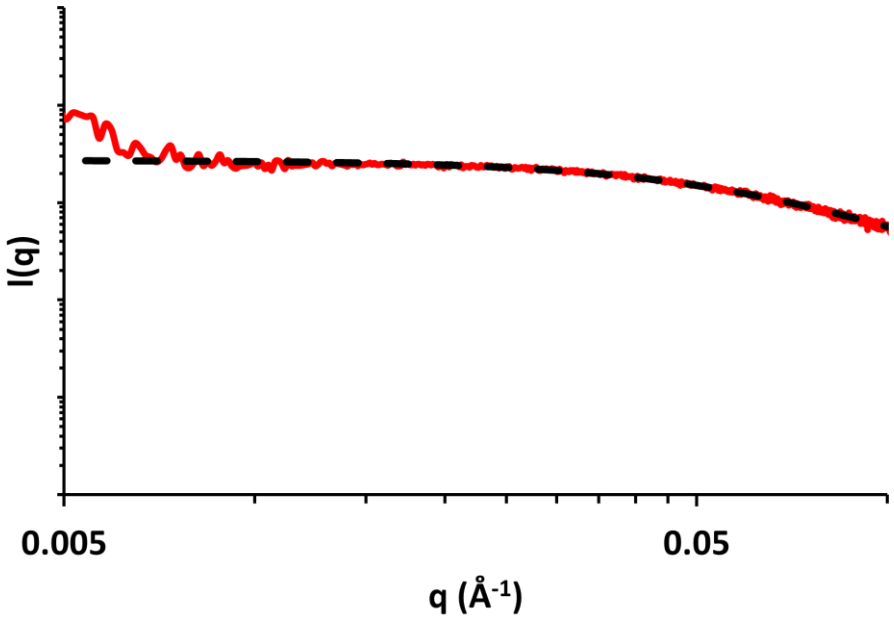

Figure 3.9. Background-subtracted SAXS data obtained for 1.0% w/w $PHEMA_{30}$-$PBzMA_{49}$ in [EMIM][DCA] at 25 °C. Dashed lines represent the model fit obtained using the Gaussian chain model (Appendix 7.1.4).

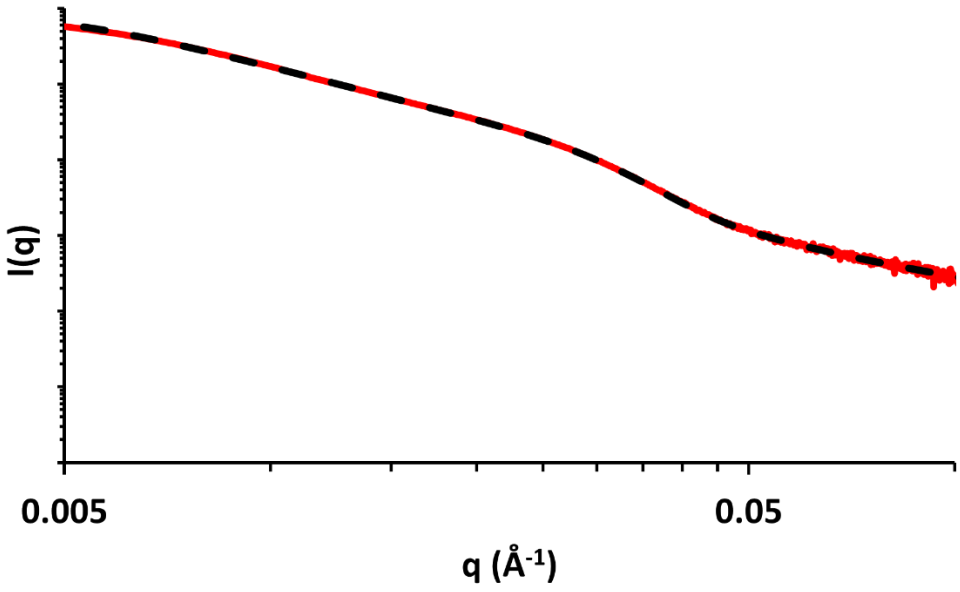

Figure 3.10. Background-subtracted SAXS data obtained for 1.0% w/w $PHEMA_{30}$-$PBzMA_{98}$ in [EMIM][DCA] at 25 °C. Dashed lines represent the model fit obtained using the spherical micelle model (Appendix 7.1.1) with an additional power law to account for the upturn in scattering at low *q*.

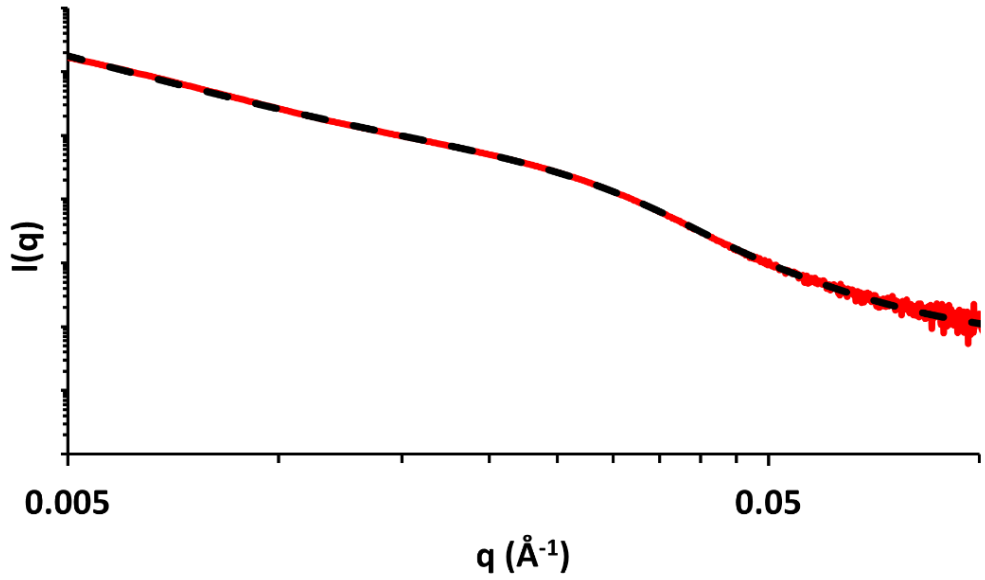

Figure 3.11. Background-subtracted SAXS data obtained for 1.0% w/w $PHEMA_{30}$-$PBzMA_{146}$ in [EMIM][DCA] at 25 °C. Dashed lines represent the model fit obtained using the spherical micelle model (Appendix 7.1.1).

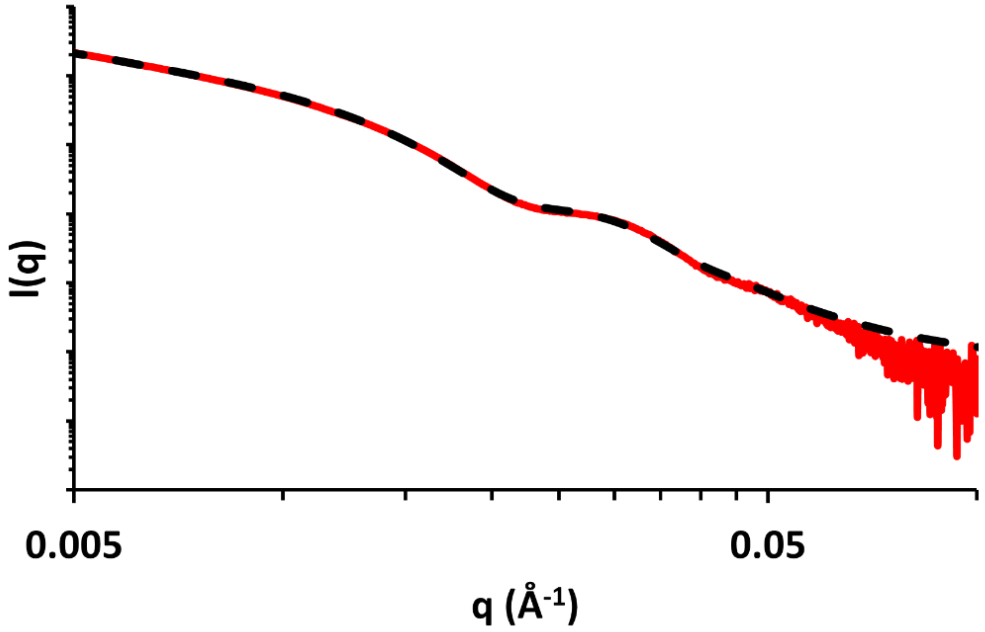

Figure 3.12. Background-subtracted SAXS data obtained for 1.0% w/w $PHEMA_{30}$-$PBzMA_{196}$ in [EMIM][DCA] at 25 °C. Dashed lines represent the model fit obtained using a combination of the spherical micelle model (Appendix 7.1.1) and worm-like micelle model (Appendix 7.1.2).

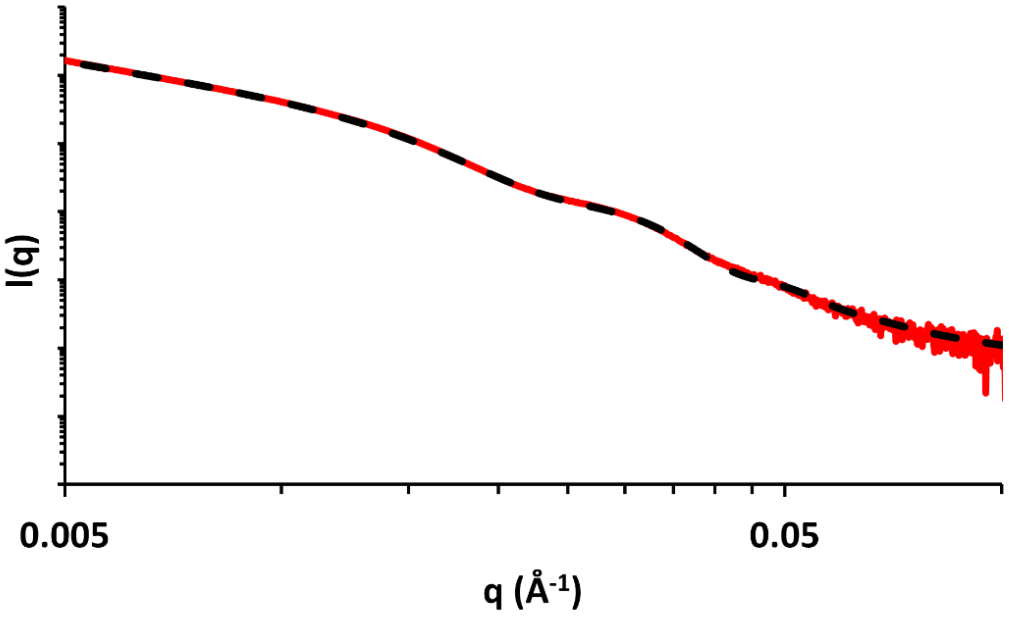

Figure 3.13. Background-subtracted SAXS data obtained for 1.0% w/w $PHEMA_{30}$-$PBzMA_{201}$ in [EMIM][DCA] at 25 °C. Dashed lines represent the model fit obtained using a combination of the spherical micelle model (Appendix 7.1.1) and worm-like micelle model (Appendix 7.1.2).

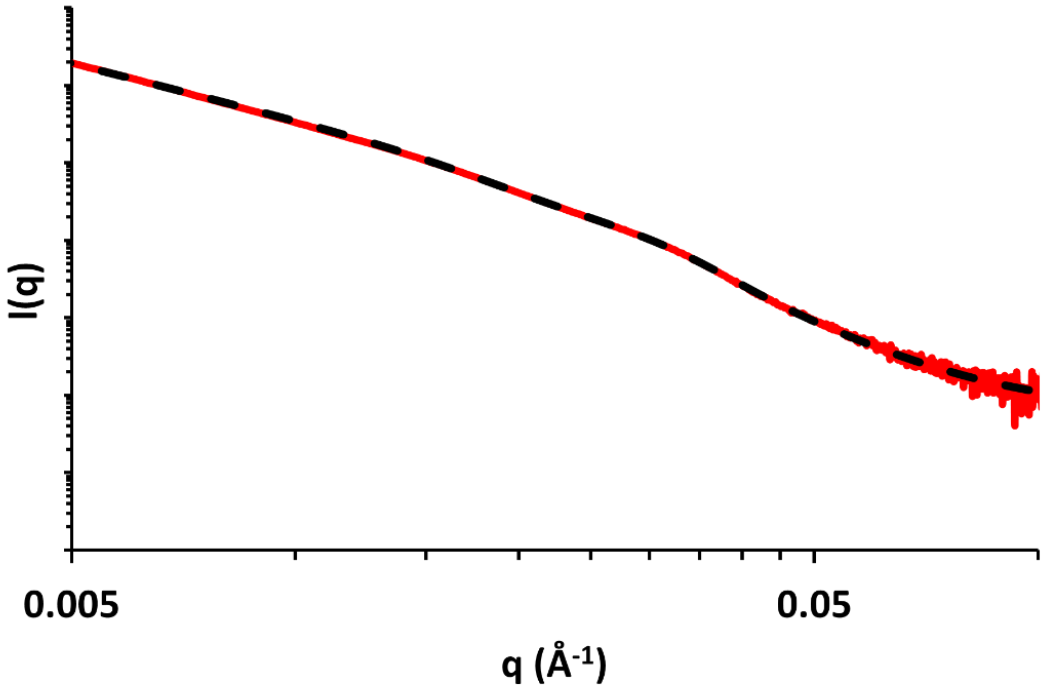

Figure 3.14. Background-subtracted SAXS data obtained for 1.0% w/w PHEMA30-PBzMA216 in [EMIM][DCA] at 25 °C. Dashed lines represent the model fit obtained using a combination of the spherical micelle model (Appendix 7.1.1) and worm-like micelle model (Appendix 7.1.2).

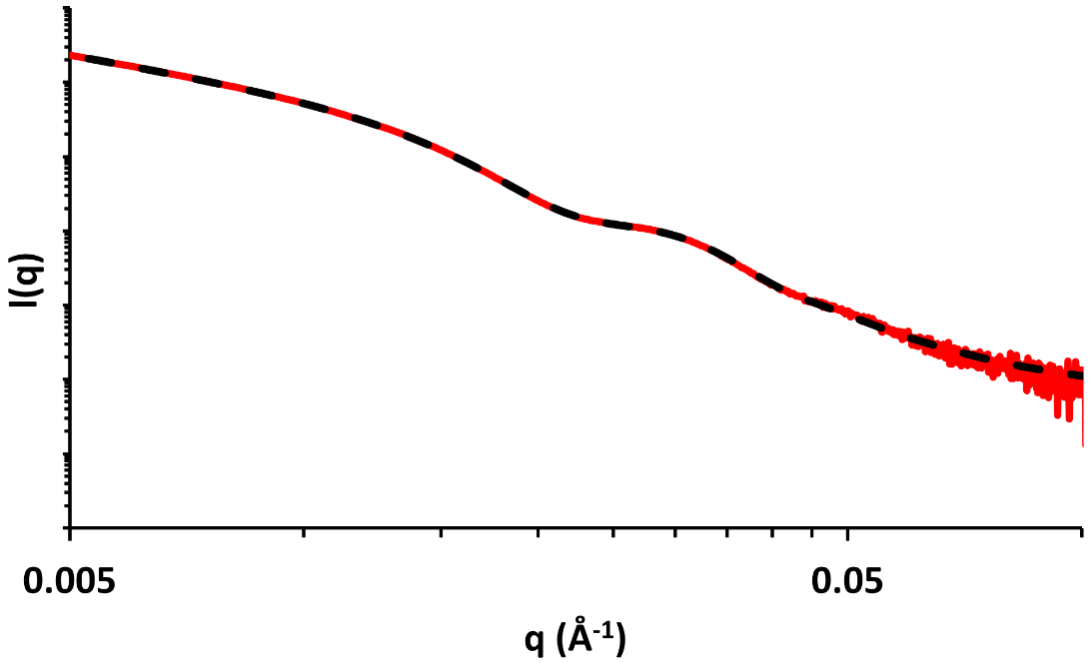

Figure 3.15. Background-subtracted SAXS data obtained for 1.0% w/w $PHEMA_{30}$-$PBzMA_{228}$ in [EMIM][DCA] at 25 °C. Dashed lines represent the model fit obtained using a combination of the spherical micelle model (Appendix 7.1.1) and worm-like micelle model (Appendix 7.1.2).

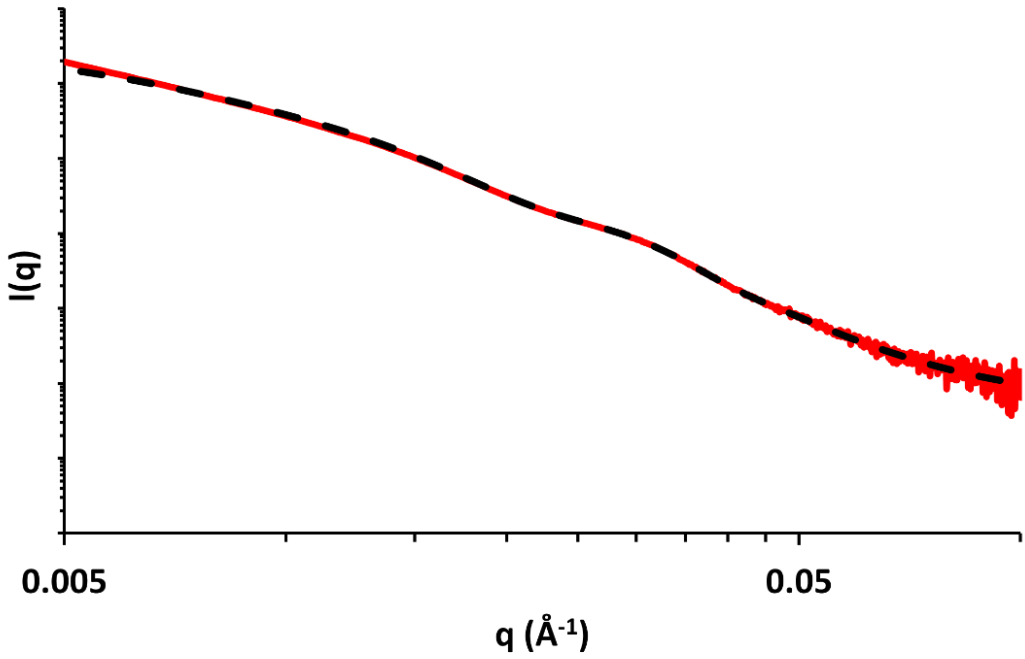

Figure 3.16. Background-subtracted SAXS data obtained for 1.0% w/w $PHEMA_{30}$-$PBzMA_{233}$ in [EMIM][DCA] at 25 °C. Dashed lines represent the model fit obtained using a combination of the spherical micelle model (Appendix 7.1.1) and worm-like micelle model (Appendix 7.1.2).

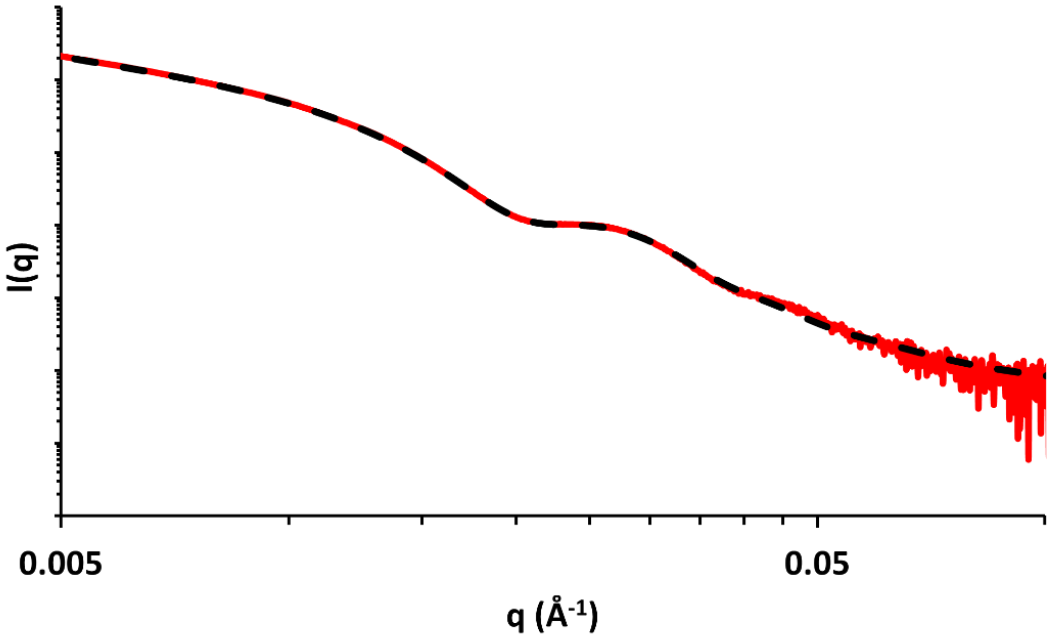

Figure 3.17. Background-subtracted SAXS data obtained for 1.0% w/w $PHEMA_{30}$-$PBzMA_{240}$ in [EMIM][DCA] at 25 °C. Dashed lines represent the model fit obtained using a combination of the spherical micelle model (Appendix 7.1.1) and worm-like micelle model (Appendix 7.1.2).

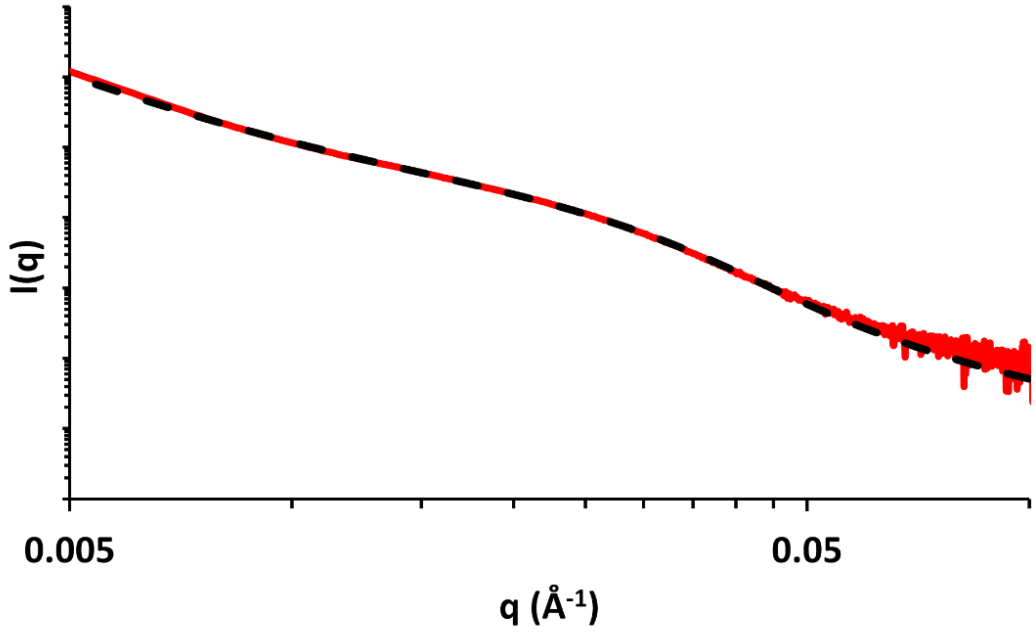

Figure 3.18. Background-subtracted SAXS data obtained for 1.0% w/w $PHEMA_{30}$-$PBzMA_{250}$ in [EMIM][DCA] at 25 °C. Dashed lines represent the model fit obtained using the worm-like micelle model (Appendix 7.1.2).

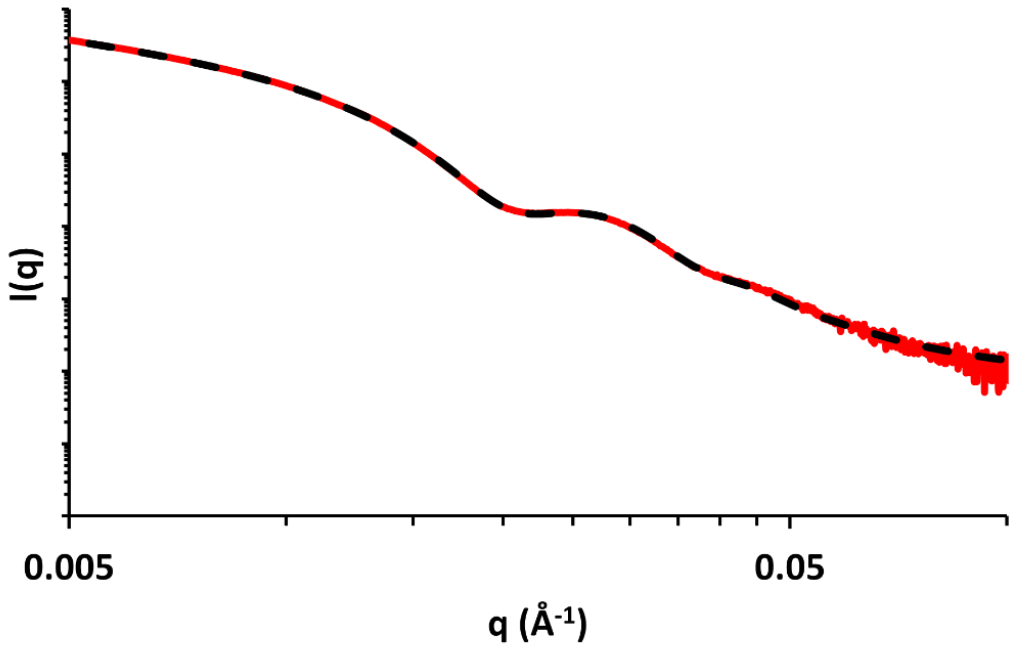

Figure 3.19. Background-subtracted SAXS data obtained for 1.0% w/w $PHEMA_{30}$-$PBzMA_{265}$ in [EMIM][DCA] at 25 °C. Dashed lines represent the model fit obtained using a combination of the spherical micelle model (Appendix 7.1.1) and worm-like micelle model (Appendix 7.1.2).

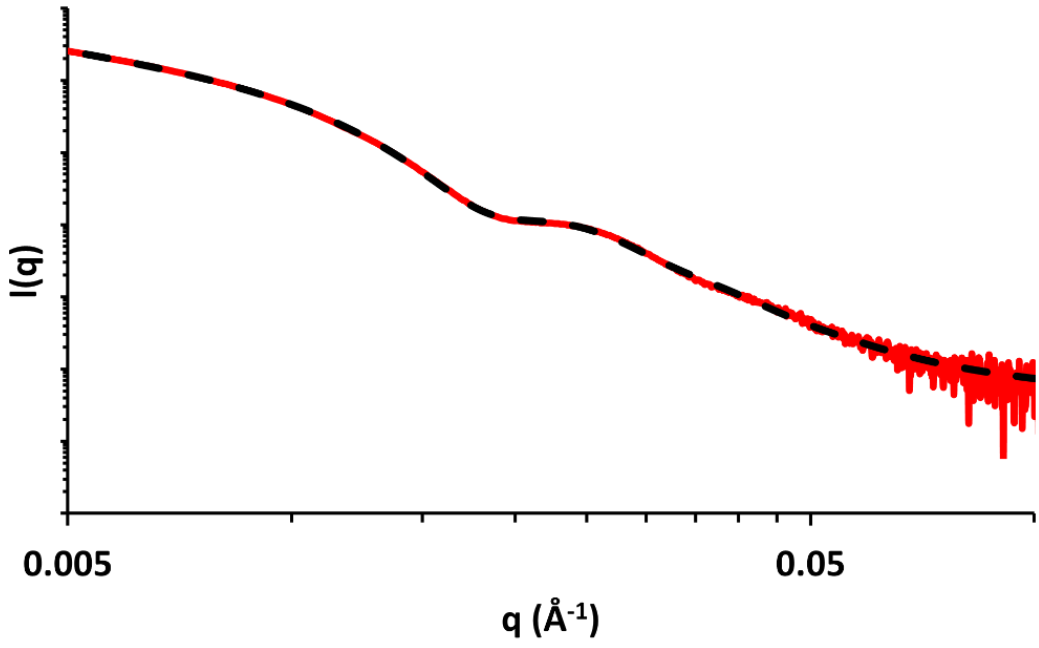

Figure 3.20. Background-subtracted SAXS data obtained for 1.0% w/w $PHEMA_{30}$-$PBzMA_{269}$ in [EMIM][DCA] at 25 °C. Dashed lines represent the model fit obtained a combination of the spherical micelle model (Appendix 7.1.1) and worm-like micelle model (Appendix 7.1.2).

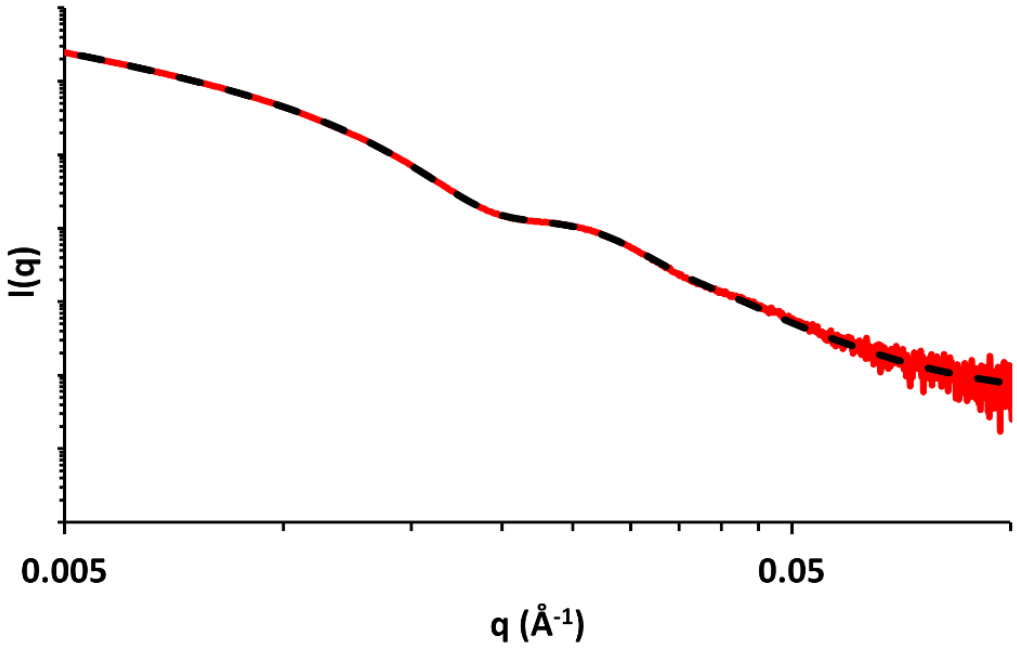

Figure 3.21. Background-subtracted SAXS data obtained for 1.0% w/w $PHEMA_{30}$-$PBzMA_{279}$ in [EMIM][DCA] at 25 °C. Dashed lines represent the model fit obtained using a combination of the spherical micelle model (Appendix 7.1.1) and worm-like micelle model (Appendix 7.1.2).

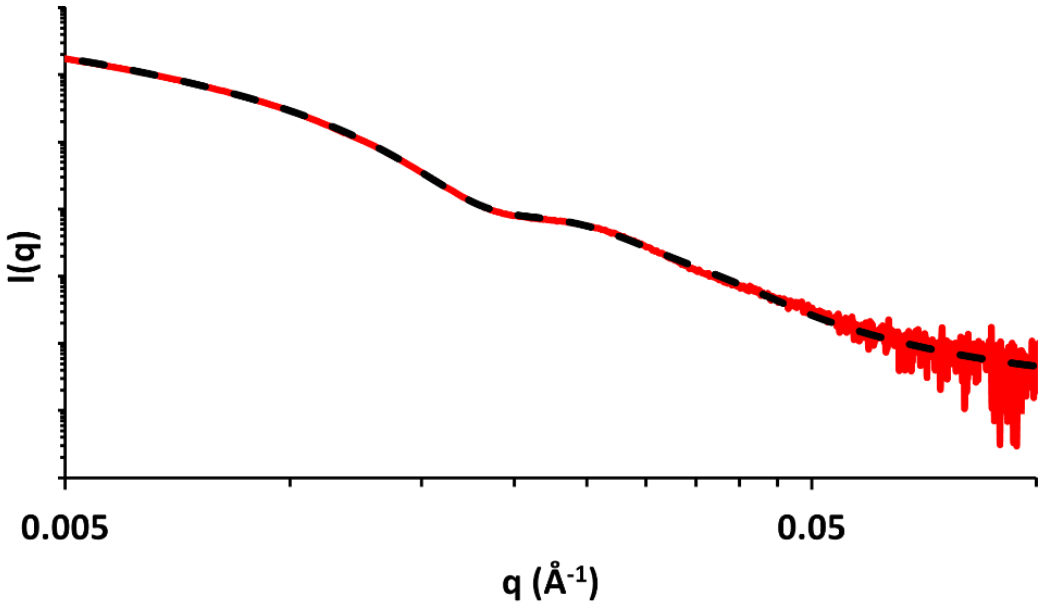

Figure 3.22. Background-subtracted SAXS data obtained for 1.0% w/w $PHEMA_{30}$-$PBzMA_{291}$ in [EMIM][DCA] at 25 °C. Dashed lines represent the model fit obtained using a combination of the spherical micelle model (Appendix 7.1.1) and worm-like micelle model (Appendix 7.1.2).

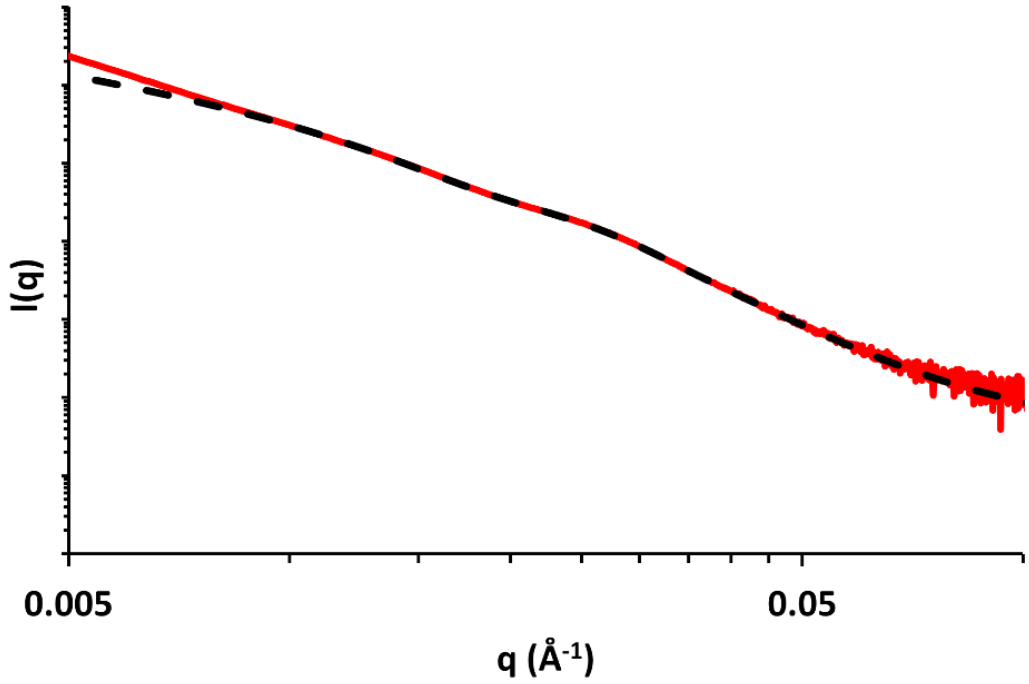

Figure 3.23. Background-subtracted SAXS data obtained for 1.0% w/w $PHEMA_{30}$-$PBzMA_{301}$ in [EMIM][DCA] at 25 °C. Dashed lines represent the model fit obtained using a combination of the spherical micelle model (Appendix 7.1.1) and worm-like micelle model (Appendix 7.1.2).

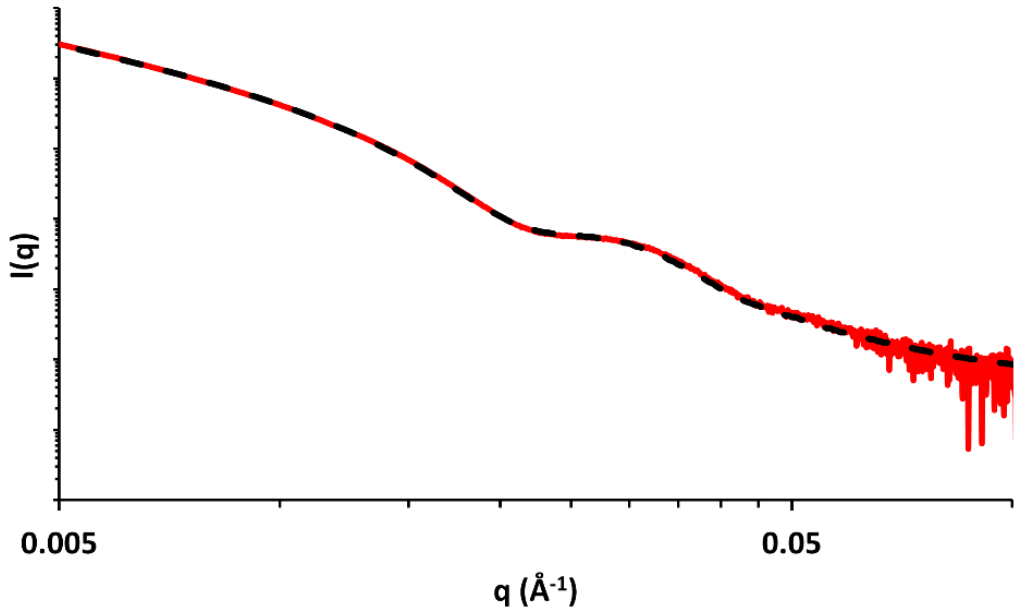

Figure 3.24. Background-subtracted SAXS data obtained for 1.0% w/w $PHEMA_{30}$-$PBzMA_{314}$ in [EMIM][DCA] at 25 °C. Dashed lines represent the model fit obtained using a combination of the worm-like micelle (Appendix 7.1.2) and vesicle models (Appendix 7.1.3).

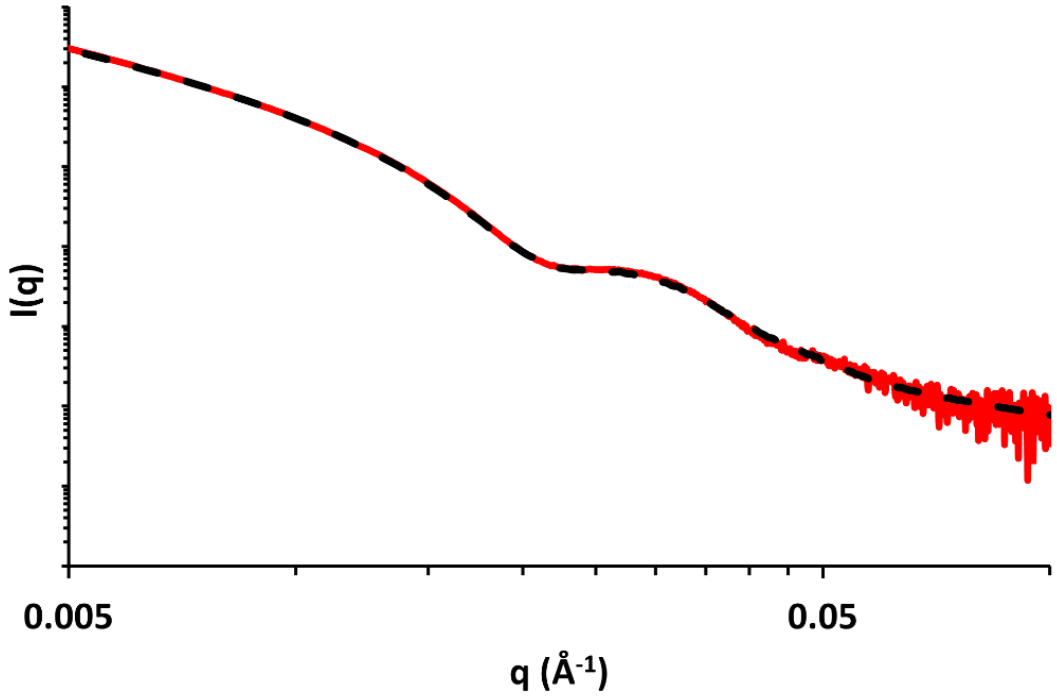

Figure 3.25. Background-subtracted SAXS data obtained for 1.0% w/w $PHEMA_{30}$-$PBzMA_{317}$ in [EMIM][DCA] at 25 °C. Dashed lines represent the model fit obtained using a combination of the worm-like micelle (Appendix 7.1.2) and vesicle models (Appendix 7.1.3).

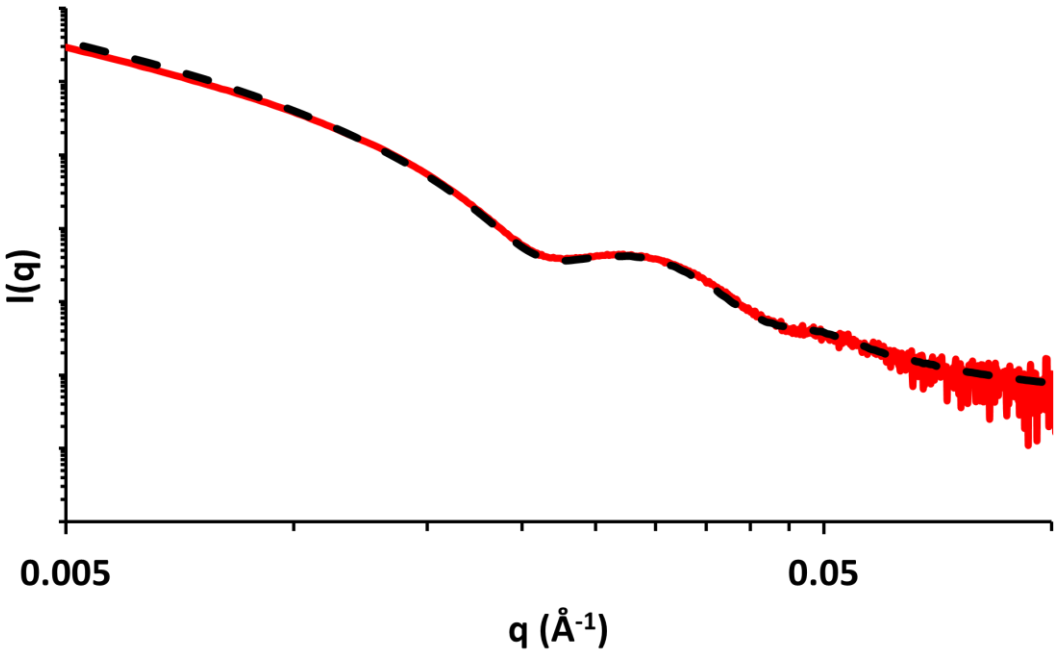

Figure 3.26. Background-subtracted SAXS data obtained for 1.0% w/w $PHEMA_{30}$-$PBzMA_{330}$ in [EMIM][DCA] at 25 °C. Dashed lines represent the model fit obtained using a combination of the worm-like micelle (Appendix 7.1.2) and vesicle models (Appendix 7.1.3).

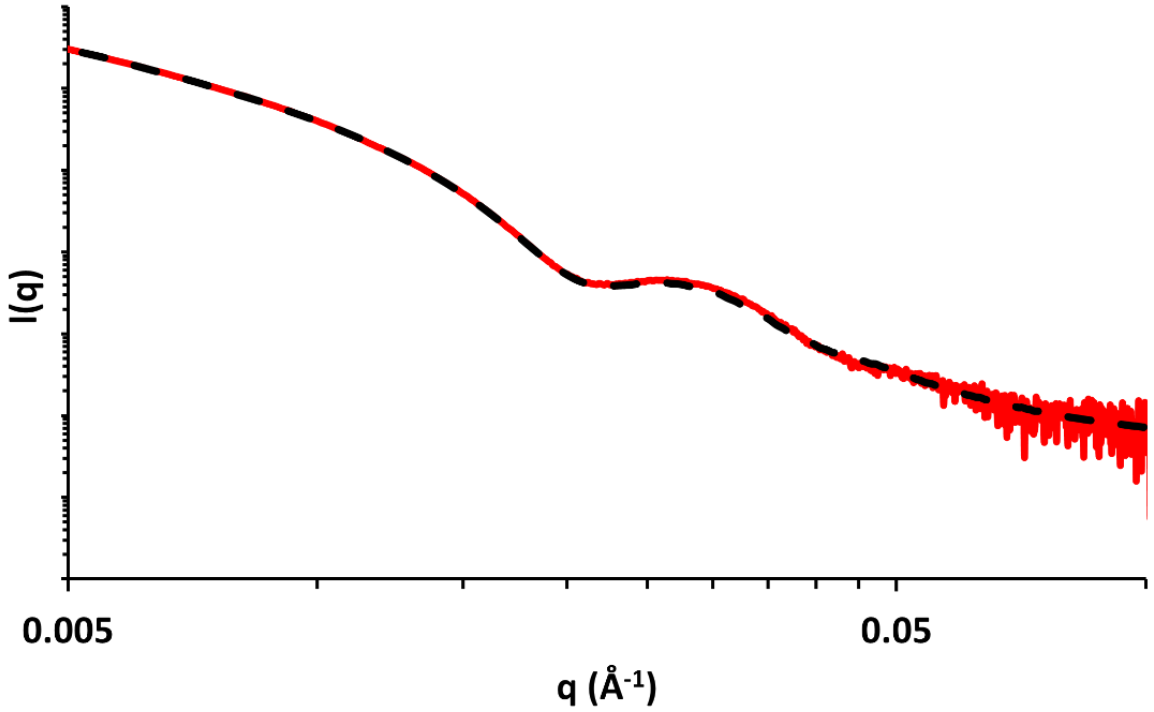

Figure 3.27. Background-subtracted SAXS data obtained for 1.0% w/w $PHEMA_{30}$-$PBzMA_{340}$ in [EMIM][DCA] at 25 °C. Dashed lines represent the model fit obtained using a combination of the worm-like micelle (Appendix 7.1.2) and vesicle models (Appendix 7.1.3).

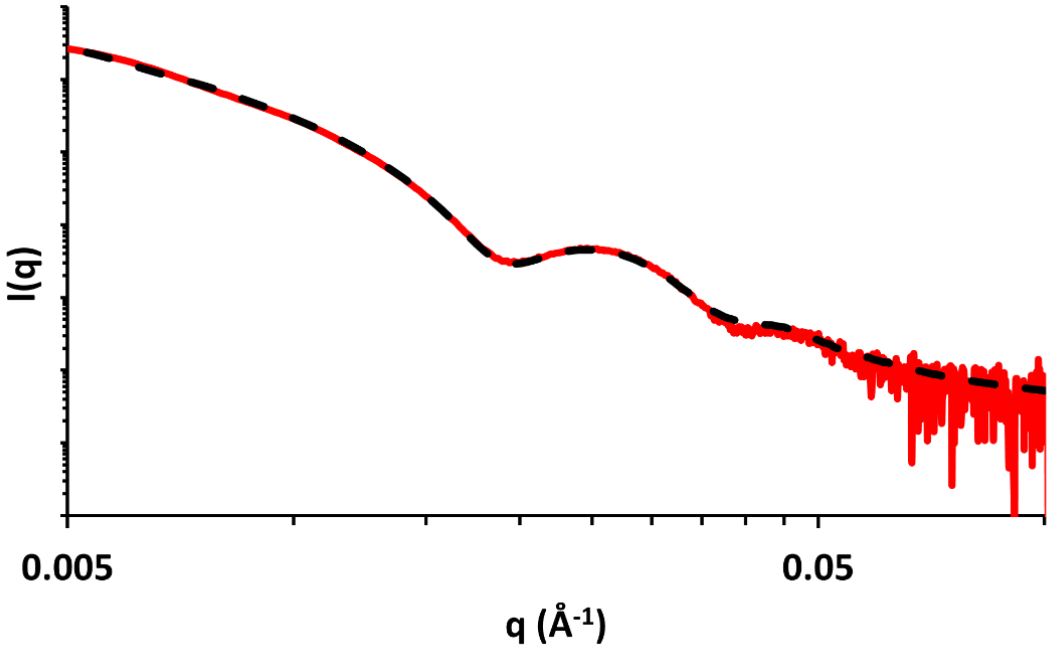

Figure 3.28. Background-subtracted SAXS data obtained for 1.0% w/w $PHEMA_{30}$-$PBzMA_{396}$ in [EMIM][DCA] at 25 °C. Dashed lines represent the model fit obtained using the vesicle model (Appendix 7.1.3).

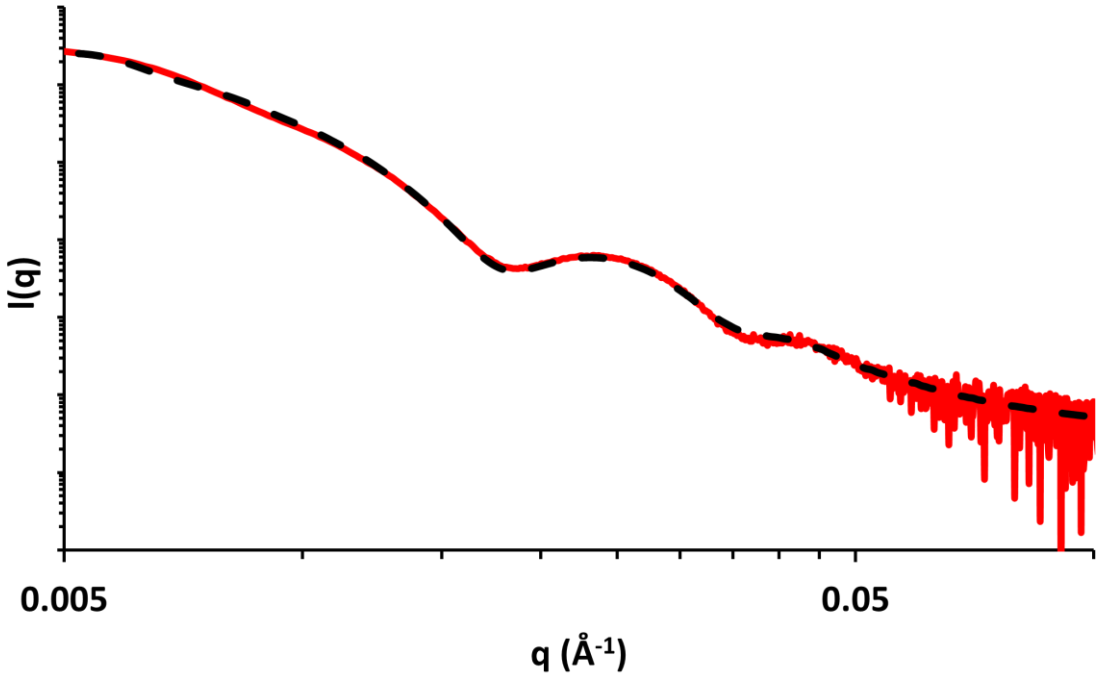

Figure 3.29. Background-subtracted SAXS data obtained for 1.0% w/w $PHEMA_{30}$-$PBzMA_{446}$ in [EMIM][DCA] at 25 °C. Dashed lines represent the model fit obtained using a vesicle model (Appendix 7.1.3).

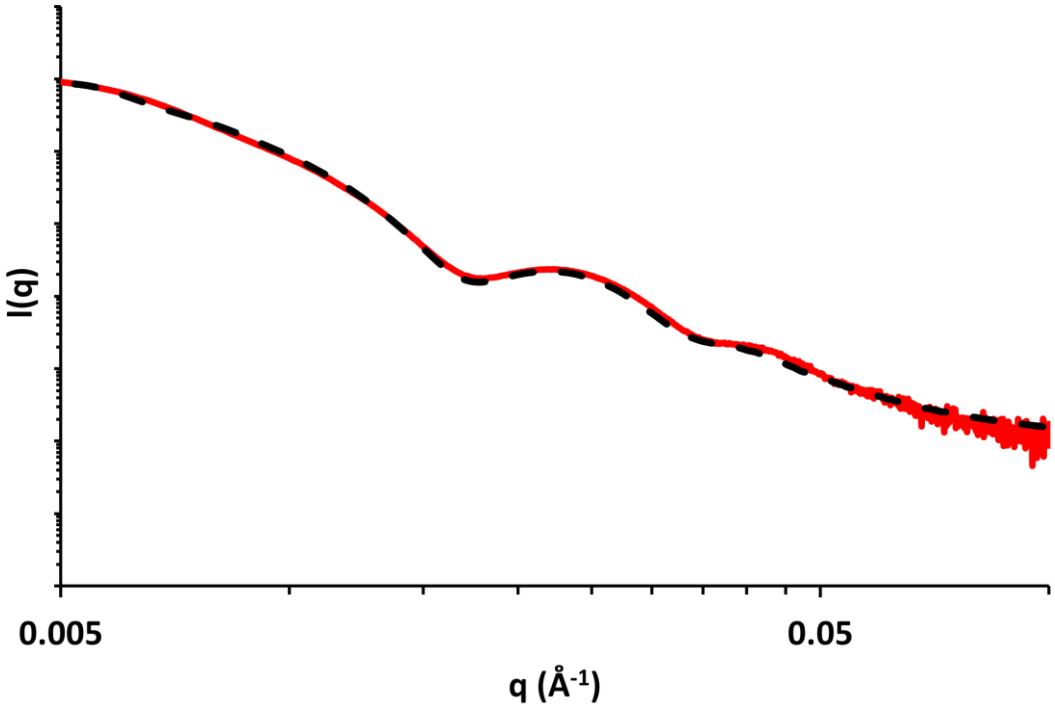

Figure 3.30. Background-subtracted SAXS data obtained for 1.0% w/w $PHEMA_{30}$-$PBzMA_{490}$ in [EMIM][DCA] at 25 °C. Dashed lines represent the model fit obtained using a vesicle model (Appendix 7.1.3).

3.4 Conclusions

In summary, a series of $PHEMA_{30}$-*b*-$PBzMA_y$ block copolymers were synthesised via RAFT dispersion polymerisation of benzyl methacrylate in [EMIM][DCA] at 70 °C and 15% w/w solids. A kinetic study carried out indicated high monomer conversions could be achieved within 120 minutes, with the critical PBzMA DP for self-assembly being determined as 72. This is the point at which the PBzMA core-forming block is sufficiently long to become insoluble in [EMIM][DCA] and thus induce self-assembly. GPC analysis of the block copolymer series demonstrated good control of the polymerisation when targeting a range of PBzMA DPs. A range of dispersions were yielded including transparent, free-flowing liquids (PBzMA DPs between 98 and 220), free-standing gels (PBzMA DPs between 233 and 330), and viscous turbid solutions (PBzMA DPs ≥340), each of which are a good indication of the presence of spheres, worms and vesicles, respectively. This was further evidenced by a combination of DLS, SAXS and TEM analyses. From SAXS analysis, it was found that the $PHEMA_{30}$-*b*-$PBzMA_{291}$ free-standing gel, which lies at the centre of the gel phase, had the highest proportion of worms (82.6% v/v) out of all the dispersions, and TEM visually confirmed the presence of worms. For the first time, this PISA formulation facilitates a more convenient and facile route to *in situ* generation of free-standing worm ionogels, which show considerable promise in future electrochemical applications as ionic liquid-based gel electrolytes. Importantly, the need for post-polymerisation processing/purification and the aid of co-solvents or crosslinkers has been eliminated, further demonstrating this formulation's promise as future gel electrolytes.

3.5 References

1. D. M. Correia, L. C. Fernandes, N. Pereira, J. C. Barbosa, J. P. Serra, R. S. Pinto, C. M. Costa and S. Lanceros-Méndez, *Appl. Mater. Today*, 2021, **22**, 100928.
2. R. Tamate, K. Hashimoto, T. Ueki and M. Watanabe, *Phys. Chem. Chem. Phys*, 2018, **20**, 25123-25139.
3. Q. Zhang and S. Zhu, *ACS Macro Lett.*, 2015, **4**, 755-758.
4. A. J. Greer, J. Jacquemin and C. Hardacre, *Molecules*, 2020, **25**.
5. A. Tsurumaki, T. Iwata, M. Tokuda, H. Minami, M. A. Navarra and H. Ohno, *Electrochim. Acta*, 2019, **308**, 115-120.
6. Y. Ding, H. Tang, X. Zhang, S. Wu and R. Xiong, *Eur. Poly. J*, 2008, **44**, 1247-1251.
7. C. M. Caldas, B. G. Soares, T. Indrusiak and G. M. O. Barra, *J. Appl. Polym. Sci*, 2021, **138**, 49814.
8. V. Bugatti, G. Viscusi, A. Di Bartolomeo, L. Iemmo, D. C. Zampino, V. Vittoria and G. Gorrasi, *Polymers*, 2020, **12**, 495.
9. Y. He and T. P. Lodge, *Chem. Commun*, 2007, 2732-2734.
10. T. P. Lodge and T. Ueki, *Acc. Chem. Res*, 2016, **49**, 2107-2114.
11. Y. He, P. G. Boswell, P. Bühlmann and T. P. Lodge, *J. Phys. Chem. B*, 2007, **111**, 4645-4652.

12. J. H. Lee, J. C. Shin, J. Kim, J.-W. Ho, W. J. Cho, M. J. Park, G.-R. Yi, M. Lee and P. J. Yoo, *J. Power Sources*, 2023, **557**, 232565.
13. Y. Xu, X. Jiang, Z. Liu, Z. Chen, S. Zhang and Y. Zhang, *J. Power Sources*, 2022, **546**, 231952.
14. L. Li, X. Yang, J. Li and Y. Xu, *Ionics*, 2018, **24**, 735-741.
15. X. Liu, Y. Zhan, C. Zhao, Y. Su, Z. Ge and Y. Luo, *Polymers*, 2020, **12**, 1513.
16. C. Liao, X.-G. Sun and S. Dai, *Electrochim. Acta*, 2013, **87**, 889-894.
17. S. Wang, Y. Jiang and X. Hu, *Adv. Mater*, 2022, **34**, 2200945.
18. M. Hoffmann, A. J. Butzelaar, C. Iacob, P. Theato and M. Wilhelm, *ACS App. Polym. Mat*, 2022, **4**, 2794-2805.
19. J. Zhang, W. Zhang, J. Guo, C. Yuan and F. Yan, *Electrochim Acta*, 2015, **165**, 98-104.
20. J. Yoon, D. k. Kang, J. Won, J.-Y. Park and Y. S. Kang, *J. Power Sources*, 2012, **201**, 395-401.
21. S.-K. Tseng, R.-H. Wang, J.-L. Wu, J. P. Jyothibasu, T.-L. Wang, C.-Y. Chu and R.-H. Lee, *Polymer*, 2020, **210**, 123074.
22. S. Shahbaz, A. A. Tahir, T. Mallick, I. A. Siyabi, B. Y. Alfaifi and S. Ahmed, *New J. Chem*, 2020, **44**, 20212-20221.
23. D. Zhou, G. M. Spinks, G. G. Wallace, C. Tiyapiboonchaiya, D. R. MacFarlane, M. Forsyth and J. Sun, *Electrochim Acta*, 2003, **48**, 2355-2359.
24. O. Kim, H. Kim, U. H. Choi and M. J. Park, *Nat. Commun*, 2016, **7**, 13576.
25. O. Kim, S. Y. Kim, B. Park, W. Hwang and M. J. Park, *Macromolecules*, 2014, **47**, 4357-4368.
26. X. Fan, S. Liu, Z. Jia, J. J. Koh, J. C. C. Yeo, C.-G. Wang, N. E. Surat'man, X. J. Loh, J. Le Bideau, C. He, Z. Li and T.-P. Loh, *Chem. Soc. Rev*, 2023, **52**, 2497-2527.
27. M. Wang, J. Hu and M. D. Dickey, *JACS Au*, 2022, **2**, 2645-2657.
28. M. A. B. H. Susan, T. Kaneko, A. Noda and M. Watanabe, *J. Am. Chem. Soc*, 2005, **127**, 4976-4983.
29. M. Zou, J. Luo, X. Wang, S. Tan, C. Wang and Y. Wu, *Ind. Eng. Chem. Res*, 2021, **60**, 3589-3596.
30. J. Lan, Y. Li, B. Yan, C. Yin, R. Ran and L.-Y. Shi, *ACS App. Mater. Interfaces*, 2020, **12**, 37597-37606.
31. M. Wang, P. Zhang, M. Shamsi, J. L. Thelen, W. Qian, V. K. Truong, J. Ma, J. Hu and M. D. Dickey, *Nat. Mater*, 2022, **21**, 359-365.
32. L. M. Zhang, Y. He, S. Cheng, H. Sheng, K. Dai, W. J. Zheng, M. X. Wang, Z. S. Chen, Y. M. Chen and Z. Suo, *Small*, 2019, **15**, 1804651.
33. X. Zhang, S. Zeng, Z. Hu, X. Liang, Q. Sun, J. Huang and G. Zu, *ACS Materials. Lett*, 2022, **4**, 2459-2468.
34. J. Rao, X. Wang, R. Yunis, V. Ranganathan, P. C. Howlett, D. R. MacFarlane, M. Forsyth and H. Zhu, *Electrochim. Acta*, 2020, **346**, 136224.
35. H. Srour, M. Leocmach, V. Maffeis, A. C. Ghogia, S. Denis-Quanquin, N. Taberlet, S. Manneville, C. Andraud, C. Bucher and C. Monnereau, *Polym. Chem*, 2016, **7**, 6608-6616.
36. Z. Yu and P. Wu, *Mater. Horiz*, 2021, **8**, 2057-2064.
37. K. G. Cho, S. An, D. H. Cho, J. H. Kim, J. Nam, M. Kim and K. H. Lee, *Adv. Funct. Mater*, 2021, **31**, 2102386.
38. R. Tamate, K. Hashimoto, T. Horii, M. Hirasawa, X. Li, M. Shibayama and M. Watanabe, *Adv. Mater*, 2018, **30**, 1802792.
39. L. Xu, Z. Huang, Z. Deng, Z. Du, T. L. Sun, Z.-H. Guo and K. Yue, *Adv. Mater*, 2021, **33**, 2105306.
40. Z. Cao, H. Liu and L. Jiang, *ACS Appl. Polym. Mater*, 2020, **2**, 2359-2365.

41. C. R. López-Barrón, D. Li, N. J. Wagner and J. L. Caplan, *Macromolecules*, 2014, **47**, 7484-7495.
42. H. Mizuno, K. Hashimoto, R. Tamate, H. Kokubo, K. Ueno, X. Li and M. Watanabe, *Polymer*, 2020, **206**, 122849.
43. S. Zhang, K. H. Lee, C. D. Frisbie and T. P. Lodge, *Macromolecules*, 2011, **44**, 940-949.
44. Y. M. Kim and H. C. Moon, *Adv. Funct. Mater*, 2020, **30**, 1907290.
45. J. Chiefari, Y. K. Chong, F. Ercole, J. Krstina, J. Jeffery, T. P. T. Le, R. T. A. Mayadunne, G. F. Meijs, C. L. Moad, G. Moad, E. Rizzardo and S. H. Thang, *Macromolecules*, 1998, **31**, 5559-5562.
46. D. Ikkene, J.-L. Six and K. Ferji, *Eur. Polym. J*, 2023, **188**, 111848.
47. J. Wan, B. Fan and S. H. Thang, *Chem. Sci*, 2022, **13**, 4192-4224.
48. F. D'Agosto, J. Rieger and M. Lansalot, *Angew. Chem. Int. Ed*, 2020, **59**, 8368-8392.
49. S. L. Canning, G. N. Smith and S. P. Armes, *Macromolecules*, 2016, **49**, 1985-2001.
50. C. Gonzato, M. Semsarilar, E. R. Jones, F. Li, G. J. P. Krooshof, P. Wyman, O. O. Mykhaylyk, R. Tuinier and S. P. Armes, *J. Am. Chem. Soc*, 2014, **136**, 11100-11106.
51. N. Zaquen, W. A. A. W. Azizi, J. Yeow, R. P. Kuchel, T. Junkers, P. B. Zetterlund and C. Boyer, *Polym Chem*, 2019, **10**, 2406-2414.
52. J. Tan, C. Huang, D. Liu, X. Zhang, Y. Bai and L. Zhang, *ACS Macro Lett*, 2016, **5**, 894-899.
53. S. Sahoo, Y. D. Gordievskaya, K. Bauri, A. A. Gavrilov, E. Y. Kramarenko and P. De, *Macromolecules*, 2022, **55**, 1139-1152.
54. L. A. Fielding, M. J. Derry, V. Ladmiral, J. Rosselgong, A. M. Rodrigues, L. P. D. Ratcliffe, S. Sugihara and S. P. Armes, *Chem. Sci*, 2013, **4**, 2081-2087.
55. E. J. Cornel, S. van Meurs, T. Smith, P. S. O'Hora and S. P. Armes, *J. Am. Chem. Soc*, 2018, **140**, 12980-12988.
56. N. J. Warren and S. P. Armes, *J. Am. Chem. Soc*, 2014, **136**, 10174-10185.
57. L. P. D. Ratcliffe, M. J. Derry, A. Ianiro, R. Tuinier and S. P. Armes, *Angew. Chem*, 2019, **58**, 18964-18970.
58. H. J. Kim, F. Ishizuka, S. Chatani, H. Niino and P. B. Zetterlund, *Polym. Chem*, 2023, **14**, 687-696.
59. J. M. Cumming, O. J. Deane and S. P. Armes, *Macromolecules*, 2022, **55**, 788-798.
60. D. L. Beattie, O. J. Deane, O. O. Mykhaylyk and S. P. Armes, *Polym. Chem*, 2022, **13**, 655-667.
61. N. Audureau, F. Coumes, J.-M. Guigner, C. Guibert, F. Stoffelbach and J. Rieger, *Macromolecules*, 2022, **55**, 10993-11005.
62. M. J. Derry, L. A. Fielding and S. P. Armes, *Prog. Polym. Sci*, 2016, **52**, 1-18.
63. D. Das, D. Gerboth, A. Postma, S. Srinivasan, H. Kern, J. Chen, D. M. Ratner, P. S. Stayton and A. J. Convertine, *Polym. Chem*, 2016, **7**, 6133-6143.
64. C. Bergerbit, F. Baffie, A. Wolpers, P.-Y. Dugas, O. Boyron, M. Taam, M. Lansalot, V. Monteil and F. D'Agosto, *Angew. Chem*, 2020, **59**, 10385-10390.
65. P. J. Docherty, M. J. Derry and S. P. Armes, *Polym. Chem*, 2019, **10**, 603-611.
66. C. György, S. J. Hunter, C. Girou, M. J. Derry and S. P. Armes, *Polym. Chem*, 2020, **11**, 4579-4590.
67. S. Boissé, J. Rieger, K. Belal, A. Di-Cicco, P. Beaunier, M.-H. Li and B. Charleux, *Chem. Commun*, 2010, **46**, 1950-1952.
68. F. L. Hatton, M. J. Derry and S. P. Armes, *Polym. Chem*, 2020, **11**, 6343-6355.

69. X. Zhang, S. Boissé, W. Zhang, P. Beaunier, F. D'Agosto, J. Rieger and B. Charleux, *Macromolecules*, 2011, **44**, 4149-4158.
70. H. Zhou, C. Liu, C. Gao, Y. Qu, K. Shi and W. Zhang, *J. Polym. Sci. Part A: Polym Chem*, 2016, **54**, 1517-1525.
71. J. Demarteau, A. Fernandez de Añastro, A. S. Shaplov and D. Mecerreyes, *Polym. Chem*, 2020, **11**, 1481-1488.
72. J. R. Lovett, M. J. Derry, P. Yang, F. L. Hatton, N. J. Warren, Patrick W. Fowler and S. P. Armes, *Chem. Sci*, 2018, **9**, 7138-7144.
73. A. N. Soriano, B. T. Doma and M.-H. Li, *J. Taiwan. Inst. Chem. Eng*, 2010, **41**, 115-121.
74. R. R. Maddikeri, S. Colak, S. P. Gido and G. N. Tew, *Biomacromolecules*, 2011, **12**, 3412-3417.
75. N. P. Cowieson, C. J. C. Edwards-Gayle, K. Inoue, N. S. Khunti, J. Doutch, E. Williams, S. Daniels, G. Preece, N. A. Krumpa, J. P. Sutter, M. D. Tully, N. J. Terrill and R. P. Rambo, *J. Synchrotron Rad*, 2020, **27**, 1438-1446.
76. J. Ilavsky and P. Jemian, *J. Appl. Crystallogr*, 2009, **42**, 347-353.
77. B. Hammouda, *Probing Nanoscale Structures – the sans Toolbox*, 2008.
78. J. Pedersen, *J. Appl. Crystallogr*, 2000, **33**, 637-640.
79. J. Bang, S. Jain, Z. Li, T. P. Lodge, J. S. Pedersen, E. Kesselman and Y. Talmon, *Macromolecules*, 2006, **39**, 1199-1208.
80. L. A. Fielding, J. A. Lane, M. J. Derry, O. O. Mykhaylyk and S. P. Armes, *J. Am. Chem. Soc*, 2014, **136**, 5790-5798.
81. M. J. Derry, L. A. Fielding and S. P. Armes, *Polym Chem*, 2015, **6**, 3054-3062.
82. M. J. Derry, L. A. Fielding, N. J. Warren, C. J. Mable, A. J. Smith, O. O. Mykhaylyk and S. P. Armes, *Chem. Sci*, 2016, **7**, 5078-5090.
83. M. Zare, A. Bigham, M. Zare, H. Luo, E. Rezvani Ghomi and S. Ramakrishna, *Int. J. Mol. Sci.*, 2021, **22**, 6376.
84. A. Blanazs, J. Madsen, G. Battaglia, A. J. Ryan and S. P. Armes, *J. Am. Chem. Soc*, 2011, **133**, 16581-16587.
85. V. J. Cunningham, A. M. Alswieleh, K. L. Thompson, M. Williams, G. J. Leggett, S. P. Armes and O. M. Musa, *Macromolecules*, 2014, **47**, 5613-5623.
86. A. Blanazs, R. Verber, O. O. Mykhaylyk, A. J. Ryan, J. Z. Heath, C. W. I. Douglas and S. P. Armes, *J. Am. Chem. Soc*, 2012, **134**, 9741-9748.

4. Characterisation of worm ionogels prepared via polymerisation-induced self-assembly in 1-ethyl-3-methylimidazolium dicyanamide

Reproduced in part with permission from [G. L. Maitland; M. Liu; T. J. Neal; J. Hammerton; Y. Han; S. D. Worrall; P. D. Topham; M. J. Derry, *Chemical Science*, **2024**, 15, 4416-4426]

4.1 Introduction

Ionogels are defined as an ionic liquid (IL) trapped in a crosslinked network such as an inorganic network or a polymer network. Depending on their targeted application, mechanical and rheological properties are essential to consider.[1] Current ionogels formulations consist of relatively soft gels which are ideal for applications such as actuators,[2-4] sensors[5] and wearable electronics.[6]

Several methods of enhancing mechanical properties of soft ionogels have been reported, such as introducing sacrificial bonds into polymer networks in order to dispel energy.[7] For example, double-network (DN) ionogels[8-10] have been found to be much tougher than single-network ionogels. DN ionogels have an elastic network, as a well as a brittle network which are both characterised as soft and brittle, respectively. Ionogels can also be toughened by incorporating non-covalent interactions between the IL and polymer network such as hydrogen bonding or electrostatic interactions. Alternatively, non-covalent interactions between polymer chains can strengthen ionogels. More relevant to this research, mechanical properties of ionogels can be improved by forming phase-separated domains of block polymers.[6, 11, 12] Specifically, block copolymers composed of an IL-philic and an IL-phobic block can phase separate in the ionic liquid to form uniform networks as a result of the breakage of non-covalent interactions in the polymer network, therefore toughening the gels when the energy dissipates. Typically, these block copolymers are synthesised via reversible addition-fragmentation chain transfer (RAFT) polymerisation, followed by purification and then mixing with the IL with the aid of a co-solvent to facilitate the formation of the ionogel. The co-solvent is then removed by evaporation, affording microphase-separated polymer networks in the chosen IL (Figure 4.1).

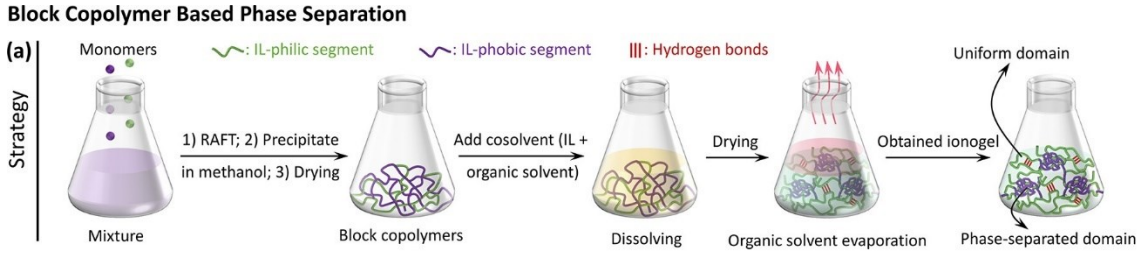

Figure 4.1. Soft but toughened ionogels synthesis from phase separation of block copolymers.[7]

The work conducted in Chapter 3 showed that *in situ* formation of block copolymer soft worm ionogels in 1-ethyl-3-methylimidazolium dicyanamide, [EMIM][DCA], is possible without the need for post-polymerisation processing or a co-solvent aid. For this Thesis, it is important to understand the rheological properties of the soft worm ionogels to ensure they are mechanically robust.

Using oscillatory rheology, it is generally acknowledged that a 'true' gel can be confirmed by a reasonably linear viscoelastic behaviour of the gels and frequency-independence of storage modulus (i.e. the elastic component) and loss modulus (i.e. the viscous component) (*G*' and *G*'', respectively), with *G*'' being substantially lower than *G*'.[13] Moreover, strain-sweeps enable the determination of the strain at which the worm ionogels degel, often termed the strain at break (Figure 4.2).

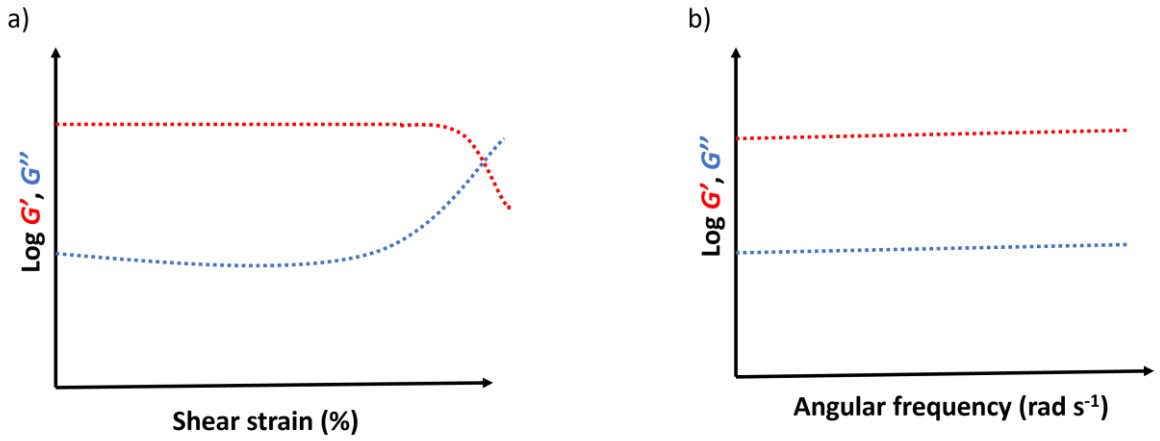

Figure 4.2. a) Representative strain-sweep trend expected for viscoelastic materials. The crossover of *G*' and *G*'' indicates the critical strain of degelation. b) Representative frequency-sweep trend expected for viscoelastic materials. *G*' and *G*'' are frequency-independent moduli, with *G*'' being considerably lower than *G*'.

Depending on the desired application, ionogels are required to operate at high temperatures and over broad temperature ranges.[1] Thermogravimetric analysis (TGA)[14] is a commonly used to obtain a thermal profile of a given polymer. In essence, this is measured by the weight change of the polymer with respect to temperature and time.[15] The weight change of the polymers can be caused by a range of physical processes such as vaporisation and desorption etc., or by oxidation and decomposition. TGA has been shown to be a well-established technique for characterising ionogels, notably demonstrating high decomposition temperatures and long-term thermal

stability at high temperatures, particularly in comparison to hydrogels with no ionic liquid (IL) content.[16]

Ionic conductivity is an essential feature of ionogels. In comparison to ionogels fabricated using poly(ionic liquids) (PILs), ionogels composed of ILs that can move freely as a mobile phase amongst host networks generally display a higher ionic conductivity.[1] Furthermore, the choice of IL affects the ionogel ionic conductivity. IL that consist of anions with weak ability to hydrogen bond such as dicyanamide ([DCA]) and hexafluorophosphate ([PF_6]) typically display improved ionic conductivity,[17] as well as ion sizes and viscosity of the ILs. However, in this Thesis, the effect of polymer content within the ionogel on the electrochemical properties of the material is investigated. The higher the proportion of ILs, the better the electrochemical properties of the ionogels are expected to be. Ionic conductivity is one way of assessing the electrochemical properties of the ionogels. For example, Chen *et al.*[18] reported the fabrication of an ionogel for strain sending consisting of poly(urethane-urea) (PUU) copolymer and [EMIM][DCA]. Systematically increasing the IL content of the ionogels from 20% w/w to 60% w/w demonstrated an increasing ionic conductivity from 0.072 S m^{-1} up to 2.25 S m^{-1}, respectively. However, tensile testing of each ionogel indicated that the IL itself acted as a plasticiser, as judged by the increasing trend in breaking strain but decreasing Young's modulus and tensile strength. In essence, as the IL content increases, the ionogels become weaker yet more flexible.

Electrochemical impedance spectroscopy (EIS)[19] is a useful technique for determining electrochemical characteristics such as diffusion and ion exchange between materials and their interfaces.[20] Notably, EIS has been used to characterise ionogels for several electrochemical applications, such as lithium-ion batteries,[21-24] supercapacitors[25-27] and dye-sensitised solar cells (DSSCs).[28] Specifically in this Chapter, EIS is used to determine the bulk resistance of the ionogels by plotting so-called Nyquist plots and extracting the x-intercept at high frequencies.

In this Chapter, rheological, electrochemical and thermal properties of the previously synthesised poly(2-hydroxyethyl methacrylate)-*block*-poly(benzyl methacrylate) (PHEMA-*b*-PBzMA) block copolymers worm ionogels prepared in [EMIM][DCA] at 15% w/w are explored. Critical gel concentration (CGC) screenings are conducted in order to assess the concentration at which degelation occurs and subsequent rheological analysis is conducted on each sample to assess the viscoelastic properties of the worm ionogels.

4.2 Experimental

4.2.1 Materials

Poly(2-hydroxyethyl methacrylate)$_{30}$ macromolecular chain-transfer agent ($PHEMA_{30}$ mCTA) was synthesised as previously described in Chapter 3 (2-hydroxyethyl methacrylate (HEMA)conversion = 40%; M_n = 8,000 g mol^{-1}, $Đ_M$ = 1.25). Benzyl methacrylate (BzMA) was purchased from Sigma Aldrich and passed through a basic alumina column prior to use in order to remove the inhibitor. 2,2'-Azobisisobutyronitrile (AIBN) was purchased from Molekula and was recrystallised from methanol prior to use. Dimethyl sulfoxide-d6 (DMSO-d6) for ^{1}H NMR analysis was purchased from Goss Scientific. 1-Ethyl-3-methylimidazolium dicyanamide, [EMIM][DCA], was acquired from BASF.

4.2.3 Oscillatory rheology

The loss and storage moduli were measured as a function of shear strain between 0.1% and 100% at a fixed angular frequency of 6.28 rad s^{-1} to assess the gel strength. The moduli were also measured as a function of frequency between 1 rad s^{-1} and 100 rad s^{-1} at a fixed complex shear strain of 1.0%. All measurements were conducted at 25 °C.

4.2.4 Electrochemical impedance spectroscopy (EIS)

Electrochemical impedance spectroscopy (EIS)[19] measurements were performed in a symmetrical two electrode configuration. Stainless steel spacers (15.5 mm diameter, 0.5 mm thickness) were used as the electrodes and were separated by either Whatman Grade 1 Qualitative Filter Paper soaked in [EMIM][DCA] or an ionogel sample, within a sealed CR2032 coin cell. EIS was performed using a PGSTAT302N potentiostat (Metrohm Autolab B.V., The Netherlands) over the frequency range 1 MHz – 200 mHz with a 10 mV RMS perturbation voltage. Bulk resistance values were extracted from Nyquist plots by taking the high frequency intercept of the x-axis. Measurements were performed in triplicate.

4.2.5 Thermogravimetric analysis (TGA)

Thermogravimetric analysis (TGA) was used to assess the thermal behaviour of the gels, focusing on their thermal degradation temperature relative to the IL alone. The thermal degradation was measured by monitoring the relative change in mass as a function of increasing temperature. TGA was performed using a PerkinElmer TGA 8000 under nitrogen atmosphere (flow rate 40 mL min^{-1}). All samples were heated from 150 °C to 600 °C at a rate of 10 °C min^{-1}.

4.2.6 Synthesis of additional poly(2-hydroxyethyl methacrylate)-*block*-poly(benzyl methacrylate) ($PHEMA_{30}$-*b*-$PBzMA_y$) block copolymers for critical gel concentration (CGC) studies

$PHEMA_{30}$-*b*-$PBzMA_y$ block copolymers were synthesised via the same protocol as reported in Chapter 3. A degree of polymerisation of 300 for the second block, PBzMA, was targeted and syntheses were conducted at copolymer concentrations ranging from 10% w/w to 1% w/w. The block copolymers were initially characterised using ^{1}H nuclear magnetic resonance (NMR) spectroscopy, gel permeation chromatography (GPC) and dynamic light scattering (DLS). The same protocols used for these were as described in Chapter 3.

4.3 Results and discussion

4.3.1 Rheological studies of worm ionogels

Rheological studies of all 15% w/w $PHEMA_{30}$-*b*-$PBzMA_y$ dispersions that were synthesised in Chapter 3 were conducted to assess their viscoelastic properties. Specifically, angular frequency and strain sweeps were conducted (see Figures 4.4). The storage modulus, *G'*, obtained at 1% strain and an angular frequency of 6.28 rad s^{-1} for each nanoparticle dispersion was plotted as a function of PBzMA DP as shown in Figure 4.3.

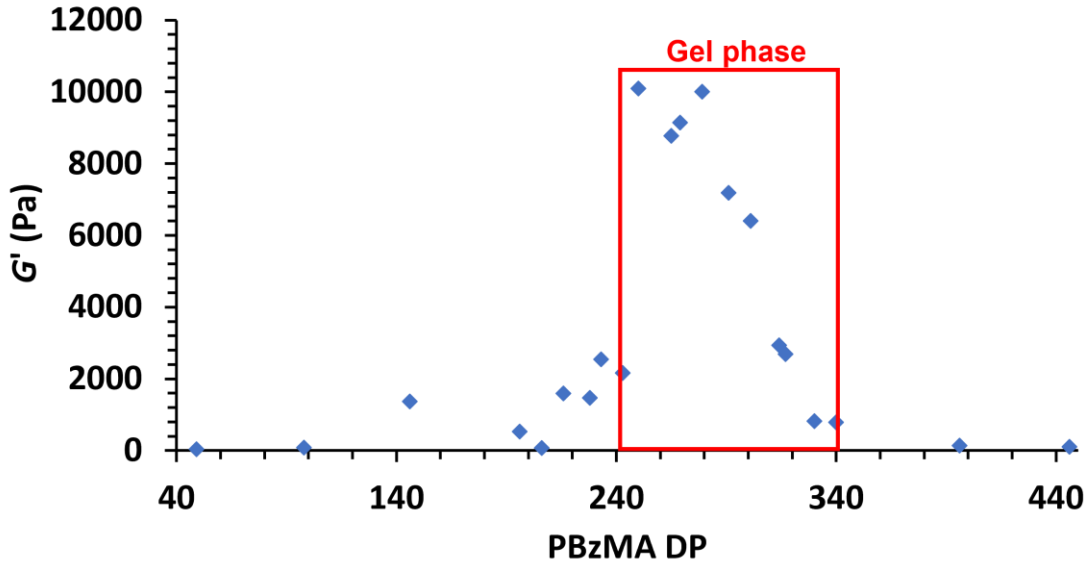

Figure 4.3. Initial G' vs. PBzMA DP for the $PHEMA_{30}$-b-$PBzMA_y$ series at 15% w/w, at a fixed angular frequency of 6.28 rad s^{-1}, shear strain of 1.0% and 25 °C. The region outlined in red denotes the gel range based on inversion tests.

Samples with PBzMA DP < 228 exhibited a relatively low initial *G*' (<2,500 Pa), which coincides with their physical form of transparent free-flowing liquids. SAXS patterns for dispersions in this PBzMA DP range show that morphologies change from dissolved chains when PBzMA < 100 (see Figure 3.9 in Section 3.3.3) to mixtures of spheres and worms for PBzMA DPs between 96 and 228. The *G*' value increased from ~2,500 Pa to ~10,000 Pa as the PBzMA DP was increased from 228 to 291, which corresponds to the DP range that forms free-standing gels (see Figure 3.5 in Section 3.3.2). Generally, this is in good agreement with fitting corresponding SAXS data which indicated the presence of worm-like particles, often with a small population of spheres, with samples that exhibited the highest *G*' value possessing the highest proportion of worms. The presence of more worm-like nanoparticles most likely results in gels with increased *G*' as a result of an increase in the number of inter-worm contacts and thus the formation of a more extended percolating network.[29] At PBzMA DPs between 314 and 330, *G*' decreases from approximately 7,000 Pa to 1,000 Pa, and fitting SAXS data indicates a substantial decrease in the proportion of worm-like structures alongside a considerable increase in the proportion of vesicles. This coincides with the physical appearance of these dispersions changing from free-standing gels to free-flowing turbid liquids over this PBzMA DP range. At PBzMA DPs > 330, *G*' decreases from approximately 1,000 Pa to a limiting value of ~100 Pa, and SAXS fittings confirm the presence of vesicular morphologies only. Additionally, oscillatory rheology studies of each free-standing gel sample confirmed their linear viscoelastic behaviour and relatively frequency-independent variation of *G*' (Figures 4.4-4.25 for all data), indicating the generation of 'true' gels.[30]

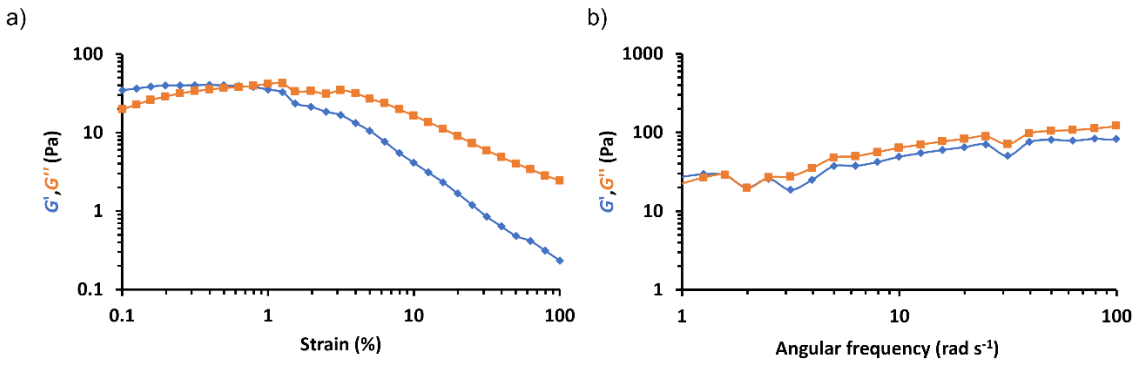

Figure 4.4. Oscillatory rheology data obtained for 15% w/w $PHEMA_{30}$-$PBzMA_{49}$ in [EMIM][DCA] at 25 °C. a) Strain sweep at a fixed angular frequency of 6.28 rad s^{-1} and b) frequency sweep at fixed a strain of 1.0%.

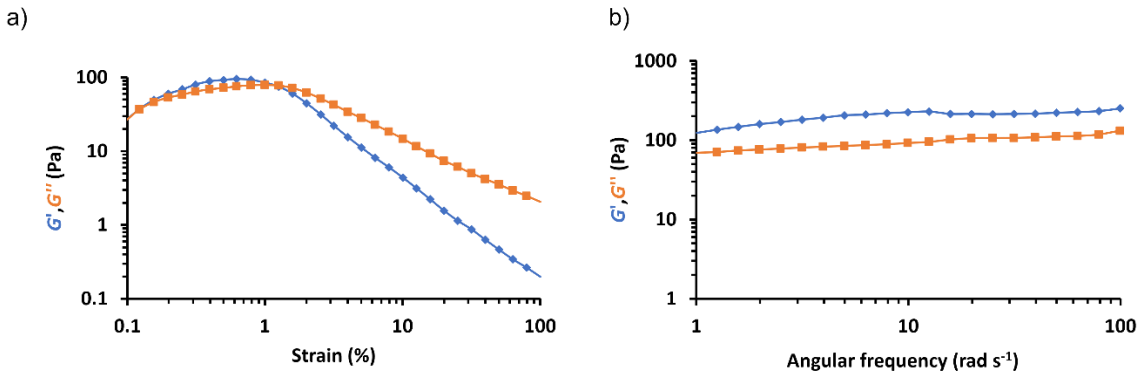

Figure 4.5. Oscillatory rheology data obtained for 15% w/w $PHEMA_{30}$-$PBzMA_{98}$ in [EMIM][DCA] at 25 °C. a) Strain sweep at a fixed angular frequency of 6.28 rad s^{-1} and b) frequency sweep at fixed a strain of 1.0%.

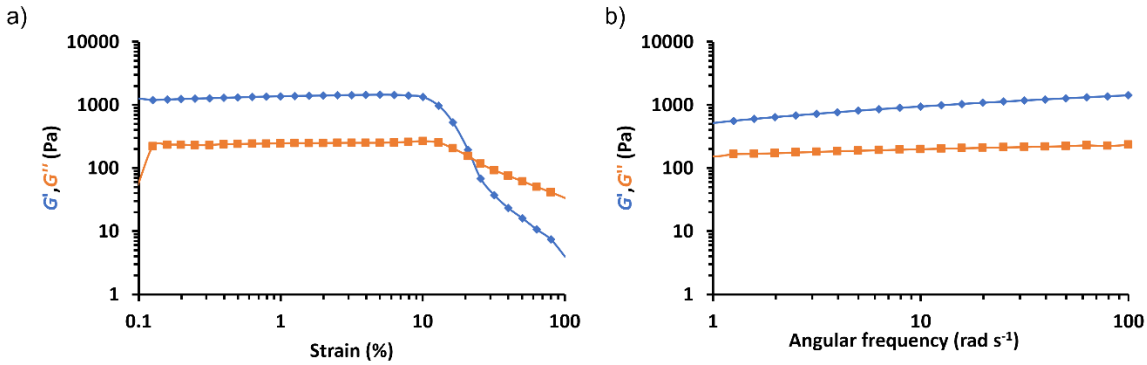

Figure 4.6. Oscillatory rheology data obtained for 15% w/w $PHEMA_{30}$-$PBzMA_{146}$ in [EMIM][DCA] at 25 °C. a) Strain sweep at a fixed angular frequency of 6.28 rad s^{-1} and b) frequency sweep at fixed a strain of 1.0%.

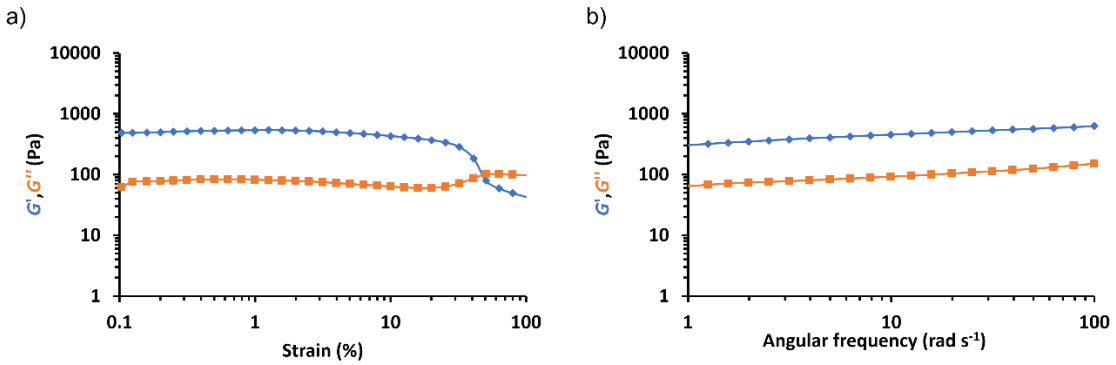

Figure 4.7. Oscillatory rheology data obtained for 15% w/w $PHEMA_{30}$-$PBzMA_{196}$ in [EMIM][DCA] at 25 °C. a) Strain sweep at a fixed angular frequency of 6.28 rad s^{-1} and b) frequency sweep at fixed a strain of 1.0%.

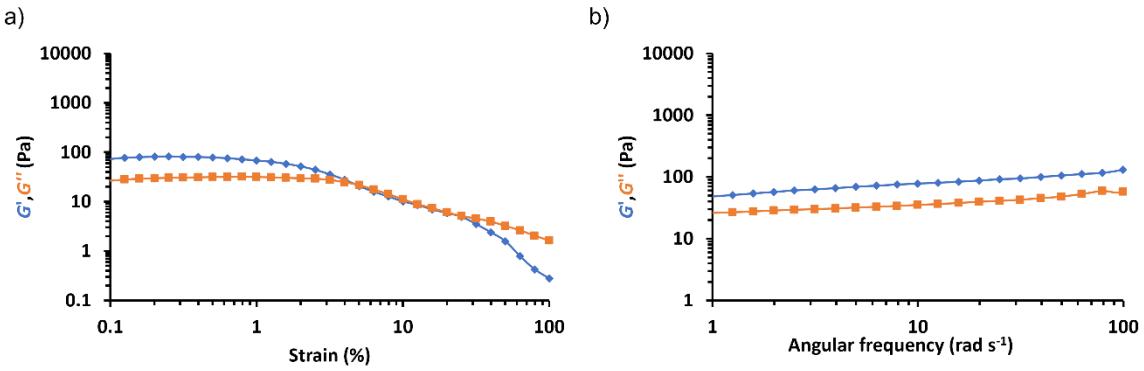

Figure 4.8. Oscillatory rheology data obtained for 15% w/w $PHEMA_{30}$-$PBzMA_{206}$ in [EMIM][DCA] at 25 °C. a) Strain sweep at a fixed angular frequency of 6.28 rad s^{-1} and b) frequency sweep at fixed a strain of 1.0%.

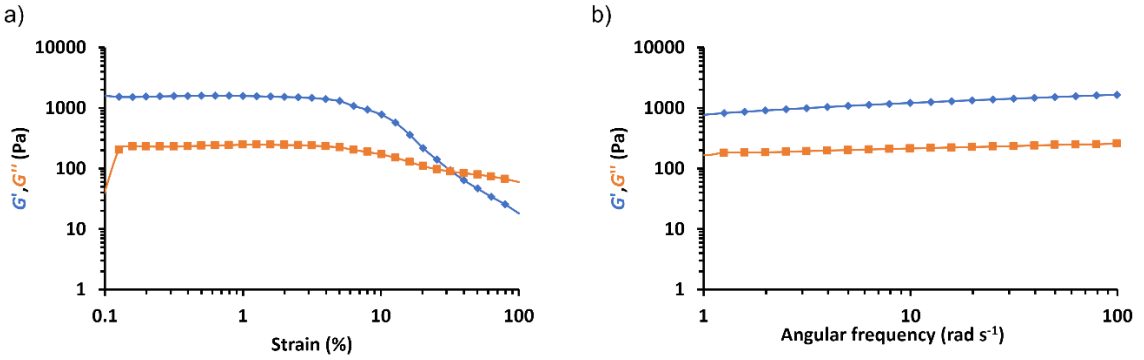

Figure 4.9. Oscillatory rheology data obtained for 15% w/w $PHEMA_{30}$-$PBzMA_{216}$ in [EMIM][DCA] at 25 °C. a) Strain sweep at a fixed angular frequency of 6.28 rad s^{-1} and b) frequency sweep at fixed a strain of 1.0%.

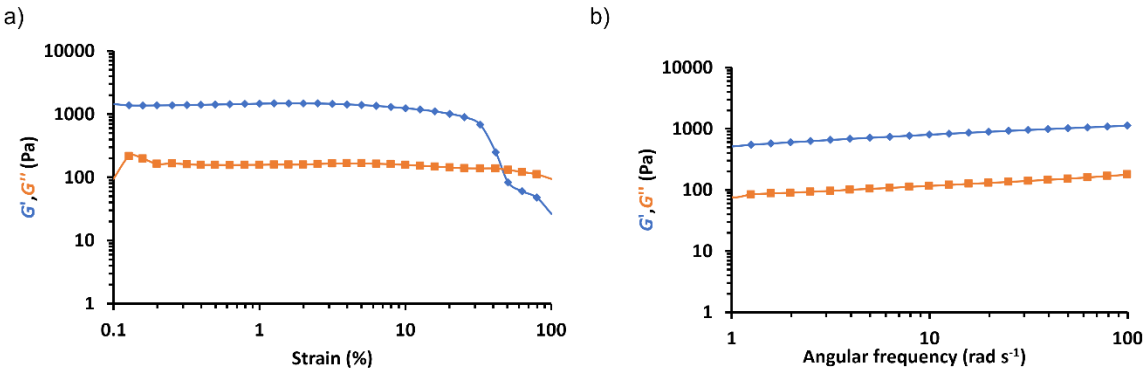

Figure 4.10. Oscillatory rheology data obtained for 15% w/w $PHEMA_{30}$-$PBzMA_{228}$ in [EMIM][DCA] at 25 °C. a) Strain sweep at a fixed angular frequency of 6.28 rad s^{-1} and b) frequency sweep at fixed a strain of 1.0%.

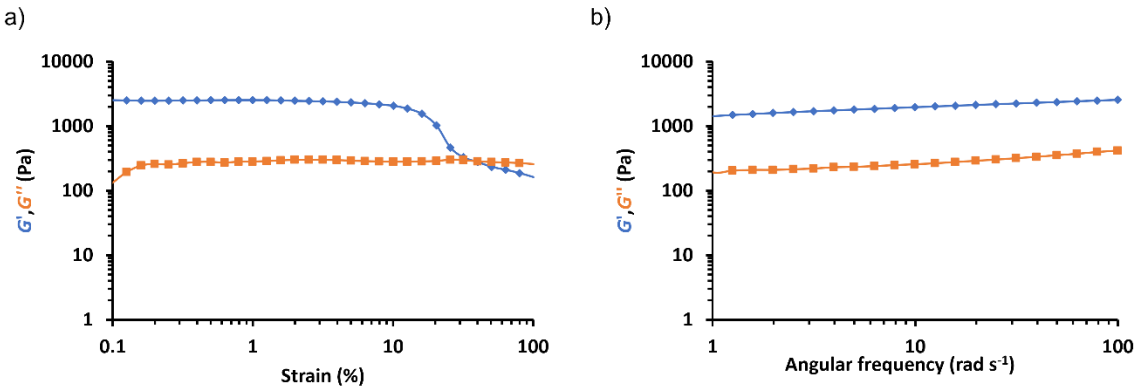

Figure 4.11. Oscillatory rheology data obtained for 15% w/w $PHEMA_{30}$-$PBzMA_{233}$ in [EMIM][DCA] at 25 °C. a) Strain sweep at a fixed angular frequency of 6.28 rad s^{-1} and b) frequency sweep at fixed a strain of 1.0%.

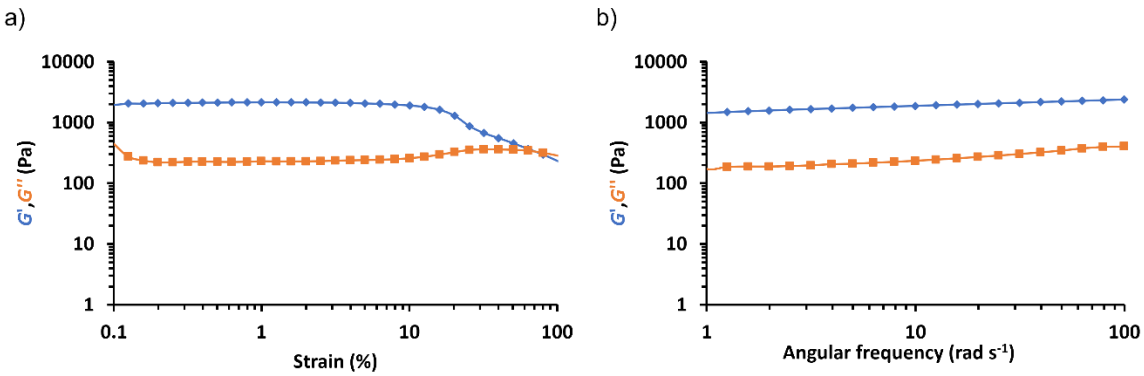

Figure 4.12. Oscillatory rheology data obtained for 15% w/w $PHEMA_{30}$-$PBzMA_{243}$ in [EMIM][DCA] at 25 °C. a) Strain sweep at a fixed angular frequency of 6.28 rad s^{-1} and b) frequency sweep at fixed a strain of 1.0%.

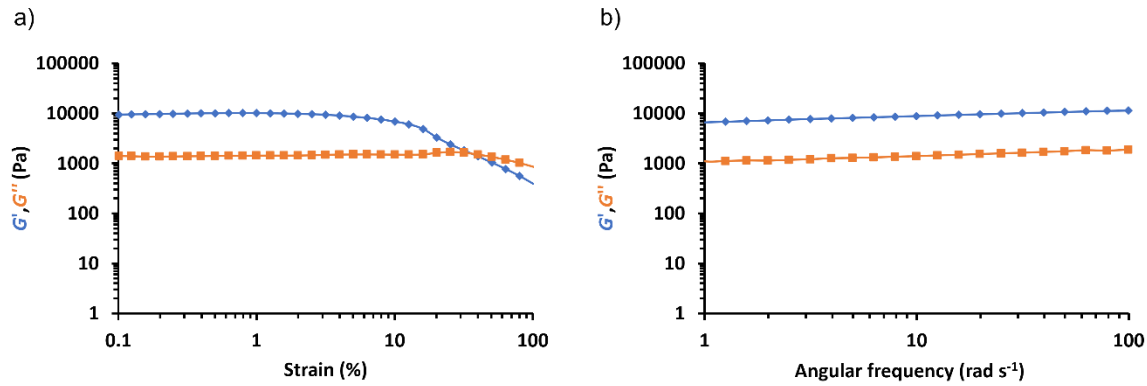

Figure 4.13. Oscillatory rheology data obtained for 15% w/w $PHEMA_{30}$-$PBzMA_{250}$ in [EMIM][DCA] at 25 °C. a) Strain sweep at a fixed angular frequency of 6.28 rad s^{-1} and b) frequency sweep at fixed a strain of 1.0%.

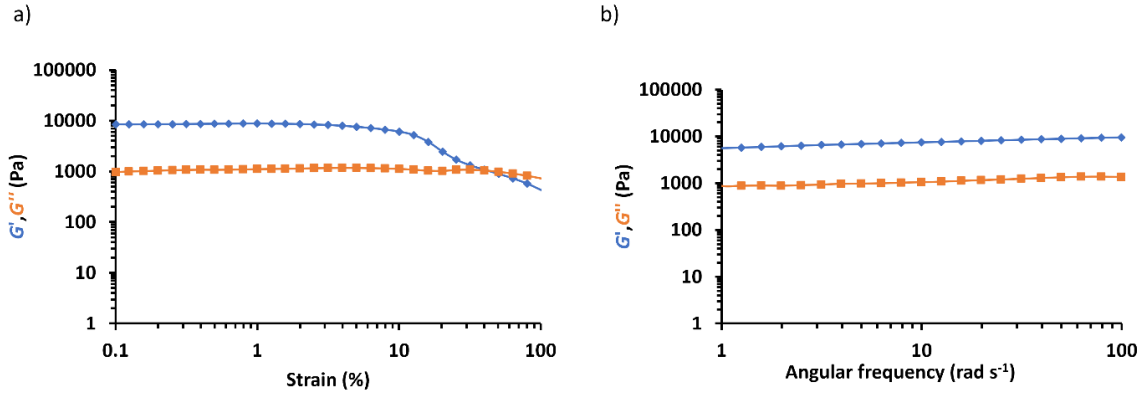

Figure 4.14. Oscillatory rheology data obtained for 15% w/w $PHEMA_{30}$-$PBzMA_{265}$ in [EMIM][DCA] at 25 °C. a) Strain sweep at a fixed angular frequency of 6.28 rad s^{-1} and b) frequency sweep at fixed a strain of 1.0%.

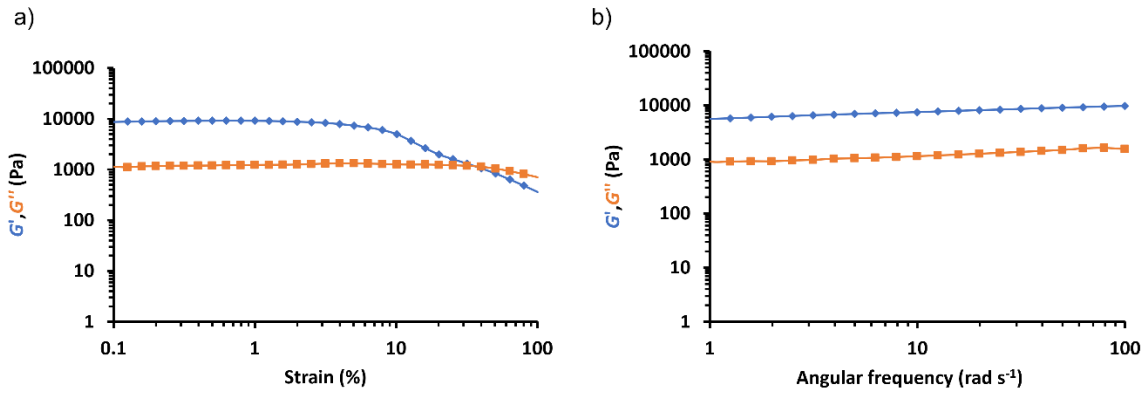

Figure 4.15. Oscillatory rheology data obtained for 15% w/w $PHEMA_{30}$-$PBzMA_{269}$ in [EMIM][DCA] at 25 °C. a) Strain sweep at a fixed angular frequency of 6.28 rad s^{-1} and b) frequency sweep at fixed a strain of 1.0%.

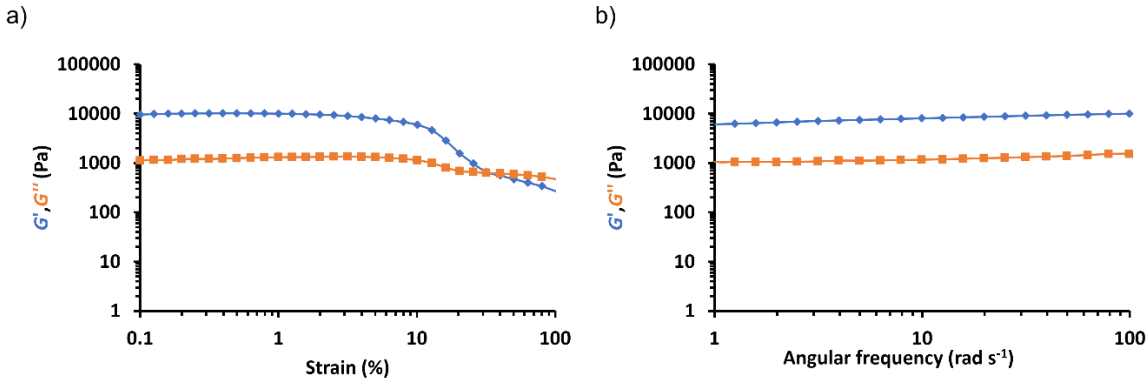

Figure 4.16. Oscillatory rheology data obtained for 15% w/w $PHEMA_{30}$-$PBzMA_{279}$ in [EMIM][DCA] at 25 °C. a) Strain sweep at a fixed angular frequency of 6.28 rad s^{-1} and b) frequency sweep at fixed a strain of 1.0%.

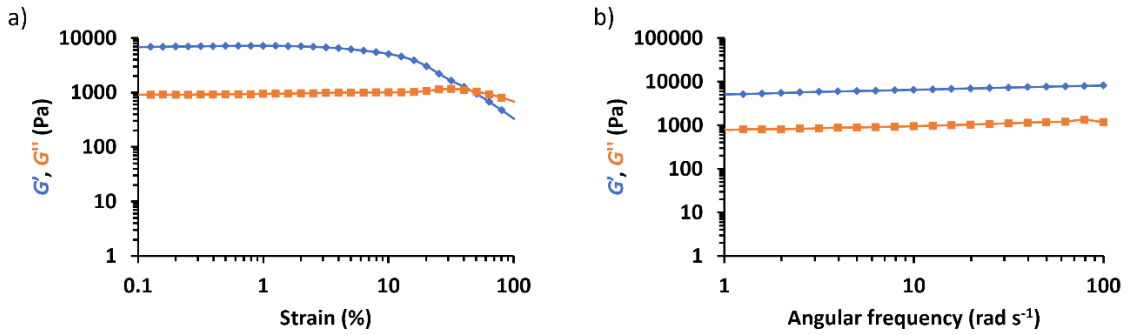

Figure 4.17. Oscillatory rheology data obtained for 15% w/w $PHEMA_{30}$-$PBzMA_{291}$ in [EMIM][DCA] at 25 °C. a) Strain sweep at a fixed angular frequency of 6.28 rad s^{-1} and b) frequency sweep at fixed a strain of 1.0%.

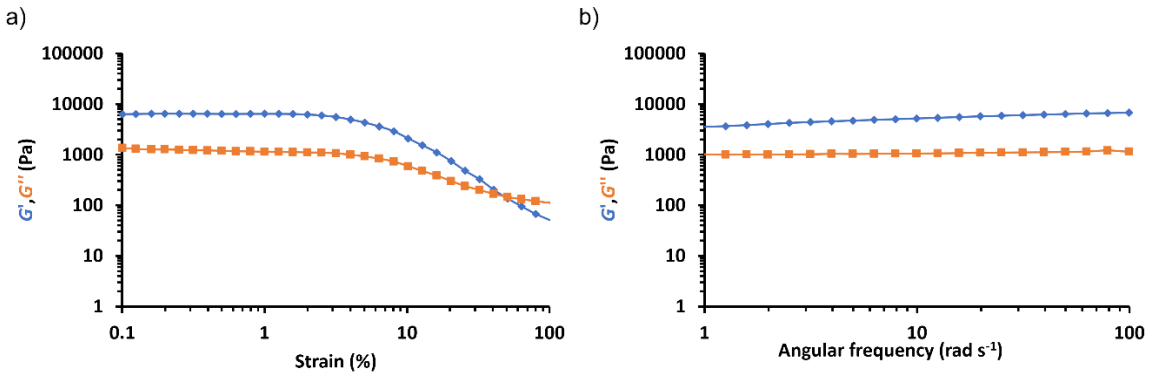

Figure 4.18. Oscillatory rheology data obtained for 15% w/w $PHEMA_{30}$-$PBzMA_{301}$ in [EMIM][DCA] at 25 °C. a) Strain sweep at a fixed angular frequency of 6.28 rad s^{-1} and b) frequency sweep at fixed a strain of 1.0%.

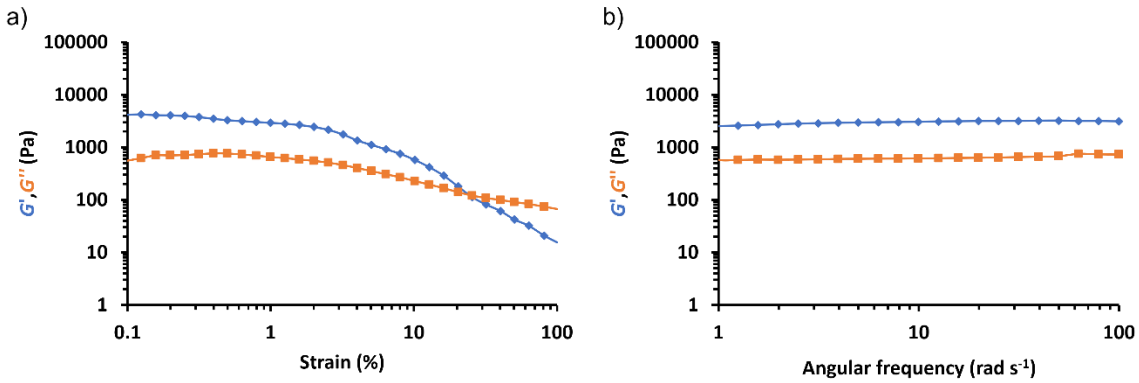

Figure 4.19. Oscillatory rheology data obtained for 15% w/w $PHEMA_{30}$-$PBzMA_{314}$ in [EMIM][DCA] at 25 °C. a) Strain sweep at a fixed angular frequency of 6.28 rad s^{-1} and b) frequency sweep at fixed a strain of 1.0%.

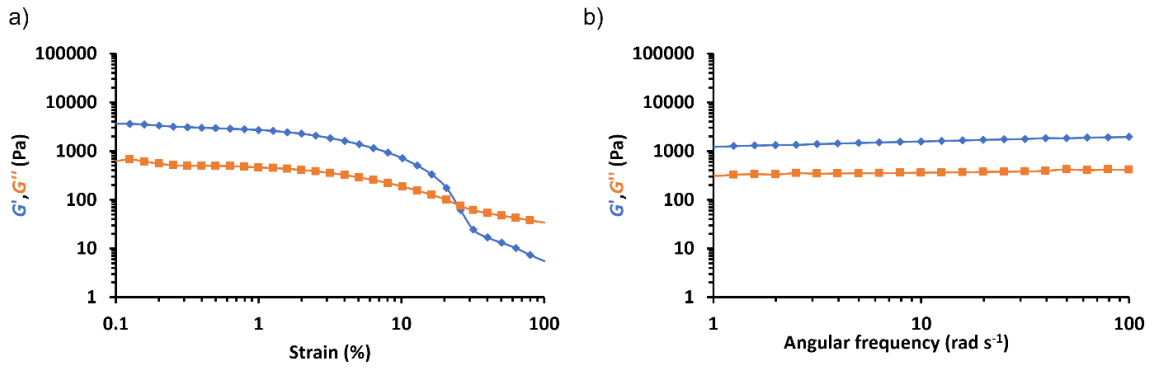

Figure 4.20. Oscillatory rheology data obtained for 15% w/w $PHEMA_{30}$-$PBzMA_{317}$ in [EMIM][DCA] at 25 °C. a) Strain sweep at a fixed angular frequency of 6.28 rad s^{-1} and b) frequency sweep at fixed a strain of 1.0%.

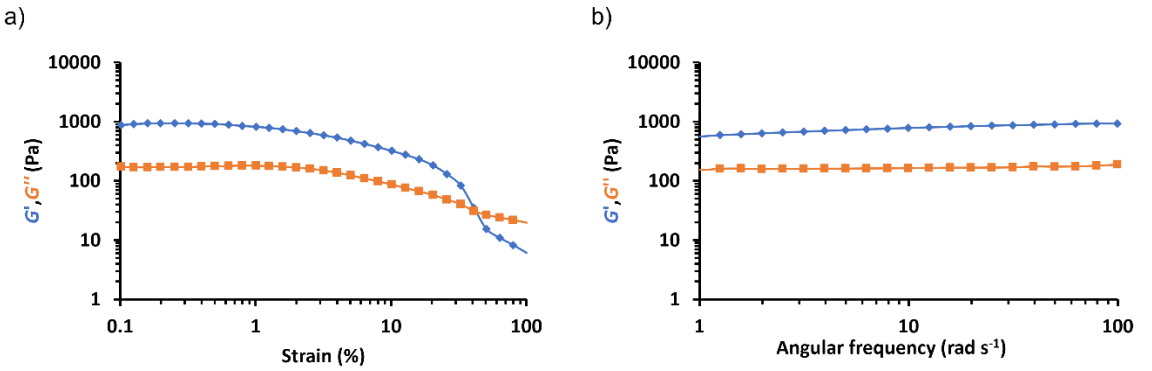

Figure 4.21. Oscillatory rheology data obtained for 15% w/w $PHEMA_{30}$-$PBzMA_{330}$ in [EMIM][DCA] at 25 °C. a) Strain sweep at a fixed angular frequency of 6.28 rad s^{-1} and b) frequency sweep at fixed a strain of 1.0%.

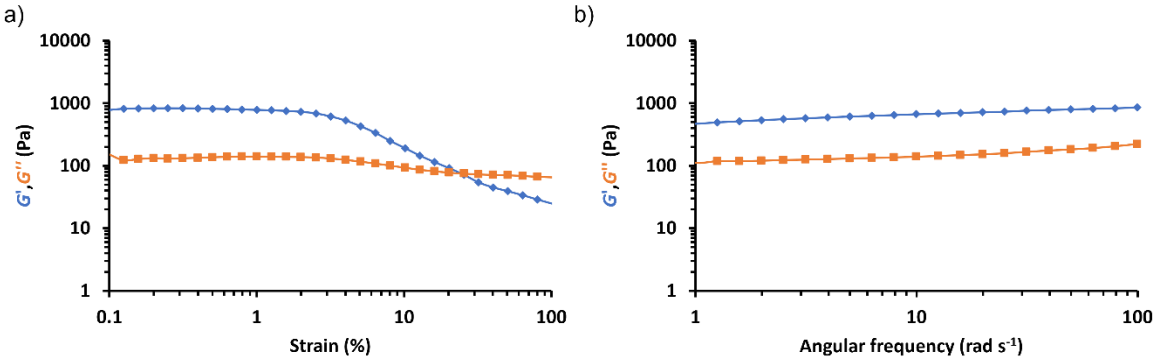

Figure 4.22. Oscillatory rheology data obtained for 15% w/w $PHEMA_{30}$-$PBzMA_{340}$ in [EMIM][DCA] at 25 °C. a) Strain sweep at a fixed angular frequency of 6.28 rad s^{-1} and b) frequency sweep at fixed a strain of 1.0%.

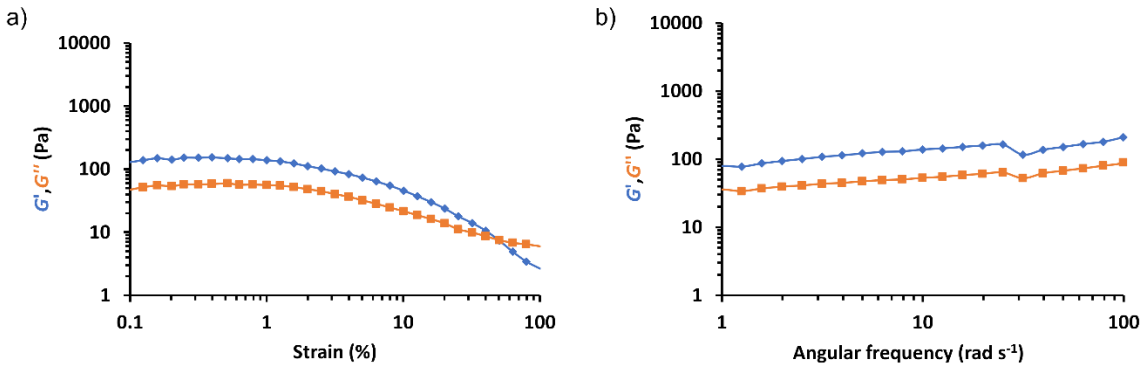

Figure 4.23. Oscillatory rheology data obtained for 15% w/w $PHEMA_{30}$-$PBzMA_{396}$ in [EMIM][DCA] at 25 °C. a) Strain sweep at a fixed angular frequency of 6.28 rad s^{-1} and b) frequency sweep at fixed a strain of 1.0%.

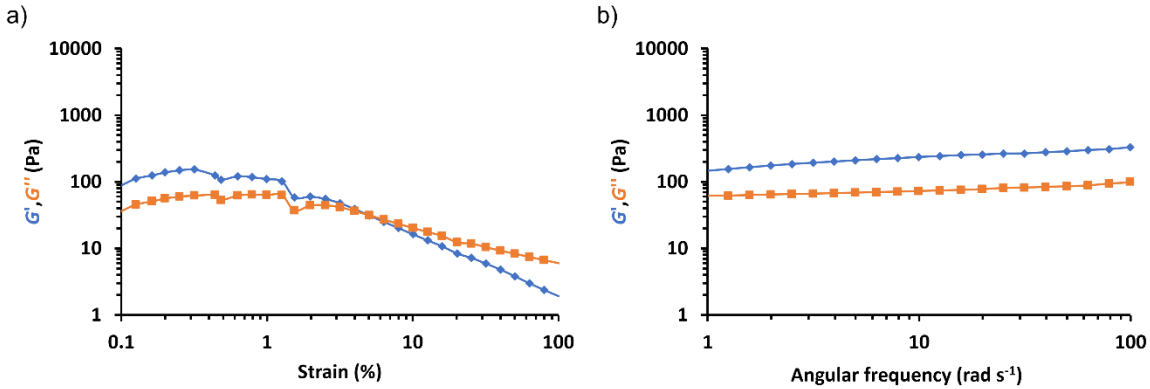

Figure 4.24. Oscillatory rheology data obtained for 15% w/w $PHEMA_{30}$-$PBzMA_{446}$ in [EMIM][DCA] at 25 °C. a) Strain sweep at a fixed angular frequency of 6.28 rad s^{-1} and b) frequency sweep at fixed a strain of 1.0%.

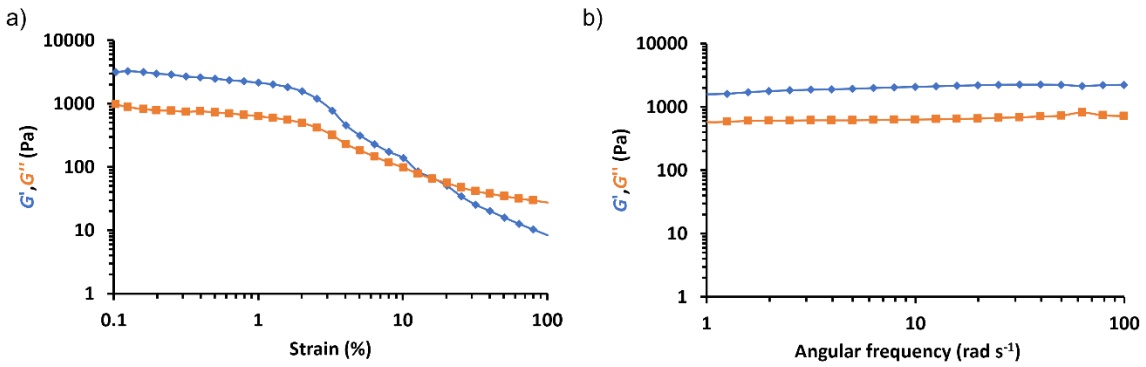

Figure 4.25. Oscillatory rheology data obtained for 15% w/w $PHEMA_{30}$-$PBzMA_{490}$ in [EMIM][DCA] at 25 °C. a) Strain sweep at a fixed angular frequency of 6.28 rad s^{-1} and b) frequency sweep at fixed a strain of 1.0%.

As previously discussed, the critical gel concentration of PHEMA$_{30}$-*b*-PBzMA$_y$ block copolymer worms appeared to be >4% w/w based on inversion tests. This was further evidenced when monitoring the *G*' of each dispersion (see Figure 4.26), which highlights a significant decrease in *G*' for copolymer concentrations ≤4% w/w. Importantly, angular frequency sweeps confirmed that *G*' > *G*" for worm dispersions at copolymer concentrations above this observed CGC (see Figure 4.26), as expected.

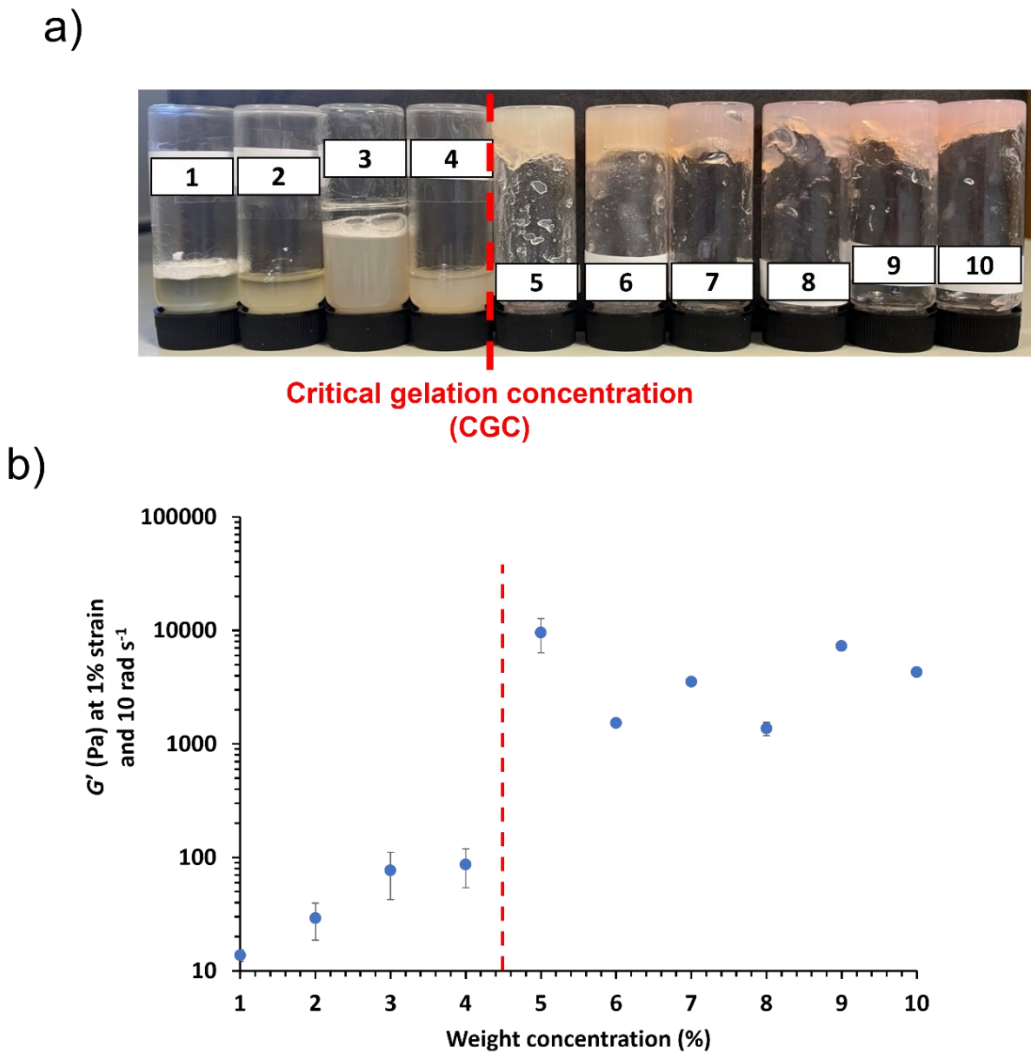

Figure 4.26. a) Digital images of critical gelation concentration (CGC) screenings conducted for the synthesis of PHEMA$_{30}$-b-PBzMA$_{300}$ (300 = target DP of PBzMA) between 1% w/w and 10% w/w. b) G' vs. % w/w solids of each gel at a fixed angular frequency of 10 rad s^{-1}, 1% strain and 25 °C. Vertical red dashed lines denote the CGC.

4.3.2 Additional syntheses of $PHEMA_{30}$-*b*-$PBzMA_y$ block copolymers for critical gelation concentration (CGC) studies

In order to maximise electrochemical properties whilst still achieving ionogel formation, it is important to reduce the polymer content. In order to assess the minimum copolymer concentration required to generate a worm ionogel for this formulation, commonly referred to as the critical gel concentration (CGC), a series of targeted $PHEMA_{30}$-*b*-$PBzMA_{300}$ block copolymers were synthesised at copolymer concentrations between 10% w/w and 1% w/w. This target composition was selected for CGC studies since it lies near the centre of the gel phase indicated in Figure 4.3 and has the highest proportion of worms as confirmed by SAXS (82.6% v/v worms) (Section 3.3.3, Figure 3.22 and Table 3.2). Free-standing gels are no longer formed at copolymer concentrations where there are insufficient worm contacts to form a physically crosslinked network, thus yielding free-flowing fluids.[29] These block copolymers were characterised by ^{1}H NMR spectroscopy, GPC and DLS prior to rheological studies. The summary of these results are found below in Table 4.1 and select DLS data is presented in Figures 4.27-4.32. Based on the work conducted in Chapter 3, where free-standing gels indicated worm gels as confirmed by nanoparticle characterisation, it was assumed that free-standing gels that were yielded at the concentrations >4% w/w in this chapter also contained a sufficient proportion of worm-like morphologies.

Table 4.1. Summary of targeted copolymer composition, BzMA conversion, actual copolymer composition, theoretical M_n, GPC M_n and $Đ_M$ (= M_w/M_n), and DLS diameter and PDI for targeted $PHEMA_{30}$-*b*-$PBzMA_{300}$ diblock copolymers prepared by RAFT dispersion polymerisation of BzMA in [EMIM][DCA] at 70 °C and various copolymer concentrations, using AIBN initiator ([$PHEMA_{30}$ macro-CTA]/[AIBN] molar ratio = 5.0). $PHPMA_{30}$-*b*-$PBzMA_y$ is denoted as H_{30}-B_y for brevity.

		^{1}H NMR spectroscopy		DMF GPC		DLS	
Copolymer concentration (% w/w)	**BzMA conversion (%)**	**Actual composition**	**$M_{n,th}$ (g mol^{-1})**	**M_n (g mol^{-1})**	**$Đ_M$**	**Diameter (nm)**	**PDI**
15	97	H_{30}-B_{291}	55,331	52,900	1.31	238	0.06
10	90	H_{30}-B_{270}	51,761	53,200	1.36	500	0.36
9	94	H_{30}-B_{282}	53,875	56,100	1.43	324	0.27
8	89	H_{30}-B_{267}	51,232	53,100	1.32	361	0.30
7	89	H_{30}-B_{267}	51,232	50,200	1.47	317	0.41
6	98	H_{30}-B_{294}	55,990	53,200	2.12	200	0.28
5	97	H_{30}-B_{291}	55,461	69,500	1.67	770	0.76
4	98	H_{30}-B_{294}	55,990	53,600	1.94	-	-
3	92	H_{30}-B_{276}	52,818	63,000	1.39	-	-
2	99	H_{30}-B_{297}	56,518	43,600	1.67	-	-
1	95	H_{30}-B_{285}	54,404	33,500	1.49	-	-

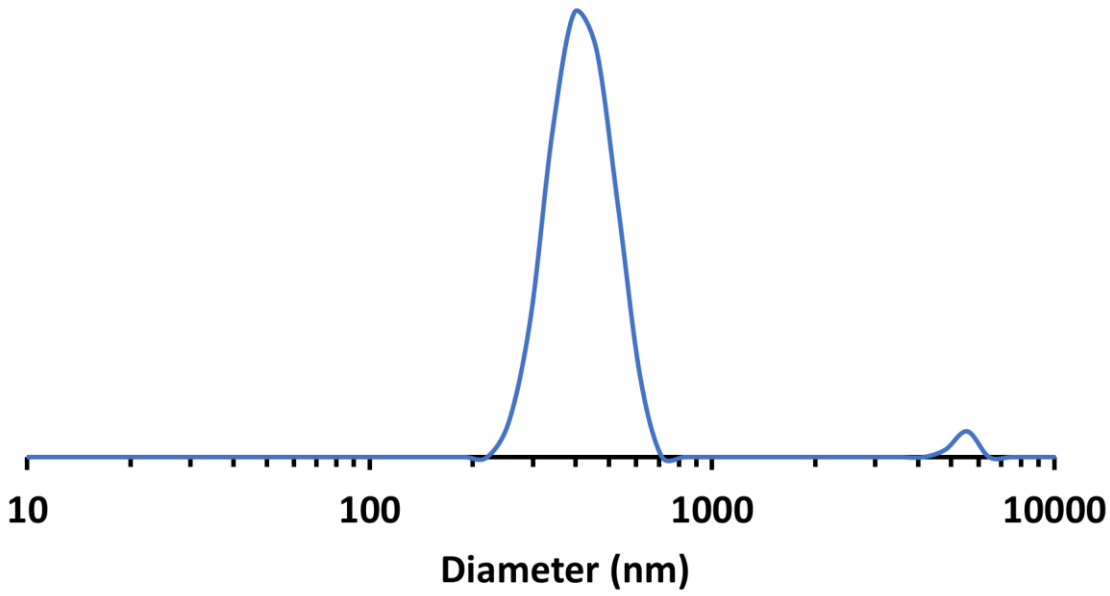

Figure 4.27. DLS data obtained for 0.15% w/w dispersion of $PHEMA_{30}$-*b*-$PBzMA_{270}$. Synthesis was carried out at 10% w/w copolymer concentration.

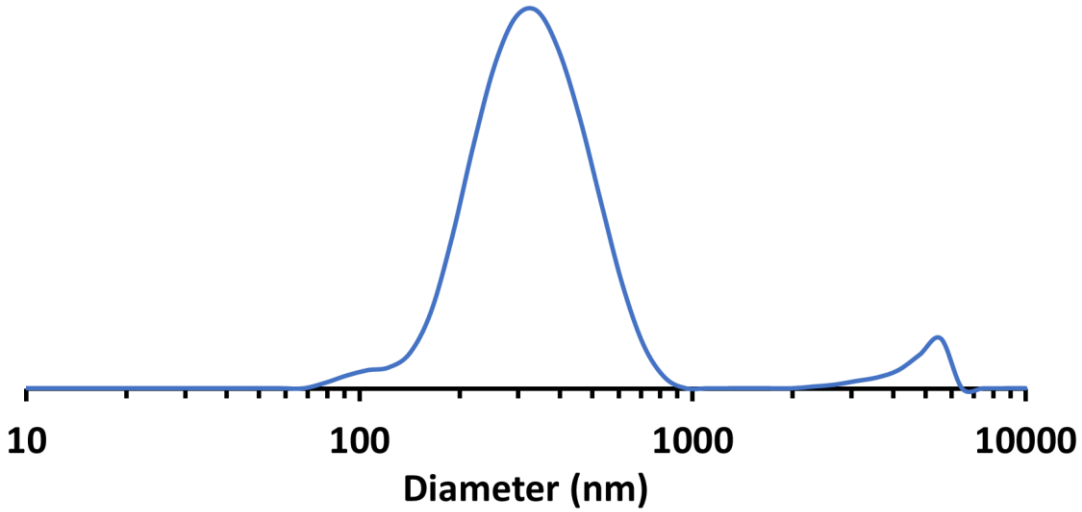

Figure 4.28. DLS data obtained for 0.15% w/w dispersion of $PHEMA_{30}$-*b*-$PBzMA_{282}$. Synthesis was carried out at 9% w/w copolymer concentration.

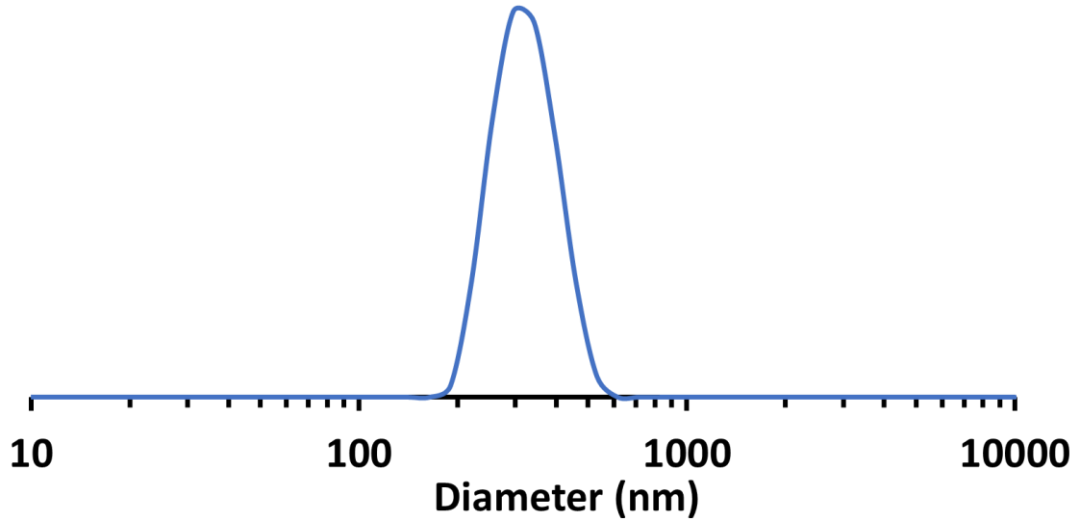

Figure 4.29. DLS data obtained for 0.15% w/w dispersion of $PHEMA_{30}$-*b*-$PBzMA_{267}$. Synthesis was carried out at 8% w/w copolymer concentration.

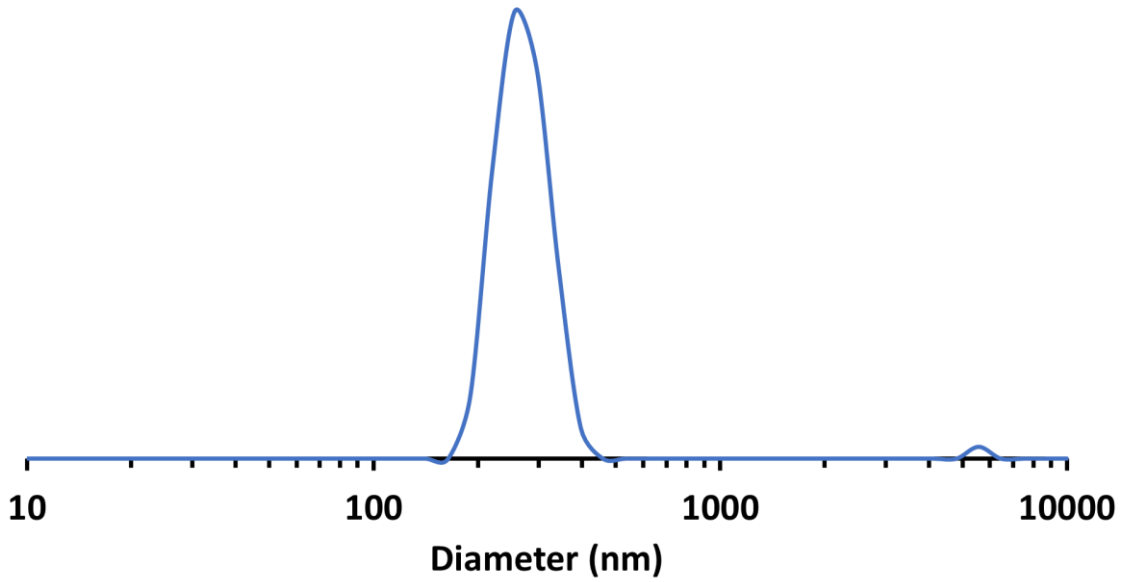

Figure 4.30. DLS data obtained for 0.15% w/w dispersion of $PHEMA_{30}$-*b*-$PBzMA_{267}$. Synthesis was carried out at 7% w/w copolymer concentration.

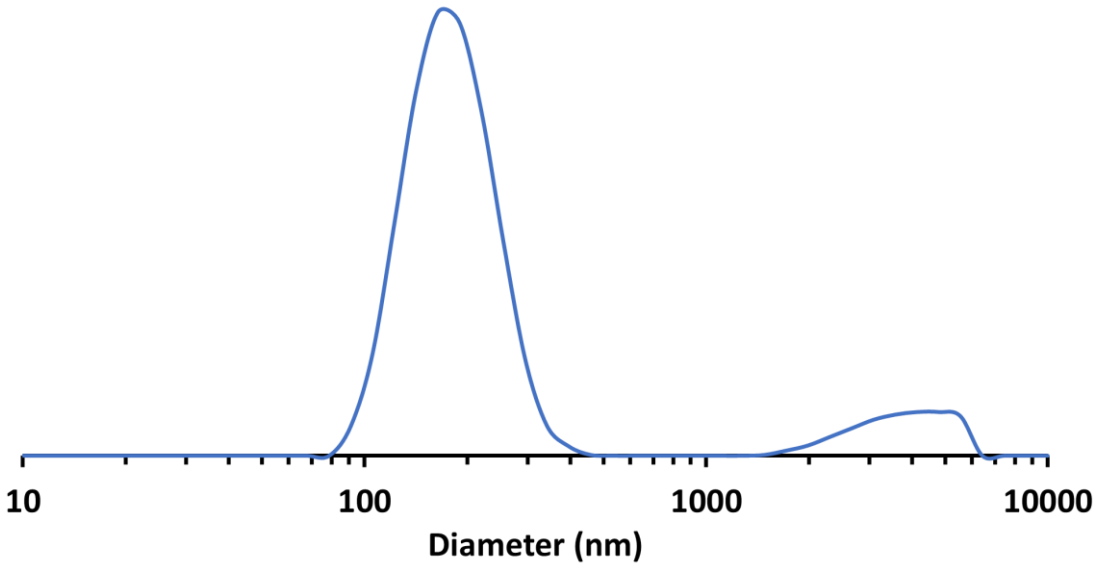

Figure 4.31. DLS data obtained for 0.15% w/w dispersion of $PHEMA_{30}$-*b*-$PBzMA_{294}$. Synthesis was carried out at 6% w/w copolymer concentration.

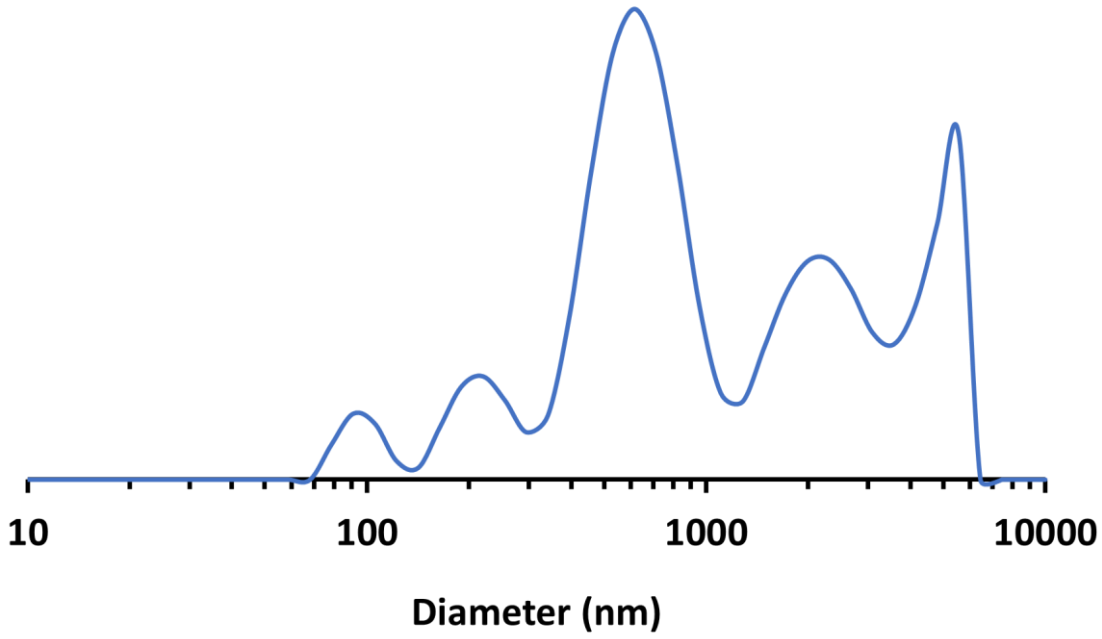

Figure 4.32. DLS data obtained for 0.15% w/w dispersion of $PHEMA_{30}$-*b*-$PBzMA_{291}$. Synthesis was carried out at 5% w/w copolymer concentration.

4.3.3 Thermal and electrochemical properties of block copolymer worm ionogels

Thermogravimetric analysis (TGA) was used to investigate the thermal stability of selected samples relative to [EMIM][DCA] (Figure 4.33). [EMIM][DCA] appeared to have an onset degradation temperature of approximately 305 °C, which is similar to previously reported studies.[31] Similarly, the 15% w/w $PHEMA_{30}$-*b*-$PBzMA_{291}$ ionogel also appeared to have a onset degradation temperature of approximately 305 °C, showing that the polymer content in the ionogel has minimal effect on the degradation temperature thus demonstrating that this formulation has good short term thermal stability, an important parameter for future polymer gel electrolytes. In order to further understand this, bulk $PHEMA_{30}$-*b*-$PBzMA_{293}$ was analysed by TGA under the same conditions (Figure 4.33). This bulk block copolymer appeared to have a lower degradation temperature of approximately 230 °C, indicating that the thermal stability of the polymer is potentially improved as a result of the presence of the IL to form the ionogel. This is also observed in TGA studies conducted on all other block copolymer samples, summarised in Table 4.2.

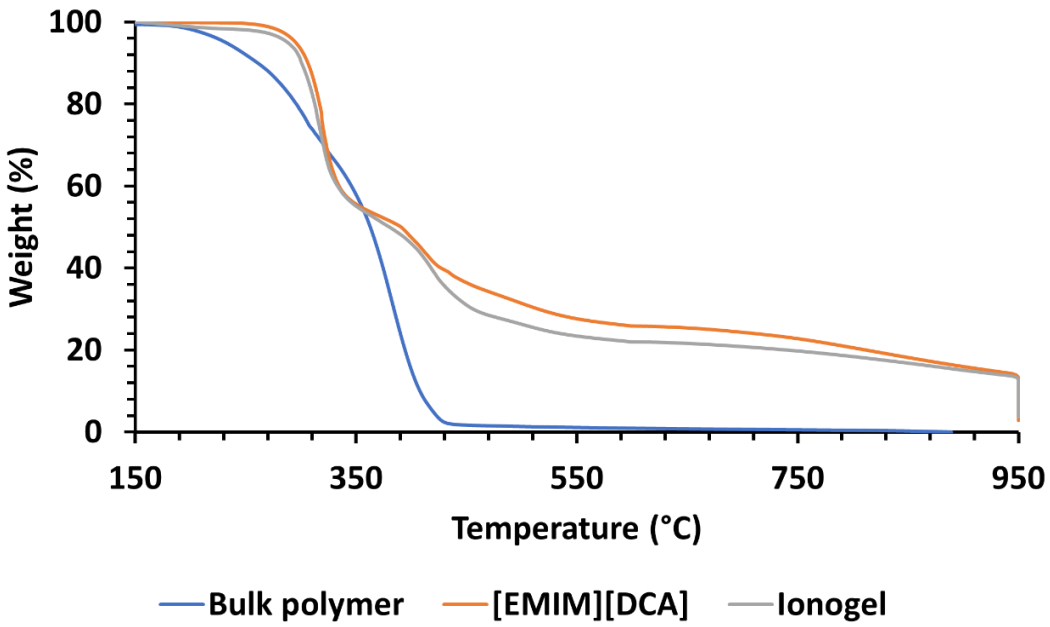

Figure 4.33. Thermogravimetric analysis (TGA) data obtained for bulk $PHEMA_{30}$-*b*-$PBzMA_{267}$ block copolymer (blue), pure [EMIM][DCA] (orange), and 15% w/w $PHEMA_{30}$-*b*-$PBzMA_{291}$ worm ionogel (grey).

Table 4.2. Summary of onset degradation temperatures obtained by thermogravimetric analysis (TGA) of each $PHEMA_{30}$-*b*-$PBzMA_y$ block copolymer. All were analysed as prepared at 15% w/w in [EMIM][DCA] with the exception of bulk [EMIM][DCA] and bulk polymer. $PHEMA_{30}$-*b*-$PBzMA_y$ is denoted as H_{30}-B_y for brevity.

Block copolymer composition	Onset degradation temperature (°C)
[EMIM][DCA]	305
Bulk H_{30}-B_{293}	230
H_{30}-B_{240}	310
H_{30}-B_{250}	290
H_{30}-B_{262}	290
H_{30}-B_{269}	289
H_{30}-B_{279}	285
H_{30}-B_{291}	305
H_{30}-B_{301}	284
H_{30}-B_{314}	285
H_{30}-B_{317}	290
H_{30}-B_{340}	281

Electrochemical impedance spectroscopy (EIS) was used to compare the bulk resistance of block copolymer worm ionogels and the ionic liquid alone (Table 4.2). The bulk resistance was obtained by generating Nyquist plots as represented in Figure 4.34.

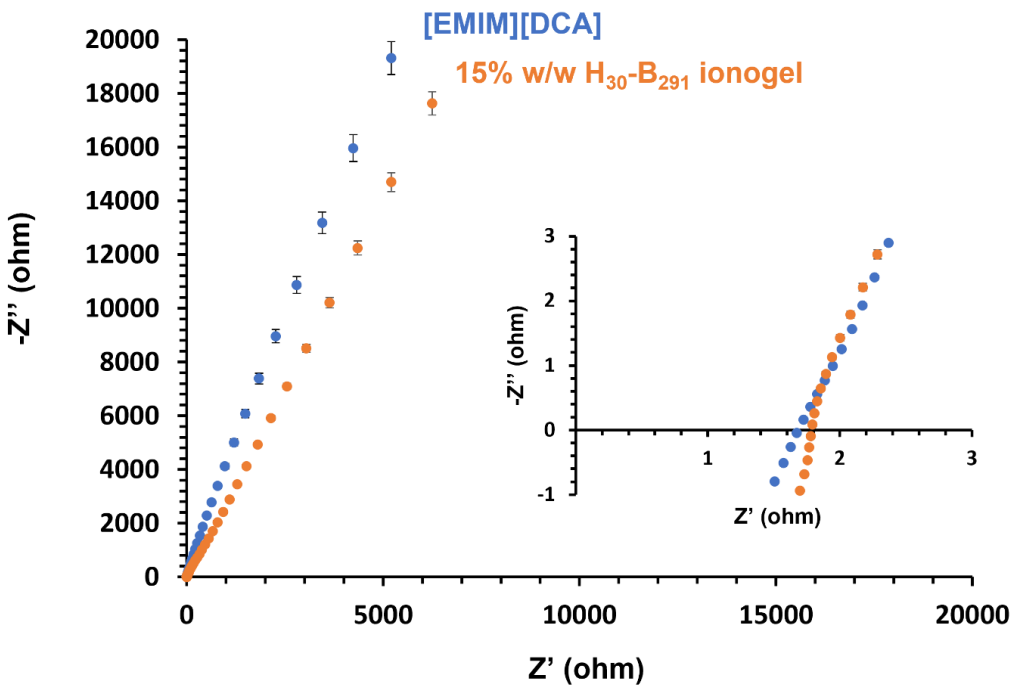

Figure 4.34. Nyquist plots obtained for [EMIM][DCA] (blue) and $PHEMA_{30}$-*b*-$PBzMA_{291}$ (orange) via electrochemical impedance spectroscopy. The inset graph shows the magnified low Z' region to better indicate the x-intercept used to determine bulk resistance.

EIS data obtained showed that the ionic liquid, [EMIM][DCA], had a marginally lower bulk resistance (1.67 ± 0.04 Ω) than that of the representative worm ionogel ($PHEMA_{30}$-*b*-$PBzMA_{291}$) which had a bulk resistance of 1.79 ± 0.15 Ω. When considering the standard deviation in these values, which were determined from repeating results in triplicate, the differences in bulk resistance of the ionogel and [EMIM][DCA] were deemed to be statistically insignificant, meaning that the presence of 15% w/w non-ionic $PHEMA_{30}$-*b*-$PBzMA_{291}$ did not negatively impact the electrochemical properties of the IL. This is also observed in the EIS analysis obtained for each of the block copolymers (Table 4.3) which shows the majority of gels displaying a lower bulk resistance. This is important and suggests that these gel electrolytes formed using this new approach have great potential for potential applications in the energy storage sector.

Table 4.3. Summary of bulk resistances obtained by electrochemical impedance spectroscopy (EIS) of each $PHEMA_{30}$-*b*-$PBzMA_y$ block copolymer gel. All were analysed as prepared at 15% w/w in [EMIM][DCA]. $PHEMA_{30}$-*b*-$PBzMA_y$ is denoted as H_{30}-B_y for brevity.

Block copolymer composition	Bulk resistance (Ω)
[EMIM][DCA]	1.67 ± 0.04
H_{30}-B_{250}	0.76 ± 0.03
H_{30}-B_{262}	0.75 ± 0.00
H_{30}-B_{269}	0.86 ± 0.00
H_{30}-B_{279}	1.19 ± 0.01
H_{30}-B_{291}	1.79 ± 0.15
H_{30}-B_{301}	0.49 ± 0.01
H_{30}-B_{314}	0.51 ± 0.01
H_{30}-B_{317}	0.59 ± 0.00

4.4 Conclusions

In summary, $PHEMA_{30}$-*b*-$PBzMA_y$ worm ionogels at 15% w/w in [EMIM][DCA] prepared in Chapter 3 were characterised by oscillatory rheology, TGA and EIS. The viscoelastic properties of all worm ionogels were investigated using oscillatory rheology. Gels that were composed of the highest proportion of worms, as confirmed by SAXS, generally exhibited higher *G*' values, indicating that the increased stiffness of gels is attributed to the increased proportion of inter-worm contacts present in the dispersions. Lower *G*' values were observed for free-flowing dispersions containing spherical nanoparticles or relatively smaller proportions of worms. Additionally, the gel dispersions were confirmed as 'true' gels due to exhibiting frequency-independent moduli. Thermal stability studies of the worm ionogels was also carried out using TGA. The onset thermal degradation of each gel was recorded and compared with that of [EMIM][DCA] to assess the effect of polymer content on the ionogels. Interestingly, bulk $PHEMA_{30}$-*b*-$PBzMA_{293}$ had an onset degradation temperature of 230 °C, whereas the [EMIM][DCA] alone had an onset degradation temperature of 305 °C. The onset degradation temperatures of the ionogels were recorded to be in the range of 280 and 310 °C indicating that the presence of the polymer content in the ionogels did not significantly affect the thermal stability provided by [EMIM][DCA]. Overall, the ionogels were shown to have good thermal stability. Additionally, EIS was used to obtain bulk resistances of each ionogel as well as [EMIM][DCA] in order to assess the effect of polymer content on the electrochemical properties provided by [EMIM][DCA]. Generally, EIS analysis demonstrated that the ionogels had comparable electrochemical properties compared to [EMIM][DCA] alone.

Therefore, it can be concluded that the polymer content merely provided the mechanical strength required for gelation and had minimal effect on the electrochemical properties in the ionogels.

In particular for electronic applications, it is important to maintain if not maximise the electrochemical properties of the [EMIM][DCA] in the ionogels. Therefore, it is fundamental that the minimum amount of polymer content that provides mechanical strength is contained within the ionogel. For this reason, CGC studies were conducted so as to determine the concentration at which inter-worm contacts are no longer possible, thus yielding free-flowing dispersions based on tube inversion tests. $PHEMA_{30}$-*b*-$PBzMA_y$ block copolymers were synthesised in [EMIM][DCA] at concentrations between 10% w/w and 1% w/w targeting a PBzMA DP of 300 for each. The screenings identified the CGC as >4 % w/w, which was in good agreement with the rheological studies carried out of each dispersion. Importantly, this research demonstrates that the PISA formulation described in Chapter 3 to generate ionogels *in situ* displays desirable electrochemical, thermal and rheological characterisation for electronic application. Moreover, this formulation requires a very low copolymer concentration to be able to form ionogels, enabling the superior electrochemical properties of the [EMIM][DCA] to be maintained when used in future potential polymer gel electrolytes.

4.5 References

1. X. Fan, S. Liu, Z. Jia, J. J. Koh, J. C. C. Yeo, C.-G. Wang, N. E. Surat'man, X. J. Loh, J. Le Bideau, C. He, Z. Li and T.-P. Loh, *Chem. Soc. Rev*, 2023, **52**, 2497-2527.
2. J. Xu, H. Hu, S. Zhang, G. Cheng and J. Ding, *Polymers*, 2023, **15**.
3. H. Hu, S. Zhang, Y. Li, X. Hu, L. Xu, A. Feng, G. Cheng and J. Ding, *J. Bionic. Eng*, 2023, **20**, 2755-2763.
4. J. Cao, Z. Zhang, L. Ye and X. Zhao, *J. Mater. Chem. A*, 2023, **11**, 19981-19995.
5. J. Lai, H. Zhou, Z. Jin, S. Li, H. Liu, X. Jin, C. Luo, A. Ma and W. Chen, *ACS Appl. Mater. Interfaces*, 2019, **11**, 26412-26420.
6. Y. M. Kim and H. C. Moon, *Adv. Funct. Mater*, 2020, **30**, 1907290.
7. M. Wang, J. Hu and M. D. Dickey, *JACS Au*, 2022, **2**, 2645-2657.
8. W. Qiu, G. Chen, H. Zhu, Q. Zhang and S. Zhu, *J. Chem. Eng*, 2022, **434**, 134752.
9. J. Sun, G. Lu, J. Zhou, Y. Yuan, X. Zhu and J. Nie, *ACS Appl. Mater. Interfaces*, 2020, **12**, 14272-14279.
10. Y. Zhang, L. Chang, P. Sun, Z. Cao, Y. Chen and H. Liu, *RSC Adv*, 2020, **10**, 7424-7431.
11. R. Tamate, K. Hashimoto, T. Horii, M. Hirasawa, X. Li, M. Shibayama and M. Watanabe, *Adv. Mater*, 2018, **30**, 1802792.
12. K. G. Cho, S. An, D. H. Cho, J. H. Kim, J. Nam, M. Kim and K. H. Lee, *Adv. Funct. Mater*, 2021, **31**, 2102386.
13. G. M. Kavanagh and S. B. Ross-Murphy, *Prog. Polym. Sci*, 1998, **23**, 533-562.
14. A. W. Coats and J. P. Redfern, *Analyst*, 1963, **88**, 906-924.

15. H. M. Ng, N. M. Saidi, F. S. Omar, K. Ramesh, S. Ramesh and S. Bashir, *Encyclopedia of Polymer Science and Technology*, 4th edn., 2018.
16. B. Yiming, X. Guo, N. Ali, N. Zhang, X. Zhang, Z. Han, Y. Lu, Z. Wu, X. Fan, Z. Jia and S. Qu, *Adv. Funct. Mater*, 2021, **31**, 2102773.
17. Z. Luo, W. Li, J. Yan and J. Sun, *Adv. Funct. Mater*, 2022, **32**, 2203988.
18. L. Chen and M. Guo, *ACS Appl. Mater. Interfaces*, 2021, **13**, 25365-25373.
19. A. C. Lazanas and M. I. Prodromidis, *ACS Meas. Sci. Au*, 2023, **3**, 162-193.
20. N. Gil-González, T. Akyazi, E. Castaño, F. Benito-Lopez and M. C. Morant-Miñana, *Sens. Actuators. B Chem*, 2018, **260**, 380-387.
21. S.-H. Wang, S.-S. Hou, P.-L. Kuo and H. Teng, *ACS Appl. Mater. Interfaces*, 2013, **5**, 8477-8485.
22. D. S. Ashby, J. Cardenas, A. S. Bhandarkar, A. W. Cook and A. A. Talin, *ACS Appl. Energy. Mater*, 2022, **5**, 12467-12474.
23. Q. Xiao, C. Deng, Q. Wang, Q. Zhang, Y. Yue and S. Ren, *ACS Omega*, 2019, **4**, 95-103.
24. S.-H. Wang, P.-L. Kuo, C.-T. Hsieh and H. Teng, *ACS Appl. Mater. Interfaces*, 2014, **6**, 19360-19370.
25. M. Brachet, T. Brousse and J. Le Bideau, *ECS Electrochem. Lett*, 2014, **3**, A112.
26. J. Park and J.-Y. Sun, *ACS Appl. Mater. Interfaces*, 2022, **14**, 23375-23382.
27. R. M. González-Gil, M. Borràs, A. Chbani, T. Abitbol, A. Fall, C. Aulin, C. Aucher and S. Martínez-Crespiera, *Nanomaterials*, 2022, **12**.
28. J. Yoon, D. k. Kang, J. Won, J.-Y. Park and Y. S. Kang, *J. Power Sources*, 2012, **201**, 395-401.
29. J. R. Lovett, M. J. Derry, P. Yang, F. L. Hatton, N. J. Warren, Patrick W. Fowler and S. P. Armes, *Chem. Sci*, 2018, **9**, 7138-7144.
30. L. A. Fielding, J. A. Lane, M. J. Derry, O. O. Mykhaylyk and S. P. Armes, *J. Am. Chem. Soc*, 2014, **136**, 5790-5798.
31. P. Navarro, M. Larriba, E. Rojo, J. García and F. Rodríguez, *J. Chem. Eng. Data*, 2013, **58**, 2187-2193.

5. Extending the scope of polymerisation-induced self-assembly in ionic liquids: RAFT dispersion polymerisation of benzyl methacrylate in 1-ethyl-3-methylimidazolium ethyl sulphate

5.1 Introduction

Polymerisation-induced self-assembly (PISA) has been shown to be a convenient and versatile technique for accessing well-defined nano-objects such as spheres, worms and vesicles.[1] These morphologies are dictated by the relative block volume fraction, i.e. the relative lengths of the stabiliser and core-forming block in a given block copolymer. In practice, however, other parameters also need to be considered in order to access higher order morphologies such as copolymer concentration and solvent choice. Some reported PISA formulations in ionic liquids (ILs) have generated only spherical morphologies such as spheres[2] or vesicles.[3] This is presumably because anisotropic worm-like nanoparticles occupy a very narrow phase space between core-forming block degrees of polymerisation (DPs) that form spheres and vesicles and thus are more inaccessible compared to other morphologies.[4-6] As previously discussed in this Thesis (Section 1.4.3), many parameters can contribute to obtaining higher order morphologies (e.g. worms and vesicles), which have been explored extensively in the literature[7-10]

Most relevant to this Chapter, dispersion PISA has been conducted in an extensive solvent selection such as alcohols,[4, 11-13] non-polar,[8, 10, 14-16] and water.[5, 17-20]. Moreover, solvent choice has been shown to affect access to higher order morphologies.[8, 21-25] For example, introduction of water into an ethanolic PISA system was explored by Jones *et al.*[21] when synthesising poly(*N,N*-dimethylacrylamide)-*block*-(poly(benzyl methacrylate) (PDMA-*b*-PBzMA) block copolymers via RAFT dispersion polymerisation of BzMA. The introduction of water into the system (ethanol: water ratio of 80:20 w/w) increased the kinetic rate of the reaction, however it hindered the formation of higher order morphologies such as worms and vesicles, both of which were able to be accessed in a pure ethanol solvent system. Derry *et al.*[8] reported the synthesis of poly(lauryl methacrylate)-*block*-poly(benzyl methacrylate) (PLMA-*b*-PBzMA) block copolymer nanoparticles via RAFT dispersion polymerisation of BzMA in two non-polar solvents. It was found that at a copolymer concentration of 20% w/w and similar block copolymer compositions, the formation of different morphologies were achieved. In mineral oil, a pure worm phase was successfully accessed, whereas in poly(α-olefin) oil, a sphere, worm and vesicle mixture was observed.

Despite the ever-increasing reports of RAFT-PISA formulations in several solvents, there is still considerable scope for developing PISA formulations in ionic liquids (ILs). Aside from studies carried out by Zhang *et al*.[3], Zhou *et al.*[26], and Yamanaka *et al.*[27], PISA in ILs has been considerably

overlooked. Chapter 3 and Chapter 4 of this Thesis explore the synthesis and characterisation of block copolymers synthesised via PISA in 1-ethyl-3-methylimdazolium dicyanamide ([EMIM][DCA]), in which spheres as well as higher order morphologies such as worms and vesicles could be obtained. Herein, a PISA formulation in 1-ethyl-3-methylimidazolium ethyl sulphate ([EMIM][$EtOSO_3$]) (Scheme 5.1) at 15% w/w and 20% w/w solids is reported, in an effort to extend the scope of PISA in ILs to generate ionogels from another hydrophilic IL. Utilising the same block copolymer as in Chapter 3, poly(2-hydroxyethyl methacrylate)-*block*-poly(benzyl methacrylate) ($PHEMA_X$-*b*-$PBzMA_y$), spherical nanoparticles could be accessed, in particular spheres. Worm gels were not attainable in this particular IL over a wide range of PBzMA core-forming block DPs (196-594) at both copolymer concentrations investigated (15% w/w and 20% w/w solids), however this formulation has paved the way to investigate other parameters to generate worm gels in this IL.

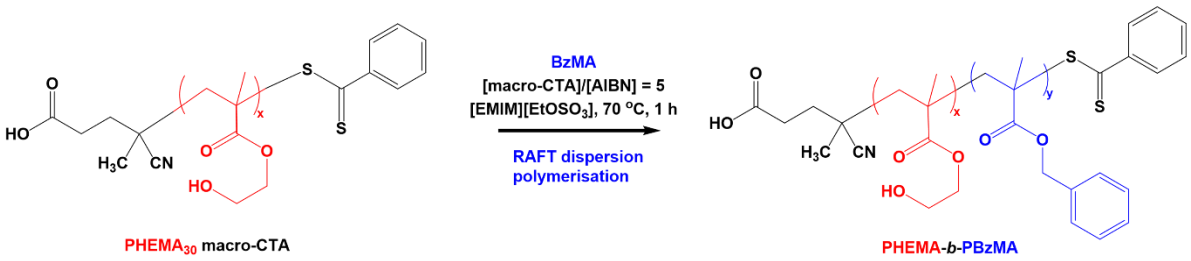

Scheme 5.1. RAFT dispersion polymerisation of benzyl methacrylate (BzMA) in [EMIM][$EtOSO_3$] at 70 °C to yield $PHEMA_{30}$-*b*-$PBzMA_y$ diblock copolymers.

5.2 Experimental

5.2.1 Materials

Poly(2-hydroxyethyl methacrylate)$_{30}$ macromolecular chain-transfer agent ($PHEMA_{30}$ mCTA) was synthesised as previously described in Chapter 3 (2-hydroxyethyl methacrylate (HEMA)conversion = 40%; M_n = 8,000 g mol^{-1}, $Đ_M$ = 1.25). Benzyl methacrylate (BzMA) was purchased from Sigma Aldrich and passed through a basic alumina column prior to use in order to remove the inhibitor. 2,2'-Azobisisobutyronitrile (AIBN) was purchased from Molekula and was recrystallised from methanol prior to use. Dimethyl sulfoxide-d6 (DMSO-d6) for ^{1}H NMR analysis was purchased from Goss Scientific. 1-Ethyl-3-methylimidazolium ethyl sulphate, [EMIM][$EtOSO_3$], was acquired from BASF.

5.2.2 ^{1}H Nuclear Magnetic Resonance (NMR) spectroscopy

^{1}H NMR spectra were obtained in DMSO-d6 using a Bruker Avance Neo 300 MHz spectrometer. . Both crude and pure samples were prepared by dissolving approximately 40 mg of sample in 0.7 mL of appropriate deuterated solvent Typically 16 scans were averaged per spectrum and all chemical shifts are expressed in ppm. ^{1}H NMR spectra were referenced using peaks present as a result of residual solvent.

5.2.3 Gel Permeation Chromatography (GPC)

Molecular weight distributions were obtained by using an Agilent Infinity II multi-detector GPC comprising a guard column and two PL gel mixed-C columns. The mobile phase contained 0.10% w/v LiBr in HPLC grade DMF and the flow rate was fixed at 1 ml min^{-1} at 80 °C. The GPC was calibrated using near-monodispersed poly(methyl methacrylate) standards (M_p range = 535-1,591,000 g mol^{-1}).

5.2.4 Dynamic light scattering (DLS)

Dynamic light scattering (DLS) studies were conducted using a Zetasizer Nano ZS instrument (Malvern Panalytical, UK) at a fixed scattering angle of 173 °. The block copolymer dispersions were diluted in [EMIM][EtOSO$_3$] (refractive index = 1.48, viscosity = 94.2 cP) at 0.10% w/w prior to light scattering studies at 25 °C against polystyrene latex standards. The polydispersity index (PDI) and average diameter (D) were calculated, and data were averaged over approximately thirteen runs each of 30 seconds duration.

5.2.5 Small-angle X-ray scattering (SAXS)

Small-angle X-ray scattering (SAXS) patterns were recorded for 1.0 % w/w copolymer dispersions in [EMIM][EtOSO$_3$] in 1.5 mm diameter polycarbonate capillaries at a synchrotron source (beamline B21[28], Diamond Light Source, UK) using monochromatic X-ray radiation (X-ray wavelength λ = 0.9408 Å, sample-to-detector distance of 3.712 m corresponding to scattering vector q ranging from 0.0045 to 0.34 Å^{-1}) and an EigerX 4M detector (Dectris, Switzerland). Scattering data were reduced using standard protocols from the beamline and were further analyzed using Irena SAS macros for Igor Pro[29]. Background-subtracted SAXS data were fitted to aspherical micelle model[30].

5.2.6 Synthesis of poly(2-hydroxyethyl methacrylate)-*b*-poly(benzyl methacrylate) diblock copolymer nanoparticles via polymerisation-induced self-assembly (PISA) in [EMIM][EtOSO$_3$]

A typical RAFT dispersion polymerisation for the synthesis of PHEMA$_{30}$-PBzMA$_{297}$ at 15% w/w solids was conducted as follows: BzMA (0.85 g; 4.8 mmol), 2,2'-azobisisobutyronitrile (AIBN; 0.5 mg; 3.2 µmol) and PHEMA$_{30}$ macro-CTA (65 mg; 16 µmol; macro-CTA/initiator molar ratio = 3.0; PBzMA target degree of polymerisation = 300) were dissolved in 1-ethyl-3-methylimidazolium ethyl sulphate ([EMIM][EtOSO$_3$]; 3.65 g) in a 14 mL sample vial. The sealed reaction mixture was purged with nitrogen for 30 minutes prior to being placed in a preheated oil bath at 70 °C whilst stirring for 1 hour (BzMA conversion = 99%; M_n = 54,500 g mol^{-1}, $Đ_M$ =1.27).

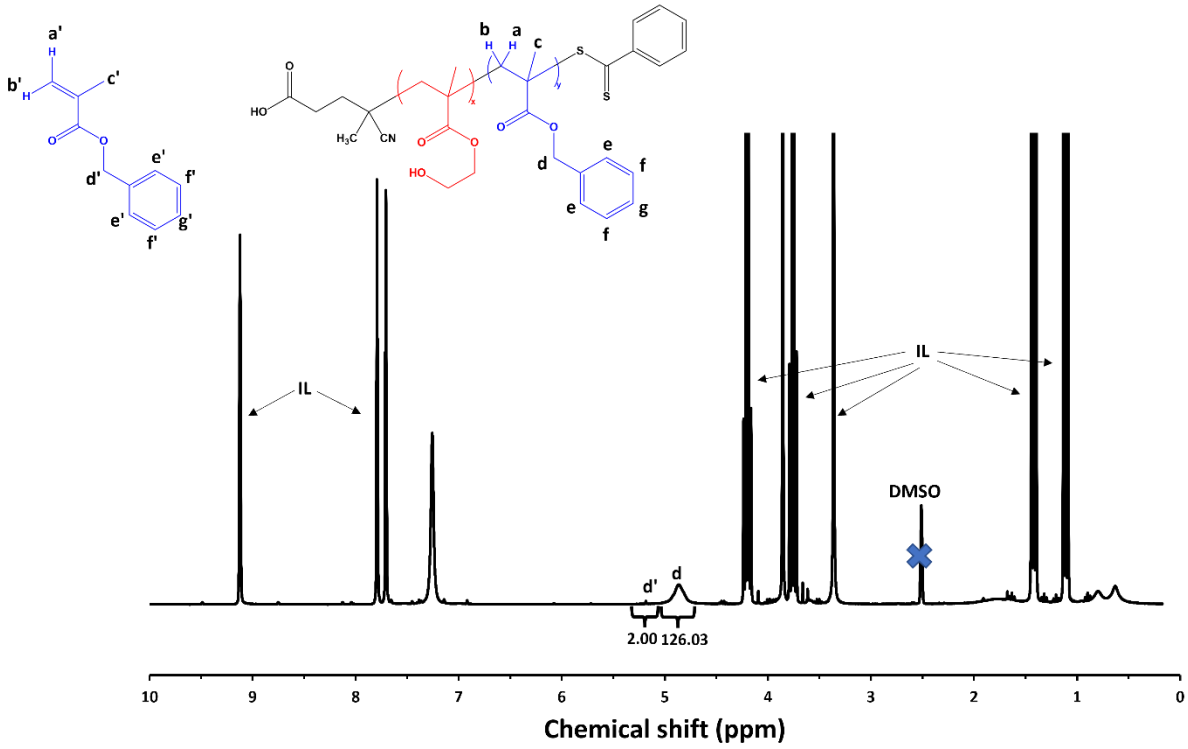

Figure 5.1. Assigned ^{1}H NMR spectrum for the reaction mixture directly after RAFT dispersion polymerisation of benzyl methacrylate in [EMIM][EtOSO$_3$] at 15% w/w solids.

As seen in Chapter 3, BzMA conversions for RAFT dispersion polymerisations in [EMIM][EtOSO$_3$] are calculated using equations 5.1, 5.2 and 5.3:

$$I_m = [Integral\ (d')] = 2H \quad (5.1)$$

$$I_p = [Integral\ (d)] \quad (5.2)$$

$$\%\ Conversion = \frac{Ip}{Im+Ip}\ x\ 100\% \quad (5.3)$$

The degree of polymerisation of the PBzMA block in each block copolymer was calculated using equation 5.4:

$$\text{PBzMA DP} = \text{BzMA conversion}\ x\ \text{target PBzMA DP} \quad (5.4)$$

5.3 Results and discussion

5.3.1 Kinetic study of the RAFT polymerisation of benzyl methacrylate in [EMIM][EtOSO$_3$]

A representative kinetic study of the chain extension of PHEMA$_{30}$ macro-CTA with BzMA in [EMIM][EtOSO$_3$] at 70 °C and 15% w/w solids was conducted when targeting a PBzMA DP of 300 (Figure 5.2). Aliquots from the reaction solution were taken at 5 minute intervals in order to monitor the polymerisation kinetics.

The critical PBzMA DP for the assembly of PHEMA$_{30}$-*b*-PBzMA$_y$ nanoparticles during PISA in [EMIM][EtOSO$_3$] was determined to be approximately 132. At this critical point in the PISA synthesis, the observed rate of polymerisation increased by a factor of approximately 7.

The first 25 minutes of the polymerisation process were comparatively slow, but after that, there was a noticeable rate enhancement, indicating the beginning of micellar nucleation, which occurs when a critical degree of polymerisation of the core-forming block is reached, above which the block copolymer becomes insoluble. The substantial increase in propagation rate is as a result of preferential migration of unreacted monomer into the micelle cores where polymerisation occurs, which results in a greater effective local monomer concentration at the polymerisation site.[8, 18] This is also observed when conducting PISA in [EMIM][DCA] for the same block copolymer (Chapter 3).

When compared to the reaction rate of the dispersion polymerisation of BzMA in [EMIM][DCA], the polymerisation rate in [EMIM][$EtOSO_3$] is noticeably faster, requiring only one hour to reach full monomer conversion. In contrast, PISA in [EMIM][DCA] requires 2 hours to reach full conversion of BzMA. This is perhaps due to the viscosity of the [EMIM][$EtOSO_3$] compared to [EMIM][DCA]. The higher viscosity may have accelerated the rate of the reaction as the heat does not as quickly dissipate upon solution mixing. Additionally, the critical DP for self-assembly was 132 in [EMIM][$EtOSO_3$], and 72 in [EMIM][DCA], indicating that a relatively longer core-forming block is required for self-assembly to occur in [EMIM][$EtOSO_3$].

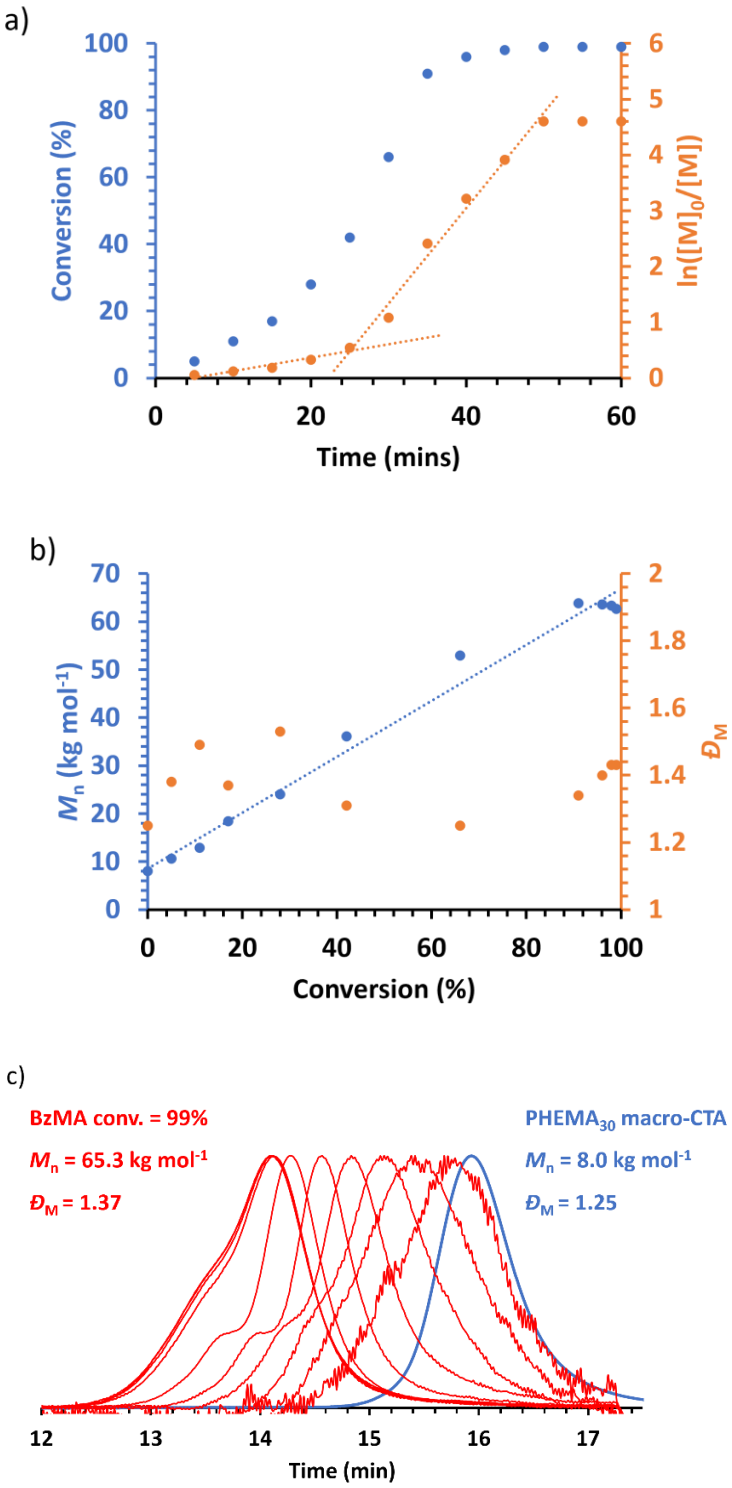

Figure 5.2. Kinetic study for the RAFT dispersion polymerisation of BzMA (target DP 300) in [EMIM][$EtOSO_3$] at 15% w/w solids using a $PHEMA_{30}$ macro-CTA: a) BzMA conversion vs. time (blue data) and semi-log kinetic (orange data) plots; b) M_n and $Đ_M$ vs. BzMA conversion. Dashed blue line indicates linear progression of molar mass growth; c) DMF GPC chromatograms. GPC data was obtained against poly(methyl methacrylate) standards.

5.3.2 Synthesis of $PHEMA_{30}$-*b*-$PBzMA_y$ diblock copolymer nanoparticles via PISA at 15% w/w solids

Following on from this kinetic study, a series of $PHEMA_{30}$-*b*-$PBzMA_y$ block copolymers were synthesised at 15% w/w in [EMIM][$EtOSO_3$] targeting PBzMA DPs from 200 to 1000, as shown in Table 5.1 and Figure 5.3 below.

Table 5.1. Summary of targeted copolymer composition, BzMA conversion, actual copolymer composition, theoretical M_n, GPC M_n and $Đ_M$ (M_w/M_n), and DLS diameter and PDI for the series of $PHEMA_{30}$-*b*-$PBzMA_y$ diblock copolymers prepared by RAFT dispersion polymerisation of BzMA in [EMIM][$EtOSO_3$] at 70 °C and 15% w/w, using AIBN initiator ([$PHEMA_{30}$ macro-CTA]/[AIBN] molar ratio = 5.0). $PHEMA_{30}$-*b*-$PBzMA_y$ is denoted as H_{30}-B_y for brevity.

Target composition	BzMA conversion[a] (%)	Actual composition	$M_{n,th}$[a] (g mol^{-1})	M_n[b] (g mol^{-1})	$Đ_M$[b]
H_{30}-B_{200}	98	H_{30}-B_{196}	38,721	38,100	1.24
H_{30}-B_{250}	99	H_{30}-B_{248}	47,884	45,800	1.23
H_{30}-B_{300}	99	H_{30}-B_{297}	52,954	54,500	1.27
H_{30}-B_{350}	98	H_{30}-B_{343}	60,508	59,900	1.28
H_{30}-B_{400}	98	H_{30}-B_{392}	68,554	65,500	1.31
H_{30}-B_{450}	96	H_{30}-B_{432}	75,123	68,000	1.52
H_{30}-B_{500}	92	H_{30}-B_{460}	79,721	79,200	1.36
H_{30}-B_{550}	-	-	94,500	66,300	2.12
H_{30}-B_{600}	95	H_{30}-B_{570}	97,784	93,700	1.42
H_{30}-B_{1000}	98	H_{30}-B_{980}	165,110	167,200	1.69

[a]*D*etermined by ^{1}H NMR spectroscopy. [b]Determined by DMF GPC against poly(methyl methacrylate) standards.

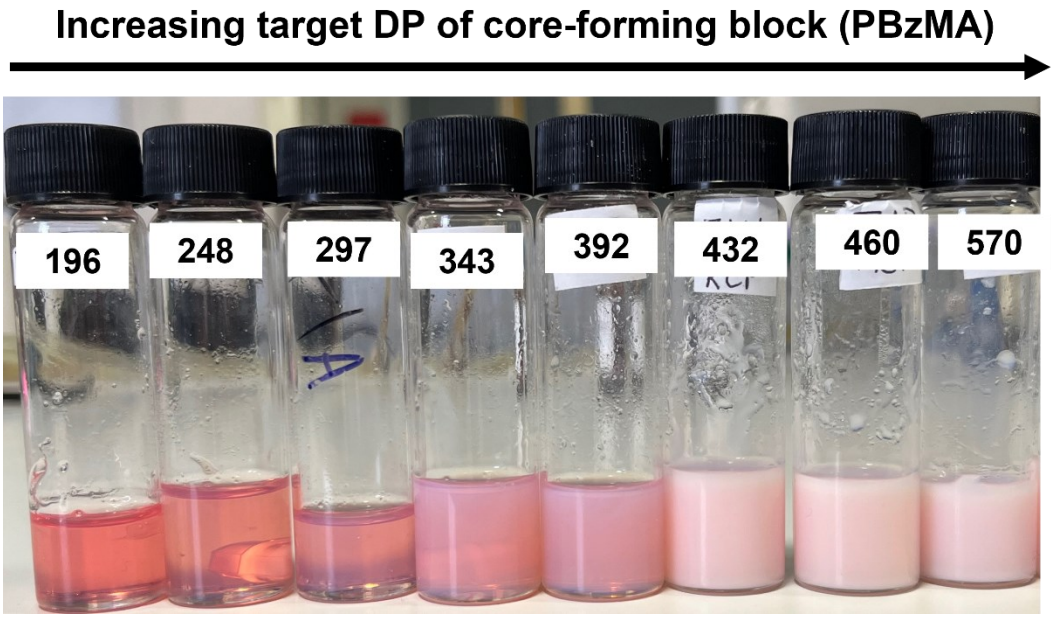

Figure 5.3. Digital image showing the physical appearance of the series of $PHEMA_{30}$-b-$PBzMA_y$ block copolymer dispersions in [EMIM][$EtOSO_3$] at 15% w/w solids. Number labels on sample vials denote the actual PBzMA core-forming block DP, as determined using ^{1}H NMR spectroscopy.

Initial observations of this block copolymer series (Figure 5.3) indicate the absence of sufficient, if any, worm-like structures that can physically crosslink and form an extended percolating network,[31] evidenced by the lack of freestanding gels. All block copolymers dispersions appeared to be free-flowing solutions. Transparent fluids at lower BzMA DPs (DP ≤ 248) and turbid solutions at higher BzMA DPs (DP ≥ 297) indicate the presence of spherical nanoparticles.[14] However, further nanoparticle analysis was required in order to distinguish the specific type of spherical nanoparticle present, i.e. spheres, vesicles or mixed phases.

GPC analysis of this $PHEMA_{30}$-*b*-$PBzMA_y$ series was conducted (Figure 5.4). As seen in the GPC chromatograms in Figure 5.4a, there is a clear shift in molecular weight upon chain extension of the $PHEMA_{30}$ macro-CTA, with no residual $PHEMA_{30}$ macro-CTA remaining in the samples as evidenced by the absence of the molecular weight peak for this precursor. This indicates efficient chain extension of the macro-CTA during the dispersion polymerisation of the BzMA.

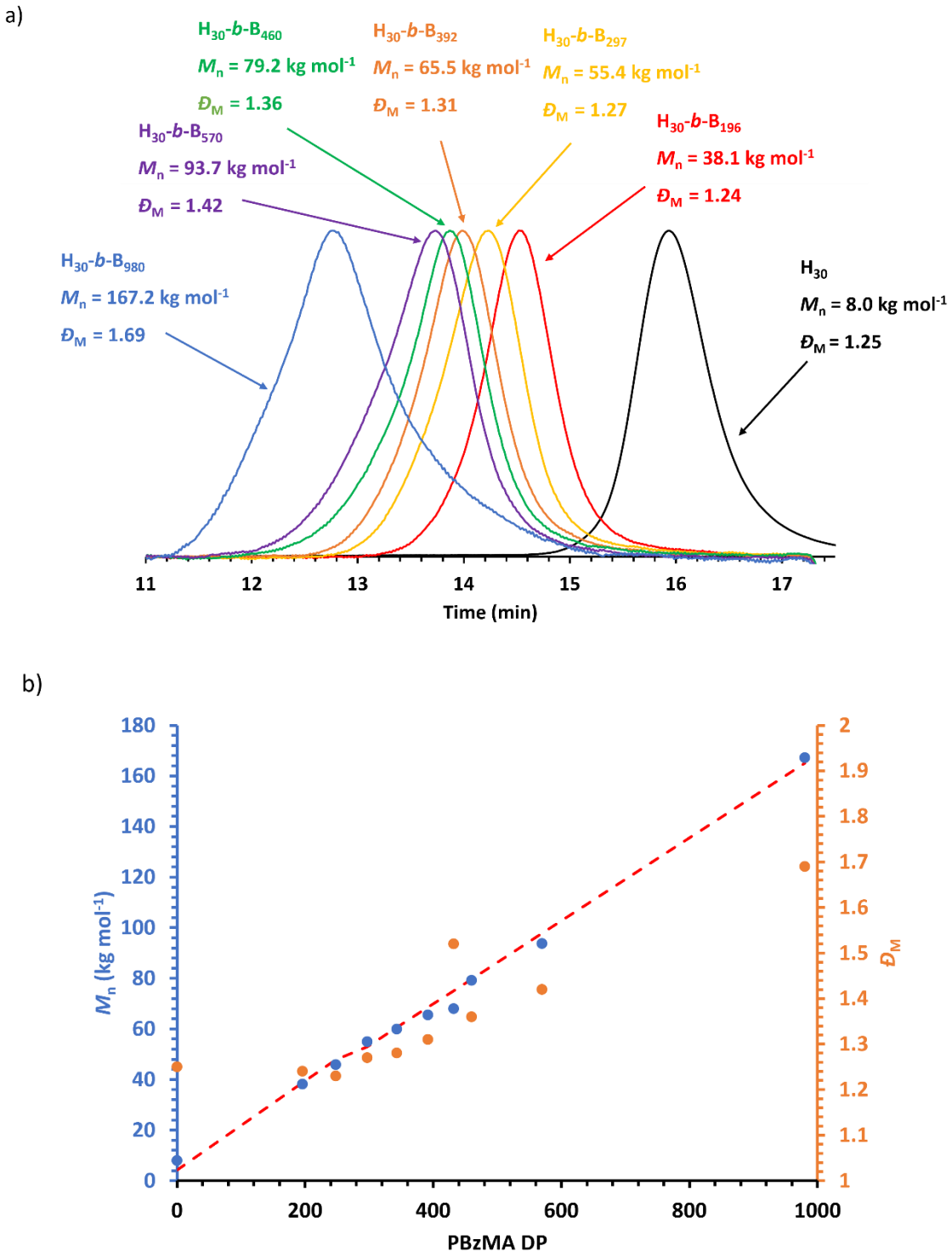

Figure 5.4. a) Selected DMF GPC chromatograms (vs poly(methyl methacrylate) standards) obtained for $PHEMA_{30}$-b-$PBzMA_y$ block copolymers synthesised via RAFT dispersion polymerisation of benzyl methacrylate in [EMIM][$EtOSO_3$] at 70 °C and 15% w/w solids; b) M_n vs PBzMA DP for $PHEMA_{30}$-b-$PBzMA_y$ block copolymers in [EMIM][$EtOSO_3$] at 15% w/w solids obtained using DMF GPC (vs. poly(methyl methacrylate) standards). The $PHEMA_{30}$ macro-CTA used for this polymerisation is also shown as a black trace for reference.

5.3.3 Synthesis of $PHEMA_{30}$-*b*-$PBzMA_y$ diblock copolymer nanoparticles via PISA at 20% w/w solids

In an effort to attempt to yield freestanding gels in [EMIM][$EtOSO_3$], a series of block copolymers were also synthesised at 20% w/w solids (Table 5.2 and Figure 5.5). Previous literature has reported that increasing the weight concentration has enabled the accessibility of worm phases (mixed and pure).[6, 10, 13, 32-34] The block copolymers were initially characterised by ^{1}H NMR spectroscopy and GPC (Figure 5.6), of which the results are summarised in Table 5.2.

Table 5.2. Summary of $PHEMA_{30}$-*b*-$PBzMA_y$ block copolymers synthesised in [EMIM][$EtOSO_3$] at 20% w/w.

Target composition	BzMA conversion[a] (%)	Actual composition	$M_{n,th}$[a] (g mol^{-1})	M_n[b] (g mol^{-1})	$Đ_M$[b]
H_{30}-B_{200}	99	H_{30}-B_{198}	33,998	42,900	1.35
H_{30}-B_{250}	99	H_{30}-B_{248}	44,908	49,400	1.42
H_{30}-B_{300}	91	H_{30}-B_{273}	49,013	52,000	1.26
H_{30}-B_{350}	99	H_{30}-B_{347}	61,165	56,700	1.47
H_{30}-B_{400}	99	H_{30}-B_{396}	69,211	61,800	1.59
H_{30}-B_{450}	99	H_{30}-B_{446}	77,422	74,400	1.49
H_{30}-B_{500}	99	H_{30}-B_{495}	85,468	77,500	1.58
H_{30}-B_{550}	98	H_{30}-B_{539}	92,693	90,500	1.46
H_{30}-B_{600}	99	H_{30}-B_{594}	101,725	96,300	1.49
H_{30}-B_{1000}	98	H_{30}-B_{980}	165,110	181,000	1.38

[a]Determined by ^{1}H NMR spectroscopy. [b]Determined by DMF GPC against poly(methyl methacrylate) standards.

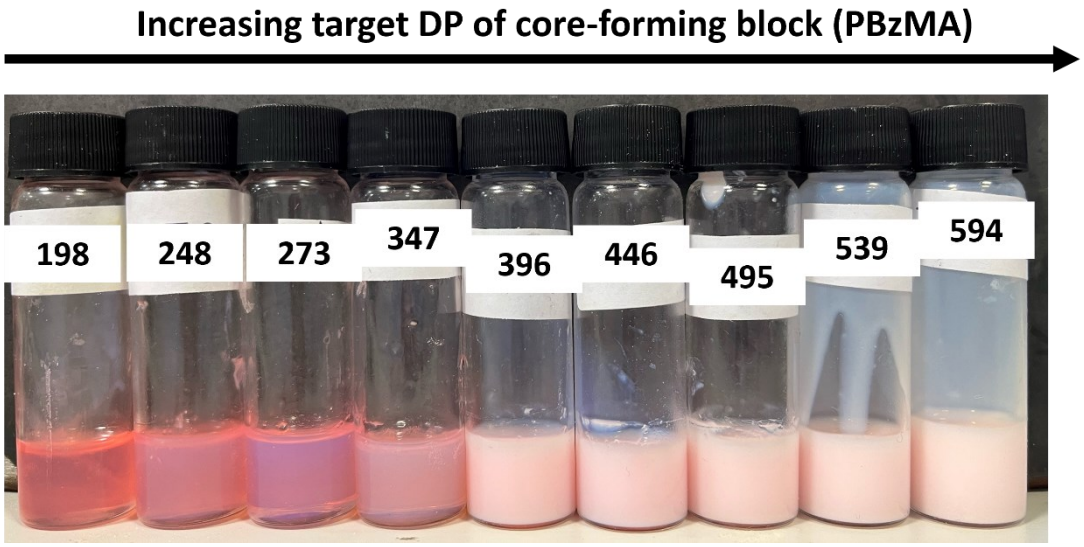

Figure 5.5. Digital image showing the physical appearance of the series of $PHEMA_{30}$-b-$PBzMA_y$ block copolymer dispersions in [EMIM][$EtOSO_3$] at 20% w/w solids. Number labels on sample vials denote the actual PBzMA core-forming block DP, as determined using ^1H NMR spectroscopy.

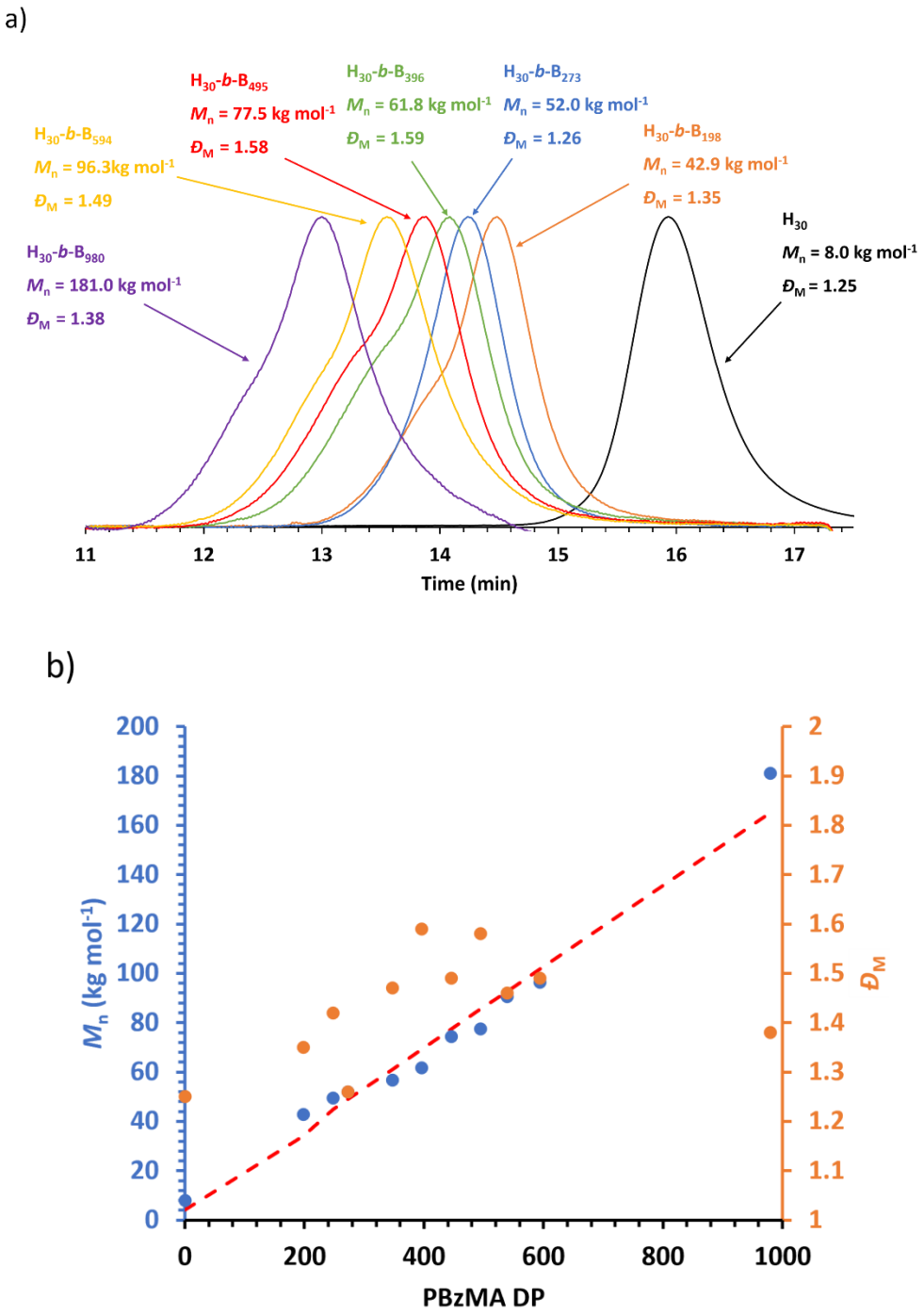

Figure 5.6. a) Selected DMF GPC chromatograms (vs. poly(methyl methacrylate) standards) obtained for $PHEMA_{30}$-b-$PBzMA_y$ block copolymers synthesised via RAFT dispersion polymerisation of benzyl methacrylate in [EMIM][$EtOSO_3$] at 70 °C and 20% w/w solids. The $PHEMA_{30}$ macro-CTA used for this polymerisation is also shown as a dashed black line for reference; b) M_n vs PBzMA DP for $PHEMA_{30}$-b-$PBzMA_y$ block copolymers in [EMIM][$EtOSO_3$] at 20% w/w solids obtained using DMF GPC (vs. poly(methyl methacrylate) standards). Theoretical M_n is shown as a dashed red line.

Similarities are observed for the block copolymer series at 20% w/w solids when compared to the block copolymers dispersions at 15% w/w solids. Firstly, at both weight concentrations, BzMA monomer conversion reach ≤99% within one hour. Secondly, only free-flowing fluids are yielded at all PBzMA DPs, indicating only spherical nanoparticles are present, and no freestanding gels are observed, indicating worm-like nanoparticles are absent. GPC also indicates efficient chain extension of the macro-CTA at 20% w/w, evidenced by a growth in molecular weight and lack of macro-CTA molecular weight peak (Figure 5.6a).

It has been established that when targeting higher DPs of the core-forming block, a loss of control over the polymerisation can be observed.[2] However, at both copolymer concentrations, there is unexpectedly no discernible trend in the dispersity. Instead, fluctuation in the dispersity is seen. This is unlike block copolymer syntheses in [EMIM][DCA] (Chapter 3), where the expected loss of control at higher PBzMA DPs is observed. Additionally, some tailing in observed in GPC traces of the block copolymers, which could be attributed to a low level of termination by combination which has been observed in previously reported syntheses involving the polymerisation of benzyl methacrylate.[35]

5.3.4 Nanoparticle characterisation of $PHEMA_{30}$-*b*-$PBzMA_y$ spherical nano-objects

DLS was initially used to confirm the presence of nanoparticles. Sphere-equivalent diameters and PDI values for each 0.15% w/w dispersion was recorded and plotted in Figures 5.7-5.8 for nanoparticles prepared at 15% w/w and Figure 5.9-5.10 for nanoparticles prepared at 20% w/w.

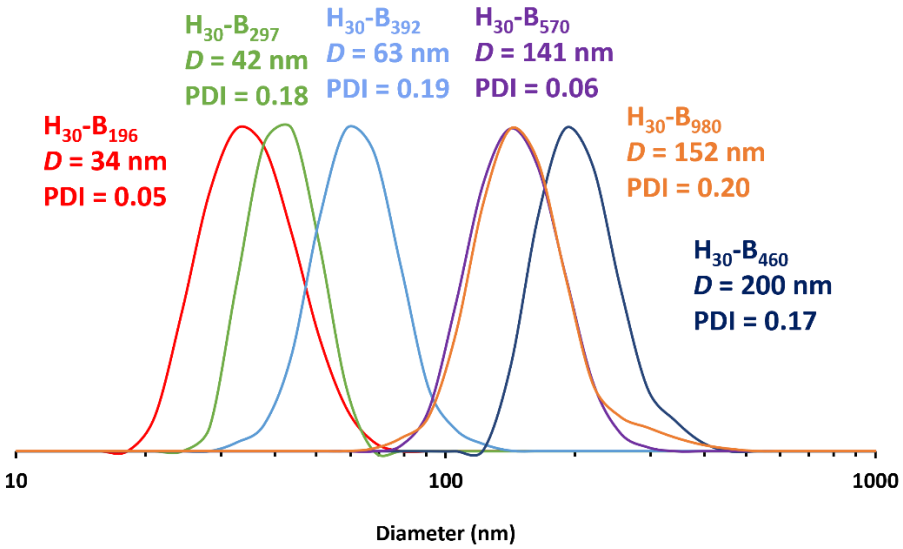

Figure 5.7. DLS data obtained for selection of 0.15% w/w dispersions of $PHEMA_{30}$-*b*-$PBzMA_y$ (H_{30}-B_y for brevity) nanoparticles synthesised at 15% w/w solids in [EMIM][$EtOSO_3$].

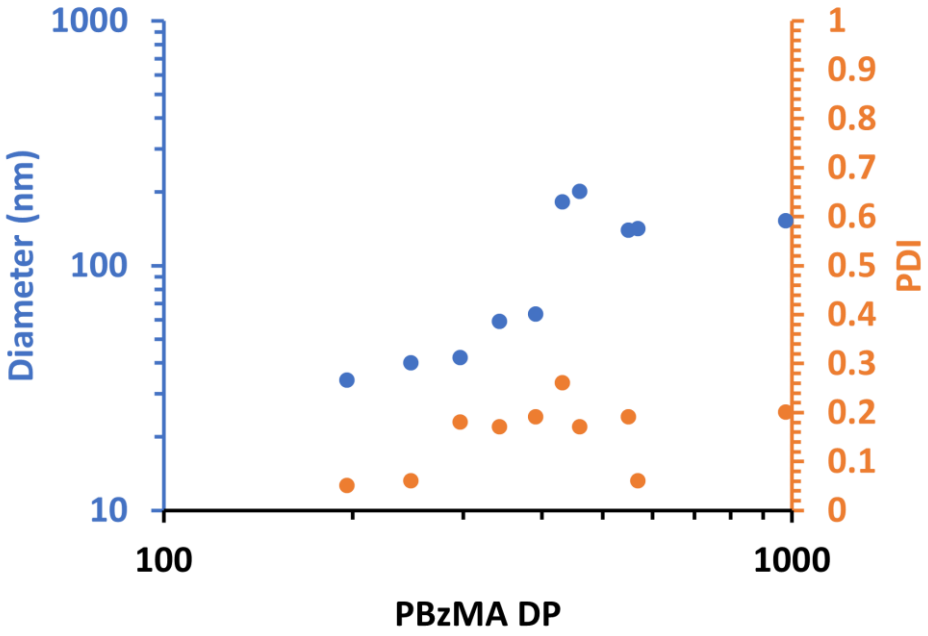

Figure 5.8. Dynamic light scattering (DLS) studies showing intensity-average diameter (blue) and polydispersity (orange) for 0.15% w/w dispersions of $PHEMA_{30}$-b-$PBzMA_y$ nanoparticles synthesised at 15% w/w solids in [EMIM][$EtOSO_3$].

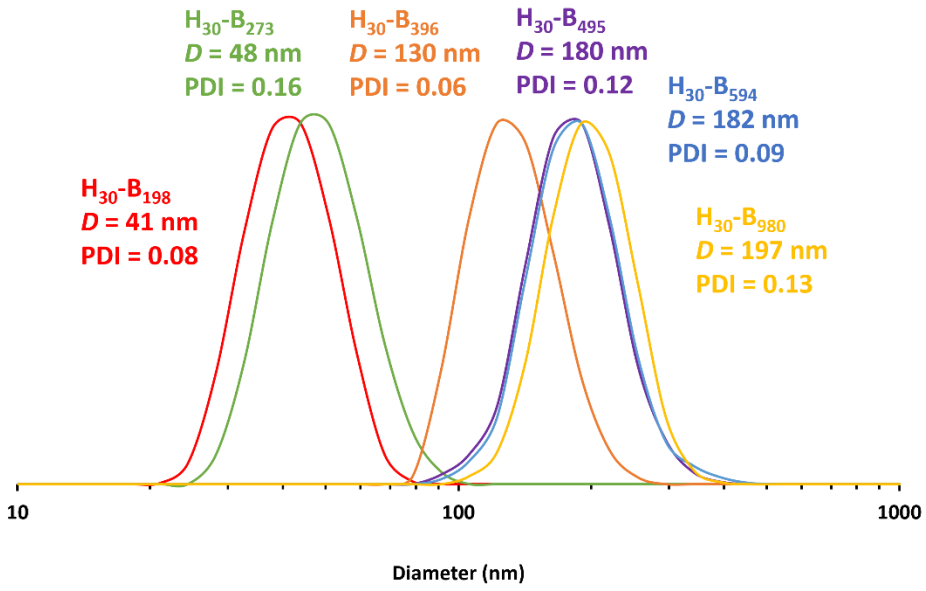

Figure 5.9. DLS data obtained for selection of 0.15% w/w dispersions of $PHEMA_{30}$-*b*-$PBzMA_y$ (H_{30}-B_y for brevity) nanoparticles synthesised at 20% w/w solids in [EMIM][$EtOSO_3$].

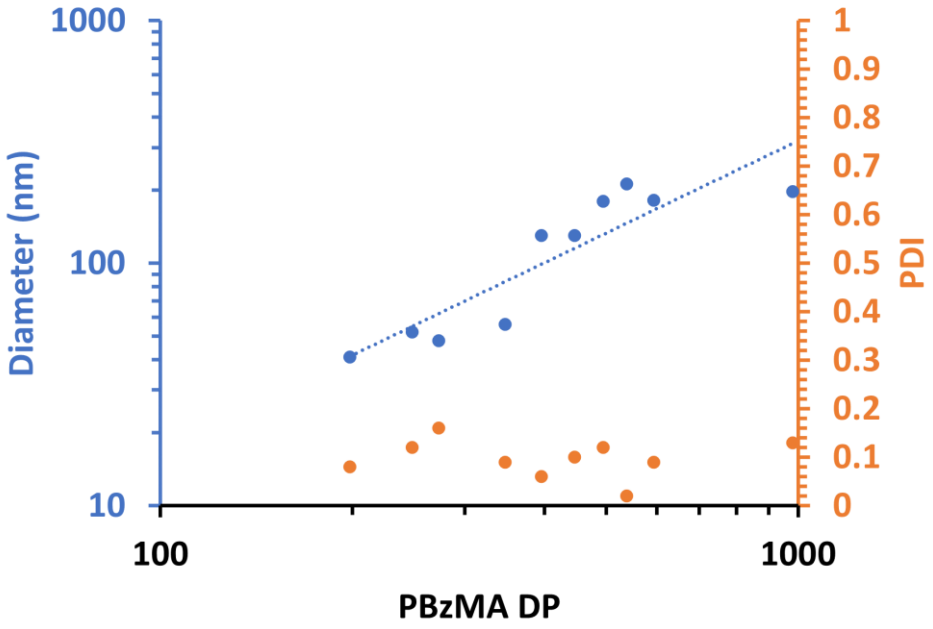

Figure 5.10. Dynamic light scattering (DLS) studies showing intensity-average diameter (blue) and polydispersity (orange) for 0.15% w/w dispersions of $PHEMA_{30}$-b-$PBzMA_y$ nanoparticles synthesised at 20% w/w solids in [EMIM][$EtOSO_3$].

When synthesised at 15% w/w solids, DLS indicated a sphere-equivalent nanoparticle size range from ~30 nm to ~200 nm. For nanoparticles with PBzMA DPs in the range of 196-392, there is a very steady increase in diameter from ~30 nm to ~60 nm. For the sample with a PBzMA DP of 432, there is a substantial jump in nanoparticle diameter to ~180 nm, after which for higher DPs, there is fluctuation in the sizes without a notable trend, therefore a power law trendline was not suitable.

In contrast, nanoparticles synthesised at 20% w/w solids had a diameter range of ~40 nm to ~210 nm. Again, there was a considerable increase in nanoparticle size at a specific PBzMA DP, but this time a slightly lower DP than those prepared at 15% w/w solids. Specifically, the nanoparticle size increases from ~60 nm to ~130 nm between a PBzMA DP of 347 to 396, respectively. After a PBzMA DP of 396, there is a noticeable, yet less dramatic jump in diameter.

The presence of spheres and vesicles was confirmed by SAXS analysis (Figures 5.11-5.14 and 5.16 and Table 5.3). All block copolymers with lower PBzMA DPs (≤343) prepared at 15% w/w and also those prepared at 20% w/w with PBzMA DPs ≤347 contained spherical nanoparticles as confirmed by fitting their respective background-subtracted scattering pattern to a well-established spherical micelle model (Figures 5.11-5.14).[30]

Table 5.3. Summary of parameters obtained when fitting SAXS data to a spherical-micelle model. φ_{sphere} is the volume fraction of spheres. D_{sphere} is the spherical nanoparticle diameter ($D_{\text{sphere}} = 2R_s + 4R_g$, where R_g is the radius of gyration of the stabiliser block and R_s is the core radius). $PHEMA_{30}$-*b*-$PBzMA_y$ is denoted as H_{30}-B_y for brevity.

Sample	Copolymer concentration during synthesis (% w/w)	φ_{sphere}	D_{sphere} (nm)
H_{30}-B_{196}	15	0.0030	26.0
H_{30}-B_{248}	15	0.0031	31.3
H_{30}-B_{297}	15	0.0041	36.3
H_{30}-B_{343}	15	0.0036	48.7
H_{30}-B_{198}	20	0.0031	28.6
H_{30}-B_{248}	20	0.0031	41.3
H_{30}-B_{273}	20	0.0044	37.5
H_{30}-B_{347}	20	0.0027	47.1

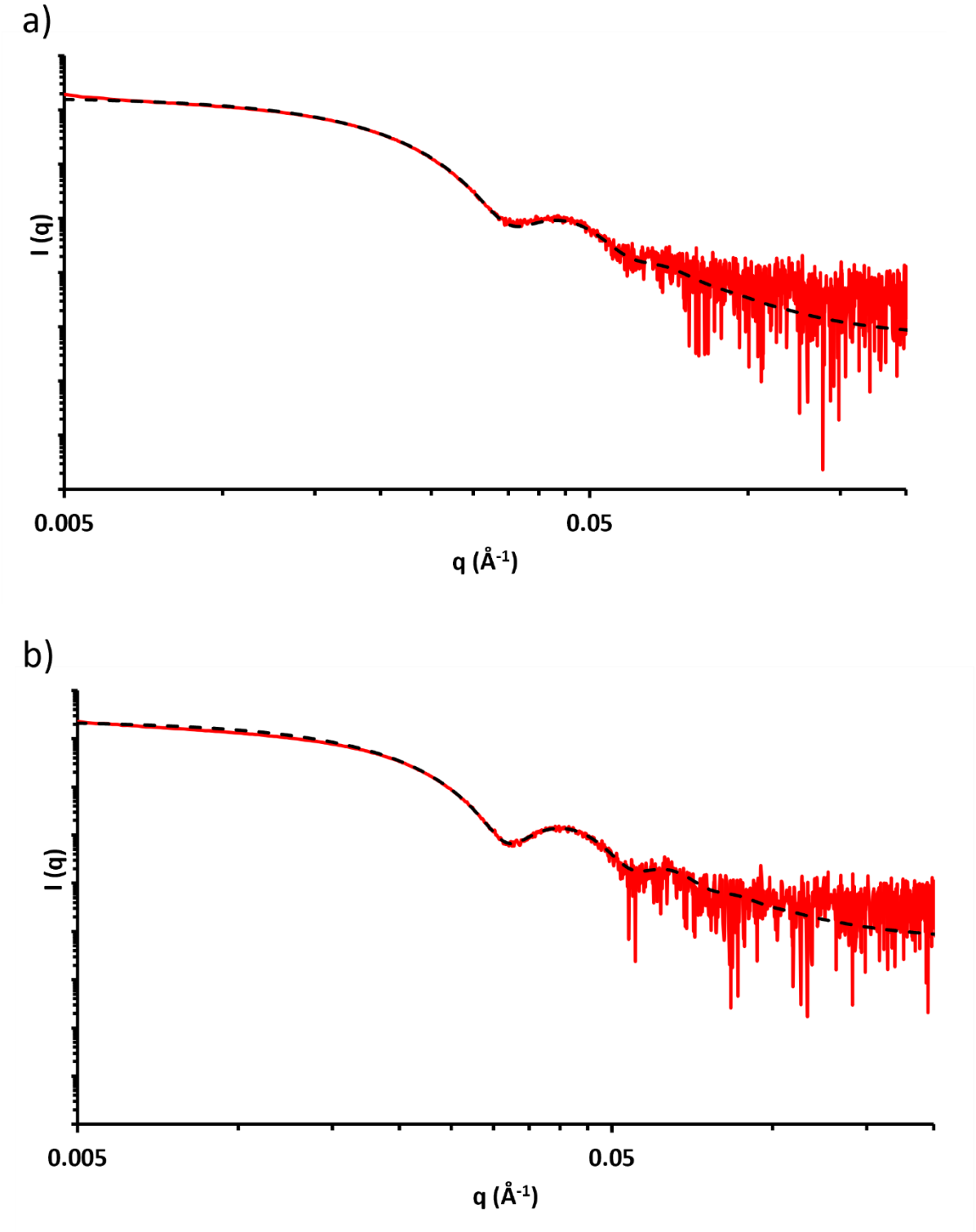

Figure 5.11. Background-subtracted SAXS data obtained for a) 1.0% w/w $PHEMA_{30}$-$PBzMA_{196}$ in [EMIM][$EtOSO_3$] at 25 °C prepared at 15% w/w, b) 1.0% w/w $PHEMA_{30}$-$PBzMA_{198}$ in [EMIM][$EtOSO_3$] at 25 °C prepared at 20% w/w. Dashed lines represent the model fit obtained using the spherical-micelle model (Appendix 7.1.1).

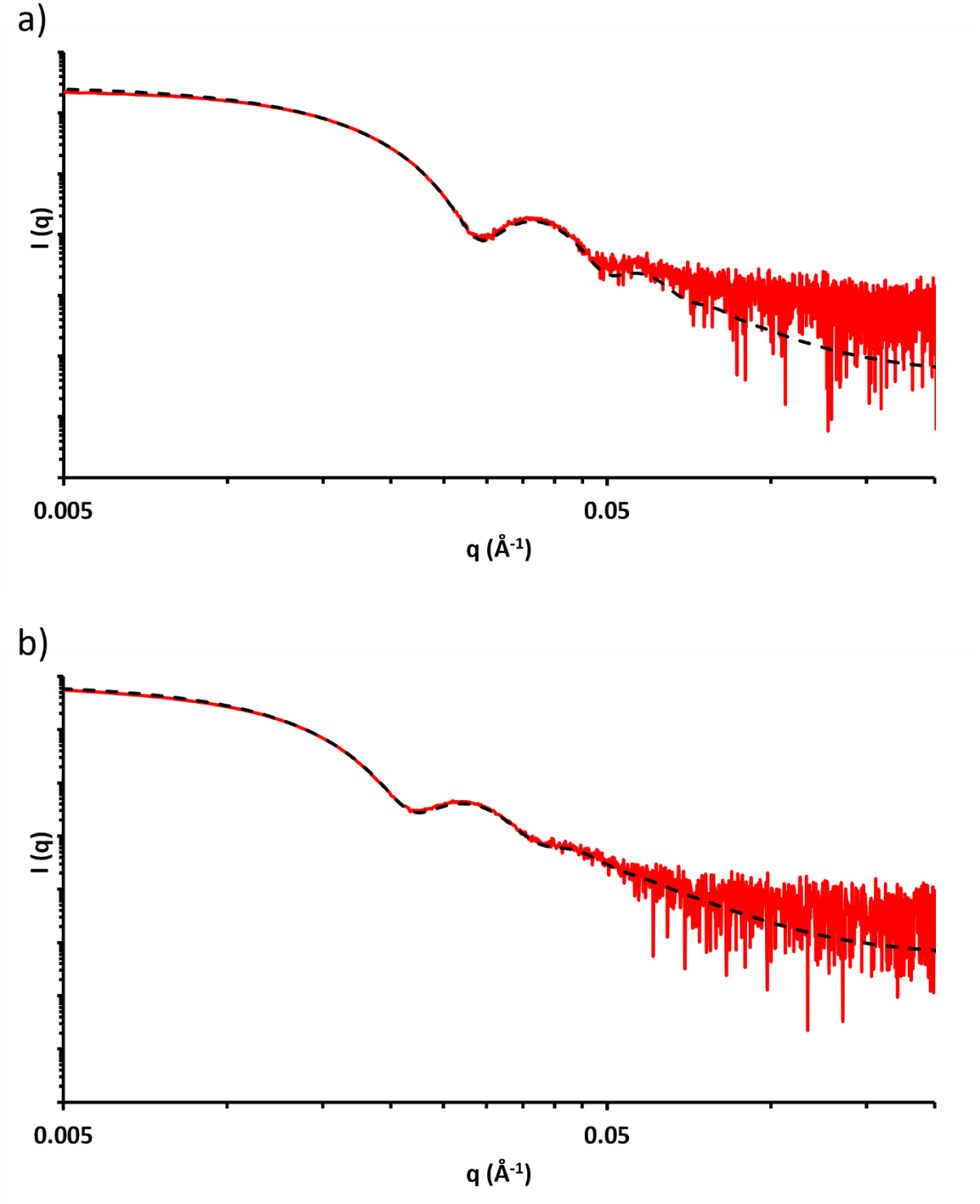

Figure 5.12. Background-subtracted SAXS data obtained for a) 1.0% w/w $PHEMA_{30}$-$PBzMA_{248}$ in [EMIM][$EtOSO_3$] at 25 °C prepared at 15% w/w, b) 1.0% w/w $PHEMA_{30}$-$PBzMA_{248}$ in [EMIM][$EtOSO_3$] at 25 °C prepared at 20% w/w. Dashed lines represent the model fit obtained using the spherical-micelle model (Appendix 7.1.1).

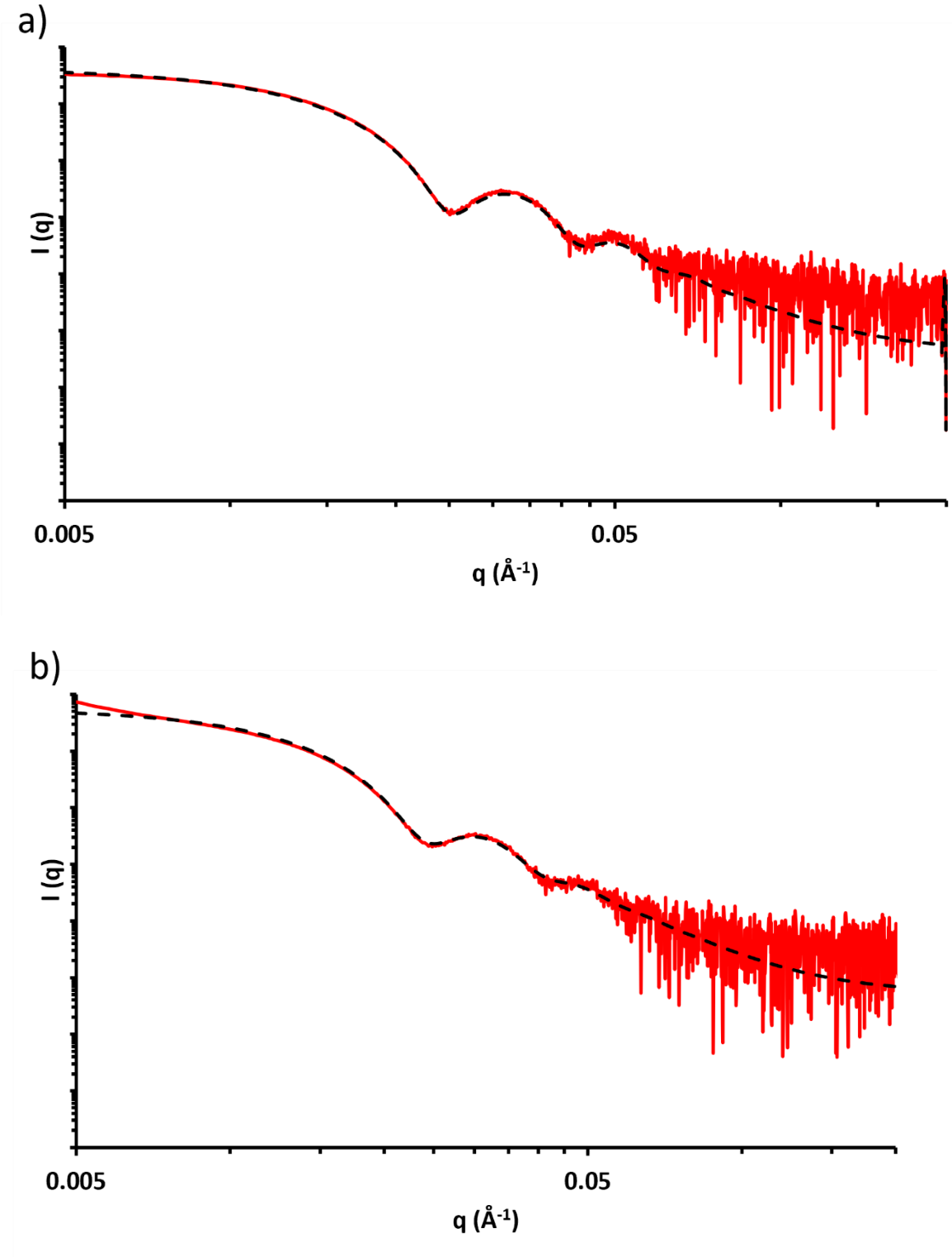

Figure 5.13. Background-subtracted SAXS data obtained for a) 1.0% w/w $PHEMA_{30}$-$PBzMA_{297}$ in [EMIM][$EtOSO_3$] at 25 °C prepared at 15% w/w, b) 1.0% w/w $PHEMA_{30}$-$PBzMA_{273}$ in [EMIM][$EtOSO_3$] at 25 °C prepared at 20% w/w. Dashed lines represent the model fit obtained using the spherical-micelle model (Appendix 7.1.1).

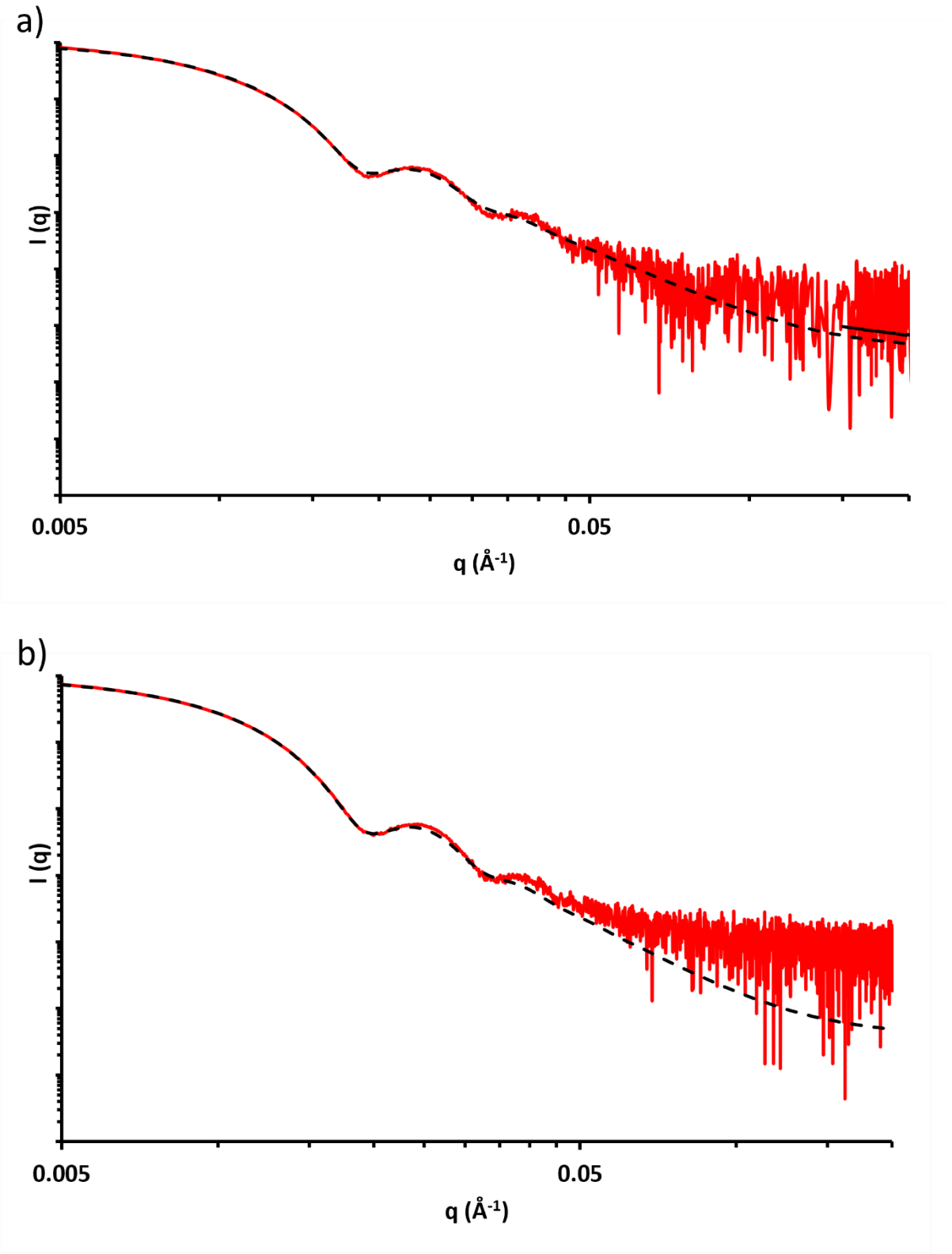

Figure 5.14. Background-subtracted SAXS data obtained for a) 1.0% w/w $PHEMA_{30}$-$PBzMA_{343}$ in [EMIM][$EtOSO_3$] at 25 °C prepared at 15% w/w, b) 1.0% w/w $PHEMA_{30}$-$PBzMA_{347}$ in [EMIM][$EtOSO_3$] at 25 °C prepared at 20% w/w. Dashed lines represent the model fit obtained using the spherical-micelle model (Appendix 7.1.1).

The diameters of the spheres in the nanoparticle dispersions were recorded from both DLS and SAXS analysis. The comparison of the values obtained is shown in Figure 5.15 below.

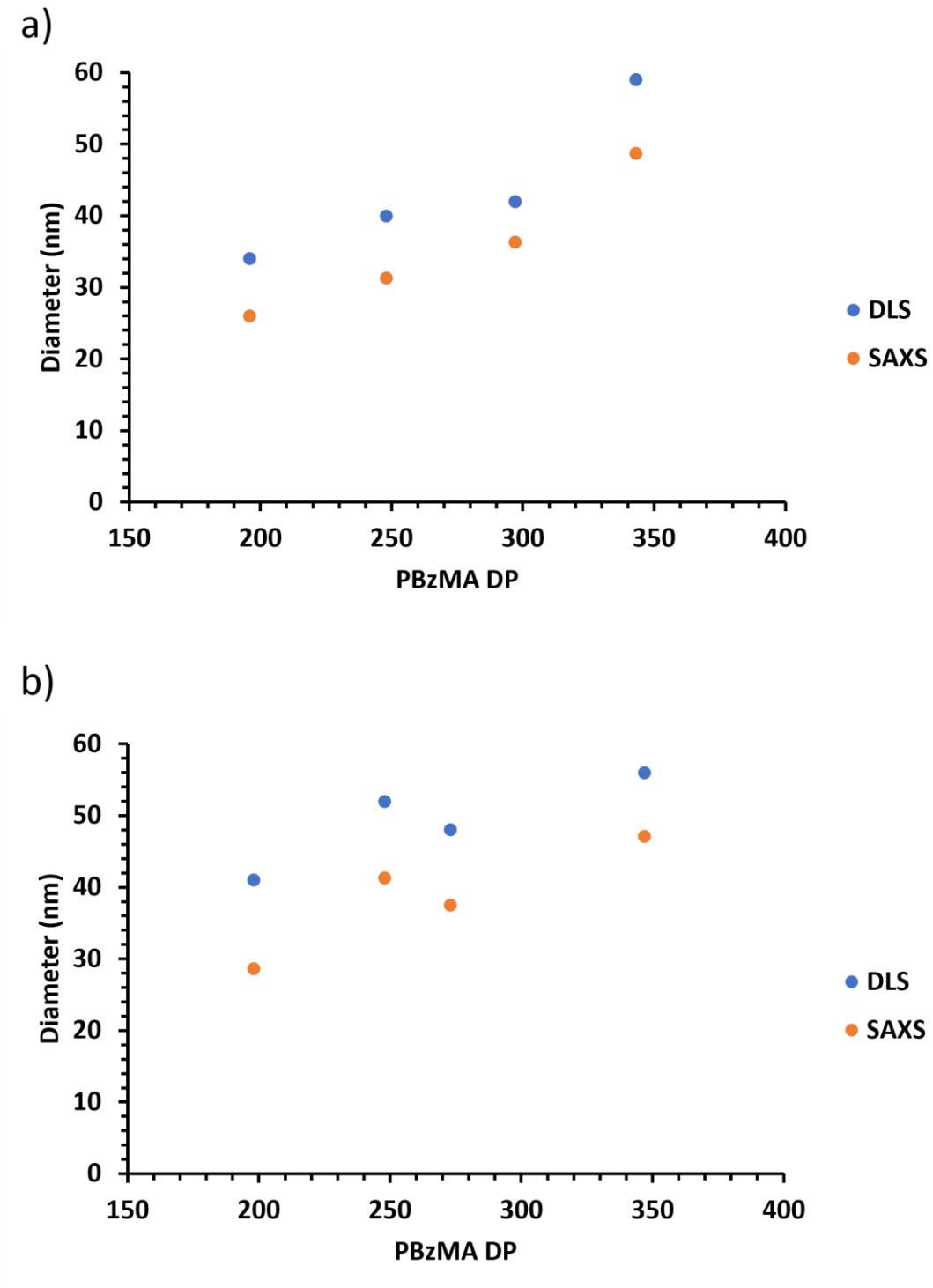

Figure 5.15. Diameter values of the spheres obtained by DLS and SAXS data in 1% w/w nanoparticle dispersions of $PHEMA_{30}$-b-$PBzMA_y$ originally prepared at a) 15% w/w solids and b) 20% w/w solids.

For both copolymer concentrations, SAXS obtained diameter values are shown to be smaller than that of DLS diameter values. Notably, for spheres prepared at 20% w/w, fluctuation in the diameter of spheres is observed for both DLS and SAXS obtained diameters.

Due to poor fitting of some models, only the background-subtracted data was plotted without the models. However, a gradient as a guide to the eye is provided to indicate that there are indeed spheres and vesicles present in the samples (Figure 5.16). In most cases at higher PBzMA DPs (target DP > 400) where the most ideal model fit would be a well-established vesicle model, it was still not possible to fit due to the vesicles appearing to be too large for fitting (Figure 5.17).

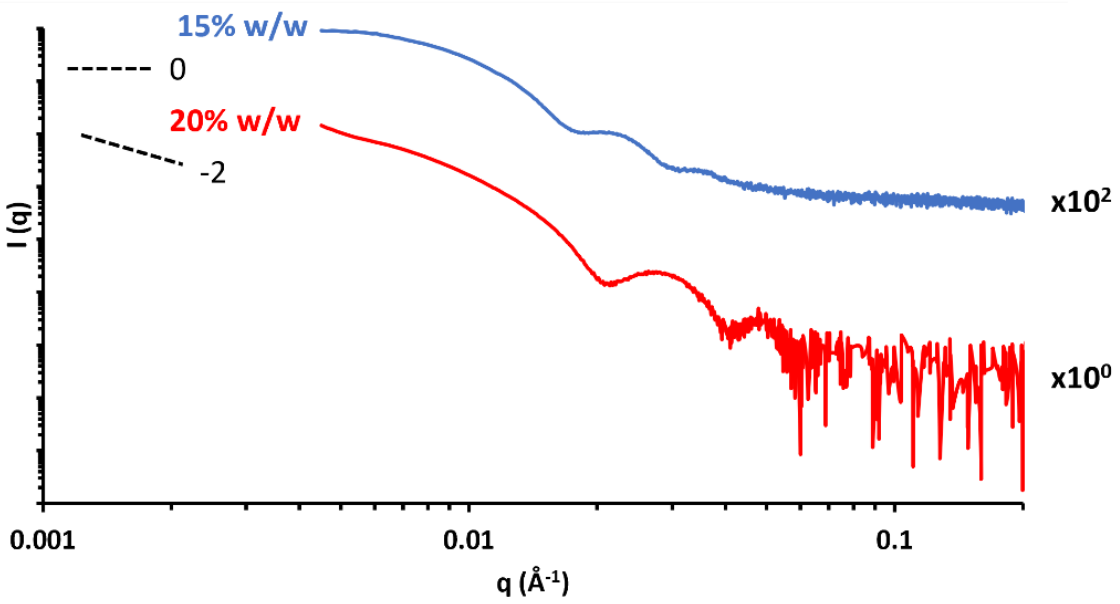

Figure 5.16. Background-subtracted SAXS data obtained for 1.0% w/w $PHEMA_{30}$-b-$PBzMA_{392}$ in [EMIM][$EtOSO_3$] at 25 °C prepared at 15% w/w (blue) and 1.0% w/w $PHEMA_{30}$-b-$PBzMA_{396}$ in [EMIM][$EtOSO_3$] at 25 °C prepared at 20% w/w (red). Gradients of 0 and -2 are shown as a guide to the eye to indicate the presence of spheres and vesicles, respectively.

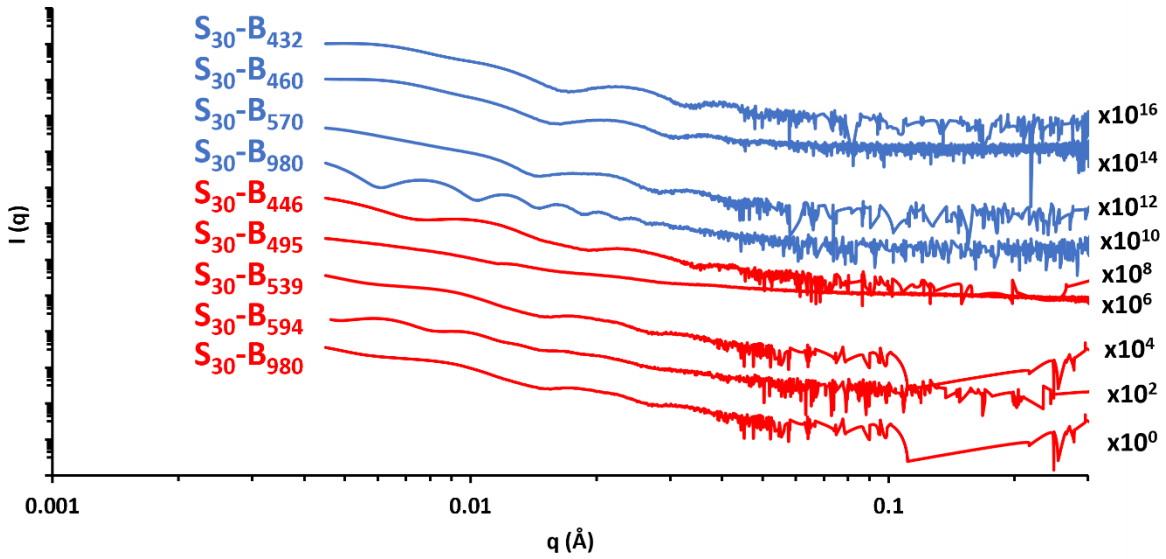

Figure 5.17. Background subtracted SAXS data obtained for 1% w/w dispersions of $PHEMA_{30}$-b-$PBzMA_y$ nanoparticles prepared at 15% w/w (blue) and 20% w/w (red). $PHEMA_{30}$-b-$PBzMA_y$ is denoted as H_{30}-B_y for brevity.

5.4 Conclusions

In summary, $PHEMA_{30}$-*b*-$PBzMA_y$ block copolymer spherical nanoparticles can be generated by polymerisation-induced self-assembly at 70 °C in [EMIM][$EtOSO_3$] at 15% w/w and 20% w/w solids. ≤99% BzMA conversion was achieved in all syntheses within 1 hour and efficient chain extension of the $PHEMA_{30}$ macro-CTA was confirmed by GPC. All block copolymer solutions were visually free-flowing liquids, which were transparent at lower PBzMA DPs (≤ 392 at 15% w/w and 343 at 20% w/w), and turbid solutions at higher PBzMA DPs. No free-standing gels were obtained as judged by the inversion test, indicating the absence of worm-like micelles, unlike previous block copolymers generated in [EMIM][DCA] (Chapter 3). DLS confirmed the presence of nanoparticles ranging in sizes from ~30 nm to ~200 nm and from ~40 nm to ~210 nm for block copolymers synthesised at 15% w/w and 20% w/w solids, respectively. For nanoparticles prepared at 15% w/w, PDI values ranged from 0.05 to 0.26 with no discernible trend. Those with much smaller PDI values (≤ 0.06) were well-defined spheres, however those with higher PDI values (≤0.17) indicated the presence of less well-defined spheres, indicating there could be some other morphologies present Further nanoparticle characterisation was conducted using SAXS, which confirmed the presence of spheres and vesicles.

To conclude, choice of solvent can greatly affect the ability to access higher order morphologies as observed in this chapter and previous literature. One reason that only spherical micelles could be accessed in [EMIM][$EtOSO_3$] could be that PBzMA core-forming block has a higher affinity for this IL in comparison to [EMIM][DCA] investigated in Chapter 3, therefore a longer core-forming block is required to induce PISA. Despite this, the scope of PISA in ionic liquids has been successfully expanded to include [EMIM][$EtOSO_3$] as a suitable PISA solvent, particularly for generating spherical nanoparticles. Other parameters can be investigated in order to include worm-like micelles in the range of morphologies that can be accessed in this IL, such as tuning the T_g of the core-forming block by incorporating a lower T_g monomer, or potentially utilising a smaller stabiliser block to potentially enable to fusion of 2D spheres to ultimately yield worms.

5.5 References

1. N. J. W. Penfold, J. Yeow, C. Boyer and S. P. Armes, *ACS Macro Lett*, 2019, **8**, 1029-1054.
2. P. J. Docherty, M. J. Derry and S. P. Armes, *Polym. Chem*, 2019, **10**, 603-611.
3. Q. Zhang and S. Zhu, *ACS Macro Lett.*, 2015, **4**, 755-758.
4. M. Semsarilar, N. J. W. Penfold, E. R. Jones and S. P. Armes, *Polym. Chem*, 2015, **6**, 1751-1757.
5. S. J. Byard, M. Williams, B. E. McKenzie, A. Blanazs and S. P. Armes, *Macromolecules*, 2017, **50**, 1482-1493.
6. F. L. Hatton, M. J. Derry and S. P. Armes, *Polym. Chem*, 2020, **11**, 6343-6355.
7. P. J. Docherty, C. Girou, M. J. Derry and S. P. Armes, *Polym. Chem*, 2020, **11**, 3332-3339.
8. M. J. Derry, L. A. Fielding and S. P. Armes, *Polym. Chem*, 2015, **6**, 3054-3062.
9. C. György, T. J. Neal, T. Smith, D. J. Growney and S. P. Armes, *Macromolecules*, 2022, **55**, 4091-4101.
10. L. A. Fielding, M. J. Derry, V. Ladmiral, J. Rosselgong, A. M. Rodrigues, L. P. D. Ratcliffe, S. Sugihara and S. P. Armes, *Chem. Sci*, 2013, **4**, 2081-2087.
11. Y. Pei and A. B. Lowe, *Polym. Chem*, 2014, **5**, 2342-2351.
12. Y. Pei, N. C. Dharsana, J. A. van Hensbergen, R. P. Burford, P. J. Roth and A. B. Lowe, *Soft Matter*, 2014, **10**, 5787-5796.
13. E. R. Jones, M. Semsarilar, A. Blanazs and S. P. Armes, *Macromolecules*, 2012, **45**, 5091-5098.
14. L. A. Fielding, J. A. Lane, M. J. Derry, O. O. Mykhaylyk and S. P. Armes, *J. Am. Chem. Soc*, 2014, **136**, 5790-5798.
15. M. J. Derry, T. Smith, P. S. O'Hora and S. P. Armes, *ACS Appl. Mater. Interfaces*, 2019, **11**, 33364-33369.
16. L. Houillot, C. Bui, C. Farcet, C. Moire, J.-A. Raust, H. Pasch, M. Save and B. Charleux, *ACS Appl. Mater. Interfaces*, 2010, **2**, 434-442.
17. N. J. Warren and S. P. Armes, *J. Am. Chem. Soc*, 2014, **136**, 10174-10185.
18. A. Blanazs, J. Madsen, G. Battaglia, A. J. Ryan and S. P. Armes, *J. Am. Chem. Soc*, 2011, **133**, 16581-16587.

19. A. Blanazs, R. Verber, O. O. Mykhaylyk, A. J. Ryan, J. Z. Heath, C. W. I. Douglas and S. P. Armes, *J. Am. Chem. Soc*, 2012, **134**, 9741-9748.
20. C. Grazon, J. Rieger, N. Sanson and B. Charleux, *Soft Matter*, 2011, **7**, 3482-3490.
21. E. R. Jones, M. Semsarilar, P. Wyman, M. Boerakker and S. P. Armes, *Polym. Chem*, 2016, **7**, 851-859.
22. Y. Kang, A. Pitto-Barry, H. Willcock, W.-D. Quan, N. Kirby, A. M. Sanchez and R. K. O'Reilly, *Polym. Chem*, 2015, **6**, 106-117.
23. P. Yang, Y. Ning, T. J. Neal, E. R. Jones, B. R. Parker and S. P. Armes, *Chem. Sci*, 2019, **10**, 4200-4208.
24. X. Luo, *Eur. Polym. J*, 2021, **158**, 110639.
25. S.-P. Wen, J. G. Saunders and L. A. Fielding, *Polym. Chem*, 2020, **11**, 3416-3426.
26. H. Zhou, C. Liu, C. Gao, Y. Qu, K. Shi and W. Zhang, *J. Polym. Sci. Part A: Polym. Chem*, 2016, **54**, 1517-1525.
27. R. Yamanaka, A. Sugawara-Narutaki and R. Takahashi, *Macromolecules*, 2023, **56**, 4354-4361.
28. N. P. Cowieson, C. J. C. Edwards-Gayle, K. Inoue, N. S. Khunti, J. Doutch, E. Williams, S. Daniels, G. Preece, N. A. Krumpa, J. P. Sutter, M. D. Tully, N. J. Terrill and R. P. Rambo, *J. Synchrotron Rad*, 2020, **27**, 1438-1446.
29. J. Ilavsky and P. Jemian, *J. Appl. Crystallogr*, 2009, **42**, 347-353.
30. J. Pedersen, *J. Appl. Crystallogr*, 2000, **33**, 637-640.
31. J. R. Lovett, M. J. Derry, P. Yang, F. L. Hatton, N. J. Warren, Patrick W. Fowler and S. P. Armes, *Chem. Sci*, 2018, **9**, 7138-7144.
32. C. György, S. J. Hunter, C. Girou, M. J. Derry and S. P. Armes, *Polym. Chem*, 2020, **11**, 4579-4590.
33. M. J. Derry, L. A. Fielding, N. J. Warren, C. J. Mable, A. J. Smith, O. O. Mykhaylyk and S. P. Armes, *Chem. Sci*, 2016, **7**, 5078-5090.
34. V. Ladmiral, M. Semsarilar, I. Canton and S. P. Armes, *J. Am. Chem. Soc*, 2013, **135**, 13574-13581.
35. V. J. Cunningham, A. M. Alswieleh, K. L. Thompson, M. Williams, G. J. Leggett, S. P. Armes and O. M. Musa, *Macromolecules*, 2014, **47**, 5613-5623.

6. Conclusions and future work

In conclusion, PISA in ionic liquids has been extended to include [EMIM][DCA] and [EMIM][$EtOSO_3$]. Most importantly, the PISA synthesis of PHEMA-*b*-PBzMA nanoparticles in [EMIM][DCA] enables access to worm ionogels via a convenient and facile synthesis route. This provides a tangible route to next generation ionogel materials for electrochemical applications. There is tremendous scope for future work, as a result of the almost inexhaustible combinations of anions and cations that form ILs, as well as the versatility of monomers that is compatible with PISA processes. Specifically, starting materials such as renewably-sourced monomers can be investigated to form sustainably-developed ionogels. Stimulus responsive worm ionogels would be a significant advancement in this field and may provide a route to fully recyclable gel electrolytes and thus provide a solution to the future problems surrounding the end-of-life prospects for batteries such as lithium-ion batteries. As ILs are readily tuneable to include desirable properties, ionogels in the future can be developed via PISA-mediated syntheses to include favourable characteristics for more specific electrochemical applications.

Various polymers were explored for their compatibility in two hydrophilic ionic liquids (ILs), 1-ethyl-3-methylimidazolium dicyanamide ([EMIM][DCA]) and 1-ethyl-3-methylimidazolium ethyl sulphate ([EMIM][$EtOSO_3$]) at the beginning of this Thesis. A range of hydrophobic and hydrophilic monomers were tested for their miscibilities in the ILs. Good miscibility with the ILs was essential for block copolymer design, particularly for generating the core-forming block via RAFT dispersion polymerisation. Any monomers that were shown to be immiscible with the ILs were eliminated from the selection and were not used for the proceeding solubility screenings of the polymers in the ILs. Firstly, polymers synthesised via free radical polymerisation were tested for their solubility in ILs. This proved to be moderately challenging as the purification of some polymers was more challenging than others. This in itself could have potentially adverse effects on the solubility screenings. Concurrently, a series of polymers were also synthesised via RAFT solution polymerisation, which resulted in lower molecular weights and a relatively more controlled polymerisation as evidenced by GPC analysis. Additionally, this was reflected in the solubility studies where selected polymers synthesised via RAFT were readily soluble in the ILs, whereas their free radical equivalents were not. This was attributed to either the lower molecular weights of the RAFT-synthesised macromolecular chain transfer agents (macro-CTAs), or the functionality of the RAFT chain transfer agent (CTA) facilitating solubility in the ILs. Those that were soluble in the ILs, particularly in the form of a macro-CTA, could have been considered as potential candidates for stabiliser blocks in future block copolymer syntheses via RAFT dispersion

polymerisation. Some polymers, synthesised by both free-radical and RAFT, were found to be insoluble in the ILs, thus demonstrating their potential suitability as core-forming blocks. As a result, poly(2-hydroxyethyl methacrylate) (PHEMA) was selected as the stabiliser block due the macro-CTA being readily soluble in both ILs. Moreover, poly(benzyl methacrylate) (PBzMA) was selected to be the core-forming block, due to the monomer being miscible with the ILs, but when it polymerises it forms an IL-insoluble polymer. This is essential for ensuing block copolymer syntheses to proceed via RAFT dispersion polymerisation, in which worm gels are known to be more readily accessible compared to emulsion polymerisation formulations. Because of the extensive number of combinations of cations and anions that can make up an IL, there is huge potential scope for expanding on a library of polymers and monomers and their solubilities in, and miscibilities with, several ILs. This would enable the design of block copolymers for their self-assembly in ILs to become much more facile and efficient.

A PHEMA macro-CTA with a mean degree of polymerisation (DP) of 30 was synthesised via RAFT solution polymerisation at 60 °C in methanol. The $PHEMA_{30}$ macro-CTA was analysed by GPC and was shown to have a relatively narrow molecular weight distribution ($Đ_M$ = 1.25) indicating the polymerisation was well-controlled. The DP of the PHEMA macro-CTA was targeted at 50 and the polymerisation was allowed to proceed for 6 hours, however due to a fairly low monomer conversion (40% HEMA conversion), the reaction afforded a PHEMA macro-CTA with an actual DP of 30. Despite not reaching an ideal conversion, the $PHEMA_{30}$ macro-CTA was actually shown to be sufficiently long to act as a stabiliser block and had an ideal DP in order to access higher order morphologies during block copolymer syntheses via polymerisation-induced self-assembly (PISA). Tuning the conditions of this reaction in order to achieve higher yield in a shorter time and thus reduce the amount of unreacted reagents warrants further research. With this in mind, it would be important to tune the conditions (i.e. lowering the target DP of the PHEMA but changing the solvent, temperature, reaction time, etc.) but ensure that the control of the polymerisation is not compromised.

The RAFT dispersion polymerisation of benzyl methacrylate in [EMIM][DCA] at 15% w/w solids was examined using the $PHEMA_{30}$ macro-CTA to generate a range of block copolymer nanoparticles by varying the DP of the PBzMA core-forming block. A representative kinetic study was carried out in order to determine the optimum time to allow the polymerisations to proceed to full BzMA conversion. The critical PBzMA DP at which self-assembly occurred was found to be 72. This is the

point at which the PBzMA block is sufficiently long enough to become insoluble and thus self-assemble. Based on the kinetic study, a series of $PHEMA_{30}$-*b*-$PBzMA_y$ block copolymers were synthesised. High monomer conversion of benzyl methacrylate was achieved in all cases (≥96%) within 2 hours and reasonably good control was maintained over the polymerisations up to a target PBzMA DP of 200 ($Đ_M \leq 1.24$) as confirmed by GPC analysis. Loss of control was observed when targeting higher DPs, which is typical when targeting higher DP of core-forming blocks. A range of dispersions was formed during these PISA syntheses from transparent free-flowing fluids, to free standing soft gels, and to turbid viscous solution, indicating the presence of spheres, worms and vesicles, respectively, based on previously reported PISA formulations. Furthermore, a combination of dynamic light scattering (DLS), small-angle X-ray scattering (SAXS) and transmission electron microscopy (TEM) analyses confirmed the presence of spheres, worms and vesicles. Importantly, the free-standing gels formed were shown to be as a result of worm-like micelles present in the samples as confirmed by a combination of nanoparticle and rheological characterisation. Clearly, the worms were sufficiently long enough to cause physical contacts and thus induce gelation.

Unlike some other reported PISA formulations that yielded worm gels, no thermoresponsive behaviour was observed. In order to make PISA formulations for electrochemical applications more interesting and practical, it would be beneficial to enable reversible worm-to-sphere transitions to occur, such that gelation can be induced at high temperatures thus reducing the risk of safety issues such as leakage. This development might also enable recyclability of gel electrolytes, something that would present a significant advancement in the battery industry. Thus, active research in this area is warranted.

As a result of these promising syntheses, further characterisation was conducted to assess their suitability as potential ionogels for electrochemical applications. Rheological studies of all dispersions were conducted to assess their viscoelastic properties. Dispersions that contained the highest proportion of worms, as confirmed by SAXS, generally exhibited the highest *G*' values, attributed to the extended percolating network formed as a result of the presence of more worms. Furthermore, oscillatory rheology studies of each gel dispersion displayed frequency-independent behaviour of *G*', indicating that these block copolymer dispersions were 'true' gels. In order to assess thermal properties of the ionogels, thermogravimetric analysis (TGA) was conducted for each gel. Notably, when bulk $PHEMA_{30}$-*b*-$PBzMA_{293}$ was analysed, the onset degradation temperature was recorded to be 230 °C. In contrast, both [EMIM][DCA] and the ionogels had

higher onset degradation temperatures of 305 °C and between 280 °C and 310 °C, respectively. Moreover, these studies demonstrated that the polymer content in the ionogel did not substantially affect the thermal onset degradation temperature, showcasing that the ionogels have good short term thermal stability. However, there is scope for further developing understanding of the thermal stability of the ionogels. For example, long-term thermal stability studies would be valuable to assess the thermal degradation of the ionogels over longer periods at higher temperatures. Long-term thermal stability is an essential characteristic for materials with potential electrochemical applications. The bulk resistance of each gel was also measured by electrochemical impedance spectroscopy (EIS), as well as [EMIM][DCA] in order to determine the effect of polymer content on the electrochemical properties provided by the [EMIM][DCA] in the ionogels. Generally, EIS demonstrated comparable electrochemical properties of the ionogel to [EMIM][DCA]. This is based on the fact that as the bulk resistance generally increases with decreasing ionic conductivity.

However, in order to obtain more understanding of the electrochemical properties of the ionogels, other electrochemical analyses would be advantageous. Specifically, investigating the performance of the ionogels in real-life applications such as lithium-ion batteries and supercapacitors would provide invaluable insight into the electrochemical properties of the currently formulated ionogel materials.

Critical gel concentration (CGC) studies were conducted to determine the concentration at which the block copolymer dispersion is no longer a free-standing gel, as a result of insufficient inter-worm contacts in order to induce physical crosslinking. In other words, this is the point at which degelation occurs, and the dispersions are no longer free-standing. In order to maintain the superior electrochemical properties of [EMIM][DCA], it is important that the minimum polymer content is contained within the gel. The block copolymer target composition selected for these screenings was $PHEMA_{30}$-*b*-$PBzMA_{300}$ since the $PHEMA_{30}$-*b*-$PBzMA_{291}$ block copolymer synthesised at 15% w/w were positioned near the centre of the gel range in the block copolymer series synthesised at 15% w/w solids, and also displayed the highest proportion of worms (82.6% v/v) as confirmed by SAXS analysis. Block copolymers were synthesised at copolymer concentrations ranging from 10% w/w to 1% w/w, and the CGC was found to be >4% w/w, based on tube inversion tests and visual observations, which were supported by the rheological studies conducted of each dispersion. This proof-of-concept synthesis and characterisation of $PHEMA_{30}$-*b*-$PBzMA_y$ worm gels

demonstrates the versatility and ease of utilising PISA to generate ionogels without the requirement for additives (e.g. co-solvents) or post-polymerisation processing or purification.

$PHEMA_{30}$-*b*-$PBzMA_y$ diblock copolymers were also synthesised in [EMIM][$EtOSO_3$] at 15% w/w and 20% w/w solids. A kinetic study of the synthesis of $PHEMA_{30}$-*b*-$PBzMA_y$ at 15% w/w solids indicated high monomer conversion of benzyl methacrylate (>99%) within 1 hour. The critical DP of self-assembly was found to be 198, a much higher DP than that in [EMIM][DCA] (critical DP of 72), indicating that the [EMIM][$EtOSO_3$] is a better solvent for the PBzMA block, therefore a longer PBzMA core-forming block is required to induce unfavourable [EMIM][$EtOSO_3$]-PBzMA interactions and thus self-assembly. DLS was used to obtain sphere-equivalent diameters of dispersions of each block copolymer, and SAXS was used to confirm the morphologies of each dispersion. The background-subtracted SAXS data for 1.0% w/w dispersions with lower PBzMA DPs (targeting ≤400) were able to be fitted to a spherical micelle model. However, background-subtracted SAXS data for 1.0% w/w dispersions containing higher PBzMA DPs (targeting >400) were not satisfactorily fitted to appropriate models, therefore future work includes fitting these samples to appropriate models to determine the vesicle diameters and mean membrane thickness. The vesicle diameters obtained can then be compared with sphere-equivalent diameters obtained by DLS. Worm-like micelles were not present at significant proportions in any of the dispersions synthesised at 15% w/w or 20% w/w, as confirmed visual observations, the tube inversion test and SAXS analysis. This could be because the PHEMA stabiliser block provides sufficient steric stabilisation such that 2D fusion of spheres is hindered, or simply that the worm phase space in this IL is extremely narrow.

Clearly, further investigation into this PISA formulation in [EMIM][$EtOSO_3$] is required in order to achieve worm-like micelles. There are multiple options for tuning the formulation based on previous research that can be implemented to access the highly desired worm gels. One variable that will be investigated in the future will be shortening the PHEMA stabiliser block so that sphere-sphere fusion can be achieved, thus enabling the formation of worms. Accessing worms can also be possible by tuning the core-forming block such that the glass transition temperature (T_g) is lowered therefore improving mobility of the core-forming block chains. For example, this could be achieved via statistical copolymerisation of BzMA and HEMA to decrease the overall solvophobic nature of this core-forming block.

7. Appendix

7.1 Structural models for Small-angle X-ray scattering (SAXS) analysis

Programming tools within the Irena SAS Igor Pro macros[1] were used to implement the scattering models.

In general, the intensity of X-rays scattered by a dispersion of nano-objects [as represented by the scattering cross-section per unit sample volume, $\frac{d\Sigma}{d\Omega}(q)$] can be expressed as:

$$\frac{d\Sigma}{d\Omega}(q) = NS(q)\int_0^\infty \dots \int_0^\infty F(q, r_{1,} \dots, r_k)^2 \Psi(r_{1,} \dots, r_k) dr_{1,} \dots, dr_k \qquad 7.1$$

where $F(q, r_1, \dots, r_k)$ is the form factor, $r_{1,} \dots, r_k$ is a set of *k* parameters describing the structural morphology, $\Psi(r_{1,} \dots, r_k)$ is the distribution function, *S*(*q*) is the structure factor and *N* is the number density of nano-objects per unit volume expressed as:

$$N = \frac{\varphi}{\int_0^\infty \dots \int_0^\infty V(r_1, \dots, r_k)\Psi(r_1, \dots, r_k) dr_1, \dots, dr_k} \qquad 7.2$$

where $V(r_1, \dots, r_k)$ is the volume of the nano-object and φ is its volume fraction within the dispersion. It is assumed that *S*(*q*) = 1 at the sufficiently low copolymer concentrations used in this study (1.0% w/w).

7.1.1 Spherical micelle model

The spherical micelle form factor for Equation 7.1 is given by[2]

$$\begin{aligned} F_{s_{mic}}(q) = {} & {N_s}^2 {\beta_s}^2 {A_s}^2(q, R_s) + N_s {\beta_c}^2 F_c(q, R_g) + N_s(N_s - 1){\beta_c}^2 {A_c}^2(q) \\ & + 2{N_s}^2 \beta_s \beta_c A_s(q, R_s) A_c(q) \end{aligned} \qquad 7.3$$

where R_s is the volume-average sphere core radius and R_g is the radius of gyration of the coronal steric stabilizer block (in this case, $PHEMA_{30}$). The X-ray scattering length contrasts for the core and corona blocks are given by $\beta_s = V_s(\xi_s - \xi_{sol})$ and $\beta_c = V_c(\xi_c - \xi_{sol})$ respectively. Here, ξ_s, ξ_c and ξ_{sol} are the X-ray scattering length densities of the core block (ξ_{PBzMA} = 10.41 x 10^{10} cm^{-2}),

corona block (ξ_{PHEMA}= 11.50 x 10^{10} cm^{-2}) and [EMIM][DCA] solvent (ξ_{sol}= 9.90 x 10^{10} cm^{-2}), respectively. V_s and V_c are the volumes of the core block (V_{PBzMA}) and the corona block (V_{PHEMA}), respectively. The sphere form factor amplitude is used for the amplitude of the core self-term:

$$A_c(q, R_s) = \Phi(qR_s)\exp\left(-\frac{q^2\sigma^2}{2}\right) \quad 7.4$$

where $\Phi(qR_s) = \frac{3[\sin(qR_s) - qR_s\cos(qR_s)]}{(qR_s)^3}$. A sigmoidal interface between the two blocks was assumed for the spherical micelle form factor (Equation 7.3). This is described by the exponent term with a width σ accounting for a decaying scattering length density at the micellar interface. This σ value was fixed at 2.5 during fitting.

The form factor amplitude of the spherical micelle corona is:

$$A_c(q) = \frac{\int_{R_s}^{R_s+2s} \mu_c(r)\frac{\sin(qr)}{qr}r^2dr}{\int_{R_s}^{R_s+2s} \mu_c(r)r^2dr} exp\left(-\frac{q^2\sigma^2}{2}\right) \quad 7.5$$

The radial profile, $\mu_c(r)$, can be expressed by a linear combination of two cubic b splines, with two fitting parameters s and a corresponding to the width of the profile and the weight coefficient respectively. This information can be found elsewhere,[3, 4] as can the approximate integrated form of Equation 7.5. The self-correlation term for the coronal block is given by the Debye function:

$$F_c(q, R_g) = \frac{2\left[\exp\left(-q^2{R_g}^2\right) - 1 + q^2{R_g}^2\right]}{q^4{R_g}^4} \quad 7.6$$

where R_g is the radius of gyration of the PHEMA coronal block. In all cases R_g was fixed to be 1.4 nm, which is estimated by assuming the total contour length of $PHMEA_{30}$ is 7.66 nm (30 × 0.255 nm, where 0.225 nm is the contour length of one HEMA monomer unit with two C-C bonds in all-trans conformation). Given a mean Kuhn length of 1.53 nm, based on the known literature value for poly(methyl methacrylate)[5], an estimated unperturbed R_g of 1.4 nm is determined using R_g = $(7.66 \times 1.53/6)^{0.5}$.

The aggregation number, N_s, of the spherical micelle is given by:

$$N_s = (1 - x_{sol})\frac{\frac{4}{3}\pi {R_s}^3}{V_s} \quad 7.7$$

where x_{sol} is the volume fraction of solvent within the PBzMA micelle cores, which was found to be zero in all cases. A polydispersity for one parameter (R_s) is assumed for the micelle model, which is described by a Gaussian distribution. Thus, the polydispersity function in Equation 7.1 can be represented as:

$$\Psi(r_1) = \frac{1}{\sqrt{2\pi {\sigma_{Rs}}^2}} exp\left(-\frac{(r_1 - R_s)^2}{2{\sigma_{Rs}}^2}\right) \quad 7.8$$

where σ_{Rs} is the standard deviation for R_s. In accordance with Equation 7.2, the number density per unit volume for the micelle model is expressed as:

$$N = \frac{\varphi}{\int_0^\infty V(r_1)\Psi(r_1)dr_1} \quad 7.9$$

where φ is the total volume fraction of copolymer in the spherical micelles and $V(r_1)$ is the total volume of copolymer within a spherical micelle $[V(r_1) = (V_s + V_c)N_s(r_1)]$.

7.1.2 Worm-like micelle model

The worm-like micelle form factor for Equation 7.1 is given by:

$$F_{w\_mic}(q) = {N_w}^2{\beta_s}^2 F_{sw}(q) + N_w{\beta_c}^2 F_c\left(q, R_g\right) + N_w(N_w - 1){\beta_c}^2 S_{cc}(q) + 2{N_w}^2\beta_s\beta_c S_{sc}(q) \quad 7.10$$

where all the parameters are the same as those described in the spherical micelle model (Equation 7.3), unless stated otherwise.

The self-correlation term for the worm core cross-sectional volume-average radius R_w is:

$$F_{sw}(q) = F_{worm}(q, L_w, b_w){A_{CS}}_{worm}{}^2(q, R_w) \quad 7.11$$

where

$${A_{CS}}_{worm}{}^2(q, R_w) = \left[2\frac{J_1(qR_w)}{qR_w}\right]^2 \quad 7.12$$

and J_1 is the first-order Bessel function of the first kind, and a form factor $F_{worm}(q, L_w, b_w)$ for self-avoiding semi-flexible chains represents the worm-like micelles, where b_w is the Kuhn length and L_w is the mean contour length. A complete expression for the chain form factor can be found elsewhere.[6]

The mean aggregation number of the worm-like micelle, N_{w}, is given by:

$$N_w = (1 - x_{sol})\frac{\pi {R_w}^2 L_w}{V_s} \quad 7.13$$

where x_{sol} is the volume fraction of solvent within the worm-like micelle cores, which was found to be zero in all cases. The possible presence of semi-spherical caps at both ends of each worm is neglected in this form factor.

A polydispersity for one parameter (R_{w}) is assumed for the micelle model, which is described by a Gaussian distribution. Thus, the polydispersity function in Equation 7.1 can be represented as:

$$\Psi(r_1) = \frac{1}{\sqrt{2\pi {\sigma_{R_{\mathrm{w}}}}^2}} exp\left(-\frac{(r_1 - R_{\mathrm{w}})^2}{2{\sigma_{R_{\mathrm{w}}}}^2}\right) \quad 7.14$$

where $\sigma_{R_{\mathrm{w}}}$ is the standard deviation for R_{w}. In accordance with Equation 7.2, the number density per unit volume for the worm-like micelle model is expressed as:

$$N = \frac{\varphi}{\int_0^\infty V(r_1)\Psi(r_1)dr_1} \quad 7.15$$

where φ is the total volume fraction of copolymer in the worm-like micelles and $V(r_1)$ is the total volume of copolymer in a worm-like micelle $[V(r_1) = (V_{\mathrm{s}} + V_{\mathrm{c}})N_{\mathrm{w}}(r_1)]$.

7.1.3 Vesicle model

The vesicle form factor in Equation 7.1 is expressed as:[7]

$$F_{ves}(q) = {N_v}^2{\beta_m}^2{A_m}^2(q) + N_v{\beta_{vc}}^2F_c\left(q, R_g\right) + N_v(N_v - 1){\beta_{vc}}^2{A_{vc}}^2(q) + 2{N_v}^2\beta_m\beta_{vc}A_m(q)A_{vc}(q) \quad 7.16$$

where all the parameters are the same as in the spherical micelle model (see Equation 7.3) unless stated otherwise.

The amplitude of the membrane self-term is:

$$A_m(q) = \frac{V_{out}\varphi(qR_{out}) - V_{in}\varphi(qR_{in})}{V_{out} - V_{in}} exp\left(-\frac{q^2{\sigma_{in}}^2}{2}\right) \quad 7.17$$

where $R_{in} = R_m - \frac{1}{2}T_m$ is the inner radius of the membrane, $R_{out} = R_m + \frac{1}{2}T_m$ is the outer radius of the membrane (R_m is the radius from the centre of the vesicle to the centre of the membrane), $V_{in} = \frac{4}{3}\pi{R_{in}}^3$ and $V_{out} = \frac{4}{3}\pi{R_{out}}^3$. It should be noted that Equation 7.16 differs subtly from the original work in which it was first described.[7] The exponent term in Equation 7.17 represents a sigmoidal interface between the blocks, with a width σ_{in} accounting for a decaying scattering length density at the membrane surface. The value of σ_{in} was fixed at 2.5 during fitting. The mean vesicle aggregation number, N_v, is given by:

$$N_v = (1 - x_{sol})\frac{V_{out} - V_{in}}{V_m} \quad 7.18$$

where x_{sol} is the volume fraction of solvent within the vesicle membrane, which was found to be zero in all cases. Assuming that there is no penetration of the solvophilic coronal blocks into the solvophobic membrane, the amplitude of the vesicle corona self-term is expressed as:

$$A_{vc}(q) = \Psi(qR_g)\frac{1}{2}\left[\frac{sin\left[q\left(R_{out} + R_g\right)\right]}{q(R_{out} + R_g)} + \frac{\sin\left[q\left(R_{in} - R_g\right)\right]}{q(R_{in} - R_g)}\right] \quad 7.19$$

where the term outside the square brackets is the factor amplitude of the corona block polymer chain such that:

$$\Psi(qR_g) = \frac{1 - \exp(-qR_g)}{(qR_g)^2} \quad 7.20$$

For the vesicle model, it was assumed that two parameters are polydisperse: the radius from the centre of the vesicles to the centre of the membrane and the membrane thickness (denoted R_m and T_m, respectively). Each parameter is considered to have a Gaussian distribution of values, so the polydispersity function in Equation 7.1 can be expressed in each case as:

$$\Psi(r_1 r_2) = \frac{1}{\sqrt{2\pi{\sigma_{Rs}}^2}} exp\left(-\frac{(r_1 - R_m)^2}{2{\sigma_{Rm}}^2}\right) \frac{1}{\sqrt{2\pi{\sigma_{Tm}}^2}} exp\left(-\frac{(r_1 - T_m)^2}{2{\sigma_{Tm}}^2}\right) \quad 7.21$$

where σ_{Rm} and σ_{Tm} are the standard deviations for R_m and T_m, respectively. Following Equation 7.2, the number density per unit volume for the vesicle model is expressed as:

$$N = \frac{\varphi}{\int_0^\infty \int_0^\infty V(r_1, r_2)\, \Psi(r_1, r_2) dr_1 dr_2} \quad 7.22$$

where φ is the total volume fraction of copolymer in the vesicles and $V(r_1, r_2)$ is the total volume of copolymers in a vesicle $[V(r_1, r_2) = (V_m + V_{vc}) N_v(r_1, r_2)]$.

7.1.4 Gaussian chain model

Data for the 1% w/w solution of $PHEMA_{30}$-*b*-$PBzMA_{49}$ were fitted to a Gaussian chain model.[8] Generally, the scattering cross-section per unit sample volume for an individual Gaussian polymer chain can be expressed as:

$$\frac{d\Sigma}{d\Omega}(q) = \varphi(\Delta\xi)^2 V_{\mathrm{mol}} F_{\mathrm{mol}}(q) \quad 7.23$$

where V_{mol} is the total molecular volume and $\Delta\xi$ is the excess scattering length density of the copolymer [$\Delta\xi = \xi_{\mathrm{PHEMA-PBzMA}} - \xi_{\mathrm{[EMIM][DCA]}} = 0.92 \times 10^{-10}$ cm^{-2}], where the scattering length

density of the copolymer, $\xi_{\mathrm{PHEMA-PBzMA}} = \frac{V_{\mathrm{PHEMA}}\xi_{\mathrm{PHEMA}} + V_{\mathrm{PBzMA}}\xi_{\mathrm{PBzMA}}}{V_{\mathrm{PHEMA-PBzMA}}}$ which for $PHEMA_{30}$-*b*-$PbzMA_{49}$ gives $\xi_{\mathrm{PHEMA-PBzMA}} = 10.72 \times 10^{-10}$ cm^{-2}, and the scattering length density of [EMIM][DCA], $\xi_{[EMIM][DCA]} = 9.90 \times 10^{-10}$ cm^{-2}. The generalized form factor for a Gaussian polymer chain is given by:

$$F_{\mathrm{mol}}(q) = \left[\frac{1}{\upsilon U^{1/(2\upsilon)}}\gamma\left(\frac{1}{2\upsilon}, U\right) - \frac{1}{\upsilon U^{1/\upsilon}}\left(\frac{1}{\upsilon}, U\right)\right] \quad 7.24$$

where the lower incomplete gamma function is $\gamma(s,x) = \int_0^x t^{s-1}\exp(-t)\,dt$ and U is the modified variable:

$$U = (2\upsilon + 1)(2\upsilon + 2)\frac{q^2 {R_{\mathrm{g}}}_{\mathrm{cop}}^{\ 2}}{6} \quad 7.25$$

Here, υ is the extended volume parameter and ${R_{\mathrm{g}}}_{\mathrm{cop}}$ is the radius of gyration of the copolymer chain.

7.2 References

1. J. Ilavsky and P. R. Jemian, *J. Appl. Crystallogr*, 2009, **42**, 347-353.
2. J. Pedersen, *J. Appl. Crystallogr*, 2000, **33**, 637-640.
3. J. S. Pedersen and M. C. Gerstenberg, *Colloids Surfaces A Physicochem. Eng. Asp.*, 2003, **213**, 175-187.
4. J. S. Pedersen, C. Svaneborg, K. Almdal, I. W. Hamley and R. N. Young, *Macromolecules*, 2003, **36**, 416-433.
5. L. J. Fetters, D. J. Lohsey and R. H. Colby, *Physical Properties of Polymers Handbook*, Springer, New York, 2nd edn., 2007.
6. J. S. Pedersen and P. Schurtenberger, *Macromolecules*, 1996, **29**, 7602-7612.
7. J. Bang, S. Jain, Z. Li, T. P. Lodge, J. S. Pedersen, E. Kesselman and Y. Talmon, *Macromolecules*, 2006, **39**, 1199-1208.
8. B. Hammouda, *Probing Nanoscale Structures – the SANS Toolbox*, 2008.